

NMR STUDIES OF SOME OSMIUM CLUSTER COMPOUNDS

by

Andrew K. Ma

B.S.(Hons.), University of Manitoba, 1983

THESIS SUBMITTED IN PARTIAL FULFILLMENT OF
THE REQUIREMENTS FOR THE DEGREE OF
DOCTOR OF PHILOSOPHY
in the Department
of
Chemistry

© Andrew K. Ma 1992

SIMON FRASER UNIVERSITY

July 1992

All rights reserved. This work may not be reproduced in whole or in part, by photocopy or other means, without permission of the author.

APPROVAL

Name: Andrew K. Ma
Degree: Doctor of Philosophy
Title of Thesis: Nuclear Magnetic Resonance Studies of Some Osmium Cluster Compounds
Examining Committee: Chair: Dr. D. Sutton

~~Dr. R.K. Pomeroy, (Professor)~~
Senior Supervisor

Dr. I.D. Gay, (Professor)
Committee Member

Dr. C.H.W. Jones, (Professor/Dean of Science)
Committee Member

Dr. A.S. Tracey, (Supervisor NMR Services)
Internal Examiner

Dr. J. Keister, (Professor)
External Examiner
Department of Chemistry
State University of New York

Date Approved: August 11, 1992

PARTIAL COPYRIGHT LICENSE

I hereby grant to Simon Fraser University the right to lend my thesis, project or extended essay (the title of which is shown below) to users of the Simon Fraser University Library, and to make partial or single copies only for such users or in response to a request from the library of any other university, or other educational institution, on its own behalf or for one of its users. I further agree that permission for multiple copying of this work for scholarly purposes may be granted by me or the Dean of Graduate Studies. It is understood that copying or publication of this work for financial gain shall not be allowed without my written permission.

Title of Thesis/Project/Extended Essay:


NMR STUDIES OF SOME OSMIUM CLUSTER COMPOUNDS

Author:


(signature)

Andrew Kwong-Yan Ma

(name)



(date)

Abstract

The first part of the thesis describes the use of nuclear Overhauser enhancement (NOE) to determine the relative positions of two or more hydrides that are chemically different in osmium clusters. Eight types of clusters with various, known arrangements of chemically inequivalent hydrides were studied. The observed enhancements were in good agreement with the predicted results.

The relaxation time, T_1 , for the hydrides in some of these clusters were also measured. It was found that terminal hydrides have the shortest T_1 values and those for the bridging hydrides depend on the identity of the neighbouring groups.

Both the NOE and T_1 measurements provide valuable information on the location of hydride ligands in metal clusters. This is often difficult to determine by X-ray crystallographic and conventional spectroscopic techniques.

The second part of the thesis describes investigations of the stereochemical nonrigidity in various trinuclear and tetranuclear osmium clusters by variable temperature ^{13}C NMR spectroscopy. In the ^{13}C NMR spectra of $\text{Os}_3(\text{CO})_{11}(\text{L})$ (L = group 15 ligand; L in an equatorial site) sets of carbonyl signals collapse at different rates between $-50\text{ }^\circ\text{C}$ and $60\text{ }^\circ\text{C}$. The results are rationalized in terms of three

exchange processes. The two lowest energy processes are thought to involve terminal-bridge CO exchange in two vertical planes of the cluster. The third, higher energy process is believed to be a trigonal-twist mechanism at one of the osmium centres. The chemical shift of the axial carbonyls of the $\text{Os}(\text{CO})_3(\text{L})$ group was taken as a measure of the electronic properties of the group 15 ligand in the clusters. These electronic parameters gave a good correlation with the activation energies for the first CO exchange process in the clusters.

In $\text{Os}_3(\text{CO})_{11}[\text{Os}(\text{CO})_{5-x}(\text{CNBu}^t)_x]$ ($x = 1, 2$), the first CO exchange process is consistent with a restricted oscillation about the dative Os-Os bond. The higher energy processes are similar to those proposed for the $\text{Os}_3(\text{CO})_{11}(\text{L})$ clusters. Interestingly, in $\text{Os}_3(\text{CO})_{11}[\text{Os}(\text{CO})_4(\text{CNBu}^t)]$ three of the carbonyls of the $\text{Os}(\text{CO})_4(\text{CNBu}^t)$ group exchange with those of the $\text{Os}_3(\text{CO})_{11}$ fragment, whereas the carbonyls of the $\text{Os}(\text{CO})_3(\text{CNBu}^t)_2$ unit do not exchange with the other carbonyls in $\text{Os}_3(\text{CO})_{11}[\text{Os}(\text{CO})_3(\text{CNBu}^t)_2]$.

In the kite-like cluster, $\text{Os}_4(\text{CO})_{15}$, the ^{13}C NMR spectrum at -121°C is consistent with rapid exchange of the carbonyls in the equatorial plane. In contrast, in $\text{Os}_4(\text{CO})_{13}(\text{PMe}_3)[\text{P}(\text{OMe})_3]$, which also has a kite arrangement of metal atoms, carbonyl exchange apparently takes place in the two vertical planes that are cis to the two phosphorus ligands. Furthermore, these exchanges have a much higher

activation energy than that in $\text{Os}_4(\text{CO})_{15}$.

In the three isomers of $\text{Os}_3(\mu\text{-H})_2(\text{CO})_9(\text{CNBu}^t)$, the NMR results are interpreted in terms of the rotation of the $\text{Os}(\text{CO})_3$ and $\text{Os}(\text{CO})_2(\text{CNBu}^t)$ units of the $(\text{OC})_3\text{Os}(\mu\text{-H})_2\text{-Os}(\text{CO})_2\text{L}$ ($\text{L} = \text{CO}, \text{CNBu}^t$) groups. Surprisingly, the hydride ligands remain rigid in these processes.

DEDICATION

To my Grandmother

Parents

Wife

ACKNOWLEDGEMENTS

It has been a great honour and privilege for me to have been supervised by Prof. Roland K. Pomeroy during the course of this research. His guidance has taught me chemistry as well as a great many other things.

The crystal structure of many osmium clusters reported in this thesis has been determined by Drs. Fred Einstein and Victor Johnston. I have also benefited from the discussions with them.

I would also like to express my thanks to other members of Dr. Pomeroy's research group for their friendship in the laboratory and the fun times outside the laboratory. Special thanks is conveyed to Dr. Harry Davis for his valuable discussion of the research and the lab techniques. I particularly want to thank Dr. Victor Johnston, Mr. Brad Gilmore and Mr. Ernest Wong who have collaborated on some of the work reported in this thesis.

Mrs. Marcie Tracey is thanked for her assistance in the operations of both the 100 MHz and 400 MHz NMR spectrometers in the department.

TABLE OF CONTENTS

Approval	ii
Abstract	iii
Dedication	vi
Acknowledgements	vii
Table of Contents	viii
List of Figures	x
List of Tables	xvii
General Introduction	1
1. A. Use of the Nuclear Overhauser Enhancement (NOE) Technique in the Characterization of Hydrido- Osmium Clusters	3
1A.1 Introduction	3
1A.2 Experimental Section	
1A.2.1 Preparation of NOE Samples	10
1A.2.2 Experimental Details	10
1A.3 Results and Discussion	14
1A.4 Conclusion	76
B. T ₁ Relaxation Times of Hydrides in Some Hydrido-Osmium Clusters	80
1B.1 Introduction	80
1B.2 Experimental Section	81
1B.3 Results and Discussion	86
1B.4 Conclusion	105
2. Nonrigidity of Os ₃ (CO) ₁₁ (ER ₃) and the Donor Ability of Group 15 Ligands	106
2.1 Introduction	106

2.2	Experimental Section	
2.2.1	General Procedure	108
2.2.2	NMR Studies	109
2.2.3	Preparation of Os ₃ (CO) ₁₁ (ER ₃)	111
2.2.4	Preparation of Os ₃ (CO) ₁₁ (PF ₃)	112
2.3	Results and Discussion	
2.3.1	Nonrigidity of Os ₃ (CO) ₁₁ (ER ₃)	116
2.3.2	Correlation of the Activation Barriers to CO-Exchange with the Properties of the Group 15 Ligand	140
3.	Stereochemical Nonrigidity of Tetraosmium Clusters ..	149
3.1	Introduction	149
3.2	Spiked-triangular Os ₄ Clusters	
	Os ₄ (CO) ₁₅ (CNBu ^t)	149
	Os ₄ (CO) ₁₄ (CNBu ^t) ₂	168
3.3	Puckered-square Os ₄ Clusters	
	Os ₄ (CO) ₁₅ (PF ₃)	179
3.4	Kite-shaped Os ₄ Clusters	
	Os ₄ (CO) ₁₅	184
	Os ₄ (CO) ₁₃ (PMe ₃) ₂ [P(OMe) ₃]	189
	Os ₄ (CO) ₁₄ (CNBu ^t)	198
4.	Nonrigidity in the Isomers of Os ₃ (μ-H) ₂ (CO) ₉ (CNBu ^t) .	202
4.1	Introduction	202
4.2	Experimental Section	203
4.3	Results and Discussion	207
4.4	Conclusion	236
	Appendix I	239
	References	251

LIST OF FIGURES

FIGURE	PAGE
1.1	Possible arrangements of hydride ligands in triangular Os ₃ clusters 4
1.2	The effect of τ_c on proton R ₁ at 100 and 400 MHz ... 15
1.3	Observed nuclear Overhauser enhancement versus the internuclear H...H distance for 2-spin interaction 20
1.4	The ¹ H NMR and NOE difference spectra of Os ₃ (μ-H) ₂ (CO) ₉ (CNBu ^t) at -70 °C 22
1.5	Molecular structure of the green isomer of Os ₃ (μ-H) ₂ (CO) ₉ (CNBu ^t) (1g) 24
1.6	Molecular structure of the red isomer (isomer b) of Os ₃ (μ-H) ₂ (CO) ₉ (CNBu ^t) 26
1.7	The ¹ H NMR and NOE difference spectra of isomers a and b of the red isomers of Os ₃ (μ-H) ₂ (CO) ₉ (CNBu ^t) at -70 °C 27
1.8	Molecular structure of HOs ₃ (μ-H)(CO) ₁₀ (CNBu ^t) 30
1.9	The ¹ H NMR and NOE difference spectra of HOs ₃ (μ-H)(CO) ₁₀ (CNBu ^t) at -70 °C 31
1.10	Molecular structure of HOs ₃ (μ-H)(CO) ₁₀ (PPh ₃) 33
1.11	Simplified relative locations of the hydride atoms and the calculated internuclear H...H and H...P distances in HOs ₃ (μ-H)(CO) ₁₀ (PPh ₃) 34
1.12	The ¹ H NMR and NOE difference spectra of HOs ₃ (μ-H)(CO) ₁₀ (PMe ₃) at -100 °C 36
1.13	Molecular structure of Os ₄ (μ-H) ₂ (CO) ₁₃ (PMe ₃) 40
1.14	The ¹ H NMR and NOE difference spectra of Os ₄ (μ-H) ₂ (CO) ₁₃ (PMe ₃) at -70 °C 42
1.15	Molecular structure of Os ₃ (μ-H) ₃ (CO) ₉ -[Ir(CO) ₂ (PPh ₃)] 45
1.16	The ¹ H NMR and NOE difference spectra of Os ₃ (μ-H) ₃ (CO) ₉ [Ir(CO) ₂ (PPh ₃)] at -100 °C 47

1.17	Molecular structure of isomer a of $\text{Os}_3(\mu\text{-H})_2(\text{CO})_{10}(\text{SnMe}_3)_2$	50
1.18	Proposed structure of isomer b of $\text{Os}_3(\mu\text{-H})_2(\text{CO})_{10}(\text{SnMe}_3)_2$	51
1.19	The ^1H NMR and NOE difference spectra of the two isomers of $\text{Os}_3(\mu\text{-H})_2(\text{CO})_{10}(\text{SnMe}_3)_2$ at -70°C	54
1.20	Molecular structure of $\text{HOs}_3(\mu\text{-H})_2(\text{CO})_{10}(\text{SiHPh}_2)$	57
1.21	The ^1H NMR and NOE difference spectra of $\text{HOs}_3(\mu\text{-H})_2(\text{CO})_{10}(\text{SiHPh}_2)$ at -70°C	58
1.22	The dependence of the nuclear Overhauser enhancement on the relative positions of the spins in a 3-spin system	63
1.23	Molecular structure of $\text{Os}_3(\mu\text{-H})_3(\text{CO})_9(\text{SiPh}_3)$	65
1.24	Simplified relative locations of the hydride ligands and the calculated $\text{H}\cdots\text{H}$ distances of $\text{Os}_3(\mu\text{-H})_3(\text{CO})_9(\text{SiPh}_3)$	66
1.25	The ^1H NMR and NOE difference spectra of $\text{Os}_3(\mu\text{-H})_3(\text{CO})_9(\text{SiPh}_3)$ at -70°C	67
1.26	Molecular structure of $\text{Os}_4(\mu\text{-H})_3(\text{CO})_{12}\text{I}$	70
1.27	The ^1H NMR and NOE difference spectra of $\text{Os}_4(\mu\text{-H})_3(\text{CO})_{12}\text{I}$ at -70°C	71
1.28	Molecular structure of $\text{Os}_4(\mu\text{-H})(\text{CO})_{14}(\text{SnMe}_3)$	73
1.29	The ^1H NMR and NOE difference spectra of $\text{Os}_4(\mu\text{-H})(\text{CO})_{14}(\text{SnMe}_3)$ at ambient temperature	75
1.30	Observed nuclear Overhauser enhancement versus the internuclear $\text{H}\cdots\text{H}$ distance for 2-spin interaction in this study	77
1.31	T_1 determination of the hydride signal, to the high field of the ^1H NMR spectrum, of $\text{Os}_3(\mu\text{-H})_2(\text{CO})_9(\text{CNBu}^t)$ (2) by the exponential method	84
1.32	T_1 determination of the hydride signal, to the low field of the ^1H NMR spectrum, of $\text{Os}_3(\mu\text{-H})_2(\text{CO})_9(\text{CNBu}^t)$ (2) by the exponential method	84
1.33	The relationship of relaxation rate, R_1 , with correlation time, τ_c , at different magnetic field ..	89

1.34	Stacked plot of an inversion-recovery experiment for the hydride nuclei of $\text{HOs}_3(\mu\text{-H})(\text{CO})_{10}(\text{CNBu}^t)$ measured at -70°C at 100.13 MHz	91
1.35	The structures and the measured T_1 's of the hydrido-osmium clusters 1 to 4	92
1.36	The structures and the measured T_1 's of the hydrido-osmium clusters 5 to 7	96
1.37	The structures and the measured T_1 's of the hydrido-osmium clusters 8 and 9	98
1.38	The molecular structure and the ^1H NMR spectrum (at -70°C) of $\text{Os}_3(\mu\text{-H})_3(\text{CO})_9(\text{SiPh}_3)$	100
1.39	The structures and the measured T_1 's of the hydrido-osmium clusters 10 to 12	102
1.40	The structures and the measured T_1 's of the hydrido-osmium clusters 13 to 15	104
2.1	IR spectrum (CO stretching region) of $\text{Os}_3(\text{CO})_{11}(\text{PPh}_3)$	113
2.2	Structure of $\text{Os}_3(\text{CO})_{11}[\text{P}(\text{OMe})_3]$	117
2.3	Diagrammatic presentation of the structure and the labelling scheme of carbonyl ligands in $\text{Os}_3(\text{CO})_{11}(\text{PMe}_3)$	120
2.4	Variable temperature ^{13}C NMR spectra for $\text{Os}_3(\text{CO})_{11}(\text{PMe}_3)$	122
2.5	Allowed planes of pairwise terminal-bridge carbonyl exchange in $\text{Os}_3(\text{CO})_{11}(\text{ER}_3)$	123
2.6	Terminal-bridge carbonyl exchange in $\text{Os}_3(\text{CO})_{11}(\text{ER}_3)$ when viewed directly along the edge of the $\text{Os}_A\text{-Os}_C$ bond	124
2.7	Calculated (A) and experimental (B) ^{13}C NMR spectra of $\text{Os}_3(\text{CO})_{11}(\text{PMe}_3)$ at -35°C	125
2.8	Diagram that shows the overlap of the expanded 5d orbitals on osmium with the π^* orbitals of the axial carbonyls on the adjacent osmium atom	127
2.9	Diagrammatic presentation of the partially restricted rotation that brings the PMe_3 group from one equatorial site to the other	130

2.10	Variable temperature ^{13}C NMR spectra of $\text{Os}_3(\text{CO})_{11}[\text{P}(\text{p-tolyl})_3]$	131
2.11	Variable temperature ^{13}C NMR spectra of $\text{Os}_3(\text{CO})_{11}(\text{PPh}_3)$	132
2.12	Variable temperature ^{13}C NMR spectra of $\text{Os}_3(\text{CO})_{11}(\text{AsPh}_3)$	133
2.13	Variable temperature ^{13}C NMR spectra of $\text{Os}_3(\text{CO})_{11}(\text{SbPh}_3)$	134
2.14	Variable temperature ^{13}C NMR spectra of $\text{Os}_3(\text{CO})_{11}[\text{P}(\text{OPh}_3)]$	135
2.15	Variable temperature ^{13}C NMR spectra of $\text{Os}_3(\text{CO})_{11}[\text{P}(\text{OCH}_2)_3\text{CCH}_3]$	136
2.16	Variable temperature ^{13}C NMR spectra of $\text{Os}_3(\text{CO})_{11}[\text{P}(\text{OCH}_2)_3\text{CCH}_3]$	137
2.17	Variable temperature ^{13}C NMR spectra of $\text{Os}_3(\text{CO})_{11}(\text{PF}_3)$	138
2.18	A plot that shows the linear correlation between the $\Delta\delta_{\text{Os}}$ and the activation energy, ΔG_1^\ddagger , for the first CO-exchange process in $\text{Os}_3(\text{CO})_{11}(\text{ER}_3)$	142
2.19	Molecular structure of $\text{Ru}(\text{CO})_4[\text{P}(\text{OCH}_3)_3]$	144
2.20	Comparison of the $\Delta\delta$ parameter in $\text{Ni}(\text{CO})_3(\text{ER}_3)$ ($\Delta\delta_{\text{Ni}}$) and $\text{Os}_3(\text{CO})_{11}(\text{ER}_3)$ ($\Delta\delta_{\text{Os}}$)	146
2.21	Plot of the $\nu(\text{CO})$ in $\text{Ni}(\text{CO})_3(\text{ER}_3)$ and $\Delta\delta_{\text{Os}}$ parameter in $\text{Os}_3(\text{CO})_{11}(\text{ER}_3)$	147
3.1	Molecular structure of $\text{Os}_4(\text{CO})_{15}(\text{CNBu}^t)$	150
3.2	Variable temperature ^{13}C NMR spectra for $\text{Os}_4(\text{CO})_{15}(\text{CNBu}^t)$	153
3.3	Diagrammatic presentation of the different conformations that result when the $\text{Os}(\text{CO})_4(\text{CNBu}^t)$ group oscillates about the Os-Os bond in $\text{Os}_4(\text{CO})_{15}(\text{CNBu}^t)$	154
3.4	Calculated model showing the steric hindrance between the CNBu^t ligand and its vicinal carbonyl during the rotation of the $\text{Os}(\text{CO})_4(\text{CNBu}^t)$ group about the Os(1)-Os(2) bond	156

3.5	Calculated model showing the steric hindrance between CO(13) and its vicinal carbonyl CO(43) during the rotation of the Os(CO) ₄ (CNBu ^t) group about the Os(1)-Os(2) bond	157
3.6	Variable temperature ¹³ C NMR spectra for Os ₄ (CO) ₁₅ (CNBu ^t)	159
3.7	Calculated (A) and experimental (B) ¹³ C NMR spectra of Os ₄ (CO) ₁₅ (CNBu ^t) at -85 °C	160
3.8	Terminal-bridge carbonyl exchange process that takes place in the axial plane that is cis perpendicular to L of Os ₃ (CO) ₁₁ (L) cluster	162
3.9	Calculated (A) and observed (B) ¹³ C NMR spectra of Os ₄ (CO) ₁₅ (CNBu ^t) at -48 °C	163
3.10	Proposed mechanism that exchanges three carbonyls of the Os(CO) ₄ (CNBu ^t) group with those of the Os ₃ (CO) ₁₁ fragment	165
3.11	The two proposed terminal-bridge carbonyl exchange processes that take place in the perpendicular plane of the Os ₃ (CO) ₁₁ (L) cluster	167
3.12	Proposed structure and the labelling scheme of Os ₄ (CO) ₁₄ (CNBu ^t) ₂	169
3.13	Variable temperature ¹³ C NMR spectra for Os ₄ (CO) ₁₄ (CNBu ^t) ₂	171
3.14	Schematic presentation of different conformations resulted when Os(CO) ₃ (CNBu ^t) ₂ group oscillates about the Os(1)-Os(2) bond	173
3.15	Diagrammatic presentation of the coalescence of two unequally populated signals when the two signals are close and far apart	174
3.16	Variable temperature ¹³ C NMR spectra for Os ₄ (CO) ₁₄ (CNBu ^t) ₂	175
3.17	Calculated (A) and observed (B) ¹³ C NMR spectra of Os ₄ (CO) ₁₄ (CNBu ^t) ₂ at -48 °C	177
3.18	Molecular structure of Os ₄ (CO) ₁₅ (PF ₃)	180
3.19	¹³ C NMR spectrum of Os ₄ (CO) ₁₅ (PF ₃) at -56 °C	182
3.20	Molecular structure of Os ₄ (CO) ₁₅	185

3.21	Labels indicating nonequivalent carbonyls in $\text{Os}_4(\text{CO})_{15}$	186
3.22	Variable temperature ^{13}C NMR spectra of $\text{Os}_4(\text{CO})_{15}$.	187
3.23	Proposed mechanism of in-plane merry-go-round equatorial CO exchange process for $\text{Os}_4(\text{CO})_{15}$	189
3.24	Molecular structure of $\text{Os}_4(\text{CO})_{13}(\text{PMe}_3)[\text{P}(\text{OMe})_3]$...	191
3.25	Variable temperature ^{13}C NMR spectra of $\text{Os}_4(\text{CO})_{13}(\text{PMe}_3)[\text{P}(\text{OMe})_3]$	193
3.26	Proposed CO exchange processes in $\text{Os}_4(\text{CO})_{13}(\text{PMe}_3)[\text{P}(\text{OMe})_3]$	196
3.27	Calculated (A) and observed (B) ^{13}C NMR spectra of $\text{Os}_4(\text{CO})_{13}(\text{PMe}_3)[\text{P}(\text{OMe})_3]$ at -6°C	197
3.28	Molecular structure of $\text{Os}_4(\text{CO})_{14}(\text{CNBu}^t)$	199
3.29	^{13}C NMR spectra of $\text{Os}_4(\text{CO})_{14}(\text{CNBu}^t)$	201
4.1	Infrared spectrum of $\text{Os}_3(\mu\text{-H})_2(\text{CO})_9(\text{CNBu}^t)$ (1g) ...	206
4.2	Interconversion of $\text{HOs}_3(\mu\text{-H})(\text{CO})_{10}(\text{CNBu}^t)$ (2) and the isomers of $\text{Os}_3(\mu\text{-H})_2(\text{CO})_9(\text{CNBu}^t)$	208
4.3	Molecular structure of $\text{Os}_3(\mu\text{-H})_2(\text{CO})_9(\text{CNBu}^t)$ (1g) .	211
4.4	Formation of the isomers of $\text{Os}_3(\mu\text{-H})_2(\text{CO})_9(\text{CNBu}^t)$ (1g , 1r) from $\text{HOs}_3(\mu\text{-H})(\text{CO})_{10}(\text{CNBu}^t)$ (2)	216
4.5	Proposed pathway for the isomerization of the isomers of $\text{Os}_3(\mu\text{-H})_2(\text{CO})_9(\text{CNBu}^t)$	220
4.6	Variable temperature 100.6 MHz ^{13}C NMR spectra of $\text{Os}_3(\mu\text{-H})_2(\text{CO})_9(\text{CNBu}^t)$ (1g). Inset: 100-MHz ^1H NMR spectrum of 1g in toluene- d_8 at 22°C	221
4.7	Proposed mechanism of CO exchange in $\text{Os}_3(\mu\text{-H})_2(\text{CO})_9(\text{CNBu}^t)$ (1g)	223
4.8	Calculated (A) and observed (B) ^{13}C NMR spectra of 1g at 8°C	226
4.9	Molecular structure of the red isomer of $\text{Os}_3(\mu\text{-H})_2(\text{CO})_9(\text{CNBu}^t)$ (1rb)	228
4.10	Variable temperature ^{13}C NMR spectra of 1r	230

4.11	Illustration of the three-fold rotations about the Os(2)-Os(3) axis in 1r	231
4.12	Calculated (A) and observed (B) ^{13}C NMR spectra of 1ra at 86 °C	234
4.13	Calculated (A) and observed (B) ^1H NMR spectra of 1r at 83 °C	237
A.1	The Solomon's diagram for a 2-spin spin-1/2 system	240
A.2	Plot of spectral density and frequency at different correlation time	242
A.3	Diagram shows the relation of τ_c and the relaxation rate at 100 and 400 MHz	242
A.4	Simulated NOE's for a one-proton multiplet and a three-proton singlet	249

LIST OF TABLES

TABLE	PAGE
1.1	Potential energies of the two types of hydrides calculated from the HYDEX program 8
1.2	The internuclear distances of the hydride ligands in the eight types of hydride arrangements as calculated from the HYDEX program 9
1.3	The observed %NOE in $\text{HOs}_3(\mu\text{-H})(\text{CO})_{10}(\text{L}')$ ($\text{L}' = \text{CO}, \text{CNBu}^t$) 32
1.4	The observed %NOE in $\text{HOs}_3(\mu\text{-H})(\text{CO})_{10}(\text{L})$ at $-100\text{ }^\circ\text{C}$ 37
1.5	The observed barrier of ligand exchange in $\text{HOs}_3(\mu\text{-H})(\text{CO})_{10}(\text{L})$ and $\text{HOs}_3(\mu\text{-H})(\text{CO})_{10}(\text{L}')$, ΔG^\ddagger , and the %NOE observed 39
1.6	The observed %NOE and the $\text{H}\cdots\text{H}$ distance in $\text{Os}_4(\mu\text{-H})_2(\text{CO})_{13}(\text{PMe}_3)$ 43
1.7	The observed %NOE in $\text{Os}_3(\mu\text{-H})_3(\text{CO})_9[\text{Ir}(\text{CO})_2(\text{PPh}_3)]$. 46
1.8	The calculated %NOE compared to the experimental %NOE in the clusters $\text{HOs}_3(\mu\text{-H})_2(\text{CO})_{10}(\text{ER}_3)$ 59
1.9	The %NOE observed in $\text{Os}_3(\mu\text{-H})_3(\text{CO})_9(\text{ER}_3)$ 68
1.10	Comparison of the calculated and the observed %NOE in $\text{Os}_3(\mu\text{-H})_3(\text{CO})_9(\text{ER}_3)$ 68
2.1	The IR frequencies of the terminal carbonyls of $\text{Os}_3(\text{CO})_{11}(\text{ER}_3)$ derivatives 114
2.2	^{13}C O chemical shifts of $\text{Os}_3(\text{CO})_{11}(\text{ER}_3)$ at $-53\text{ }^\circ\text{C}$.. 115
2.3	The chemical shift difference between the axial carbonyls of the $\text{Os}(\text{CO})_3(\text{ER}_3)$ group of $\text{Os}_3(\text{CO})_{11}(\text{ER}_3)$ and that in $\text{Os}_3(\text{CO})_{12}$, and the activation energies of the two terminal-bridge CO exchange processes in $\text{Os}_3(\text{CO})_{11}(\text{ER}_3)$ 139
4.1	Selected molecular dimensions for $\text{Os}_3(\mu\text{-H})_2(\text{CO})_9(\text{CNBu}^t)$ (1g) 212
4.2	The observed H-H coupling constants and the dihedral angles in some selected unsaturated triosmium clusters 218

General Introduction

Nuclear magnetic resonance spectroscopy is the most important technique for the study of molecules in solution. New NMR techniques are continually being introduced that provide more and more detail of the solution structure and dynamics of complex molecules. For a review of the application of some of these techniques to the study of organometallic compounds the reader is referred to the review by Mann.¹

The thesis concerns itself with the study of osmium carbonyl clusters by NMR spectroscopy. The first chapter deals with the application of NOE and T_1 measurements to various hydrido-osmium carbonyl clusters in order to provide information on the positions of the hydride ligands in the cluster. (It has often proven difficult to locate hydride ligands in clusters by conventional spectroscopic techniques.) The other three chapters describe investigations of the stereochemical nonrigidity exhibited by various osmium carbonyl clusters as studied by variable temperature ^1H and ^{13}C NMR spectroscopy. Metal carbonyl clusters often exhibit stereochemical nonrigidity on the NMR time scale.¹⁻⁵ The studies reported here are concerned with the elucidation of the probable mechanism of the stereochemical nonrigidity, and the effect the auxiliary ligands on the activation barriers to the nonrigidity in

some of the clusters. The studies were also carried out with the long term goal of ascertaining why one particular exchange mechanism has a low activation barrier whereas another seemingly similar process has a much larger barrier.

CHAPTER 1

Section A Use of the Nuclear Overhauser Enhancement (NOE) Technique in the Characterization of Hydrido-Osmium Clusters

1A.1 Introduction

There are several different arrangements that two hydride ligands can adopt in a triangular Os_3 framework. In Fig. 1.1, eight possible arrangements (A to H) are shown with the estimated internuclear hydride distances in brackets. The distances were estimated either from known cluster compounds in which the positions of the hydrides were located by X-ray or neutron diffraction, or with the HYDEX program.⁶ The HYDEX program predicts the positions of hydride ligands in organometallic compounds from the positions of the non-hydrogen atoms of the molecule as determined by X-ray diffraction.

In an NOE experiment the effect of saturating one NMR resonance on the intensity of the other signals in the spectrum is observed (in the form of a difference spectrum). This chapter is concerned with homonuclear ^1H NOE studies, that is, one signal in the ^1H NMR spectrum of a cluster is saturated and its effect on the intensity of the other signals in the spectrum determined. The maximum enhancement to the other signals that can be observed is 50%. As

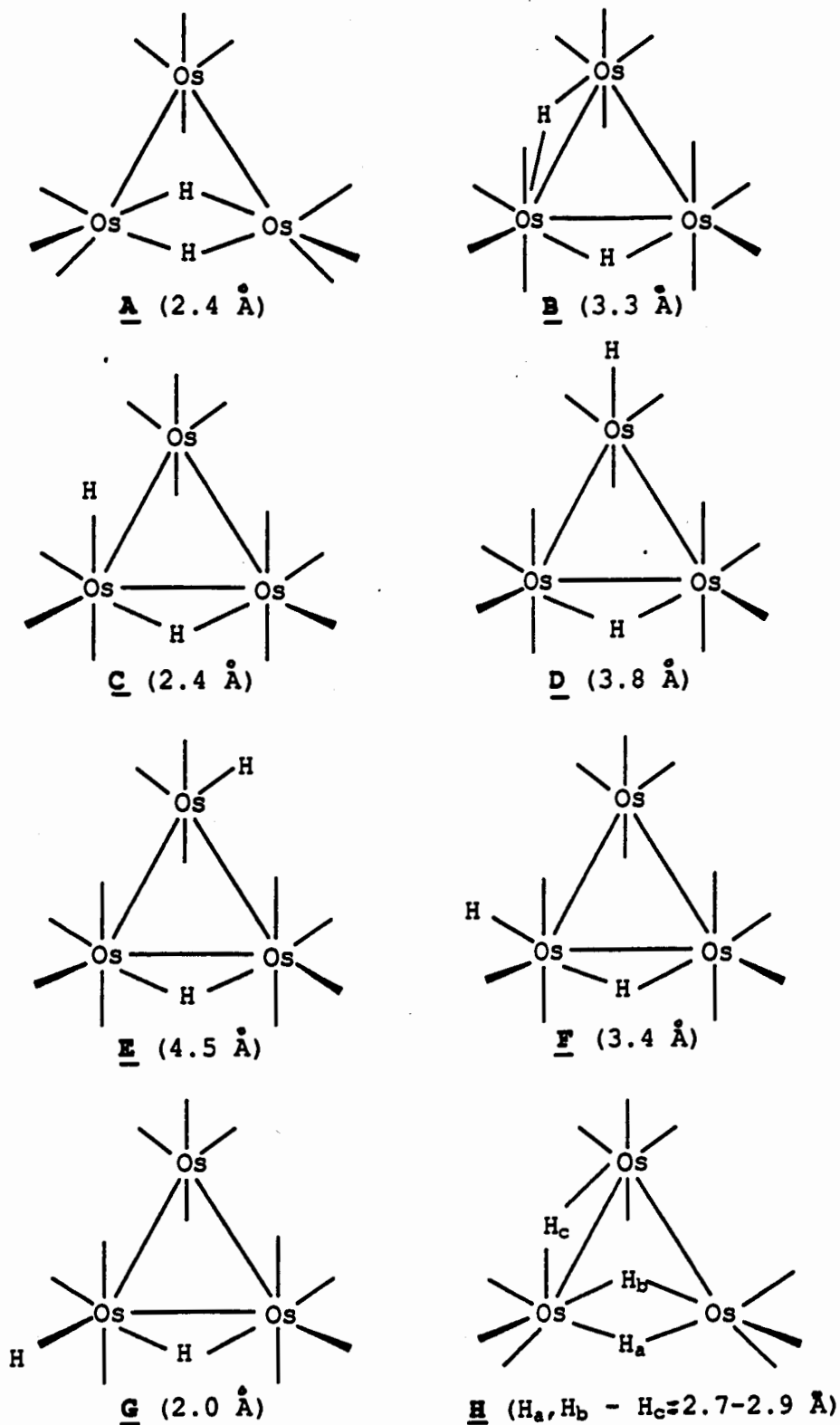


Fig. 1.1 Possible arrangements of hydride ligands in triangular Os_3 clusters. Approximate H...H internuclear distances are given in brackets.

mentioned in Appendix I and in the discussion section, there are several conditions required in order for an NOE to be observed. One of these conditions is the close proximity of the two nuclei in question. Bell and Saunders have reported a study of NOE's observed in a series of organic compounds.⁷ A plot of the percent enhancement (%NOE) versus the reciprocal of the sixth power of the internuclear H...H distance was reported. It was assumed that intramolecular dipole-dipole interaction was the only effective relaxation route in the compounds studied. The plot is shown in Fig. 1.3 (page 20). The plot shows that for an internuclear distance of about 3.0 Å, an enhancement of about 10% is observed. For longer internuclear H...H distances, smaller NOE's (i.e., <10%) are observed. These, however, were subject to a larger uncertainty due to the poor signal-to-noise ratio of the NOE difference spectra.

Based on the internuclear H...H distances in the arrangements **A** to **H** in Fig. 1.1 and the results of Bell and Saunders, the following observations are expected from an NOE experiment for a 2-spin system and if dipole-dipole relaxation is the only relaxation mechanism involved: no enhancement for **D** and **E** because of the large H...H distance; small enhancements for **B** and **F**; medium enhancement for **A** and **C**; and a large enhancement for **G**. The arrangement **H** which should be treated as a 3-spin system was also studied.

Since the internuclear distances of the hydrides in **A** and **C** are similar, to distinguish these two types of hydride arrangements from NOE results alone may not be feasible. However, the chemical shifts of the ^1H NMR resonances of the two hydrides in **C** are expected to be very different because of the different types of bonding of the hydrides to the metal centres (i.e., terminal, Os-H, and bridging, Os(μ -H)Os, hydrides).⁸ Also, hydride signals typically show a ^1H - ^1H coupling of approximately 4 Hz when the nuclei are in this configuration.^{9,10} The chemical shifts of the ^1H NMR resonances of the hydrides in **A** are, on the other hand, usually similar because they are in similar chemical environments. The resonances also exhibit only a small ^1H - ^1H coupling, of approximately 1 Hz (see Chapter 4 of this thesis). Therefore, by using the NOE results in conjunction with the chemical shifts and the coupling data of the hydride resonances, clusters of types **A** and **C** should be readily distinguishable.

Some triosmium clusters of known structure were used in the NOE study and the experimental results with the calculated NOE's were compared. Of the possible arrangements of the hydrides shown in Fig. 1.1, arrangements **D** and **E** have not been observed. The other configurations are known and either exist alone or in combination with other configurations. The eight different types of hydrido-triosmium and -tetraosmium clusters studied in this thesis

are given below:

- Type 1. $\text{Os}_3(\mu\text{-H})_2(\text{CO})_9(\text{CNBu}^t)$ - Green and red isomers
- Type 2. $\text{HOs}_3(\mu\text{-H})(\text{CO})_{10}(\text{L})$ L = CO, CNBu^t , PMe_3 , PPh_3 ,
 $\text{P}(\text{OMe})_3$, AsPh_3 , SbPh_3
- Type 3. $\text{Os}_4(\mu\text{-H})_2(\text{CO})_{13}(\text{PMe}_3)$
- Type 4. $\text{Os}_3(\mu\text{-H})_3(\text{CO})_{10}[\text{Ir}(\text{CO})_2(\text{PPh}_3)]$
- Type 5. $\text{Os}_3(\mu\text{-H})_2(\text{CO})_{10}(\text{L})_2$ L = SiPh_3 , SnPh_3 , SnMe_3
- Type 6. $\text{HOs}_3(\mu\text{-H})_2(\text{CO})_{10}(\text{L})$ L = SiHPh_2 , GePh_3 , SnPh_3
- Type 7. $\text{Os}_3(\mu\text{-H})_3(\text{CO})_9(\text{L})$ L = SiPh_3 , SiHPh_2 , SnPh_3
- Type 8. $\text{Os}_4(\mu\text{-H})_3(\text{CO})_{12}\text{I}$

An NOE study on $\text{Os}_4(\mu\text{-H})(\text{CO})_{14}(\text{SnMe}_3)$ was also carried out and is reported in this chapter.

The structure of at least one cluster of each type has been confirmed by X-ray crystallography, but the positions of the hydrides were, in most cases, not directly located. The position of hydride ligands can, however, often be predicted from ligand orientations and the metal-metal bond lengths in the cluster.¹¹ Calculation of the potential energy of a hydride ligand in a certain position in a cluster may also be used. The position of the hydride ligand is assumed to be that which gives the lowest potential energy of interaction with all the other atoms present in the cluster. This was carried out in the present study with the computer program HYDEX written by Orpen.⁶ In his original study, Orpen used the program to examine over

40 organometallic complexes and clusters where the positions of the hydride ligands had been located either by X-ray crystallography or neutron diffraction techniques. The predicted positions were in excellent agreement with the positions determined in the diffraction investigations. The range of the potential energies of the hydride ligands of two bonding types are shown in Table 1.1.

Table 1.1 Potential energies of the two types of hydrides calculated from the HYDEX program.⁶

Type of Hydride	Site Energies	
	Range	Average
Terminal	2.2 - 7.5	4.8
Edge bridging	0.2 - 10.6	2.76

In order to calculate the potential energies of the hydrides, the atomic coordinates of all the non-hydrogen atoms in the molecule must be known. That is, a crystal structure of the cluster compound must have been determined. The positions of the hydride ligands in the eight types of clusters were calculated with the HYDEX program. From the calculated hydride positions, the H...H internuclear distances were then calculated and are reported in Table 1.2.

	Site Energy			Internuclear H...H Distances (Å)			Other Relevant Internuclear Distances (Å)
	H1	H2	H3	D(H1-H2)	D(H2-H3)	D(H1-H3)	
Type 1 (Green Isomer) (Red Isomer)	0.5 0.2	0.4 0.4	---	2.4 2.4	---	---	D(H1-HMe) = 3.0
Type 2 (L = PPh3)	2.4	2.4	---	2.4	---	---	D(H2-H26) = 2.1
Type 3	2.2	0.9	---	3.0	---	---	D(H1-P) = 2.7 D(H1-Me) = 2.9
Type 4	4.3	3.0	1.6	2.9	4.2	2.9	D(H3-P) = 2.7
Type 5 (L = SnMe3)	2.9	2.5	---	3.3	---	---	D(H1, H2-Me) ≈ 3.1-3.2
Type 6 (L = SiHPh2)	3.7	3.0	1.8	3.4	3.3	2.0	D(H3-HSi) = 2.7
Type 7 (L = SiPh3)	0.5	0.6	2.0	2.5	2.7	3.0	D(H1-H76) = 2.4 D(H3-H62) = 2.4
Type 8	3.9*	3.5	---	3.1	---	---	D(H1-H1a) = 4.2
Os4(μ-H)(CO)14 ⁻ (SnMe3)	2.4	---	---	---	---	---	D(H1-Me) = 3.0

* Same for both H1 and H1a.

Table 1.2 The internuclear distances of the hydride ligands in the eight types of hydride arrangements as calculated from the HYDEX program. The labelling schemes and structures of these clusters are given in the text.

1A.2 Experimental Section

1A.2.1 Preparation of NOE Samples

All the NOE samples were prepared in a dry box under an O₂ free atmosphere. About 2 - 3 mg of the recrystallized cluster compound was dissolved in dichloromethane-d₂ if the NOE study was carried out at -90 °C or above. When a very low temperature was needed for the NOE study (i.e., less than -90 °C), a mixture of CS₂ and CD₂Cl₂ (1:1 ratio) was used as the solvent. The sample was filtered through Celite and then degassed with at least three freeze-pump-thaw cycles, followed by sealing the sample under vacuum. NMR tubes with a Teflon screw-top were used in this study. It was found that these tubes maintained a vacuum throughout a given experiment even with the samples at -100 °C.

1A.2.2 Spectroscopic Details

The NOE experiments were carried out on a Bruker SY100 NMR spectrometer operating at a proton frequency of 100.13 MHz. All NOE experiments were performed with the use of the standard pulse sequence:¹²



The delay times, D1 and D2, are for the complete relaxation of the hydride ligands: D1 was usually set at 2 s and D2 was

set at five times the longest T_1 of the hydride ligand of the cluster under investigation. The irradiation was carried out by the homogated decoupling, HG_1 . The irradiation frequency was set at the resonance frequency of the hydride that was to be saturated. The FID was collected immediately after the irradiation. An NOE spectrum was therefore obtained by the first part of the sequence, $(D1 - HG_1 - D2)_8$, which was repeated eight times. The second part of the sequence, $(D1 - HG_2 - D2)_8$, was used to generate a normal NMR spectrum so that when this spectrum was subtracted from the NOE spectrum an NOE difference spectrum was obtained. The irradiation offset, HG_2 , was set at a remote point in the high frequency region of the spectrum which was away from all other resonances. It is required that the saturation field is turned on at all times in an NOE experiment. Therefore, the irradiation offset, HG_2 , was moved to off-resonance when the NMR intensity was measured. The subtraction of the spectra was done by adding the inverted NOE spectrum to the normal NMR spectrum. (The inversion was carried out with the negate memory command, NM.) The cycle was continued n times until a desired signal-to-noise ratio was obtained for the difference spectrum.

The minimum decoupling power (DP) was used in the saturation of a signal. This varied for different compounds. The optimum power was adjusted by trial and

error until the irradiated signal had just disappeared into the base line. In the cases where the hydride signals were close to each other, the DP was chosen so that only one hydride signal was saturated and the adjacent signal was not affected.

The irradiation frequency for a singlet was chosen at the on-resonance point. In the case of a doublet with a small coupling constant, the irradiation frequency was taken at the mid-point of the two components of the doublet so that the decoupling power was distributed equally. The same offset was chosen for multiplets, i.e., at the mid-point of the multiplet. However, when a doublet with a large coupling constant was to be saturated, two separate saturation pulses on-resonance at each of the two components was used. Use of just one decoupling signal large enough to cover the frequency range of the doublet was undesirable because saturation of other signals would probably occur. The use of two separate pulses was especially useful when another signal was close to this doublet.

In $\text{HOs}_3(\mu\text{-H})(\text{CO})_{10}(\text{PR}_3)$, the ^1H NMR resonance of the bridging hydride exhibits a doublet-of-doublets with a coupling constant of 12 Hz to the phosphorus, and 4 Hz to the terminal hydride. Only one saturation pulse of optimal power was applied at the centre of the multiplet in the NOE experiments on this cluster. The resonance of the terminal hydride is about 1000 Hz away from this multiplet and was

therefore not affected by an irradiation signal of this saturation power.

The subtraction of an NOE spectrum from the normal NMR spectrum often resulted in a difference spectrum with a low signal-to-noise ratio, which in turn resulted in an unreliable integration of the enhancement especially when small enhancements were measured. This problem was minimized by applying a reasonably large line broadening parameter to the signals before the Fourier transform process. An optimum value of line broadening can reduce the noise level of the base line. However, the resolution of the difference spectrum is degraded.

The integrations were obtained electronically on the NMR spectrometer. At least three independent integrations were taken in each experiment. The average NOE value was then used to compare with the enhancement from the Bell and Saunders plot (for 2-spin systems) and the calculated enhancement (for 3 or more spin systems, as reported in Appendix I).

Most of the cluster compounds used in the NOE study undergo hydride exchange. Hydride exchange completely destroys the NOE experiment. Indeed, saturation of one signal due to a hydride ligand undergoing exchange with a second will cause spin saturation transfer to the signal of the second hydride. In other words, the signal due to the second hydride will decrease in intensity rather than

increase as in an NOE situation. The NOE experiments were, therefore, carried out at low temperatures where the exchange processes were completely stopped on the NMR time scale. Most of the NOE experiments were carried out at $-70\text{ }^{\circ}\text{C}$ except for the $\text{HOs}_3(\mu\text{-H})(\text{CO})_{10}(\text{L})$ clusters and $\text{Os}_3(\mu\text{-H})_3(\text{CO})_9[\text{Ir}(\text{CO})_2(\text{PPh}_3)]$ where the NOE studies were carried out at $-100\text{ }^{\circ}\text{C}$. For $\text{Os}_4(\mu\text{-H})(\text{CO})_{14}(\text{SnMe}_3)$, the NOE experiment was carried out at room temperature.

1A.3 Results and Discussion

As mentioned in the Introduction, nuclear Overhauser enhancement is a change of intensity of an NMR signal of a nuclear spin when the NMR signal of another spin is saturated.¹³⁻¹⁷ The nuclear spins return to their equilibrium states through spin-lattice relaxation which requires magnetic field fluctuations at a frequency of the order of the Larmor precession frequency, ω_0 , i.e., $10^8 - 10^9$ Hz. Because the necessary field fluctuations are produced by proton tumbling at a rate $(\tau_c)^{-1}$, spin-lattice relaxation is the most efficient, i.e., at a maximum relaxation rate, R_1 , when $\omega_0\tau_c \approx 1$, or $\tau_c \approx 10^{-8}$ s (where τ_c is the correlation time). Since ω_0 depends on the magnetic field strength, $\omega_0 = |\gamma|H_0$ where γ is the gyromagnetic ratio of the spin, the relaxation rate is field dependent. Figure 1.2 shows the effect of τ_c on proton R_1 at field strengths of 100 and 400 MHz.¹⁷ When τ_c is 10^{-9} s

the maximum relaxation rate, R_1 , is observed. The figure also shows that the relaxation rate at a field strength of 100 MHz is higher than that at 400 MHz. This suggests that better NOE results are obtained at lower field strength (see Appendix I). All the NOE experiments reported in this thesis were therefore carried out with the use of a 100 MHz NMR spectrometer. Some NOE experiments were carried out at an operating frequency of 400 MHz and the results were, indeed, found to be inferior to those obtained at an operating frequency of 100 MHz.

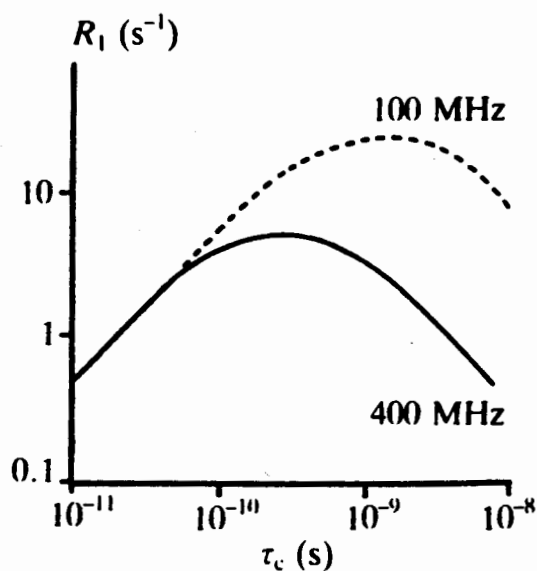


Fig. 1.2 The effect of τ_c on proton R_1 at 100 and 400 MHz.¹⁷

If distance information is to be obtained from NOE measurements, the major relaxation route of the observed

nucleus should be through intramolecular dipole-dipole interaction with the irradiated spin- $\frac{1}{2}$ nucleus. Intermolecular dipole-dipole relaxation is undesirable because it affects the intramolecular NOE which in turn makes the interpretation of the results difficult. Intermolecular dipole-dipole interaction is most effective when high concentrations of nuclei with large magnetic moments are present such as ^1H , ^{31}P and ^{19}F . There are four sources of intermolecular dipole-dipole interactions to be considered. These are interactions of spin- $\frac{1}{2}$ nuclei in the molecule under consideration with other solute molecules, with the solvent, with the lock sample if an internal lock is used, and with paramagnetic impurities.

To reduce the intermolecular dipole-dipole relaxation from other solute molecules, a dilute sample was used.⁷ In this study, 2 - 3 mg of the cluster compound was employed in ≈ 0.5 mL of solvent which corresponds to a concentration of 4 to 6 mM (for a molecular weight of 1000 g mol^{-1}). It was found that this low concentration of sample was adequate to obtain an NOE spectrum with a good signal-to-noise ratio at low temperature within a reasonable period of time.

The best solvents for NOE experiments are those which contain non-magnetic or low-magnetic nuclei such as CS_2 , CCl_4 , and SO_2 etc. Since deuterated solvents can be obtained commercially in high isotopic purity, i.e., less than 1% proton impurities, solvents such as dichloromethane-

d_2 and toluene- d_8 are also adequate. This is because the direct dipole-dipole interaction of a proton from a heteronucleus such as deuterium (spin 1) is small. The relaxation effect due to a deuterium is reduced from that due to a proton, at the same concentration, and is given by:¹³

$$\rho_{IS}^{dd} = \frac{\gamma_I^2 \gamma_S^2 h^2 \tau_c}{r_{IS}^6} S(S+1)$$

$$\frac{\rho_{HD}}{\rho_{HH}} = \frac{\gamma_D^2 1(1+1)}{\gamma_H^2 \frac{1}{2} (\frac{1}{2} + 1)} = \frac{8\gamma_D^2}{3\gamma_H^2}$$

$$= 0.06 \quad (6\%)$$

where I and S are the spin quantum numbers for spins I and S, ρ_{IS}^{dd} is the dipolar relaxation between I and S, r_{IS} is the distance between the spins I and S.

In this NOE study, dichloromethane- d_2 was used as the solvent for the following reasons: it is a low-magnetic solvent; it is available commercially with less than 0.5% proton impurities;^a it serves as a convenient source for the field lock; it has a low viscosity at low temperature so that the correlation time of the solute molecules are not

a. The dichloromethane- d_2 used in the study was purchased from ICN Biomedicals, Inc., Cambridge, MA. It was claimed to have more than 99.5% D-atom.

dramatically decreased at low temperatures (this will be discussed in Appendix I and in Section B where T_1 relaxation times of hydrides are reported); it is also a good solvent for all the cluster compounds investigated even at low temperature. When a very low temperature was needed (i.e., less than -90 °C), a mixture of CS_2 and CD_2Cl_2 (1:1 ratio) was used as the solvent. This mixture gave a homogeneous solution at -100 °C, and it possessed all the advantages mentioned above. (Carbon disulphide was distilled and stored under nitrogen before use.) It should be noted that at low temperatures the tumbling rate of a molecule is slowed down and therefore the relaxation rate decreases. This in turn will lower the observed enhancements (see Appendix I).

Paramagnetic impurities must be strictly eliminated from the NOE samples. Unpaired electrons generate large magnetic moments which interact with the nuclear spins to cause efficient relaxation. The dipole-dipole interaction is related to the square of the gyromagnetic ratios of the two spins involved in the interaction. In this case, the spins are the electron and the proton.¹³⁻¹⁶ The gyromagnetic ratio of an electron is about 1000 times that of a proton, and, therefore, the relaxation of a proton by an unpaired electron is so efficient that any NOE will be totally quenched. The most common paramagnetic species is dissolved oxygen in the sample. The samples were therefore

rigorously degassed and sealed under vacuum for all the NOE experiments.

As mentioned previously, Bell and Saunders have measured the H...H nuclear Overhauser enhancements of two-spin systems in a number of organic molecules.⁷ They assumed that only intramolecular dipole-dipole relaxation was present in the molecules. A linear relationship of %NOE and the inverse of the sixth power of the internuclear H...H distance was found (Fig. 1.3).⁷ This plot can be used to estimate the internuclear H...H distances in other compounds if the experimental conditions and the compounds under consideration are reasonably similar. The experimental conditions include the choice of solvent, the concentration of sample, the lock sample and the sample preparation.

The hydrido-osmium carbonyl clusters studied here are larger than the organic molecules studied by Bell and Saunders. Furthermore, the NOE investigations had to be carried out at low temperature where hydride exchange was negligible on the NMR timescale. Both factors would increase the correlation time of the osmium clusters such that the extreme narrowing condition (Appendix I) may not have applied. This in turn would result in decreased NOE and consequently distance information obtained from such measurements would be erroneous.

In this study the NOE between two chemically different hydride ligands in osmium clusters were measured and

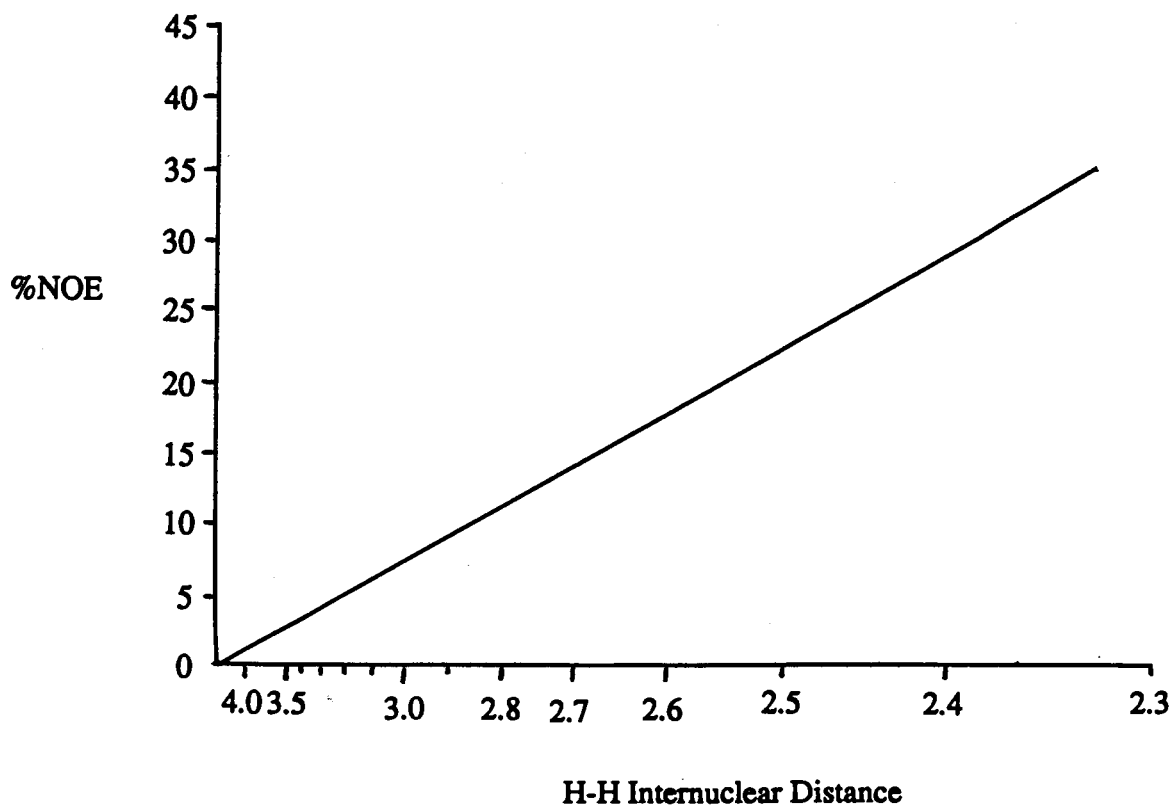


Fig. 1.3 Observed nuclear Overhauser enhancement versus the internuclear H···H distance for 2-spin interaction. (Taken from reference 1)

compared with an H...H internuclear separation estimated from imperical calculations. The results were in turn compared to those of Bell and Saunders.

**Type 1 Compounds: $\text{Os}_3(\mu\text{-H})_2(\text{CO})_9(\text{CNBu}^t)$ - Green and Red
Isomers**

The Green Isomer

The preparation and characterization of this cluster will be discussed in Chapter 4. A ^{13}C NMR study showed that all the carbonyls are rigid at -30°C but at higher temperatures the carbonyls within an individual $\text{Os}(\text{CO})_3$ unit undergo exchange. The ^1H NMR spectrum at room temperature shows two doublets which indicates the hydride ligands are rigid at this temperature. The NOE experiment was, however, carried out at -70°C to be consistent with the other experiments reported below.

The NOE spectrum of the green isomer is shown in Fig. 1.4. In osmium clusters, the signals due to terminal hydrides usually occur between -9 and -15 ppm.⁸ It has been found, however, that the resonances of hydrides of the formally unsaturated $\text{Os}(\mu\text{-H})_2\text{Os}$ linkage also occur in this region, e.g., in $\text{Os}_3(\mu\text{-H})_2(\text{CO})_{10}$ the resonance appears at -11.5 ppm,¹⁸ in $\text{Os}_3(\mu\text{-H})_3(\text{CO})_9(\text{SiPh}_3)$ the signals appear in the region -8 to -13 ppm.¹⁹

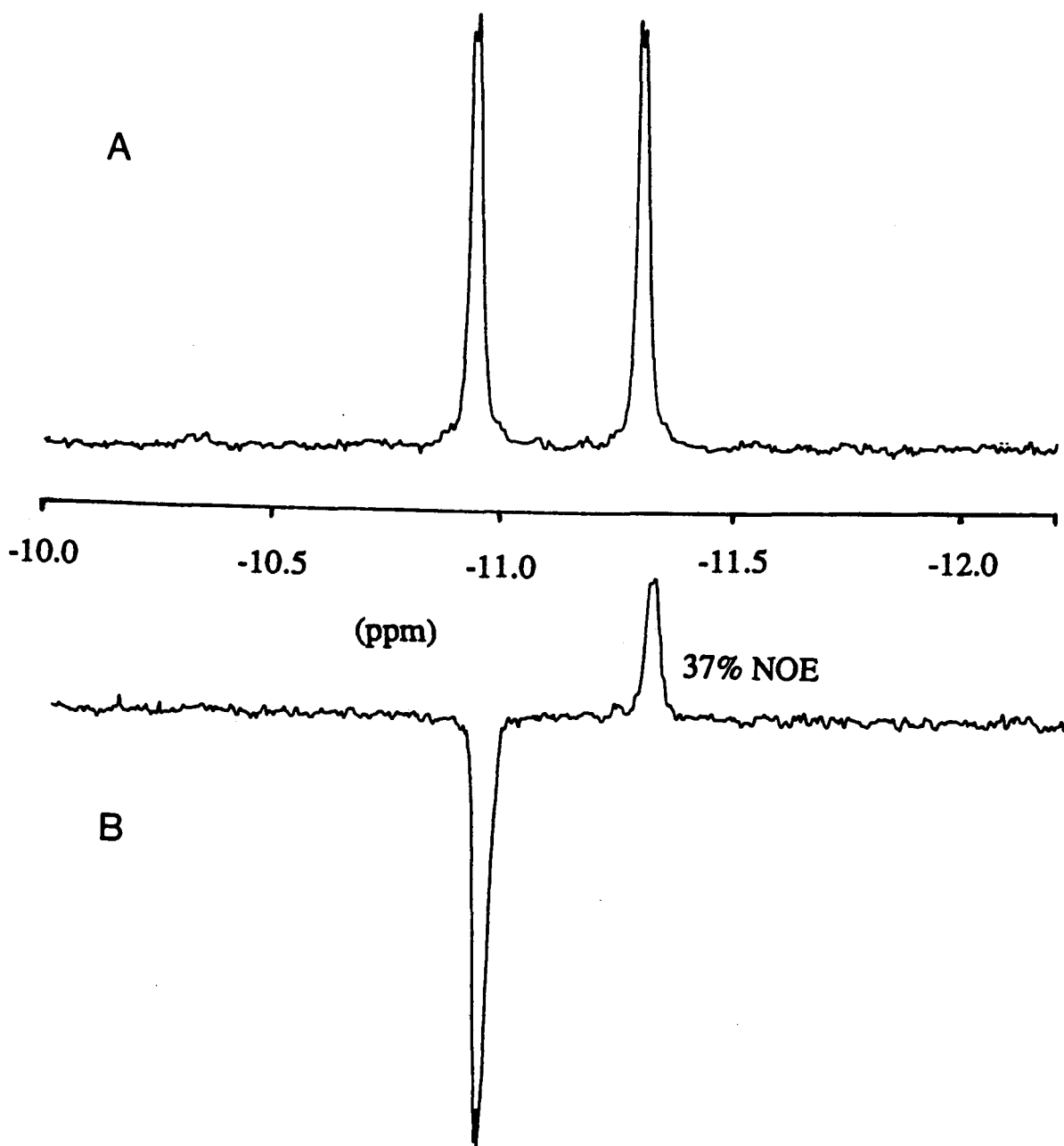


Fig. 1.4 (A) ¹H NMR spectrum of the green isomer of $\text{Os}_3(\mu\text{-H})_2(\text{CO})_9(\text{CNBu}^t)$ in CD_2Cl_2 at -70°C ; (B) The NOE difference spectrum (signal at δ -10.83 was saturated) obtained under the same conditions.

In the green isomer the hydride resonances occur at δ -10.83 and -11.22 with an H-H coupling constant of 1.2 Hz for both signals. When the resonance at δ -10.83 was irradiated, an enhancement of 37% was observed at the other hydride signal. No enhancement was observed at the signal due to the tert-butyl group when either of the hydride signals were irradiated. This probably indicates that the tert-butyl group is remote from the hydride ligands. The NOE may, therefore, be considered as a 2-spin system. The 37% enhancement projects to an H...H distance of 2.3 - 2.4 Å from Fig. 1.3. The observations of the chemical shifts, coupling constants and the NOE result suggest that the hydrides adopt the type A arrangement shown in Fig. 1.1.

The molecular structure of the green isomer is shown in Fig. 1.5.²⁰ The X-ray diffraction study shows a short Os-Os vector (2.680 Å), characteristic of an Os(μ -H)₂Os linkage.^{11,21} The X-ray structure also indicates that the isocyanide group is located in an axial position of the osmium centre which is not associated with the short Os-Os vector. The NMR and NOE results are consistent with this structure.

The closest distance of the methyl hydrogen of the tert-butyl group from the hydride was estimated to be approximately 3 Å. However, the rotation of the CN-C(CH₃)₃ bond lengthens the H...H(Bu^t) distances such that the average distance of a tert-butyl hydrogen to a bridging

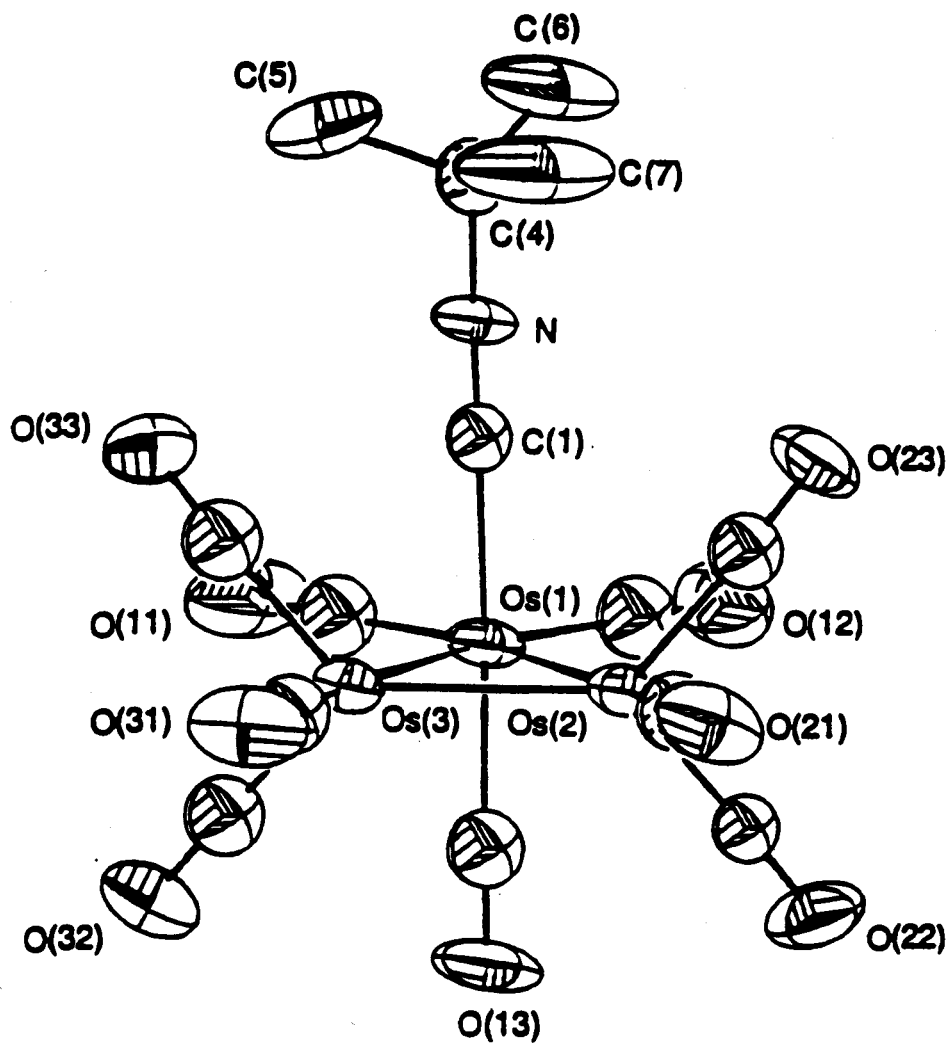


Fig. 1.5 Molecular structure of the green isomer of $\text{Os}_3(\mu\text{-H})_2(\text{CO})_9(\text{CNBut})$.²⁰ Important bond lengths (Å) are as follows: $\text{Os}(1)\text{-Os}(2) = 2.812(1)$; $\text{Os}(1)\text{-Os}(3) = 2.812(1)$; $\text{Os}(2)\text{-Os}(3) = 2.680(1)$.

hydride is approximately 3.5 Å. For this reason, no NOE would be expected at the signal of the butyl-hydrogen when the hydride signals are irradiated.

The Red Isomers

Two red isomers of $\text{Os}_3(\mu\text{-H})_2(\text{CO})_9(\text{CNBu}^t)$ had been previously observed in solution. One of the isomers (isomer b) had been characterized by X-ray crystallography.²² The molecular structure of this isomer is shown in Fig. 1.6. As can be seen from the figure, the isocyanide group adopts the equatorial position on the $\text{Os}(\text{CO})_2(\text{CNBu}^t)$ unit. Like the green isomer, the Os-Os bond length of the $\text{Os}(\mu\text{-H})_2\text{Os}$ grouping is 2.690 (1) Å and is substantially shorter than the other two Os-Os bond lengths of 2.826 (1) Å and 2.827 (1) Å. The hydride ligands were therefore proposed to both bridge the short Os-Os vector for the same reason as given for the green isomer. The two hydrides in this isomer (isomer b) are chemically equivalent and no NOE experiments could therefore be carried out on this compound.

The other isomer (isomer a) is the major isomer in solution and is in equilibrium with isomer b. The ^1H NMR spectrum of isomer a exhibits two resonances at δ -11.28 and -12.71 with an H-H coupling constant of 1.2 Hz, indicating that the two hydride ligands are chemically nonequivalent. This isomer was proposed to have the isocyanide ligand in a pseudoaxial site in the $(\text{OC})_3\text{Os}(\mu\text{-H})_2\text{Os}(\text{CO})_2(\text{CNBu}^t)$ unit as

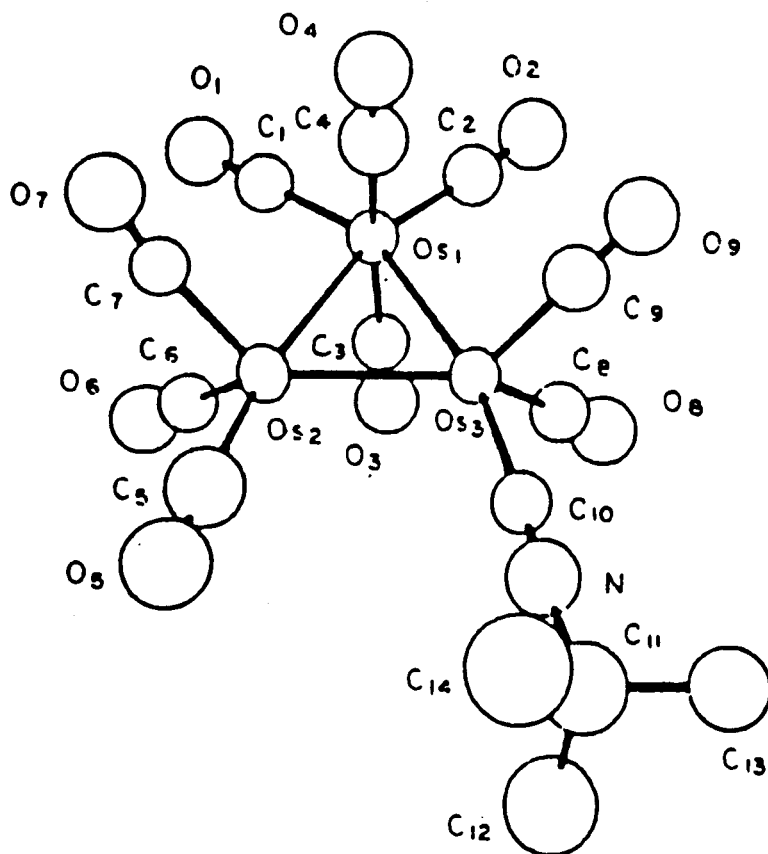


Fig. 1.6 Molecular structure of the red isomer (isomer b) of $\text{Os}_3(\mu\text{-H})_2(\text{CO})_9(\text{CNBut})$.²² Important bond lengths (Å): $\text{Os}(1)\text{-Os}(2) = 2.826(1)$; $\text{Os}(1)\text{-Os}(3) = 2.827(1)$; $\text{Os}(2)\text{-Os}(3) = 2.690(1)$.

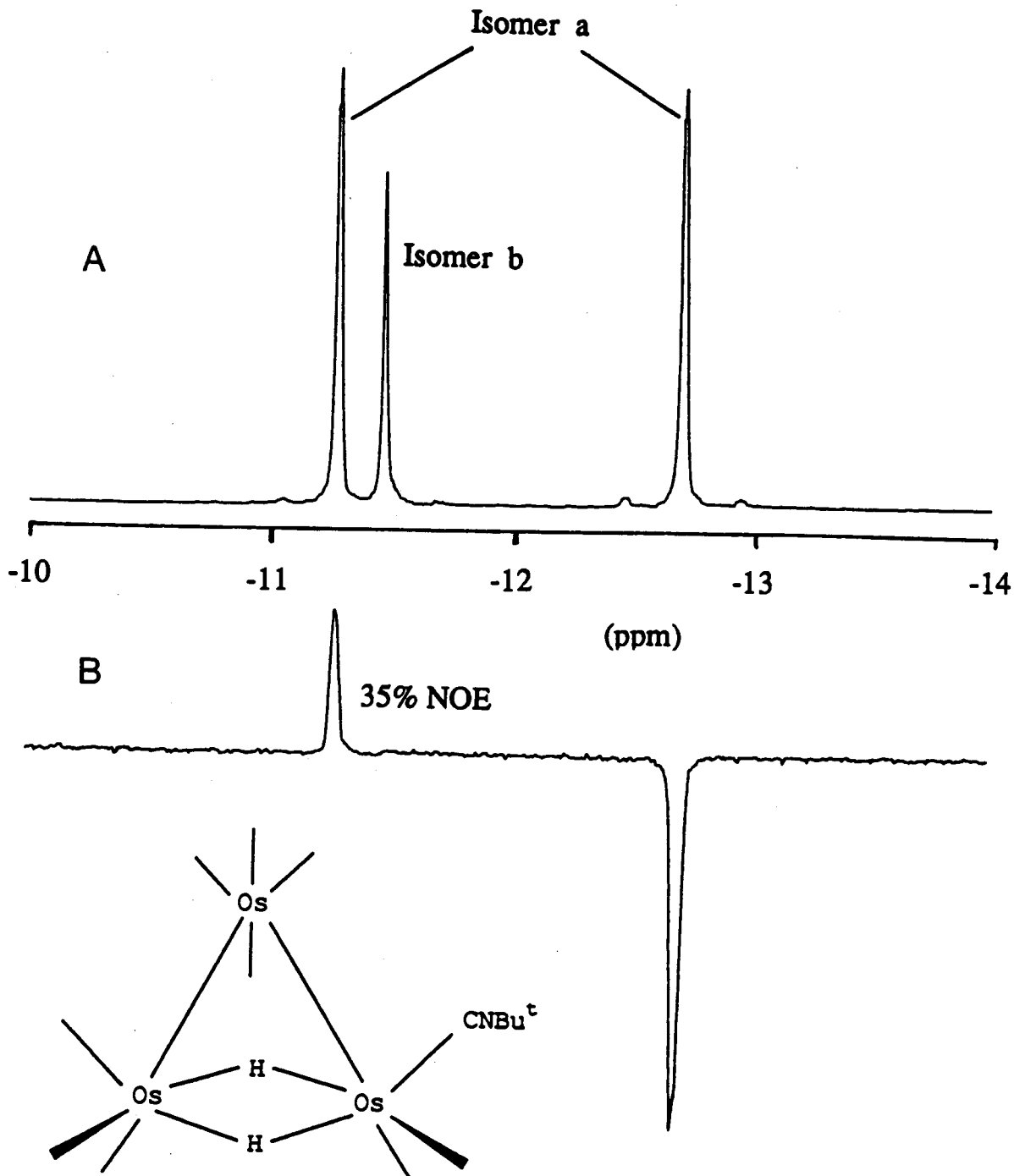


Fig. 1.7 (A) ^1H NMR spectrum (hydride region) of isomers a and b of the red isomers of $\text{Os}_3(\mu\text{-H})_2(\text{CO})_9(\text{CNBu}^t)$ in CD_2Cl_2 at -70°C ; (B) The NOE difference spectrum of isomer a (signal at δ -11.28 was saturated) under the same conditions. (Inset: Proposed structure of isomer a)

shown in the inset of Fig. 1.7. The ^{13}C NMR studies which are discussed in detail in Chapter 4 were also consistent with the CNBu^t ligand in this position.

In the NOE experiment on isomer a, an average enhancement of 35% was observed (Fig. 1.7), i.e., similar to that observed for the green isomer. Once again, enhancement was not observed at the tert-butyl signal which indicates that the tert-butyl group is probably too far from either hydride. A 2-spin system was therefore assumed and the NOE result projects to an $\text{H}\cdots\text{H}$ distance of 2.3 to 2.4 Å.

Type 2 Compounds: $\text{HOs}_3(\mu\text{-H})(\text{CO})_{10}(\text{L})$ ($\text{L} = \text{CO}, \text{CNBu}^t, \text{PPh}_3, \text{PMe}_3, \text{P(OMe)}_3, \text{AsPh}_3, \text{SbPh}_3$)

The $\text{HOs}_3(\mu\text{-H})(\text{CO})_{10}(\text{L})$ clusters can be divided into two groups: the first where the ligand L occupies an axial site ($\text{L}' = \text{CO}, \text{CNBu}^t$), and the second where L is in an equatorial site ($\text{L} = \text{SbPh}_3; \text{AsPh}_3; \text{PR}_3, \text{R} = \text{Me}, \text{OMe}, \text{Ph}$). The structures of the CO ,²³ CNBu^t ²² and PPh_3 ²⁴ derivatives have been determined by X-ray crystallography. The two types of clusters are discussed separately.

(a) $\text{HOs}_3(\mu\text{-H})(\text{CO})_{10}(\text{L}')$ ($\text{L}' = \text{CO}, \text{CNBu}^t$) Clusters

In the structural determinations of these two derivatives by X-ray crystallography the hydrides were not located. The molecular structure of $\text{HOs}_3(\mu\text{-H})(\text{CO})_{10}(\text{CNBu}^t)$

(Fig. 1.8) revealed an empty site at the axial position at Os(2), on the opposite side of the Os₃ plane as the CNBu^t ligand of the Os(CO)₃(CNBu^t) group. The bond length between Os(2) and Os(3) at 3.000 (1) Å is considerably longer than the other Os-Os vectors of 2.876 (1) Å and 2.930 (1) Å in the molecule. It is well-known that the Os-Os bond lengths of Os(μ-H)Os are considerably longer than unbridged Os-Os bonds.²⁴ The positions of the two hydrides can therefore be placed from the molecular geometry and Os-Os bond lengths: a terminal hydride at Os(2) at the empty site, and a bridging hydride across the longer Os(2)-Os(3) vector. A similar structure was found for HOs₃(μ-H)(CO)₁₁.²³ These molecules therefore have a type **C** arrangement of hydride ligands (Fig. 1.1).

Both clusters exhibit similar ¹H NMR spectra at low temperature: one signal in the terminal hydride region (-10 ppm) and one in the bridging hydride region (-20 ppm) as expected from the solid state structures. An H-H coupling constant of 4.0 Hz was observed for each signal. The results of the NOE experiments are shown in Table 1.3. The NOE spectra for HOs₃(μ-H)(CO)₁₀(CNBu^t) are shown in Fig. 1.9. An average enhancement of 39% was observed. The enhancement yields an H...H distance of 2.3 to 2.4 Å from Fig. 1.3 which is in excellent agreement with the estimated distance of 2.36 Å for both molecules from the HYDEX program.

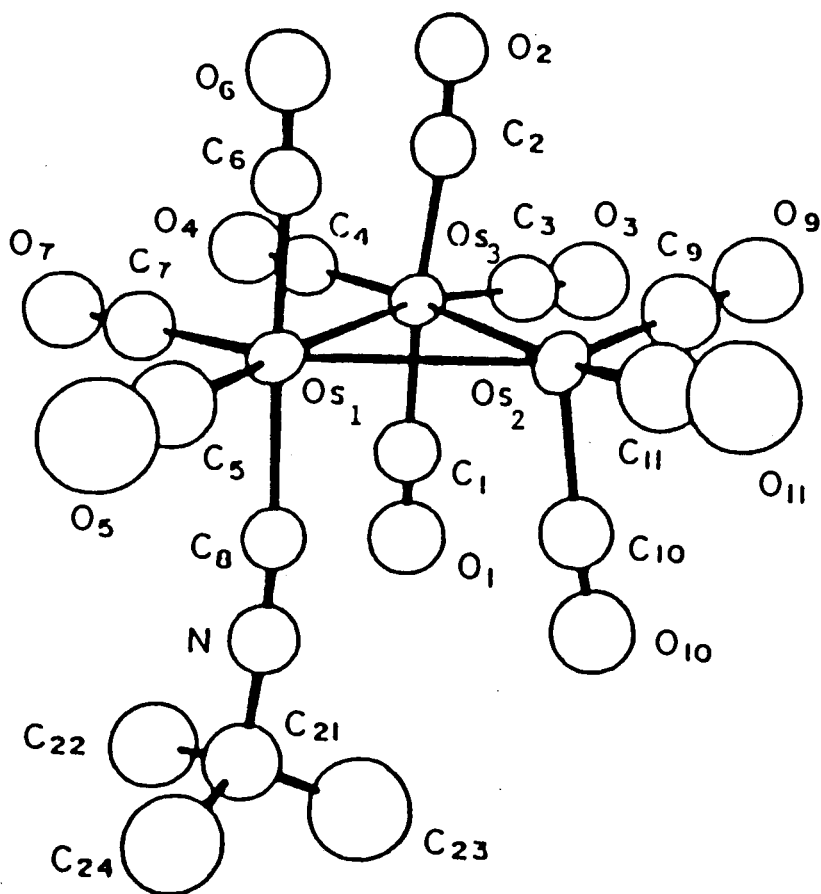


Fig. 1.8 Molecular structure of $\text{HOs}_3(\mu\text{-H})(\text{CO})_{10}(\text{CNBut}) \cdot 22$
 Important bond lengths (Å) are as follows:
 $\text{Os}(1)\text{-Os}(3) = 2.876(1)$; $\text{Os}(1)\text{-Os}(3) = 2.930(1)$;
 $\text{Os}(1)\text{-Os}(2) = 3.000(1)$.

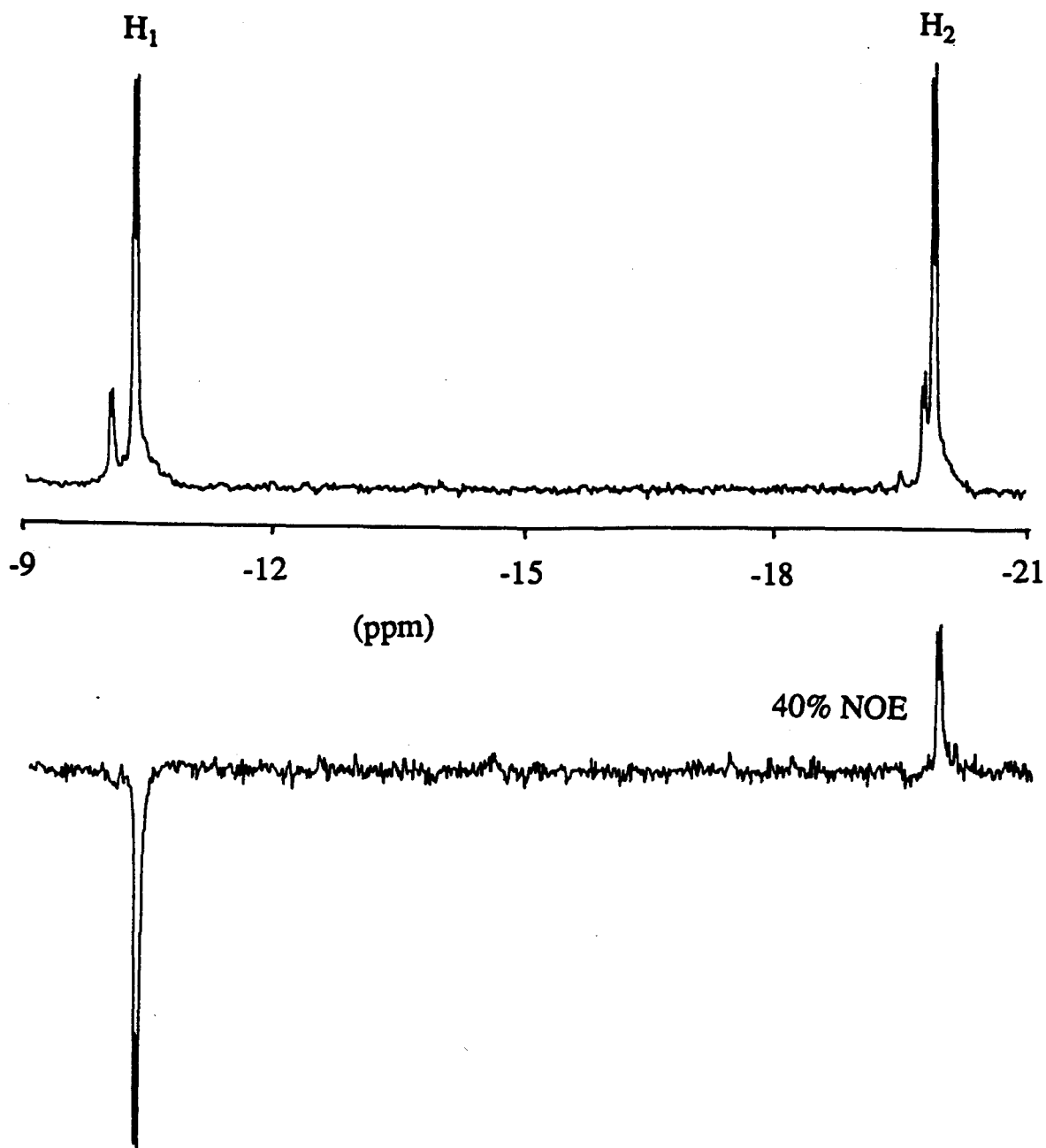


Fig. 1.9 (A) ^1H NMR spectrum of $\text{HOs}_3(\mu\text{-H})(\text{CO})_{10}(\text{CNBu}^t)$ (hydride region) in CD_2Cl_2 at -70°C ; (B) The NOE difference spectrum of $\text{HOs}_3(\mu\text{-H})(\text{CO})_{10}(\text{CNBu}^t)$ (signal at $\delta -10.07$ was irradiated) under the same conditions. The weak signals to the left of each major signal are due to a second isomer of $\text{HOs}_3(\mu\text{-H})(\text{CO})_{10}(\text{CNBu}^t)$.

Table 1.3 The observed %NOE in $\text{HOs}_3(\mu\text{-H})(\text{CO})_{10}(\text{L}')$ ($\text{L}' = \text{CO}, \text{CNBu}^t$).

L'	Observed %NOE	
CO	$f_2(1)^a$	37%
	$f_1(2)$	39%
CNBut	$f_2(1)$	40%

a. $f_2(1)$ = enhancement of spin 2 (i.e., H_2) when spin 1 is saturated (i.e., H_1).

(b) $\text{HOs}_3(\mu\text{-H})(\text{CO})_{10}(\text{L})$ ($\text{L} = \text{PPh}_3, \text{P}(\text{OMe})_3, \text{PMe}_3, \text{SbPh}_3$ and AsPh_3) Clusters

In the structural determination of $\text{HOs}_3(\mu\text{-H})(\text{CO})_{10}(\text{PPh}_3)$ both hydride ligands were located.²⁴ The structure revealed that the terminal hydride, H_1 , is in an axial position on Os(2) with the bridging hydride along the Os(1)-Os(2) vector (Fig. 1.10). The PPh_3 group is in an equatorial position on Os(1) cis to the bridging hydride, H_2 . It is a general observation that bridging hydrides will occupy the positions that are cis to phosphorus donor ligands in metal clusters.²⁵ Such positions are believed to be more electron rich because of the poorer π -acceptor character of the phosphorus ligand compared to CO.²⁶ The $\text{H}_1 \cdots \text{H}_2$ distance is 2.26 Å from the crystallographic data. The solid state structure also revealed that one of the ortho-hydrogen atoms (H_{26}) on a phenyl ring is in close proximity to the bridging hydride, at a distance of 2.06 Å.

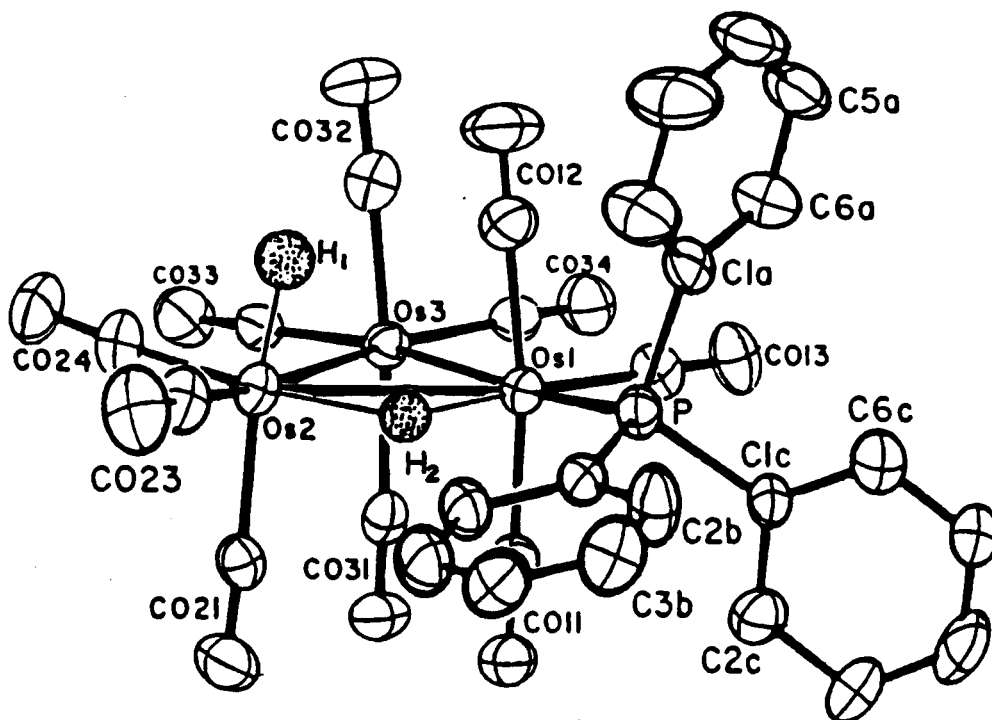


Fig. 1.10 Molecular structure of $\text{HOs}_3(\mu\text{-H})(\text{CO})_{10}(\text{PPh}_3)$.²⁴
 Important bond lengths (Å) are as follows:
 $\text{Os}(1)\text{-Os}(2) = 3.0185$ (6); $\text{Os}(1)\text{-Os}(3) = 2.9170$ (5);
 $\text{Os}(2)\text{-Os}(3) = 2.8645$ (7).

In solution the phenyl rings would rotate and hence any NOE arising from the interaction of this hydrogen with the hydride ligands would be close to zero. The ^{31}P atom of the PPh_3 group has a spin $\frac{1}{2}$ and 100 % natural abundance; it is about 2.98 Å from the bridging hydride H_2 . The phosphorus atom, therefore, should be taken into account in the calculation of the %NOE. The arrangement of the spins involved in the calculation is simplified and shown in Fig. 1.11.

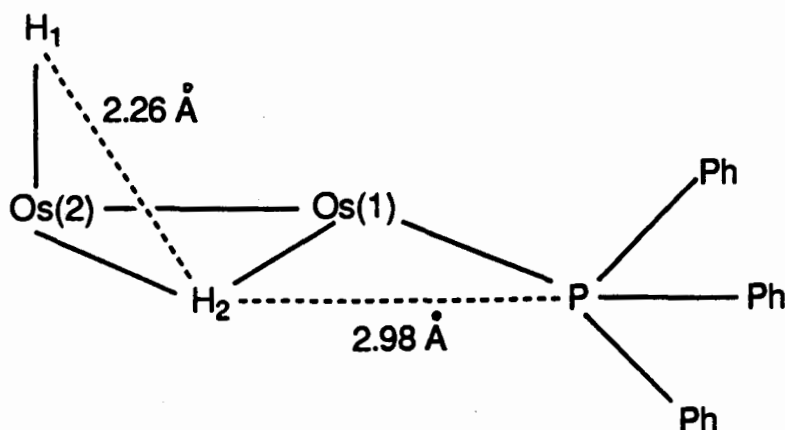


Fig. 1.11 Simplified relative locations of the hydrogen atoms and the calculated internuclear $\text{H}\cdots\text{H}$ and $\text{H}\cdots\text{P}$ distances in $\text{HOs}_3(\mu\text{-H})(\text{CO})_{10}(\text{PPh}_3)$.

The clusters $\text{HOs}_3(\mu\text{-H})(\text{CO})_{10}(\text{PR}_3)$ all exhibit similar ^1H NMR spectra in the hydride region at low temperature: one doublet ($J_{\text{H-H}} = 3.7 - 4.0$ Hz) in the terminal hydride region

and a doublet-of-doublets ($J_{H-H} = 3.7 - 4.0$ Hz, $J_{H-P} = 10.5 - 12.5$ Hz) in the bridging hydride region. For $\text{HOs}_3(\mu\text{-H})(\text{CO})_{10}(\text{EPh}_3)$ ($\text{E} = \text{As}, \text{Sb}$) a doublet was observed in the bridging hydride region. The $\text{HOs}_3(\mu\text{-H})(\text{CO})_{10}(\text{PR}_3)$ molecule was treated as a pseudo 2-spin system by irradiating at the resonance of the bridging hydride H_2 and observing the enhancement at the signal of the terminal hydride H_1 , i.e., $f_1(2)$. There were two reasons for doing this. First, in the enhancement of the signal of the bridging hydride, H_2 , it would appear that it should be considered as part of a 3-spin system due to its close proximity to the phosphorus atom (Fig. 1.11) and the other hydride ligand. Calculation of %NOE for a 3-spin system is complicated (see Appendix I), and the interpretation of the NOE results is, therefore, difficult. Second, due to the couplings of the bridging hydride, H_2 , to both the terminal hydride and the phosphorus atom, the NOE at the doublet-of-doublets is more difficult to measure than at the terminal hydride which shows a doublet in the NMR spectrum (see Appendix I). For these reasons the enhancement at the signal H_2 , when the signal due to H_1 was saturated, was not investigated. The results of the NOE experiments for the $\text{HOs}_3(\mu\text{-H})(\text{CO})_{10}(\text{L})$ clusters are reported in Table 1.4. The NOE spectra of the cluster $\text{HOs}_3(\mu\text{-H})(\text{CO})_{10}(\text{PMe}_3)$ is shown in Fig. 1.12.

For a separation of 2.26 Å in a 2-spin hydride system, the expected enhancement is about 40% from Fig. 1.3.

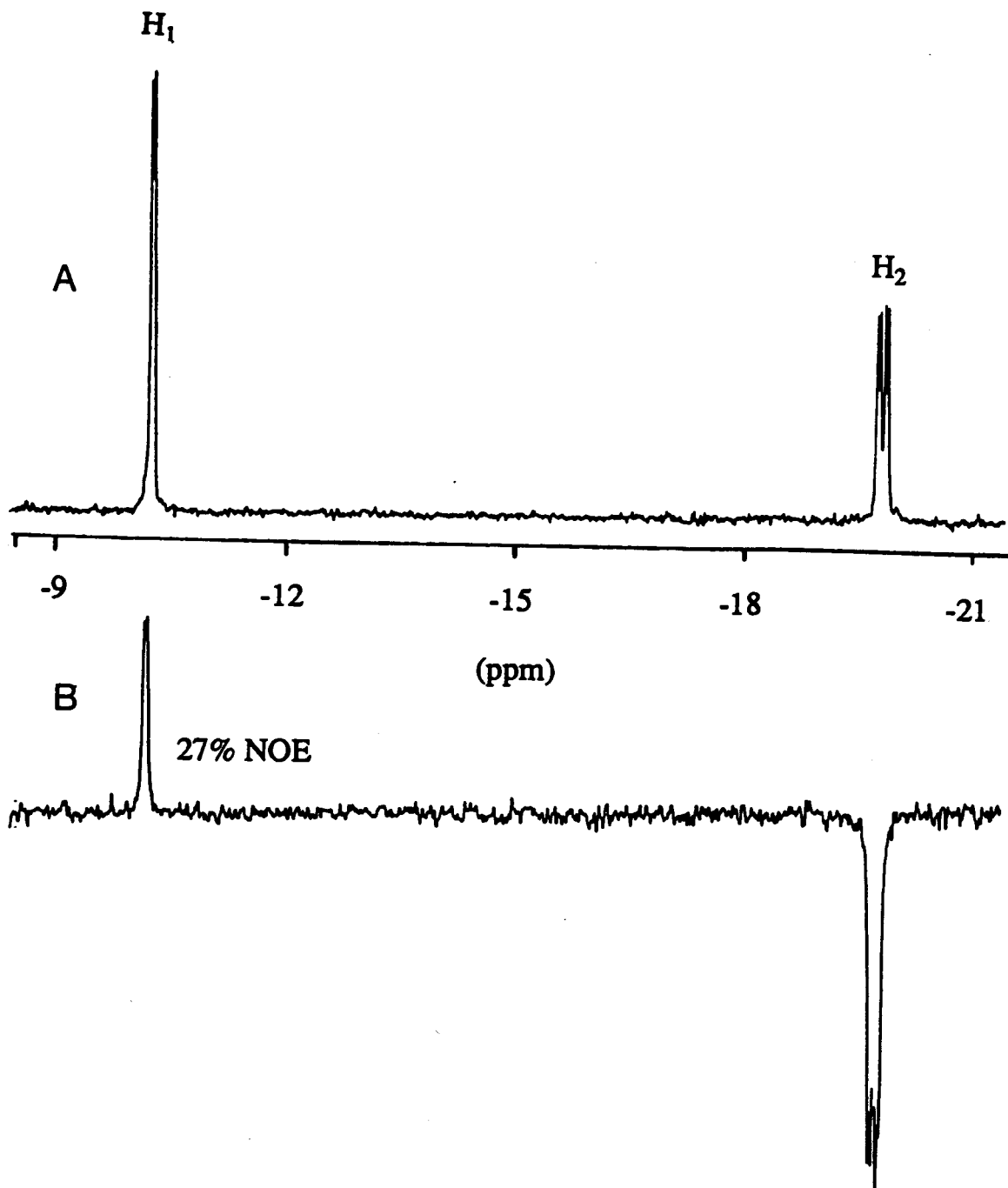


Fig. 1.12 (A) ^1H NMR spectrum of $\text{HO}_3(\mu\text{-H})(\text{CO})_{10}(\text{PMe}_3)$ (hydride region) in $\text{CS}_2/\text{CD}_2\text{Cl}_2$ at -100°C ;
 (B) The NOE difference spectrum of $\text{HO}_3(\mu\text{-H})(\text{CO})_{10}(\text{PMe}_3)$ (signal at $\delta -20.84$ was irradiated) under the same conditions.

However, the observed enhancements in $\text{HOs}_3(\mu\text{-H})(\text{CO})_{10}(\text{L})$ varied from 19 to 33% depending on the ligand L. It would be expected that all the $\text{HOs}_3(\mu\text{-H})(\text{CO})_{10}(\text{L})$ clusters would exhibit similar NOE's because of their similar structures. The discrepancy of the results were attributed to slow hydride exchange in these clusters even at -100°C . When the NOE experiment on $\text{HOs}_3(\mu\text{-H})(\text{CO})_{10}(\text{PMe}_3)$ was carried out at -70°C , a large negative enhancement was observed. This indicates that H-H exchange is still significant at -70°C . As mentioned previously, a negative signal results when there is spin saturation transfer from the irradiated spin to the spin with which it exchanges. The NOE results in Table 1.4 were for experiments carried out at -100°C . If the exchange was still not completely stopped at this temperature, the NOE's would be decreased somewhat.

Table 1.4 The observed %NOE for $\text{HOs}_3(\mu\text{-H})(\text{CO})_{10}(\text{L})$ at -100°C . (The bridging hydride was irradiated.)

L	Observed %NOE, $f_1(2)$
$\text{P}(\text{OMe})_3$	33%
PPh_3	27%
PMe_3	27%
AsPh_3	21%
SbPh_3	19%

The H-H exchange process is thought to involve the two hydride ligands and two carbonyls of the $\text{HO}(\text{CO})_3$ unit. The barrier to this exchange, ΔG^\ddagger , depends on the steric and

electronic properties of the ligand L.²⁷ The ΔG^\ddagger values for a given L are shown in Table 1.5. It shows that the PMe_3 , AsPh_3 and SbPh_3 derivatives have the lowest exchange barriers and, accordingly, the enhancements observed in these derivatives were lower than expected.

The general lower enhancements (compared to the CO and CNBu^t derivatives) might be attributed to the larger size of the clusters and also experimental uncertainties. Larger clusters will have a longer τ_c especially at low temperatures which will result in low spectral density, $J(\omega)$, and, in turn, will reduce the NOE (Appendix I). Experimental uncertainties include the presence of relaxation mechanisms other than dipole-dipole interactions; instability of the NMR spectrometer; subtractions of the NOE spectra from the original NMR spectra which may result in low signal-to-noise ratio in the NOE difference spectra which, in turn, will give inaccurate intensity measurements. Another reason for the low observed enhancement might simply be the difficulty in measuring NOE's in the complicated multiplet structure of the spin system in the clusters, especially the clusters containing phosphorus. Proper calculation of %NOE should involve the direct dipole-dipole interaction of all spins, e.g., the interaction of the hydrides with the phosphorus atom (and perhaps the hydrogen atoms of the phenyl rings and the methyl groups). The presence of these other relaxation interactions at the

Table 1.5 The observed barrier of ligand exchange in $\text{HOs}_3(\mu\text{-H})(\text{CO})_{10}(\text{L})$ and $\text{HOs}_3(\mu\text{-H})(\text{CO})_{10}(\text{L}')$, ΔG^\ddagger ,²⁷ and the %NOE observed in this study. T(K) is the temperature where ΔG^\ddagger was measured.

L	ΔG^\ddagger (kcal mol ⁻¹)	T(K)	% NOE
CO	12.9	240	38%
CNBut	12.8	259	40%
PPh ₃	12.5	236	27%
PMe ₃	11.3	216	27%
P(OMe) ₃	12.3	241	33%
AsPh ₃	11.9	224	21%
SbPh ₃	11.5	225	19%

observed hydride may also result in lower enhancement (see Appendix I).

Type 3 Compound: $\text{Os}_4(\mu\text{-H})_2(\text{CO})_{13}(\text{PMe}_3)$

The X-ray crystal structure of $\text{Os}_4(\mu\text{-H})_2(\text{CO})_{13}(\text{PMe}_3)$ is shown in Fig. 1.13.²⁸ The ¹H NMR spectrum at room temperature exhibits two resonances in the bridging hydride region: an unresolved doublet at δ -18.3 and a doublet-of-doublets at δ -20.4 ($J_{\text{H-H}} = 1.2$ Hz, $J_{\text{H-P}} = 10.2$ Hz). The H-P coupling constant of 10.2 Hz is consistent with a cis arrangement of the hydride giving rise to this signal and the PMe₃ ligand, i.e., the hydride, H₁, bridges the Os(2)-Os(3) vector. The long Os(2)-Os(3) bond length (3.115 Å) is consistent with a single hydride bridging this vector.^{11,21} By the same argument the second hydride ligand (H₂) might be expected to bridge the Os(1)-Os(4) bond which is the second

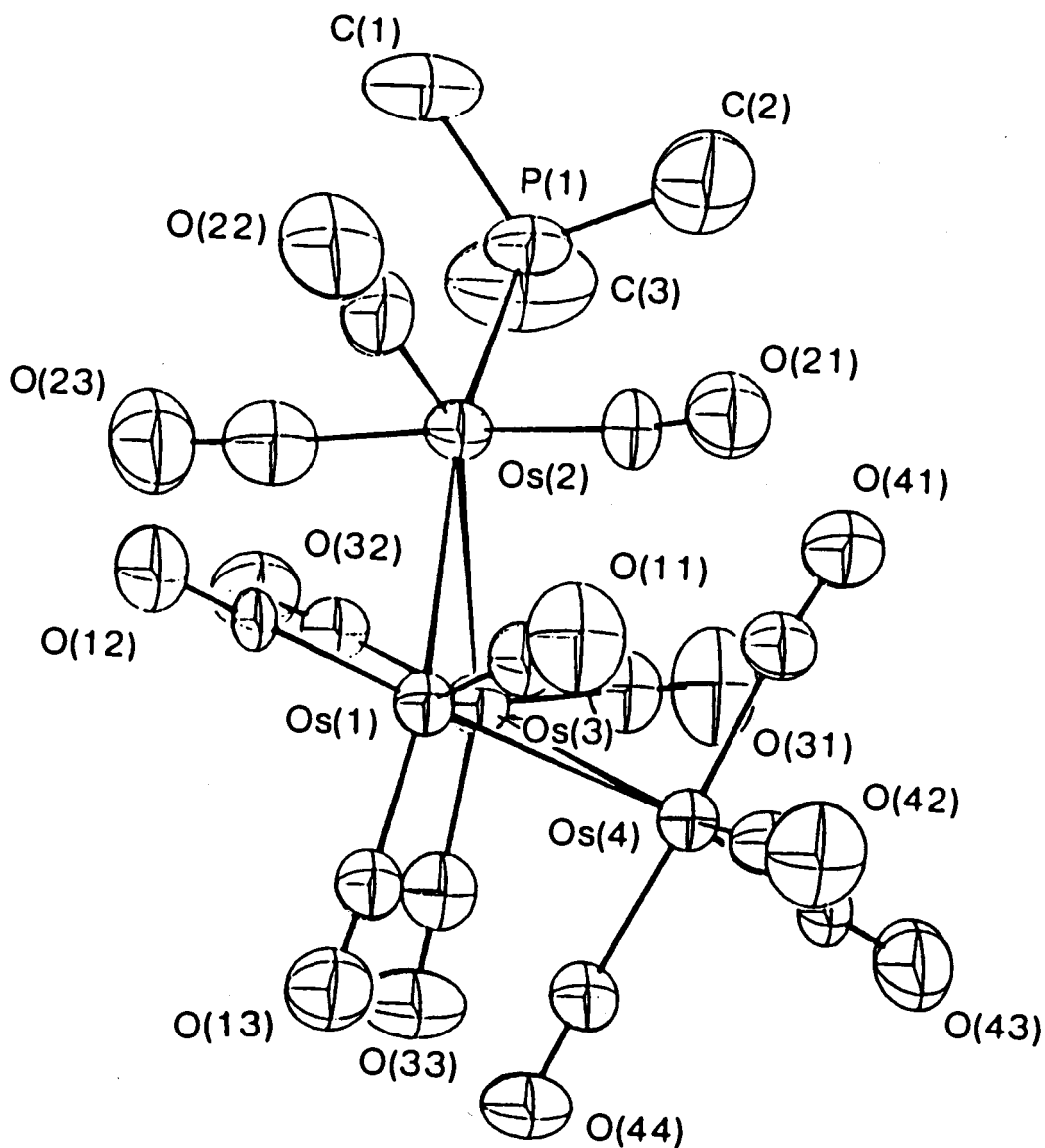


Fig. 1.13 Molecular structure of $\text{Os}_4(\mu\text{-H})_2(\text{CO})_{13}(\text{PMe}_3)\cdot 28$
 Important bond lengths (Å): $\text{Os}(1)\text{-Os}(2) = 2.868(1)$;
 $\text{Os}(1)\text{-Os}(3) = 2.886(1)$; $\text{Os}(1)\text{-Os}(4) = 2.939(1)$;
 $\text{Os}(2)\text{-Os}(3) = 3.115(1)$; $\text{Os}(3)\text{-Os}(4) = 2.850(1)$.
 The hydride ligands are believed to bridge at the
 $\text{Os}(1)\text{-Os}(3)$ and the $\text{Os}(2)\text{-Os}(3)$ vectors.

longest Os-Os vector (2.939 Å) in the structure. The H-H coupling of 1.2 Hz between the two hydride ligands was believed to exclude this possibility (no coupling would be expected if the second hydride ligand bridged Os(1)-Os(4)). Martin et al. presented evidence that H₂ bridges the hinge bond, Os(1)-Os(3), even though this bond is relatively short (2.886 (1) Å).

A HYDEX calculation was carried out for this molecule. It also favored the position of H₂ at the hinge of the butterfly structure with a calculated potential energy of 0.9 (see Table 1.1); the calculated potential energy for H₂ bridging Os(1)-Os(4) was 9.6. In the static structure the bridging hydride H₁ is closer to the phosphorus atom and one of the methyl hydrogens than to the hydride H₂. The closest calculated distances of H₁···P and H₁···a methyl hydrogen are about 2.66 Å and 2.94 Å, respectively, while the H₁···H₂ distance is about 2.98 Å as estimated by the HYDEX program (Table 1.2). The average distance of H₁ and a methyl hydrogen when the PMe₃ group is rotating about the Os(2)-P bond is, however, about 4.5 Å.

The NOE experiments were carried out at -70 °C and are shown in Fig. 1.14. The small H-H coupling observed in the spectrum at room temperature was not resolved at -70 °C. The results from the NOE experiments and the hydride distances, estimated from Fig. 1.3, are summarized in Table 1.6. The distance between H₂ and the phosphorus atom

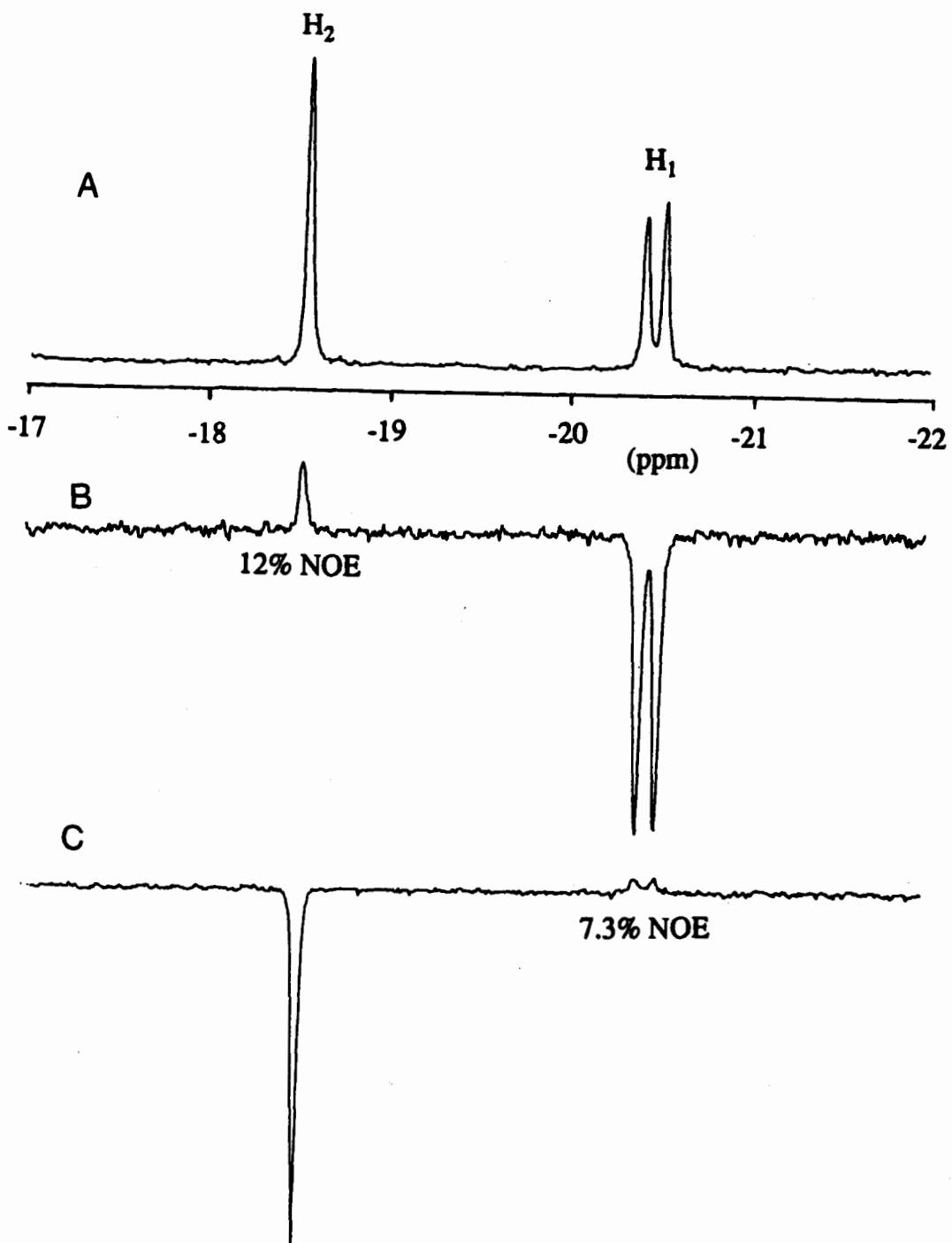


Fig. 1.14 (A) ^1H NMR spectrum of $\text{Os}_4(\mu\text{-H})_2(\text{CO})_{13}(\text{PMe}_3)$ (hydride region) in CD_2Cl_2 at -70°C ; (B) The NOE difference spectrum when the resonance at $\delta -20.4$ and (C) at $\delta -18.3$ were saturated under the same conditions.

Table 1.6 The observed %NOE and the H...H distances, as estimated from Fig 1.3, in $\text{Os}_4(\mu\text{-H})_2(\text{CO})_{13}(\text{PMe}_3)$.

	Observed %NOE	Internuclear H...H Distance ^a
$f_1(2)$	7.3%	3.0 - 3.1 Å
$f_2(1)$	12%	2.7 - 2.8 Å

a. a 2-spin system was assumed.

is long compared to those of $\text{H}_1\cdots\text{H}_2$ and $\text{H}_1\cdots\text{P}$. The direct dipole-dipole interaction of a proton to a ^{31}P nucleus (i.e., $\rho_{\text{H-P}}$) is about 16% (by a similar calculation as that shown on p 17) of that between two protons at the same internuclear distance and concentration. It is believed that the long distance and the small dipole-dipole interaction of $\text{H}_2\cdots\text{P}$ result in a negligible direct dipolar interaction of $\text{H}_2\cdots\text{P}$ in $\text{Os}_4(\mu\text{-H})_2(\text{CO})_{13}(\text{PMe}_3)$. The approximation that this molecule could be treated as a 2-spin system for $f_2(1)$, therefore, appeared justified.

The result of $f_2(1)$ is probably more reliable for reasons mentioned above and in the discussion for the $\text{HOs}_3(\mu\text{-H})(\text{CO})_{10}(\text{PR}_3)$ clusters, i.e., H(2) only undergoes strong dipole-dipole interaction with H(1) and is therefore part of a 2-spin system. The H...H internuclear distance of 2.7 - 2.8 Å supports the view that the hydride H_2 bridges the hinged Os(1)-Os(3) vector.

A similar NOE would be expected if H₂ bridged the Os(1)-Os(2) vector, i.e., trans to the phosphine ligand. However, H₂ should then exhibit a large coupling to the phosphorus atom which was not observed in the ¹H NMR spectrum. In conclusion, the NOE experiment has given strong evidence that H₂ is located along the hinge bond in this cluster and illustrates the usefulness of the technique for the location of hydrides in cluster compounds.

Type 4 Compound: Os₃(μ-H)₃(CO)₉[Ir(CO)₂(PPh₃)]

The molecular structure of this mixed metal cluster compound is shown in Fig. 1.15.²⁹ The Ir(CO)₂(PPh₃) moiety caps the Os₃ triangular fragment to give a distorted tetrahedral metal framework. The hydride ligands were not directly located but were proposed to be bridged at the three longest metal-metal vectors in the cluster: Os(3)-Ir (2.917 (3) Å), Os(2)-Os(3) (2.934 (3) Å) and Os(1)-Os(2) (2.925 (3) Å). It was reported that broad ¹H signals due to hydride exchange were obtained even at -50 °C;²⁹ the NOE experiments were therefore carried out at -100 °C to ensure that the hydride exchange processes were stopped.

Two isomers in a ratio of 3:1 were detected from the ¹H NMR spectrum. The minor isomer had not been reported in the original study. Three hydride resonances were observed in the bridging hydride region at -100 °C for each isomer: the major isomer shows resonances at δ -18.18 (d, J_{H-p} =

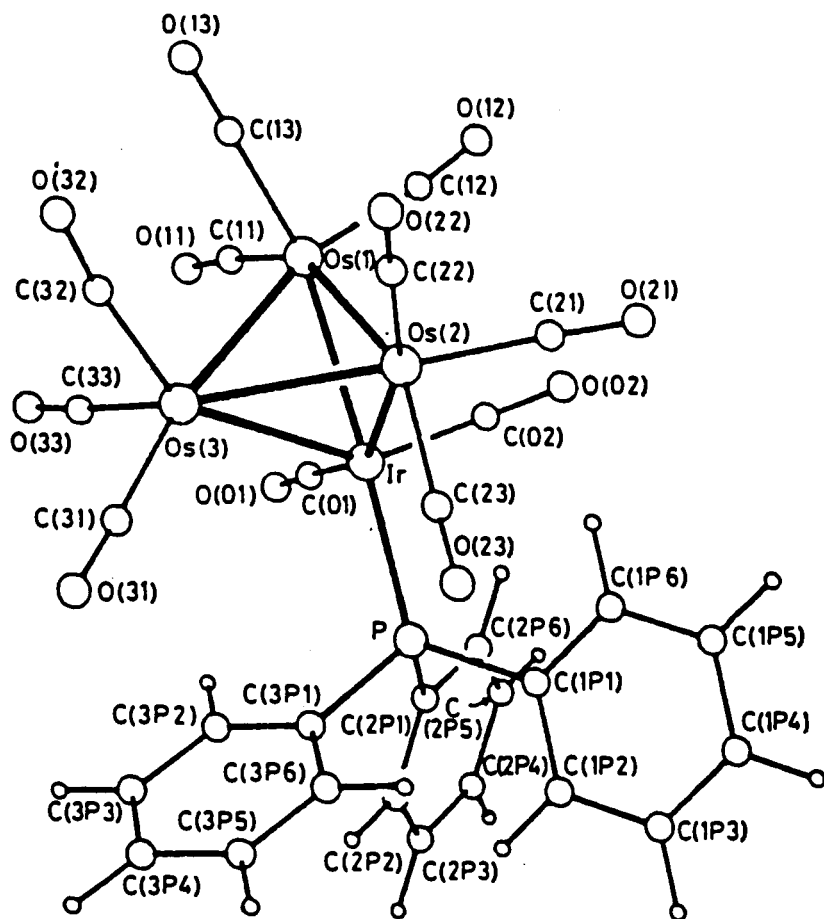


Fig. 1.15 Molecular structure of $\text{Os}_3(\mu\text{-H})_3(\text{CO})_9\text{-}[\text{Ir}(\text{CO})_2(\text{PPh}_3)]$.²⁹ Important bond lengths (Å) are: $\text{Os}(1)\text{-Ir} = 2.759(3)$; $\text{Os}(2)\text{-Ir} = 2.789(2)$; $\text{Os}(3)\text{-Ir} = 2.917(3)$; $\text{Os}(1)\text{-Os}(2) = 2.925(3)$; $\text{Os}(1)\text{-Os}(3) = 2.787(3)$; $\text{Os}(2)\text{-Os}(3) = 2.934(3)$.

11.3 Hz), -19.96 (s) and -20.89 (s); the minor isomer shows resonances at δ -19.27 (d, $J_{H-P} = 7.9$ Hz), -19.76 (br s), -20.37 (br s). The broad signals of the minor isomer suggested that hydride exchange was still taking place in this molecule which would nullify any NOE. Only the major isomer was, therefore, investigated by the NOE technique. The NOE spectra are shown in Fig. 1.16 and the results reported in Table 1.7.

Table 1.7 The results obtained in the NOE experiments of $Os_3(\mu-H)_3(CO)_9[Ir(CO)_2(PPh_3)]$.

signal irradiated (δ ppm)	observed %NOE		
	H ₁	H ₂	H ₃
H ₁ (-20.89)	--	8.7	6.0
H ₂ (-19.96)	6.0	--	0.0
H ₃ (-18.18)	7.7	0.0	--

The H-P coupling constant of 11.3 Hz exhibited by the 1H NMR resonance at δ -18.18 is consistent with a bridging hydride in a cis arrangement to the PPh₃ ligand, i.e., H₃ bridges the Ir-Os(3) bond in Fig. 1.15. This is consistent with the view mentioned previously that hydrides usually bridge metal-metal bonds that are cis to phosphorus ligands. When the resonance of H₃ was saturated, only the signal at δ -20.89 exhibited an enhancement, of 7.7%. When the signal at δ -20.89 was irradiated, enhancement was observed at the other two hydride signals (Table 1.7). If 2-spin systems

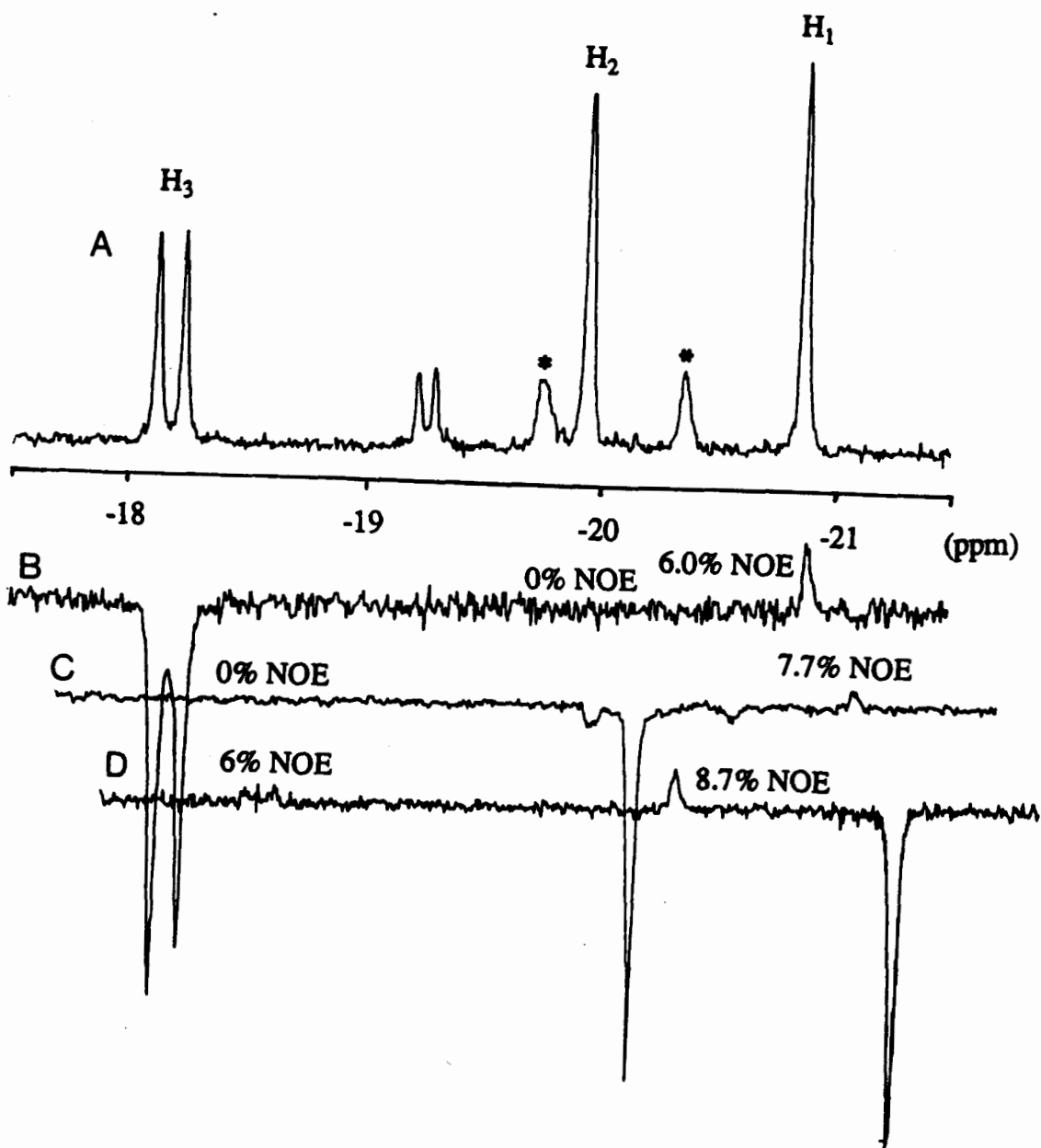


Fig. 1.16 (A) ^1H NMR spectrum of $\text{Os}_3(\mu\text{-H})_3(\text{CO})_9\text{-}[\text{Ir}(\text{CO})_2(\text{PPh}_3)]$ (hydride region) in CD_2Cl_2 at $-100\text{ }^\circ\text{C}$; the NOE difference spectrum where the signal at $\delta -18.18$ (B); at $\delta -19.96$ (C); and at $\delta -20.89$ (D) were saturated under the same conditions. (Signals marked with an asterisk are due to second isomer.)

are assumed, the results imply that hydride H₃ is close to hydride H₁ but not to H₂, and that hydride H₁ is close to both the other hydrides. The enhancement of 7.7% gives an internuclear H...H distance of 2.9 - 3.0 Å from Fig. 1.3. The hydride H₁ is therefore thought to bridge either the Os(1)-Os(3) or the Os(2)-Os(3) vectors because only at these positions would the resonance of H₁ exhibit an NOE effect. An unambiguous location of H₁ cannot be assigned based on the NOE results alone, however, H₁ probably bridges the Os(2)-Os(3) vector since it has a long bond length. A similar enhancement would be observed if hydride H₁ bridged the Ir-Os(1) or Ir-Os(2) vectors. These possibilities, however, are excluded because hydrides located at these positions would be expected to give ¹H NMR resonances that exhibit a large hydrogen-phosphorus coupling due to the trans arrangement of the hydride with the PPh₃ ligand, and this was not observed. The positions of the hydrides deduced from the results of the NOE experiments are consistent with those calculated with HYDEX program.

The hydride H₂ can be unambiguously located as along the Os(1)-Os(2) bond based on the observed NOE's when H₁ and H₃ were, in turn, saturated. The relative positions of the hydrides H₁ and H₂ are similar to that found in Os₃(μ-H)₂(CO)₁₀(ER₃)₂ clusters, which will be discussed in the next section. The enhancement observed in both cases fall in the same range of 6 - 9% which corresponds to a distance of

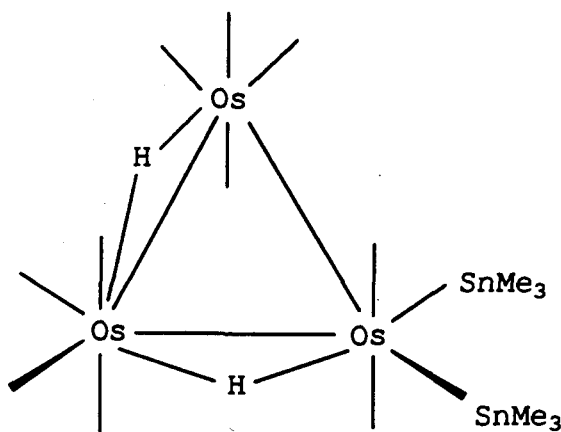
about 3 Å.

In the NOE difference spectrum where the signal of H₂ was saturated, i.e., spectrum (C) of Fig. 1.16, negative signals were observed at δ -19.76 and -20.37 of the minor isomer of Os₃(μ-H)₃(CO)₉[Ir(CO)₂(PPh₃)]. Due to the closeness of the signal of H₂ and that at δ -19.76, the latter was probably also saturated during the experiment. It is believed that spin saturation transfer then occurred from the signal at δ -19.76 to the signal at δ -20.37 of the minor isomer. Moreover, if the two isomers exchange at -100 °C, the doublet of the minor isomer should be broadened at the same rate as the other two signals. The sharp doublet observed at -100 °C, therefore, indicates that the two isomers do not exchange. Further evidence, that there is no exchange between the two isomers at -100 °C is that in the spectrum at -70 °C the signals due to the major isomer were still sharp. Almost certainly had there been exchange at the lower temperature then the signals in the spectrum at -70 °C would have shown significant broadening.

Type 5 Compounds: Os₃(μ-H)₂(CO)₁₀(ER₃)₂ (ER₃ = SnMe₃, SnPh₃, SiPh₃)

For Os₃(μ-H)₂(CO)₁₀(SnMe₃)₂, the ¹H NMR data indicates that there are two isomers in solution. One of the isomers (isomer a) has been characterized by X-ray crystallography. The hydrides were not located in the study, but are believed

to be bridge the two long Os-Os vectors (Fig. 1.17).³⁰ The second isomer (isomer b) only exists in solution and its structure is unknown. It has been proposed, however, that the two SnMe₃ groups of isomer b are probably located on one osmium centre that is also associated with one of the bridging hydrides as shown in Fig. 1.18.³⁰ In the proposed structure the individual osmium atoms do not have 18-electron configurations although the cluster itself is electron precise. This situation has been observed before in clusters of this type and, indeed, isomer a is such an example.



Carbonyls are omitted for clarity.

Fig. 1.18 The proposed structure of the isomer b of $\text{Os}_3(\mu\text{-H})_2(\text{CO})_{10}(\text{SnMe}_3)_2$.³⁰

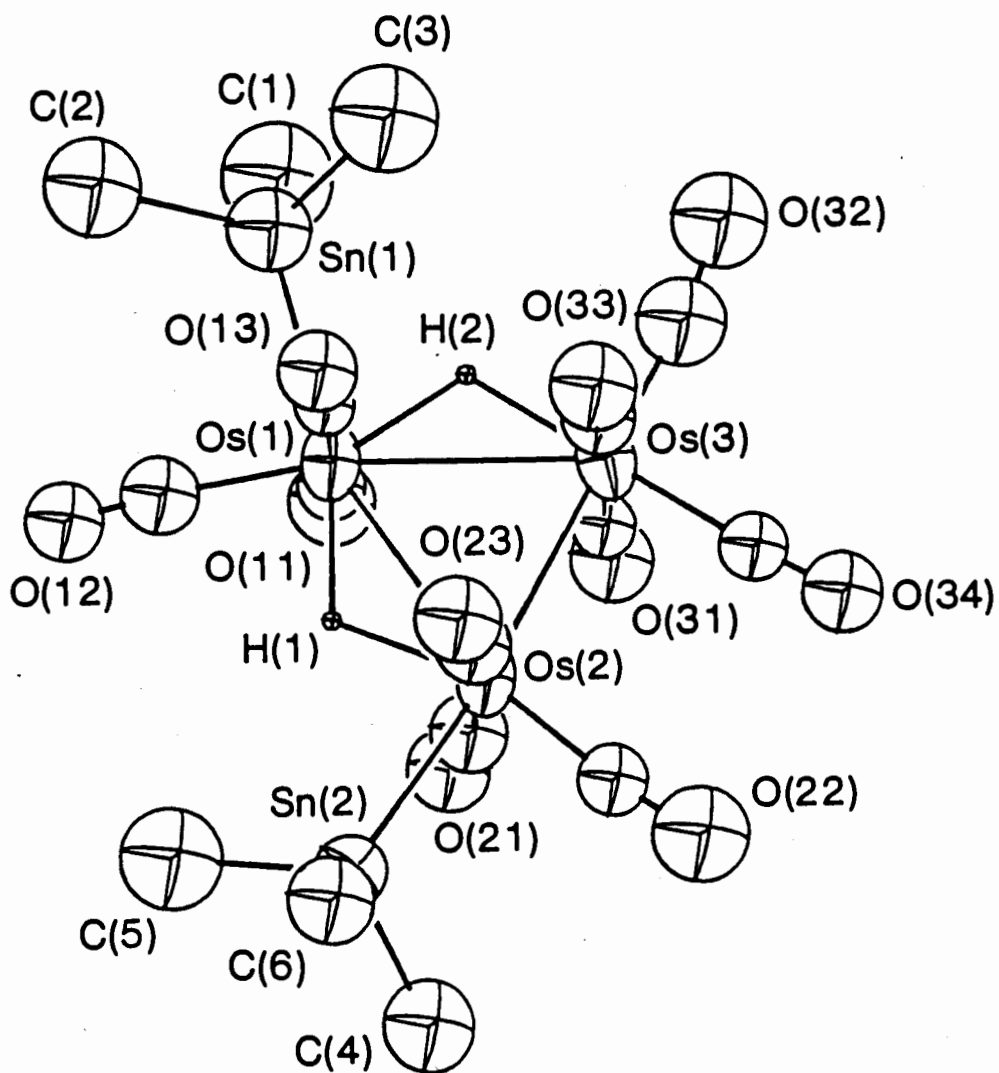


Fig. 1.17 Molecular structure of isomer **a** of $\text{Os}_3(\mu\text{-H})_2(\text{CO})_{10}(\text{SnMe}_3)_2$.³⁰ Important bond lengths (Å) are as follows: $\text{Os}(1)\text{-Os}(2) = 3.021(3)$; $\text{Os}(1)\text{-Os}(3) = 3.070(2)$; $\text{Os}(2)\text{-Os}(3) = 2.896(3)$.

The ^1H NMR spectrum of $\text{Os}_3(\mu\text{-H})_2(\text{CO})_{10}(\text{SnMe}_3)_2$ exhibits four resonances in the bridging hydride region: isomer a: δ -16.92 ($J_{\text{H-H}} = 2.1$ Hz, $J_{\text{Sn-H}} = 30.9$ Hz), -17.76 ($J_{\text{H-H}} = 1.5$ Hz, $J_{\text{Sn-H}} = 39.2$ Hz); isomer b: δ -16.70 (br. s), -18.73 ($J_{\text{H-H}} = 1.3$ Hz, $J_{\text{Sn-H}} = 23.6$ and 36.7 Hz). When a bridging hydride is cis to a stannyl substituent, a Sn-H coupling in the range of 28 - 45 Hz is usually observed.³¹ For example, in the cluster $\text{HOs}_3(\mu\text{-H})_2(\text{CO})_{10}(\text{SnPh}_3)$, $J_{\text{Sn-H}} = 28.5$ Hz;³² in $\text{Os}_4(\mu\text{-H})(\text{CO})_{14}(\text{SnMe}_3)$, $J_{\text{Sn-H}} = 34.5$ Hz;³³ in $\text{Os}_3(\mu\text{-H})_3(\text{CO})_9(\text{SnPh}_3)_3$, $J_{\text{Sn-H}} = 37.2$ Hz;³² and $\text{Os}_3(\mu\text{-H})_2(\text{CO})_{10}(\text{SnPh}_3)$, $J_{\text{Sn-H}} = 45.3$ Hz.³² The Sn-H coupling constants observed in isomer a therefore indicate that each hydride is cis to a SnMe_3 group as found in the solid state. If the hydrides of isomer a are located as shown in Fig. 1.17, the ^1H NMR signal due to the hydride H_1 should exhibit two H-Sn couplings due to the cis and trans SnMe_3 groups. In $\text{Os}_3(\mu\text{-H})_2(\text{CO})_{10}(\text{SnPh}_3)_2$, which exists as only one isomer in solution (believed to be analogous to isomer a), two Sn-H couplings of 13.7 and 30.7 Hz were observed to the hydride signal at lower field while only one Sn-H coupling of 45.3 Hz was observed to the hydride signal at higher field. (This implies that the trans Sn-H coupling is smaller than the cis Sn-H coupling in this molecule, an unusual result.) The signal with two Sn-H couplings was therefore assigned to the bridging hydride H_1 . However, only one set of Sn-H couplings was observed for $\text{Os}_3(\mu\text{-H})_2$ -

$(\text{CO})_{10}(\text{SnMe}_3)_2$. This may have been due to the broadness of the hydride signals which would obscure small couplings. (The width of this signal was about 11 Hz near the base line which would hide a Sn-H coupling of 10 Hz.) The broadness of the signals was almost certainly due to unresolved H-H coupling. Furthermore, both of the hydrides showed the same T_1 value of 1.40 s which indicates that they probably have similar neighbouring groups (see Section B). The hydride resonances of isomer **a** of $\text{Os}_3(\mu\text{-H})_2(\text{CO})_{10}(\text{SnMe}_3)_2$, therefore, could not be assigned unambiguously.

In the NOE experiment, the resonance at δ -17.76 was saturated. An enhancement of 7.5% was observed at δ -16.92 from which an internuclear H...H distance of 3.0 - 3.1 Å was estimated from Fig. 1.3. (The H...H distance calculated from the HYDEX program was 3.3 Å.) The NOE spectrum is shown in Fig. 1.19. The result, however, is consistent with the two hydrides bridging two different Os-Os vectors as in the type **B** arrangement shown in Fig. 1.1. This is in good agreement with the positions predicted with the HYDEX program and, of course, the X-ray structure.

For isomer **b**, the ^1H NMR resonance at δ -18.73 exhibits two Sn-H couplings. A short T_1 of 0.95 s was measured for this resonance (discussed in Section B). The signal at δ -16.70, on the other hand, does not show any Sn-H coupling, and it has a longer T_1 of 2.16 s. These observations are consistent with the location of the two

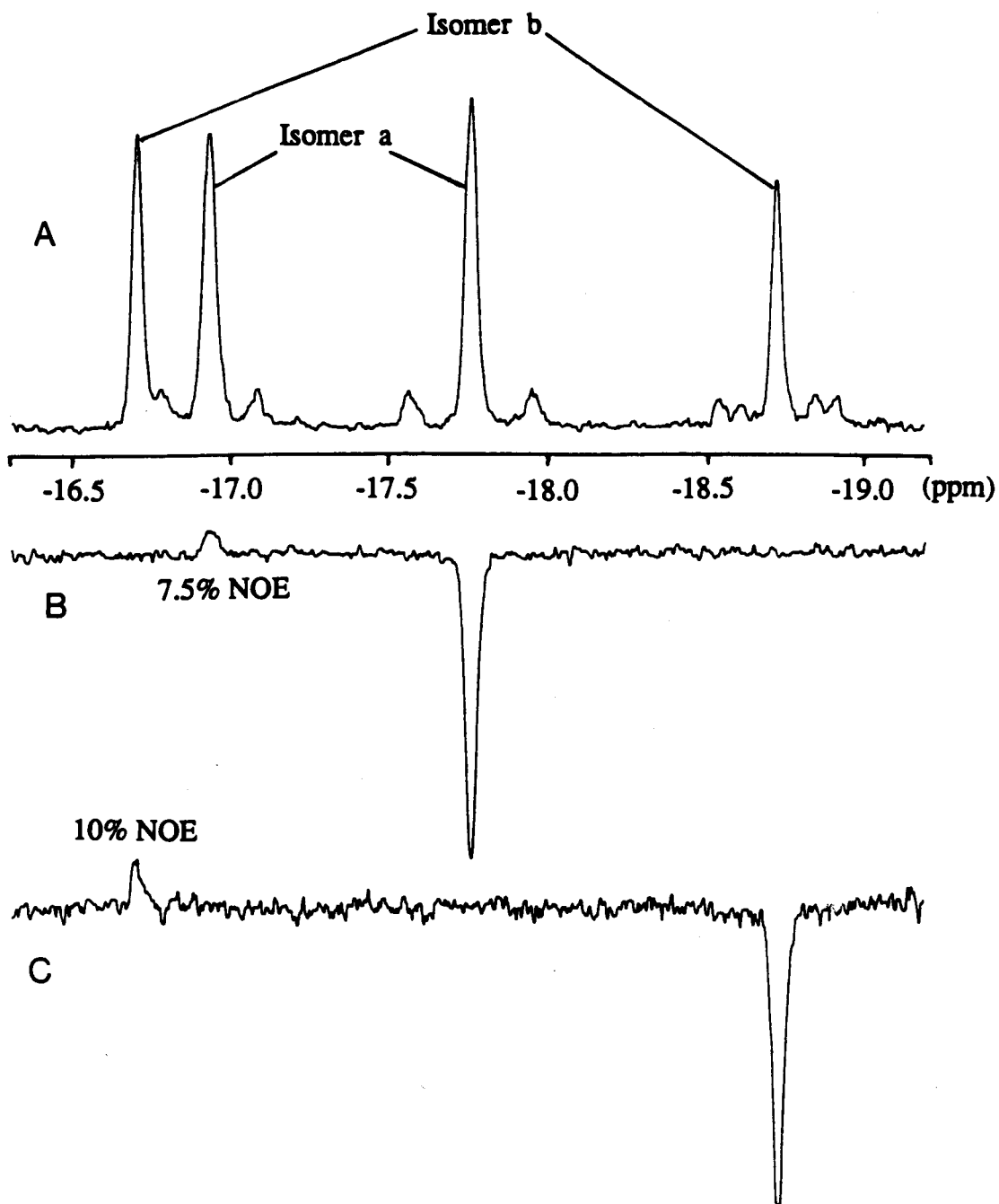


Fig. 1.19 (A) ^1H NMR spectrum (hydride region) of the two isomers of $\text{Os}_3(\mu\text{-H})_2(\text{CO})_{10}(\text{SnMe}_3)_2$ in CD_2Cl_2 at -70°C ; (B) The NOE difference spectrum of isomer **a** (signal at δ -17.76 was saturated); and (C) of isomer **b** (signal at δ -18.73 was saturated) under the same conditions.

SnMe_3 groups at the same osmium centre that is associated with the hydride (Fig. 1.18) that gives rise to the ^1H NMR resonance that exhibits two Sn-H couplings and the shorter T_1 . When the signal at $\delta -18.73$ was saturated, an enhancement of 10% was observed for the signal at $\delta -16.70$. This yields an internuclear $\text{H}\cdots\text{H}$ distance of 2.8 - 2.9 Å. The short $\text{H}\cdots\text{H}$ distance, however, is not consistent with the proposed structure in which the $\text{H}\cdots\text{H}$ distance should be approximately 3.1 Å (as in isomer a). A 5% enhancement would be expected for this distance from Fig. 1.3. The poor agreement may have been due to experimental uncertainty due to the poor signal-to-noise ratio in the NOE difference spectrum.

The structure of $\text{Os}_3(\mu\text{-H})_2(\text{CO})_{10}(\text{SnPh}_3)_2$ has not been determined. As previously stated, it is believed to have a similar structure to isomer a of the SnMe_3 analogue. Consistent with this is that the hydrides had similar T_1 's (0.78 and 0.81 s) in accordance with a similar environment for these ligands. The ^1H NMR spectrum exhibits two resonances in the bridging hydride region at $\delta -17.03$ ($J_{\text{H-H}} = 1.5$ Hz, $J_{\text{Sn-H}} = 13.7$ and 30.7 Hz) and -17.57 ($J_{\text{H-H}} = 1.5$ Hz, $J_{\text{Sn-H}} = 45.3$ Hz). The saturation of the signal at $\delta -17.03$ resulted in an enhancement of 7.4% at $\delta -17.57$. This yields an internuclear $\text{H}\cdots\text{H}$ distance of 3.0 - 3.1 Å. This is consistent with the arrangement of the hydrides as in the isomer a of the SnMe_3 analogue, which

yielded a similar NOE.

The structure of $\text{Os}_3(\mu\text{-H})_2(\text{CO})_{10}(\text{SiPh}_3)_2$ is similar to the SnPh_3 congener according to their infrared and ^1H NMR spectra. The ^1H NMR spectrum exhibits two resonances in the bridging hydride region at δ -14.63 (br s) and -14.78 (d, $J_{\text{H-H}} = 1.2$ Hz). No enhancement was observed in the NOE experiment when the two signals were in turn saturated. This was attributed to the overlap of the two hydride signals which are only 15 Hz apart. Although a minimum saturation power was used, the saturation pulse might be transferred to the neighbouring signal which would saturate the latter signal and thus obscure the observation of any enhancement, especially as the NOE is expected to be about 7% analogous to that found for the SnPh_3 derivative.

**Type 6 Compounds: $\text{HOs}_3(\mu\text{-H})_2(\text{CO})_{10}(\text{ER}_3)$ ($\text{ER}_3 = \text{SiHPh}_2$,
 GePh_3 , SnPh_3)**

The molecular structure of $\text{HOs}_3(\mu\text{-H})_2(\text{CO})_{10}(\text{SiHPh}_2)$ as determined by X-ray crystallography is shown in Fig. 1.20.³⁰ Evidence for the silicon hydrogen, $\text{H}(\text{Si})$, and the hydride ligands were found in the structural determination, but their positions were not refined. The positions of the hydrides were estimated from average osmium-hydride bond lengths of $\text{Os}(\mu\text{-H})\text{Os}$ and Os-H systems of known length.^{30,34}

A typical ^1H NMR spectrum of these compounds is shown in Fig. 1.21 (A). The spectrum exhibits three signals in

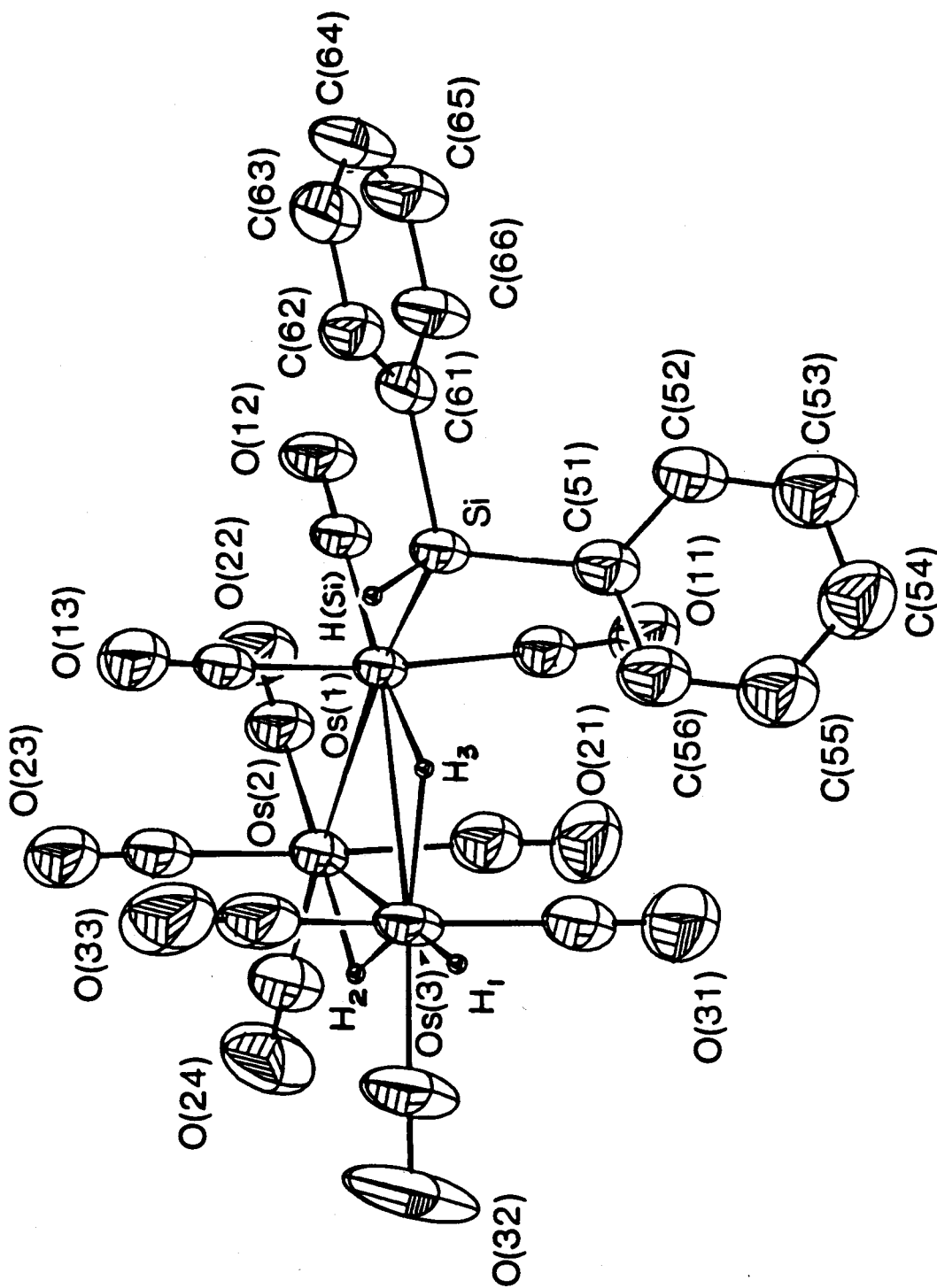


Fig. 1.20 Molecular structure of $\text{HOs}_3(\mu\text{-H})_2(\text{CO})_{10}(\text{SiHPh}_2) \cdot 30$. Important bond lengths (Å) are as follows:
 $\text{Os}(1)\text{-Os}(2) = 2.9383$ (6); $\text{Os}(1)\text{-Os}(3) = 3.0369$ (4);
 $\text{Os}(2)\text{-Os}(3) = 3.0847$ (5).

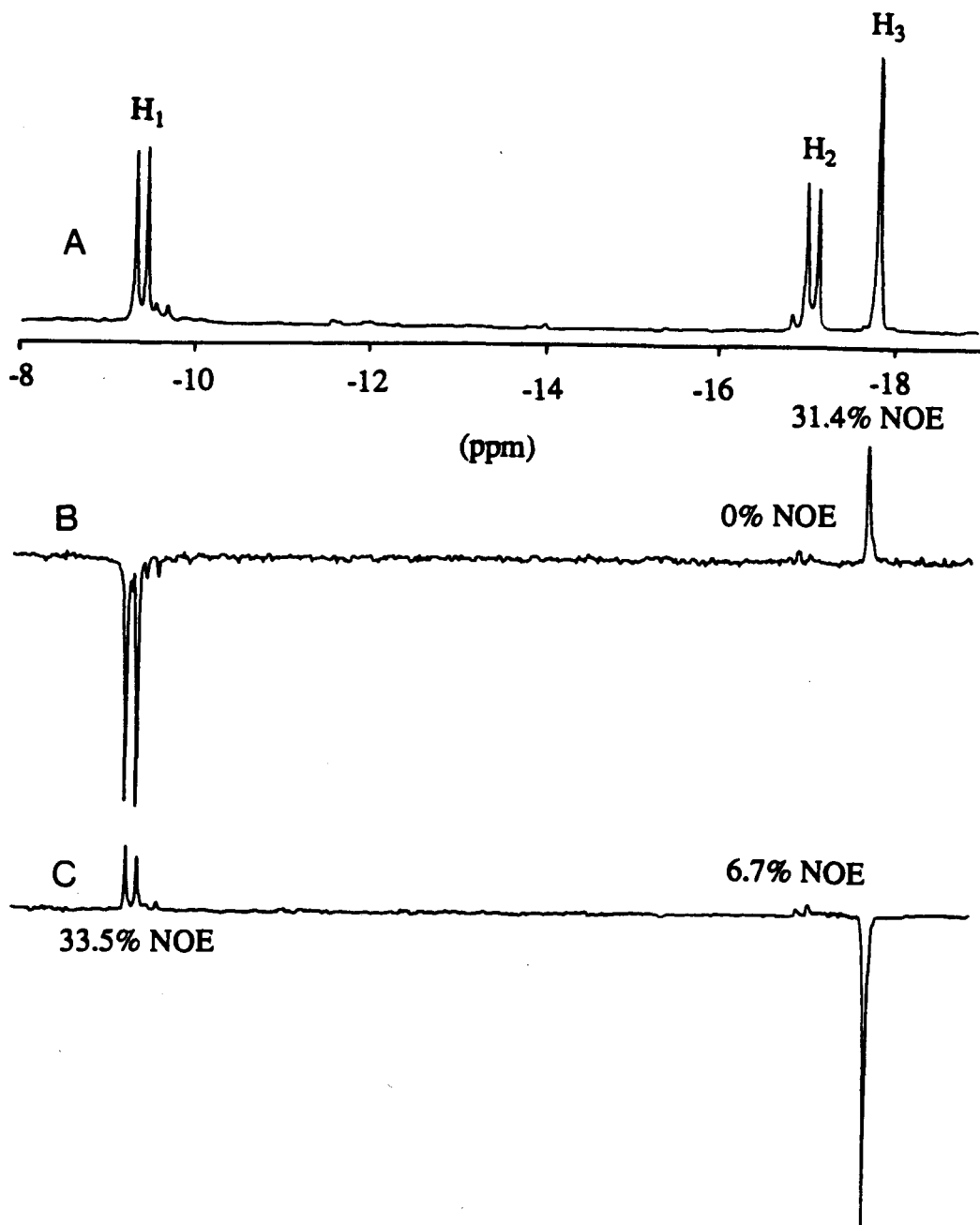


Fig. 1.21 (A) ^1H NMR spectrum of $\text{HOs}_3(\mu\text{-H})_2(\text{CO})_{10}(\text{SiHPh}_2)$ (hydride region) in CD_2Cl_2 at -70°C ; (B) The NOE difference spectrum of the same cluster when the hydride signal of H_1 at δ -9.54 was saturated (small enhancement at the resonance of $\text{H}(\text{Si})$ not shown); (C) Same as (B) but the signal of H_3 at δ -18.21 was saturated.

the hydride region. The doublet in the terminal hydride region (at about -9.5 ppm) is assigned to the terminal hydride H₁. This signal exhibits an average trans H-H coupling of about 13 Hz to the bridging hydride H₂. One doublet and one singlet are observed in the bridging hydride region. The doublet is assigned to the hydride H₂ whereas the singlet is assigned to the hydride H₃ which is cis to the ER₃ substituent. The assignment of the hydride signal due to H₃ is also supported by the observed Sn-H coupling (28.5 Hz) exhibited by this signal when ER₃ = SnPh₃.

The average observed and the calculated %NOE of the three derivatives of HOS₃(μ-H)₂(CO)₁₀(ER₃) are shown in Table 1.8. The calculated %NOE's where a 3-spin system was

Table 1.8 The calculated %NOE compared to the average %NOE observed in the clusters HOS₃(μ-H)₂(CO)₁₀(ER₃).

	Calculated %NOE ^a	H···H distance	Experimental %NOE	H···H distance ^b
f ₁ (3)	48%	2.04 Å	33%	2.3 - 2.4 Å
f ₂ (3)	18%	3.28 Å	6%	3.2 - 3.3 Å
f ₂ (1)	8%	3.43 Å	≈0%	---
f ₃ (1)	47%	2.04 Å	32%	2.3 - 2.4 Å
f _H (Si)(3)	41%	2.70 Å ^c	5%	3.2 - 3.3 Å
f _H (Si)(1)	-14%	3.80 Å ^c	small -ve	---

- calculation for 3-spin system;
- 2-spin interaction is considered and the H···H distances are obtained from Fig. 1.3;
- the distance between the hydrogen atoms was predicted from the HYDEX program, the value shown corresponds to the closest distance in solid state; when rotation occurs the average H···H distance is much longer (see text).

assumed were obtained from Eqn. A.3 (Appendix I). The NOE spectra for $\text{HOS}_3(\mu\text{-H})_2(\text{CO})_{10}(\text{SiHPh}_2)$ are shown in Fig. 1.21. The spectra for the other two derivatives were similar.

For $f_1(3)$ and $f_3(1)$, if only a two-site interaction is assumed, the maximum NOE of 50% would be expected in both cases due to the close proximity of the two hydrides. The calculated values reported in Table 1.8 also predicted a large NOE of 47-48%. However, the observed enhancements were only 32-33%. This was attributed to a long τ_c resulting from a large cluster compound in solution at low temperature and also to the experimental uncertainties.

For $f_2(3)$, if the molecule is considered as a 2-spin system (i.e., H_2 and H_3 only), the observed 6% enhancement leads to an internuclear $\text{H}\cdots\text{H}$ distance of 3.2 to 3.3 Å (from Fig. 1.3) which is in excellent agreement with the calculated distance of 3.28 Å. Since H_2 is an "isolated" spin, the total direct relaxation rate of H_2 is, therefore, slow. This is also consistent with the long T_1 relaxation time for H_2 which suggests little interaction of H_2 with other hydrogen atoms in the molecule (Section B). The 2-spin approximation therefore appeared justified. The lower observed NOE in $f_2(3)$ may be due to experimental uncertainty. Since NOE is dependent to the inverse of the sixth power of the distance between the spins involved, a small discrepancy in %NOE will not yield a great difference in the distance information, as in $f_2(3)$. The small

calculated $f_2(1)$ is due to the long distance between H_1 and H_2 . The discrepancy between the observed and the calculated $f_2(3)$ and $f_2(1)$ is attributed to a long correlation time although experimental uncertainties may account for much, if not all, of the observed discrepancy.

For the case where $ER_3 = SiHPh_2$, the silicon-hydrogen, $H(Si)$, is about 2.7 Å (Table 1.2) from the bridging hydride H_3 in the solid state. The other hydride ligands are more than 5 Å from this hydrogen atom and should not interact with it. When the resonance of H_3 was saturated, an enhancement of approximately 5% was observed at the resonance of $H(Si)$. However, an enhancement of 41% was calculated for the arrangement of the hydrogen atoms in the solid state. The calculation assumed that $H(Si)$ relaxes only through dipole-dipole interaction with H_1 and H_3 while the interactions of $H(Si)$ with the phenyl hydrogens were ignored. The distances between $H(Si)$ and the two hydrides under consideration vary upon the rotation of the $SiHPh_2$ group about the $Os(1)-Si$ bond in solution. The farthest distances of $H(Si)$ from H_1 and H_3 are about 6 Å and 4 Å, respectively. If the $SiHPh_2$ group is assumed to rotate freely about the $Os(1)-Si$ bond then average distances between $H(Si)$ and the hydrides H_1 and H_3 are 4.4 Å and 3.0 Å. The calculated NOE in $f_{H(Si)}(3)$ is, therefore, 42% which is similar to that calculated for the arrangement of the spins in the solid state. The discrepancy between the

observed and the calculated NOE's is attributed to the relaxation interactions of H(Si) with the phenyl groups which were not considered in the calculations. It is believed, from the T_1 measurements (see Section B), that the phenyl groups are the relaxation source for H(Si). In Appendix I it is shown that the NOE in a 3-spin system is inversely proportional to the total relaxation rate (R) of the observed spin. If the interactions of H(Si) and the phenyl groups are taken into account, i.e., the value of R increased, the NOE should, therefore, be diminished.

Eqn. A.2 in Appendix I shows that NOE's in a 3-spin systems are angle dependent, i.e., the angle between the spins involved as shown in the inset of Fig. 1.22.¹³ There exists an angle for which zero enhancement can be observed when the distance between spins 1 and 2 is not necessarily large. Indeed, there exists some angles at which negative enhancements are expected. These observations emphasize that it is the relative positions of all interacting spins that determines the size of the enhancement rather than simply the distance between the irradiated and the observed spins.

For $f_{H(Si)}(1)$, a negative enhancement of -14% was calculated based on a 3-spin system arranged as in the solid state (i.e., H_1 , H_3 and H(Si)). If the rotation of $SiHPh_2$ was considered, i.e., the average distances between the spins were used as mentioned above, the calculated NOE was

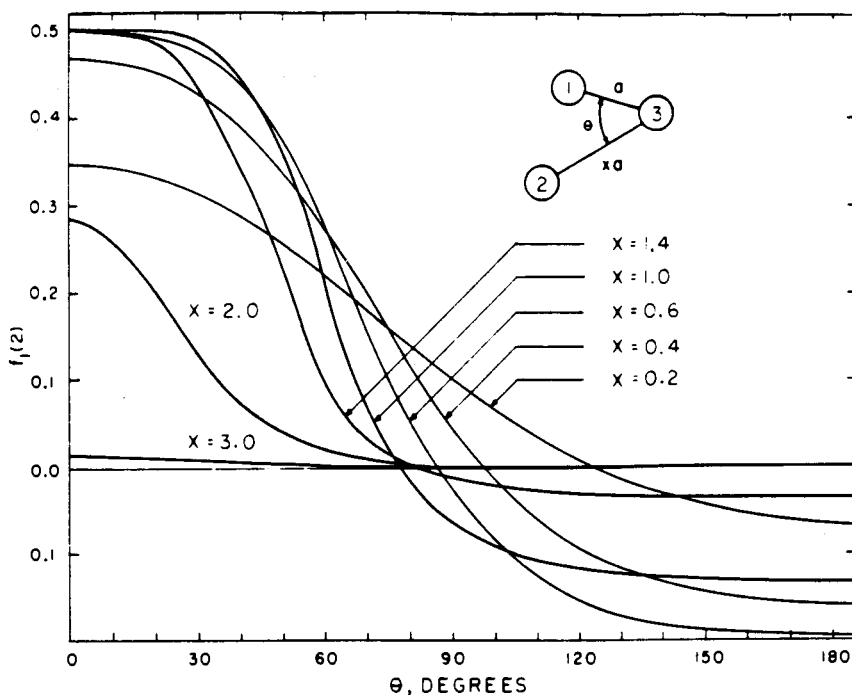


Fig. 1.22 The dependence of the nuclear Overhauser enhancement on the relative positions of the spins in a 3-spin system.¹³

-17% whereas a small negative enhancement was observed. The negative enhancement, however, reflects the arrangement of the three hydrides. From Fig. 1.22, it can be shown that, to observe a negative NOE, the angle sustaining spins H_1 and $H(\text{Si})$ on H_3 is probably greater than 90° . This is consistent with the calculated angle of 105.6° in the solid state (calculated from the positions of H-atoms estimated by the HYDEX program). The discrepancy in the observed and the calculated %NOE was probably due to the same reason as discussed above for $f_{H(\text{Si})}(3)$.

Type 7 Compounds: $\text{Os}_3(\mu\text{-H})_3(\text{CO})_9(\text{ER}_3)$ ($\text{ER}_3 = \text{SiPh}_3, \text{SiHPh}_2, \text{SnPh}_3$)

The structure of $\text{Os}_3(\mu\text{-H})_3(\text{CO})_9(\text{SiPh}_3)$ has been determined by X-ray crystallography (Fig. 1.23).¹⁹ The three hydride ligands were not located. From bond length arguments, however, one of the hydrides is believed to bridge the long Os(1)-Os(2) vector while the other two hydrides are thought to bridge the same short Os(1)-Os(3) vector as shown in Fig. 1.23. The ^1H NMR spectrum of this cluster exhibits three signals in the hydride region at δ -8.56 ($J_{\text{Os-H}} = 44.1$ Hz), -12.45 ($J_{\text{Os-H}} = 31.3$ and 35.4 Hz) and -12.56 ($J_{\text{Os-H}} = 44.9$ Hz). The resonances at δ -8.56 and -12.56 were assigned to the hydrides H_1 and H_2 because of their similar $^{187}\text{Os-H}$ coupling constants; the resonance at δ -12.45 was assigned to the hydride H_3 on the basis of its smaller $^{187}\text{Os-H}$ coupling constants.¹⁹ In this case, the coupling to the two different Os atoms was resolved. The resonances of the hydrides H_1 and H_2 , however, could not be assigned further. From the T_1 study reported below, the ^1H NMR resonance at δ -8.56 and -12.56 were assigned to the hydrides H_2 and H_1 , respectively.

The positions of the hydride ligands were consistent with those estimated with the HYDEX program. The calculations also indicated that in the solid state the hydride H_1 is quite close to an ortho-hydrogen atom on one of the phenyl groups at a distance of about 2.3 Å and

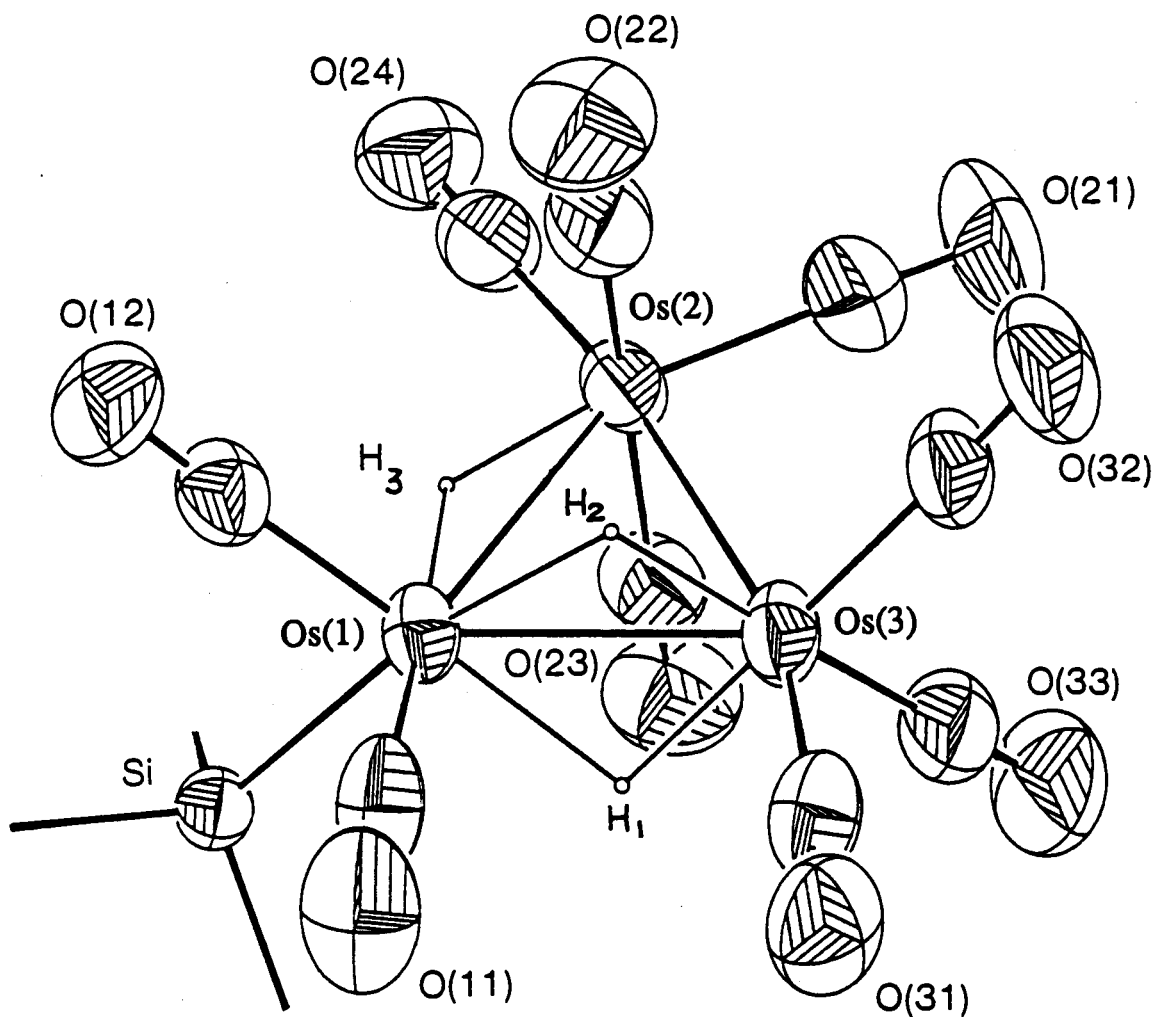


Fig. 1.23 Molecular structure of $\text{Os}_3(\mu\text{-H})_3(\text{CO})_9(\text{SiPh}_3)$
 (the phenyl groups have been omitted).¹⁹
 Important bond lengths (Å) are as follows:
 $\text{Os}(1)\text{-Os}(2) = 3.0103$ (4); $\text{Os}(1)\text{-Os}(3) = 2.7079$ (4);
 $\text{Os}(2)\text{-Os}(3) = 2.8550$ (4).²⁹

hydride H₃ is close to another ortho-hydrogen atom on a different phenyl group at a similar distance. However, due to the rotation of the SiPh₃ group about Os(1) when the molecule is in solution the interactions of the hydrides with the phenyl hydrogens are probably very small. The arrangement of the hydrides involved in the NOE calculations is shown in Fig. 1.24.

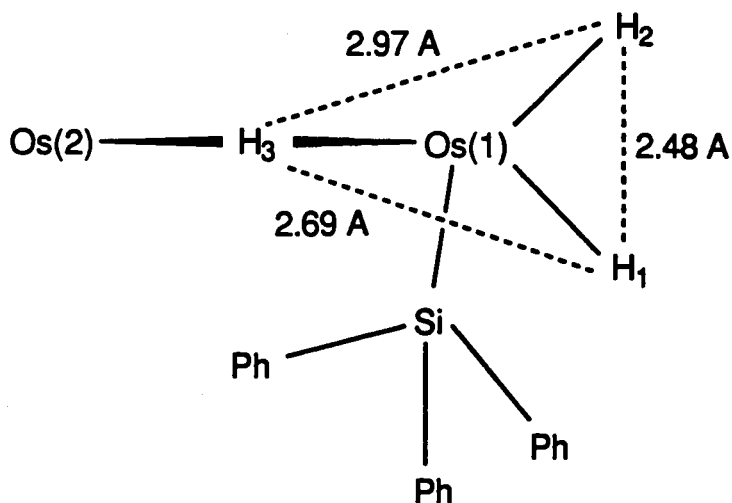


Fig. 1.24 Simplified relative locations of the hydride ligands and the calculated internuclear H...H distances of $\text{Os}_3(\mu\text{-H})_3(\text{CO})_9(\text{SiPh}_3)$.

Due to the partial overlap of the two hydride signals to higher field, saturation of only one of these signals was not possible. Therefore, only the hydride signal to lower field was irradiated and the enhancements at the other two hydride signals observed. The NOE spectra of $\text{Os}_3(\mu\text{-H})_3(\text{CO})_9(\text{SiPh}_3)$ are shown in Fig. 1.25. The results from the three derivatives of this type of cluster are

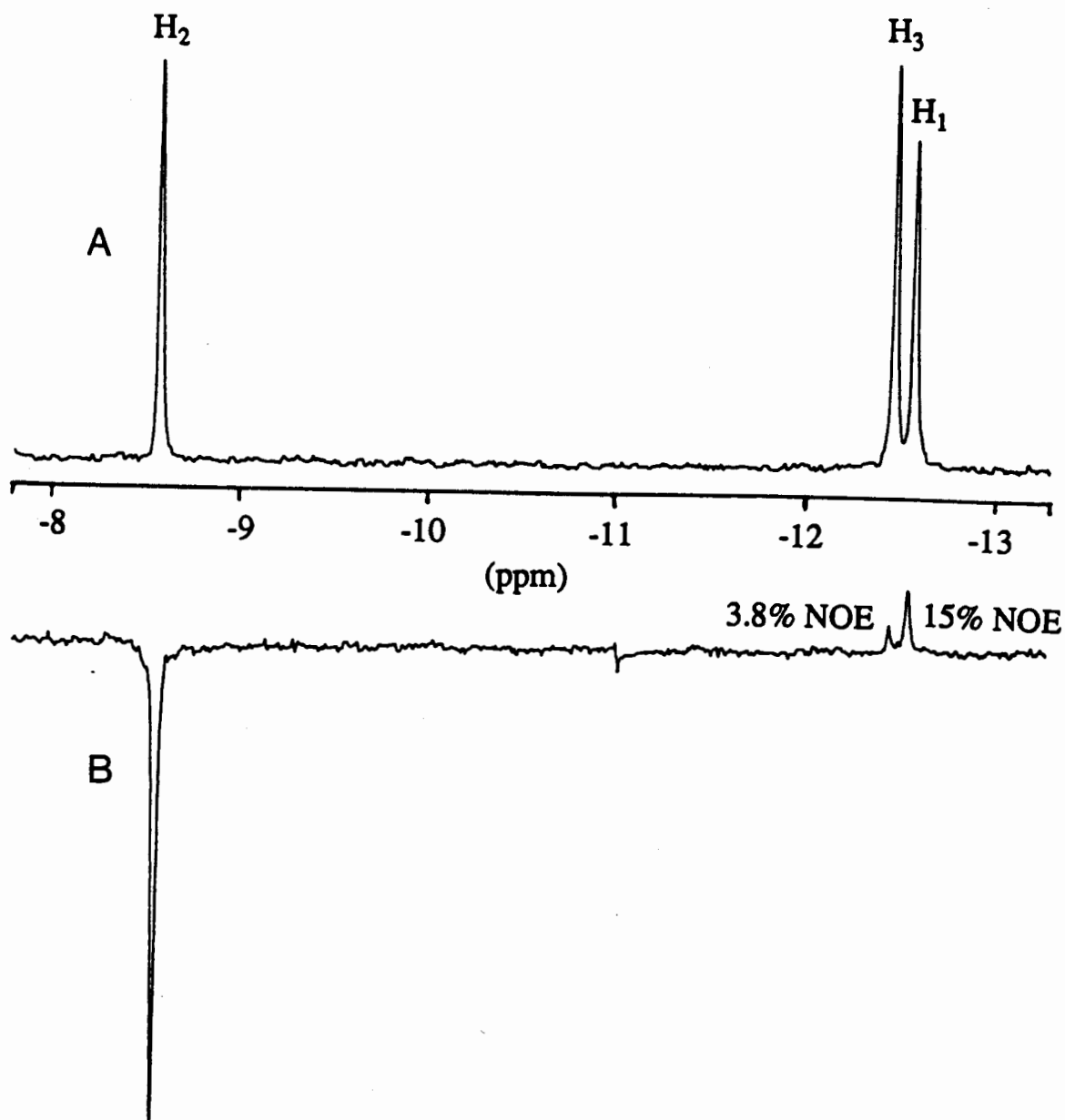


Fig. 1.25 (A) ^1H NMR spectrum of $\text{Os}_3(\mu\text{-H})_3(\text{CO})_9(\text{SiPh}_3)$ (hydride region) in CD_2Cl_2 at -70°C ; (B) The NOE difference spectrum of $\text{Os}_3(\mu\text{-H})_3(\text{CO})_9(\text{SiPh}_3)$ (signal at δ -8.56 was saturated) under the same conditions.

tabulated in Table 1.9. The experimental results and the calculated enhancements based on a 3-spin system are shown in Table 1.10.

Table 1.9 The NOE enhancements observed in $\text{Os}_3(\mu\text{-H})_3(\text{CO})_9(\text{ER}_3)$.

ER_3	$f_1(2)$	$f_3(2)$
SiPh_3	15%	3.8%
SiHPh_2	13%	4.6%
SnPh_3	13%	4.0%

In $\text{Os}_3(\mu\text{-H})_3(\text{CO})_9(\text{ER}_3)$ clusters if a 3-spin system (the three hydrides) is assumed, the calculated values of $f_1(2)$ and $f_3(2)$ are 29% and 8.4%, respectively. It may be that due to the relaxation of H_1 and H_3 through the phenyl-hydrogen atoms, which was not considered in the calculations, the calculated values of $f_1(2)$ and $f_3(2)$ of these clusters should be smaller. This is similar to the case of $\text{HOs}_3(\mu\text{-H})_2(\text{CO})_{10}(\text{SiHPh}_2)$ discussed before.

Table 1.10 Comparisons of the calculated (based on a 3-spin system) and the average observed %NOE.

	Average experimental %NOE	Calculated %NOE
$f_1(2)$	14%	29%
$f_3(2)$	4.1%	8.4%

There is strong evidence that $\text{Os}_3(\mu\text{-H})_3(\text{CO})_9(\text{SiPh}_3)$ is a true 3-spin system since in the other clusters studied with the $\text{Os}(\mu\text{-H})_2\text{Os}$ unit (the green and red isomers of $\text{Os}_3(\mu\text{-H})_2(\text{CO})_9(\text{CNBu}^t)$; type 1 above) a 37% enhancement was observed for these protons.

Type 8 Compound: $\text{Os}_4(\mu\text{-H})_3(\text{CO})_{12}\text{I}$

The structure of the compound $\text{Os}_4(\mu\text{-H})_3(\text{CO})_{12}\text{I}$ has been determined by neutron diffraction and the hydride ligands were refined.³⁵ The molecular structure is shown in Fig. 1.26. The structure has a 2-fold axis that passes through the iodine atom and the hydride H_2 which bridges the $\text{Os}(2)$ and $\text{Os}(2a)$ centres. The hydrides H_1 and H_{1a} are, therefore, equivalent. The distance of $\text{H}_1 \cdots \text{H}_2$ ($\text{H}_{1a} \cdots \text{H}_2$) is 3.08 Å observed from the neutron diffraction data and the distance between the two equivalent hydrides is 4.21 Å.

The ^1H NMR spectrum of $\text{Os}_4(\mu\text{-H})_3(\text{CO})_{12}\text{I}$ at -70°C exhibits two signals in the ratio of 1:2 in the bridging hydride region at δ -17.37 (1H, assigned to H_2) and -17.76 (2H, assigned to H_1 and H_{1a}). The NOE spectra are shown in Fig. 1.27.

When the resonance of the H_1 's was saturated, an NOE of 24% was observed at the signal of H_2 , i.e., $f_2(1)$. The calculated NOE is 26% which is in excellent agreement with the experimental value. To calculate the NOE for $f_1(2)$, one of H_1 's is regarded as the third spin (e.g., H_3). It is

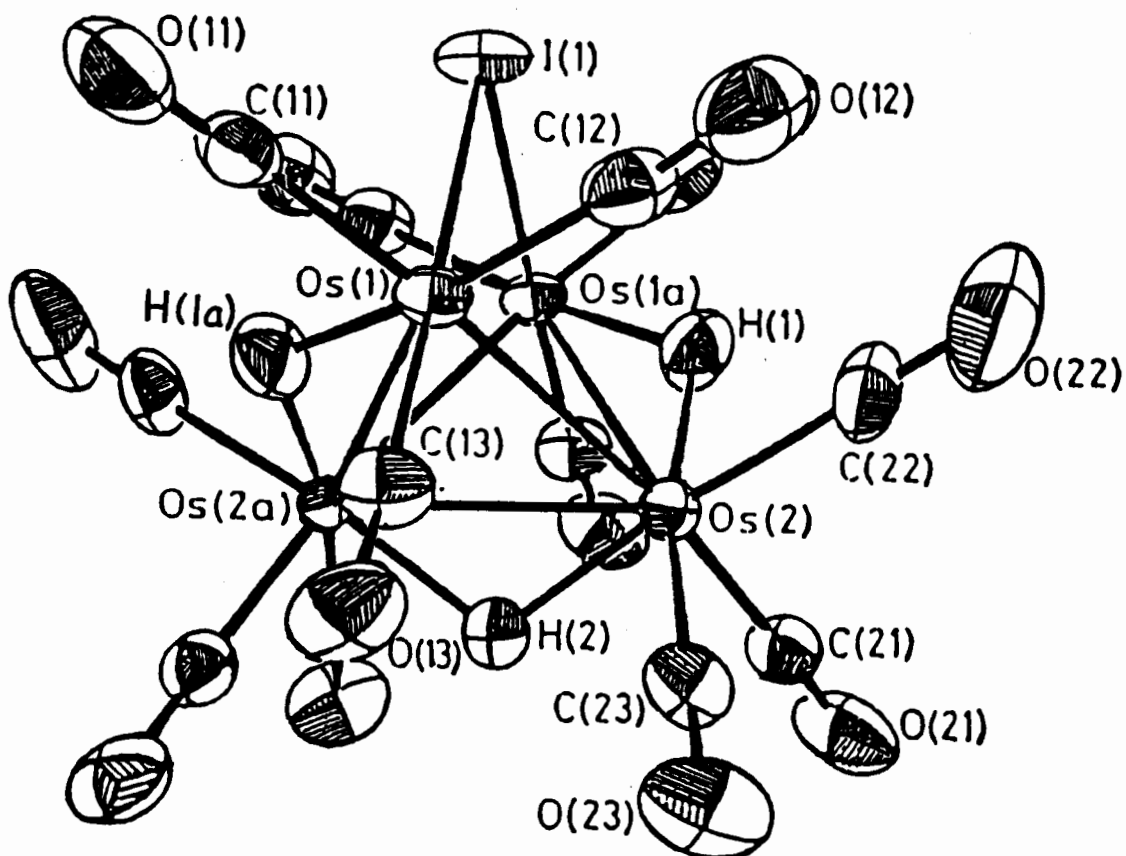


Fig. 1.26 Molecular structure of $\text{Os}_4(\mu\text{-H})_3(\text{CO})_{12}\text{I}\cdot 35$
 Important bond lengths (Å) are as follows:
 $\text{Os}(1)\text{-Os}(2) = 2.877(1)$; $\text{Os}(2)\text{-Os}(1a) = 3.055(1)$;
 $\text{Os}(2)\text{-Os}(2a) = 2.927(2)$.

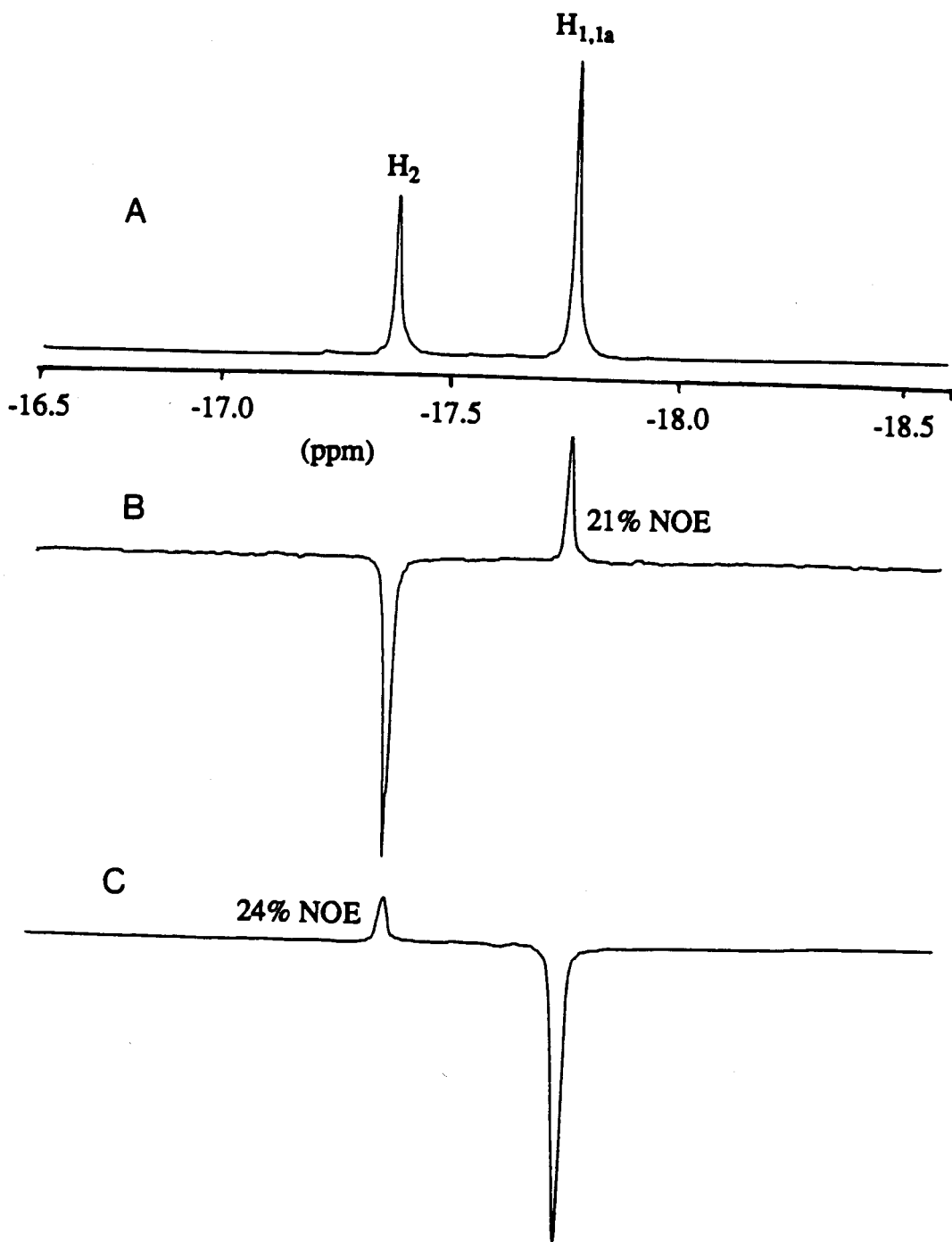


Fig. 1.27 (A) ^1H NMR spectrum of $\text{Os}_4(\mu\text{-H})_3(\text{CO})_{12}\text{I}$ (hydride region) in CD_2Cl_2 at -70°C ; (B) The NOE difference spectra of $\text{Os}_4(\mu\text{-H})_3(\text{CO})_{12}\text{I}$ where the signal at δ -17.37; and (C) at δ -17.76 were saturated under the same conditions.

noted that $\rho_{12} = \rho_{23}$. The calculated NOE, from Eqn. A.3, is 41% where 21% was observed in the NOE experiment. The discrepancy in $f_1(2)$ is, however, not known.

Os₄(μ -H)(CO)₁₄(SnMe₃)

The NOE experiment can also be applied to the situation where there is only one hydride in the cluster, provided a hydrogen-containing ligand is present. This was demonstrated with the tetraosmium cluster Os₄(μ -H)(CO)₁₄(SnMe₃).

The X-ray crystal structure of Os₄(μ -H)(CO)₁₄(SnMe₃) is shown in Fig. 1.28.³³ The methyl hydrogens were refined at calculated positions with 0.96 Å as the C-H bond length. The hydride ligand, however, could not be located. Based on the bond length argument that an Os-Os vector will be lengthened by a bridging hydride (presented earlier), one would predict that the hydride ligand in Os₄(μ -H)(CO)₁₄(SnMe₃) bridges the Os(2)-Os(3) vector since it has the longest Os-Os bond length (3.050 (1) Å) in the structure. This cluster is, however, related to some tetranuclear clusters of osmium that contain long (~3 Å) Os-Os bonds but do not contain hydride ligands, e.g., (η^5 -C₅Me₅)(OC)Ir-Os₃(CO)₁₁,³⁶ Os₄(CO)₁₅,³⁶ and Os₄(CO)₁₄(PMe₃).³⁷ The long Os-Os bond in Os₄(μ -H)(CO)₁₄(SnMe₃) might not, therefore, be indicative of a hydride ligand across this bond.

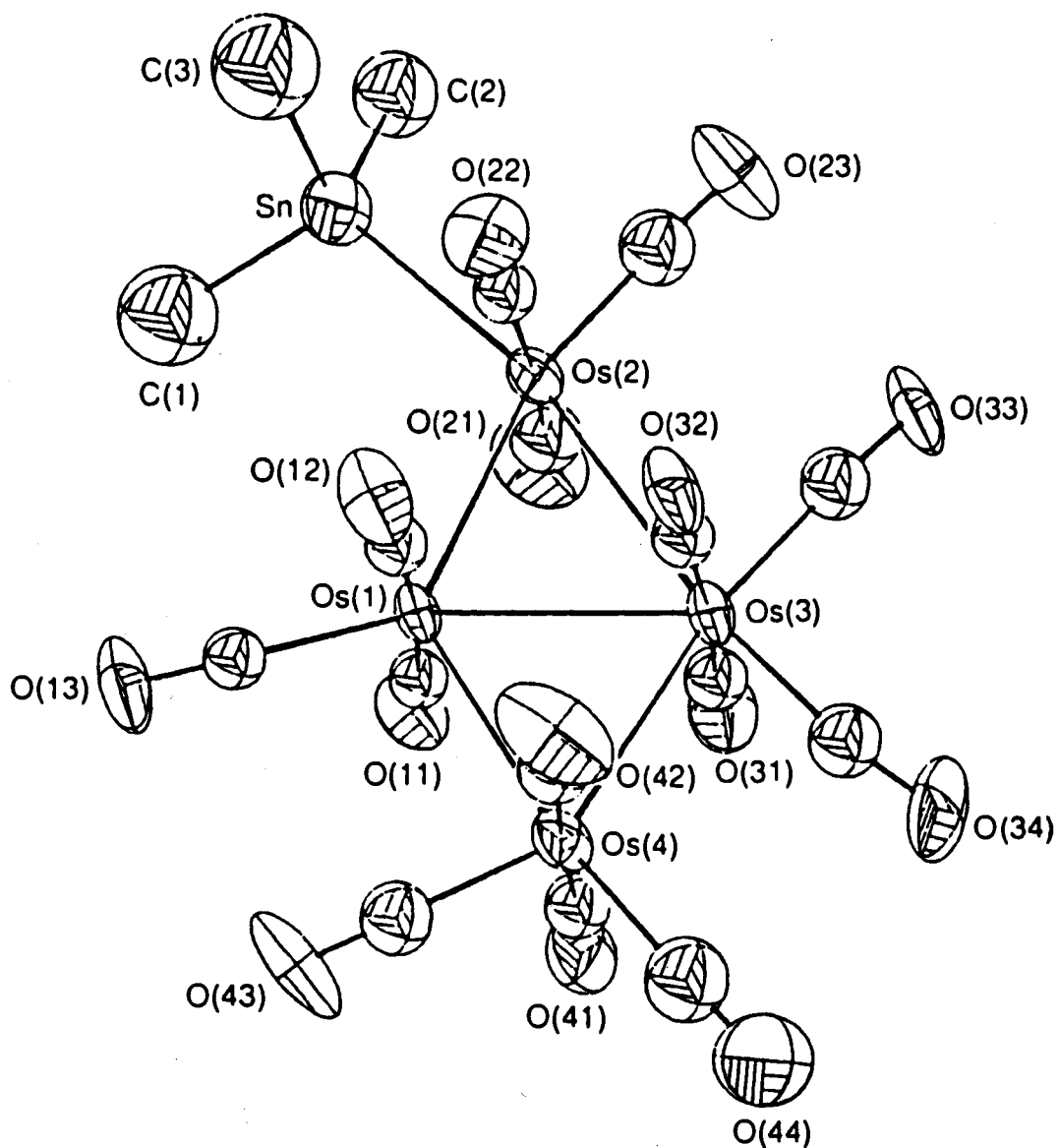


Fig. 1.28 Molecular structure of $\text{Os}_4(\mu\text{-H})(\text{CO})_{14}(\text{SnMe}_3) \cdot 33$
 Important bond lengths (Å):
 $\text{Os}(1)\text{-Os}(2) = 2.807(1)$; $\text{Os}(1)\text{-Os}(3) = 2.875(1)$;
 $\text{Os}(1)\text{-Os}(4) = 2.810(1)$; $\text{Os}(2)\text{-Os}(3) = 3.050(1)$;
 $\text{Os}(3)\text{-Os}(4) = 2.851(1)$.

The ^1H NMR spectrum of the cluster at room temperature exhibits one resonance in the bridging hydride region at δ -14.11 with a Sn-H coupling constant of 34.5 Hz. As discussed above, the magnitude of this coupling constant is consistent with a cis arrangement of the hydride with the trimethyltin group. A similar Sn-H coupling of 30.2 Hz was observed for the signal at δ -18.3 of $\text{HOs}_3(\mu\text{-H})_2(\text{CO})_{10}\text{-}(\text{SnMe}_3)$. The structure of this cluster is believed to be similar to that of $\text{HOs}_3(\mu\text{-H})_2(\text{CO})_{10}(\text{SiHPh}_2)$ in which one hydride ligand is cis to the Si group but with no hydride ligands trans to the group 14 atom.

The NOE experiment was carried out at room temperature because the ^{13}C NMR spectrum indicated that the cluster was rigid at this temperature. The NOE spectra are shown in Fig. 1.29. The methyl signal was saturated and an enhancement of 18% was observed at the hydride signal. This enhancement projects to an average internuclear $\text{H}\cdots\text{H}$ distance of about 2.6 Å from Fig. 1.3. It indicates that the hydride ligand bridges the Os(1)-Os(2) vector and is cis to the trimethyltin group in agreement with the ^1H and ^{13}C NMR data. A calculation with the HYDEX program also gave the same result, that is, the hydride bridges Os(1)-Os(2) vector and not the long Os(2)-Os(3) bond.

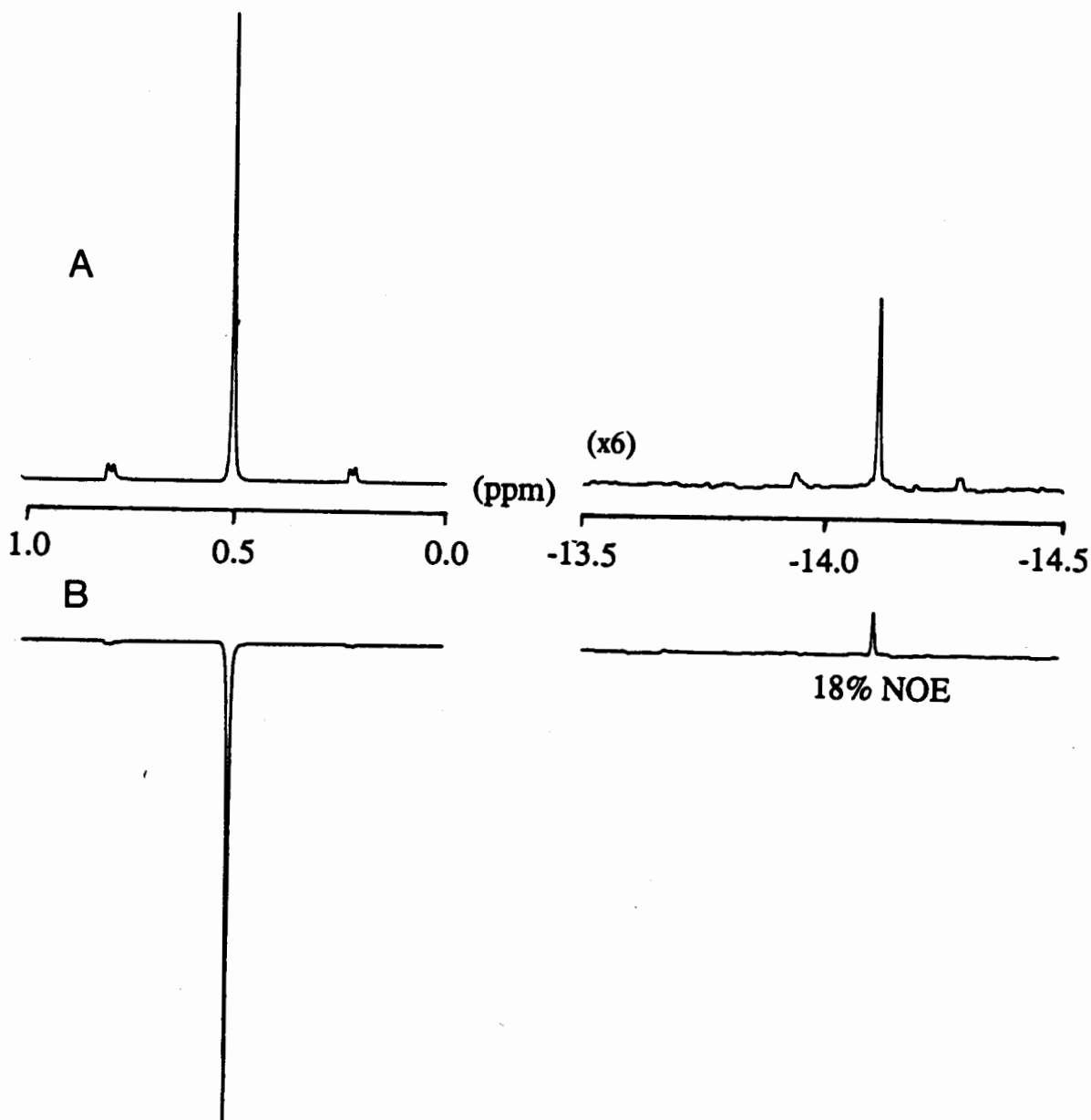


Fig. 1.29 (A) ^1H NMR spectrum of $\text{Os}_4(\mu\text{-H})(\text{CO})_{14}(\text{SnMe}_3)$ (methyl and hydride region) in CD_2Cl_2 at ambient temperature; (B) The NOE difference spectrum when the resonance of the methyl groups at δ 0.58 was saturated under the same conditions.

1A.4 Conclusion

From the results of this study (limited to the 2-spin cases) a graph similar to the Bell and Saunders plot (Fig. 1.3) can be obtained which relates the H...H internuclear distances (estimated from the HYDEX program) to the %NOE observed (Fig. 1.30). A good correlation was obtained (correlation coefficient $r = 0.92$). The slope of the line (slope = 29.2) is very similar to that reported by Bell and Saunders (slope = 27.8).¹³ However, the line in Fig. 1.30 is shifted to a higher position on the y-axis than that in the Bell and Saunders plot. This indicates that the NOE observed in this study is higher at any H...H internuclear distances. This may be due to several reasons: the clusters studied may have much longer correlation times than the organic molecules studied by Bell and Saunders and, therefore, might not be in the fast correlation time limit; the uncertainties in the H...H distances estimated from the HYDEX program; not enough data points for 2-spin systems from this study; the experimental errors.

The results presented in this study indicate that the nuclear Overhauser enhancement experiments provide a useful tool to locate the relative positions of chemically different hydride ligands in hydrido-metal clusters, but the method has its limitations.

Compounds which possess a very low barrier to H-H exchange are not suitable for the experiment. This has been

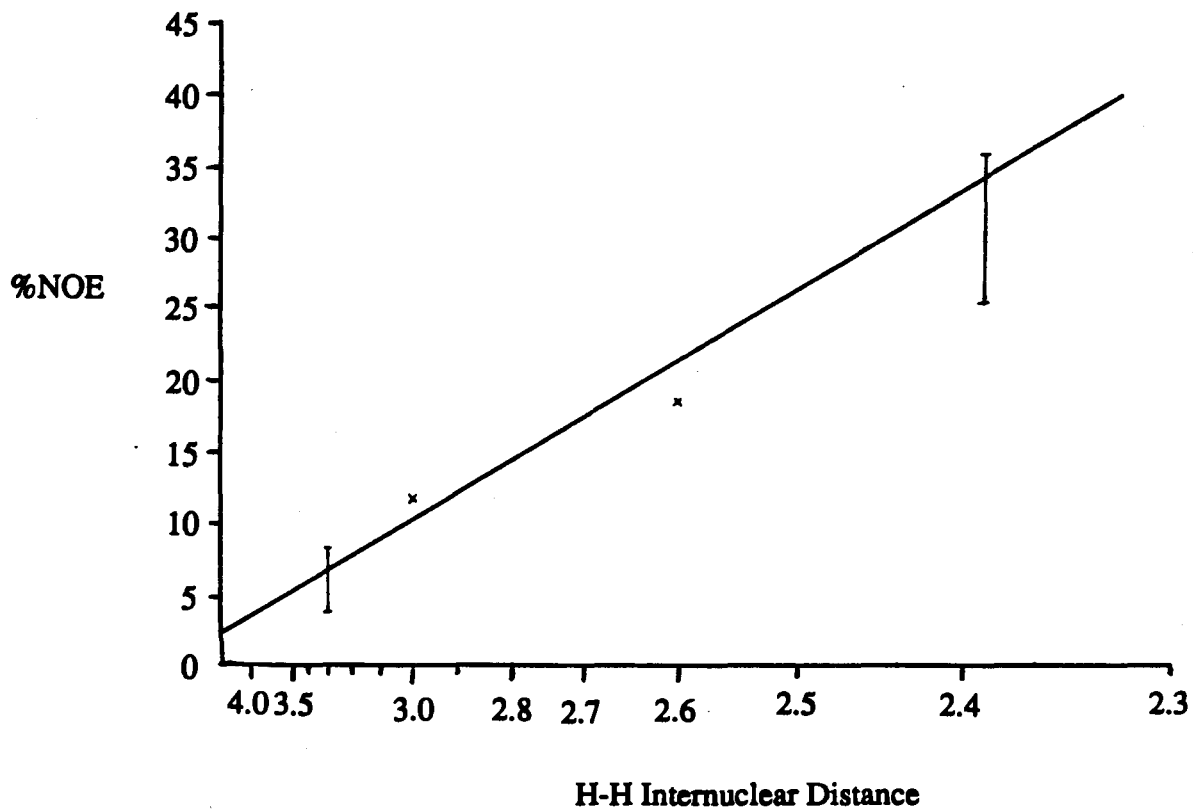


Fig. 1.30 Observed nuclear Overhauser enhancement obtained in this study versus the H...H internuclear distance for 2-spin interaction.

demonstrated in some of the type 4 compounds, $\text{HOs}_3(\mu\text{-H})\text{-}(\text{CO})_{10}(\text{L})$. At -100°C , although these compounds exhibit a spectrum of reasonably sharp resonances it is believed H-H exchange was still significant such that the size of the NOE's was therefore diminished. In other words, exchange between the hydrides must be stopped on the NMR time scale in order for NOE to yield reliable results as to the relative disposition of the hydrides.

When the hydride ligands in question are magnetically similar, the ^1H NMR resonances may not be fully resolved, i.e., the signals may not be completely separated in the base line. The saturation of only one of the resonances may therefore be difficult to carry out because the saturation power may transfer to the other signal. For example, in $\text{Os}_3(\mu\text{-H})_3(\text{CO})_9(\text{SiPh}_3)$, the two hydride signals at high field were not fully separated in the base line and saturation of only one of the two signals was not possible. The cluster $\text{Os}_3(\mu\text{-H})_2(\text{CO})_{10}(\text{SiPh}_3)_2$ provides another example where the enhancement was obscured by the closeness of the two hydride resonances. This problem could be overcome by using a high field NMR spectrometer so that the signals are better separated, but as mentioned previously high field spectrometers apparently do not give NOE spectra of the quality of low field spectrometers.

In order to get approximate distances of the hydrides from NOE experiments, the intramolecular dipole-dipole

interaction must be the main relaxation route for the observed nuclei. The presence of other more efficient relaxation routes such as paramagnetic relaxation will lower or completely eliminate the NOE. Samples must therefore be oxygen-free and not contain any other paramagnetic impurities such as transition metal ions. This did not appear to be a problem in this study.

When inconclusive results of an NOE experiment are obtained, the T_1 relaxation time of the nuclei under study should be determined. A short T_1 relaxation time of the observed nucleus may diminish or eliminate the NOE if the relaxation interaction is not mainly with the saturated spin. The T_1 relaxation times of the hydrides may also give information on the positions of the hydrides in a cluster. The T_1 relaxation times of the hydrides in some of triosmium clusters studied above were determined and are discussed in the following section.

Section B T_1 Relaxation Times of Hydrides in Some Hydrido-Osmium Clusters.

1B.1 Introduction

From the previous section, it was remarked that the NOE is quenched if there exist relaxation pathways, other than dipole-dipole relaxation interaction, for the nucleus under investigation. The presence of these "unwanted" interactions may be revealed by the T_1 relaxation time at the observed nucleus.

The T_1 relaxation times of hydride ligands in some hydrido-metal complexes and clusters have been reported.^{38,39} It was found that terminal hydrides usually exhibit shorter T_1 's than those of bridging hydrides. The relaxation times also varied according to the neighbouring groups. The results obtained in this study also show similar patterns.

In hydrido-metal clusters the T_1 relaxation times of the hydrides can provide information for the interpretation of the results of the NOE experiments. The T_1 values can be related to the environment of the nucleus in question and hence be useful in the assignment of the NMR resonances. This will be demonstrated for $Os_3(\mu-H)_2(CO)_9(CNBut)$ (green isomer) and $Os_3(\mu-H)_3(CO)_9(SiPh_3)$.

1B.2 Experimental Section

The T_1 measurements were carried out on a Bruker SY100 NMR spectrometer with an ^1H operating frequency of 100.13 MHz. The inversion-recovery method was used for the T_1 measurements. The pulse sequence was as follows:

$$[\pi - D(t_1) - \pi/2 - \text{FID} - D(t_2)]_n$$

where $D(t_1)$ is the delay time for the decay of the magnetization after the π pulse; $\pi/2$ pulse is the observing pulse; $D(t_2)$ is the delay time for the complete relaxation of the magnetization, i.e., for the magnetization to return to equilibrium. A delay time of greater than $5T_1$ was used for $D(t_2)$, where T_1 was the longest relaxation time of the hydrogen atoms in the cluster under investigation. The pulse sequence was repeated n times until a good signal-to-noise ratio was obtained (n was usually 80).

The pulse width for the π pulse is important in the determination of T_1 relaxation times. A π pulse was determined by the conventional method:^{12,17} With a sample of $\text{H}_2\text{O}/\text{D}_2\text{O}$ (9:1) an FID was acquired with a pulse width which is between a $\pi/2$ and π pulse (about $6 \mu\text{s}$ for the NMR spectrometer used in this study). After the Fourier transform (FT) process, a ^1H NMR spectrum of water was phase-corrected for a positive absorption signal. The phase constant was stored in the FT program for the phase-

correction of later spectra so that a negative signal could be recognized. The recognition of a negative phase is crucial especially when the signal is small (see below). A series of ^1H NMR spectra of water were then obtained in a similar way except that the pulse width was increased in about $0.5 \mu\text{s}$ intervals for every acquisition. The procedure was continued until a phased-corrected spectrum which exhibited a negative absorption signal for water was obtained. A π pulse was achieved when the H_2O signal in the spectrum gave a null intensity. The pulse width for a π pulse for the NMR spectrometer used in this study was found to be $11.6 \mu\text{s}$. The pulse width for a $\pi/2$ pulse is, therefore, exactly half of that for a π pulse, i.e., $5.8 \mu\text{s}$. The pulse width was checked occasionally during the period when the T_1 relaxation times of the hydrides were studied and found to be reasonably constant.

All T_1 measurements were carried out at -70°C except for $\text{HOs}_3(\mu\text{-H})(\text{CO})_{10}(\text{PMe}_3)$ where the T_1 's were measured at -100°C . The low temperature condition ensures that H-H exchange processes are stopped and no magnetization transfer will take place from one site to the other. The samples used in the T_1 studies were carefully degassed, with the use of three freeze-pump-thaw cycles, to remove any dissolved oxygen. The tube was sealed with a Teflon valve. Dilute samples in a low magnetic solvent, such as CD_2Cl_2 (for the experiments carried out at -70°C) and $\text{CS}_2/\text{CD}_2\text{Cl}_2$ (1:1, for

the experiments carried out at $-100\text{ }^{\circ}\text{C}$), were used to minimize intermolecular dipole-dipole relaxation interactions. This has been discussed in more detail in the previous section on NOE.

At least seven spectra were collected for each sample in the T_1 measurements. The spectra were obtained by varying the delay time $D(t_1)$ from 0.0 s to $5T_1$. The T_1 's of the hydrides can then be obtained by the exponential fit method. From the Bloch equation:

$$\frac{dM_z}{dt} = \frac{-1}{T_1}(M_z - M_0)$$

where M_z = magnetization in the z-axis;

M_0 = magnetization at time zero;

after integration, the exponential recovery of the magnetization can be written in terms of the signal intensity, I , since the magnetization is proportional to I :¹⁷

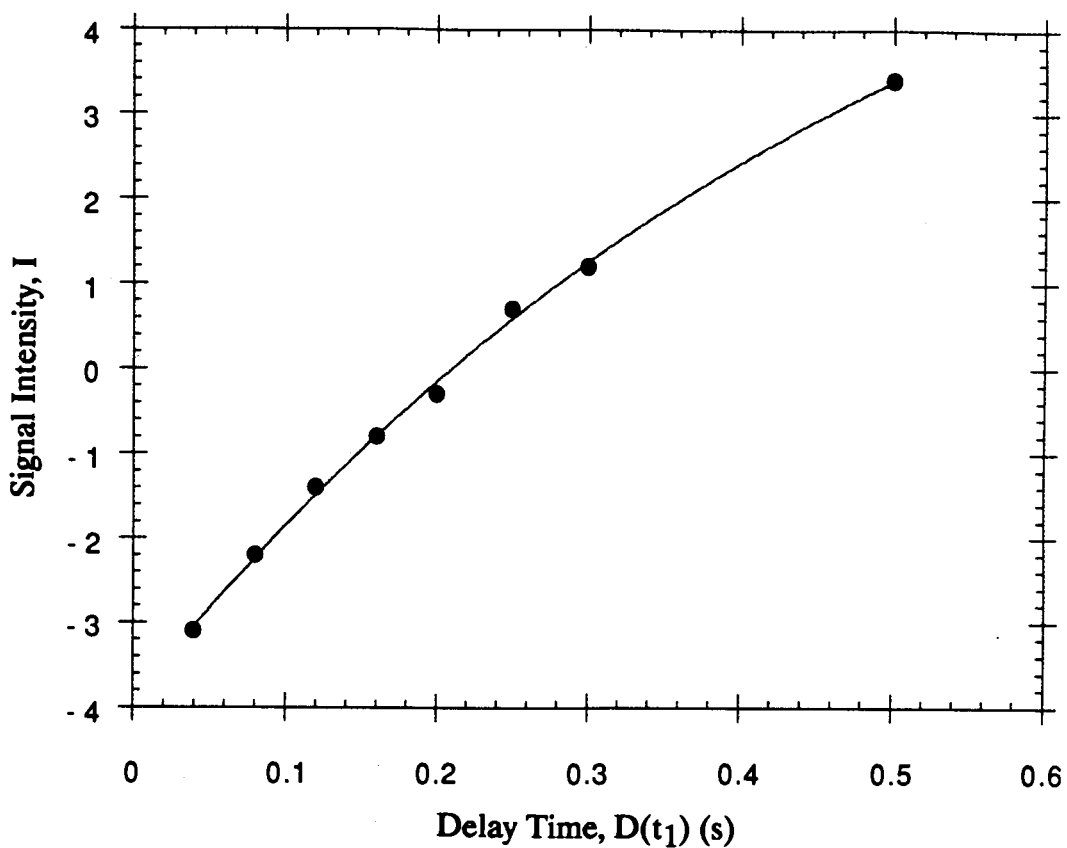
$$I_t = I_{\infty} - 2I_{\infty} \exp\left[-\frac{D(t_1)}{T_1}\right]$$

..... Eqn. 1.1

where I_t = signal intensity at time t ;

I_{∞} = signal intensity at time ∞ ;

When the intensity of the hydride signal is plotted against the delay time $D(t_1)$, the values of I_{∞} and $-1/T_1$ can be calculated from the exponential fit program. The value of T_1 can therefore be obtained. This is shown in Fig. 1.31 and 1.32 for the hydrides of $\text{Os}_3(\mu\text{-H})_2(\text{CO})_9(\text{CNBu}^t)$ (2 in

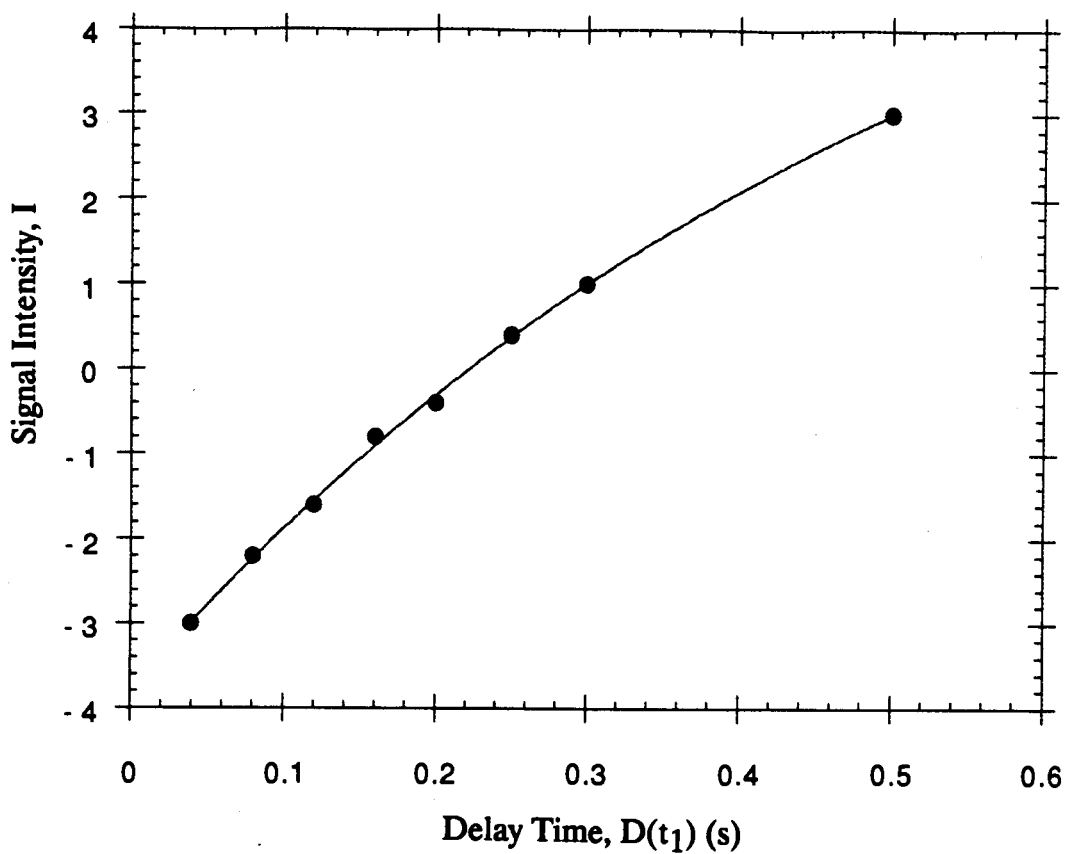


$$I_{\infty} = 8.05 \pm 1.01$$

$$\frac{1}{T_1} = 1.89 \pm 0.25 \text{ s}^{-1}$$

$$T_1 = 0.53 \pm 0.06 \text{ s}$$

Fig. 1.31 T_1 determination of the hydride signal, to the high field of the ^1H NMR spectrum, of $\text{Os}_3(\mu\text{-H})_2(\text{CO})_9(\text{CNBu}^t)$ (2) by the exponential method.



$$I_{\infty} = 7.46 \pm 0.73$$

$$\frac{1}{T_1} = 1.85 \pm 0.19 \text{ s}^{-1}$$

$$T_1 = 0.54 \pm 0.06 \text{ s}$$

Fig. 1.32 T_1 determination of the hydride signal, to the low field of the ^1H NMR spectrum, of $\text{Os}_3(\mu\text{-H})_2(\text{CO})_9(\text{CNBu}^t)$ (2) by the exponential method.

Fig. 1.33). The T_1 's of the hydrides were found to be 0.53 ± 0.06 s and 0.54 ± 0.06 s for the high and the low field signals, respectively (see Discussion).

The T_1 's of the hydrides can also be obtained from the stacked plot (Fig. 1.34). The delay time that gives a signal of zero intensity, $D(t_1)_0$, can be related to the T_1 relaxation time by the following:¹⁵

$$D(t_1)_0 = T_1 \ln 2 \quad \dots\dots \text{Eqn. 1.2}$$

Although the latter method of T_1 measurements is fast, it is subject to a larger uncertainty. All values of T_1 's reported in this thesis were obtained by the latter method.

1B.3 Results and Discussion

The T_1 relaxation time reflects the efficiency of the relaxation of a nucleus. The dipole-dipole relaxation mechanism requires magnetic fields which are fluctuating at the appropriate frequency to cause relaxation. In diamagnetic molecules, the magnetic fields are usually due to the magnetic moments of other hydrogen atoms as the molecule tumbles in solution. This is because hydrogen, i.e. the proton, has the largest magnetic moment among the elements. The magnetic fields generated by other nuclei are almost negligible in comparison. The efficiency of the dipole-dipole interaction depends on the strength and frequency of the fluctuating field which depend on three

factors: the distance between the nuclei in question, r ; the correlation time, τ_c ; and the nature of the nuclei such as the magnetic moment and, in turn, the gyromagnetic ratio, γ . The T_1 relaxation time can be expressed by the following equation:¹³

$$\frac{1}{T_1} = \frac{2}{3} \gamma^2 \langle H_L \rangle^2 \tau_c / (1 + \omega_0^2 \tau_c^2) \quad \dots\dots \text{Eqn. 1.3}$$

where $\langle H_L \rangle$ is the average value of the local magnetic field ($\langle H_L \rangle^2 \propto 1/r^6$), ω_0 is the Larmor frequency of the nuclear spin. All nuclear interactions which contribute to the $\langle H_L \rangle$ term can cause relaxation (except quadrupole relaxation). In the case of the intramolecular dipole-dipole relaxation, T_1^{DD} , it can be expressed as follows:

$$\frac{1}{T_1^{DD}} = \frac{3}{10} \frac{\gamma^4 \hbar^2}{\sum r^6} \left[\frac{\tau_c}{1 + \omega_0^2 \tau_c^2} + \frac{4\tau_c}{1 + 4\omega_0^2 \tau_c^2} \right] \quad \dots\dots \text{Eqn. 1.4}$$

Depending on the correlation time, τ_c , two extreme cases can be considered from Eqn. 1.3:

1. In the case of small molecules in non-viscous liquids where isotropic tumbling is fast, $\omega_0^2 \tau_c^2 \ll 1$ (i.e., the extreme narrowing condition), the expression of T_1^{DD} can be approximated as follows:

$$\frac{1}{T_1^{DD}} = \frac{3}{2} \frac{\gamma^4 \hbar^2}{\sum r^6} \quad \dots\dots \text{Eqn. 1.5}$$

The correlation time τ_c can be related to the size of the molecule in terms of the radius of that molecule, R:¹³

$$\tau_c = \frac{4\pi\eta R^3}{3kT} \quad \dots\dots \text{Eqn. 1.6}$$

where η is the viscosity of the solvent at temperature T, and k is the Boltzmann constant. For a small spherical molecule, the dipole-dipole relaxation time T_1 is, therefore, inversely proportional to the correlation time.

2. For molecules in viscous liquid or for large molecules, the correlation time becomes long (Eqn. 1.6) and the extreme narrowing condition is no longer valid, i.e., $\omega_0^2 \tau_c^2 \gg 1$. In this case T_1 is approximated as follows:

$$\frac{1}{T_1^{DD}} = \frac{3}{5} \frac{\gamma^4 \hbar^2}{\sum r^6} \left[\frac{1}{\omega_0^2 \tau_c} \right] \quad \dots\dots \text{Eqn. 1.7}$$

The relationship of the T_1 relaxation rate ($R_1 = 1/T_1$) with the correlation time τ_c at different magnetic fields is shown in Fig. 1.33. The details of the figure are discussed in Appendix I. It is important that the extreme narrowing condition applies to the cluster compounds when T_1 values are compared between compounds. This will be discussed

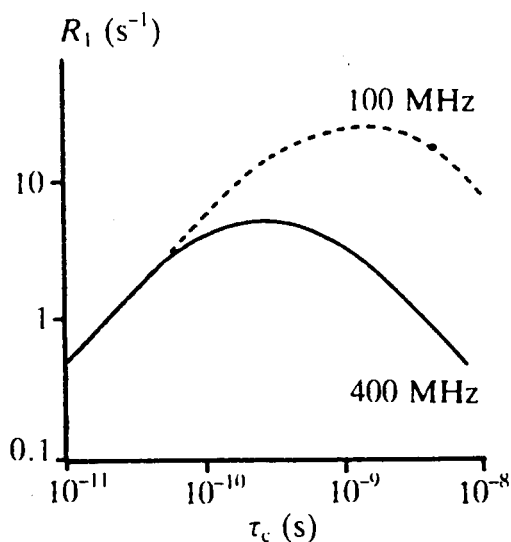


Fig. 1.33 The relationship of relaxation rate, R_1 ($R_1 = 1/T_1$), with correlation time, τ_c , at different magnetic field.¹⁷

further in the section on $\text{Os}_3(\mu\text{-H})_2(\text{CO})_{10}$.

There are five mechanisms of relaxation to a spin that will contribute to the observed T_1 : dipole-dipole interactions with other nuclei, chemical shift anisotropy, spin-rotation interactions, scalar interactions, and interactions with unpaired electrons. Since only diamagnetic molecules were used in this study and molecular oxygen was excluded in the NMR samples, the relaxation pathway which involves the interaction with unpaired electrons can be neglected in this discussion. The other four types of interactions may contribute to the observed T_1 relaxation times for the hydride ligands of the cluster

compounds. The T_1 values reported in this thesis may, therefore, not be entirely due to dipole-dipole interactions. However, among the four interactions only the dipole-dipole interaction is distance-related (Eqn. 1.4).

The structure of the cluster compounds and the T_1 values of the hydrides are shown in Fig. 1.35 to 1.37, 1.39 and 1.40. A typical stack plot for the T_1 determination of the hydride ligands in the two isomers of $\text{HOs}_3(\mu\text{-H})(\text{CO})_{10}\text{(CNBu}^t\text{)}$ is shown in Fig. 1.34. The spectra were acquired with varied delay times, $D(t_1)$ (shown on each spectrum), as mentioned before. The T_1 values of the hydrides were calculated with Eqn. 1.2. For the major isomer of $\text{HOs}_3(\mu\text{-H})(\text{CO})_{10}\text{(CNBu}^t\text{)}$ (5) the T_1 of both hydrides is approximately 0.75 s; the T_1 of both hydrides of the minor isomer (6) is about 0.79 s.

The T_1 relaxation times of the hydrides in the clusters reported in this thesis range from 0.16 s to 2.2 s calculated from Eqn. 1.2. It appears reasonable that interactions of the hydride ligand with the neighbouring groups such as methyls, phenyls or other hydride ligands are responsible for the short T_1 's.

The hydridotriosmium cluster $\text{Os}_3(\mu\text{-H})_2(\text{CO})_{10}$ (1, Fig. 1.35) has two equivalent bridging hydrides. The T_1 of the hydrides is 1.2 s when measured in CD_2Cl_2 at -70°C . This value is in agreement with the value of 1.0 s at -60°C and 6.5 s at $+20^\circ\text{C}$ measured by Aime and co-workers.³⁹ The

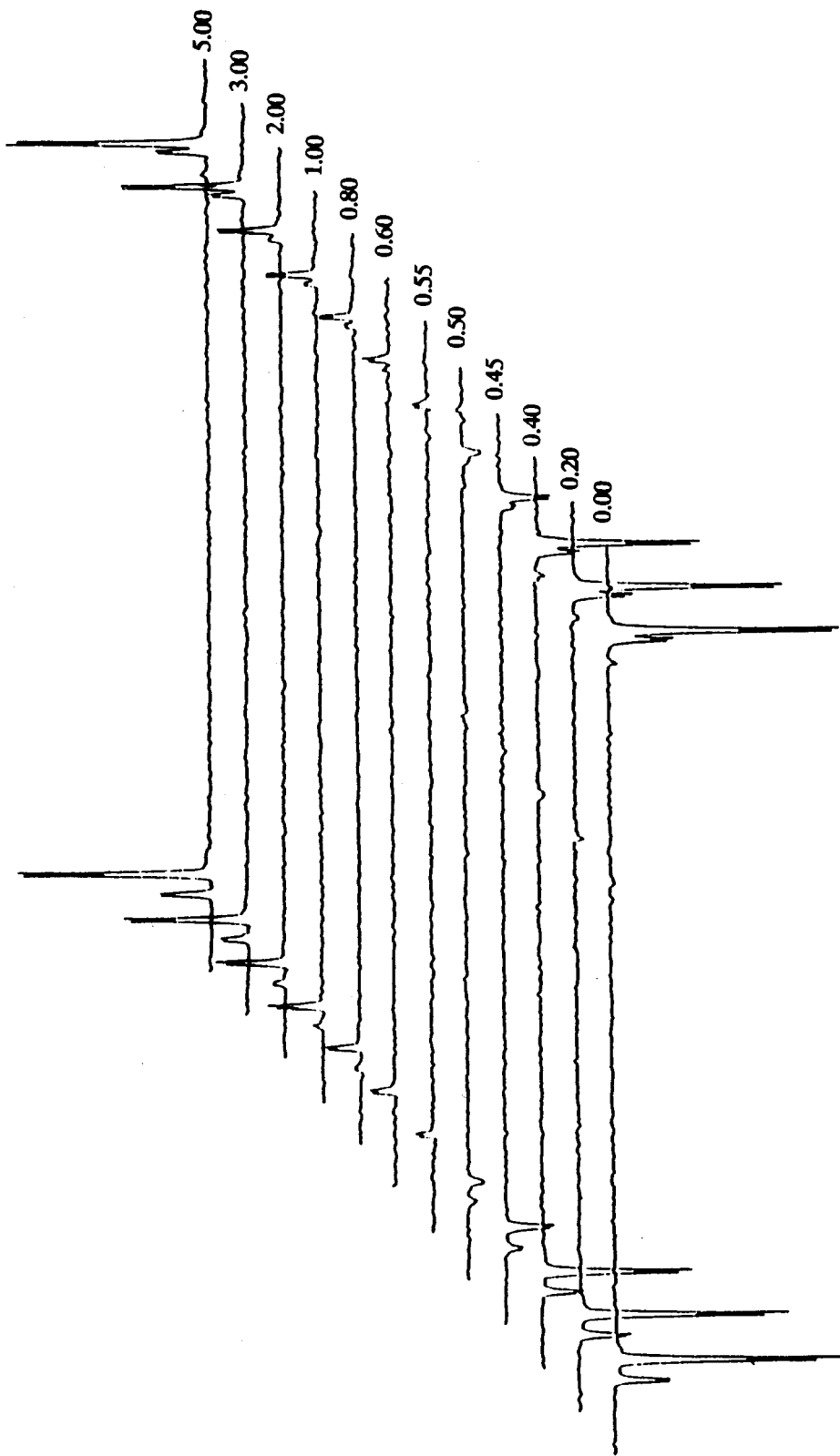


Fig. 1.34 Stacked plot of an inversion-recovery experiment for the hydride nuclei of $\text{HOs}_3(\mu\text{-H})(\text{CO})_{10}(\text{CNBut})$ measured at -70°C at 100.13 MHz. The values reported at the right of the spectra are the delay times, $D(t_1)$, in seconds.

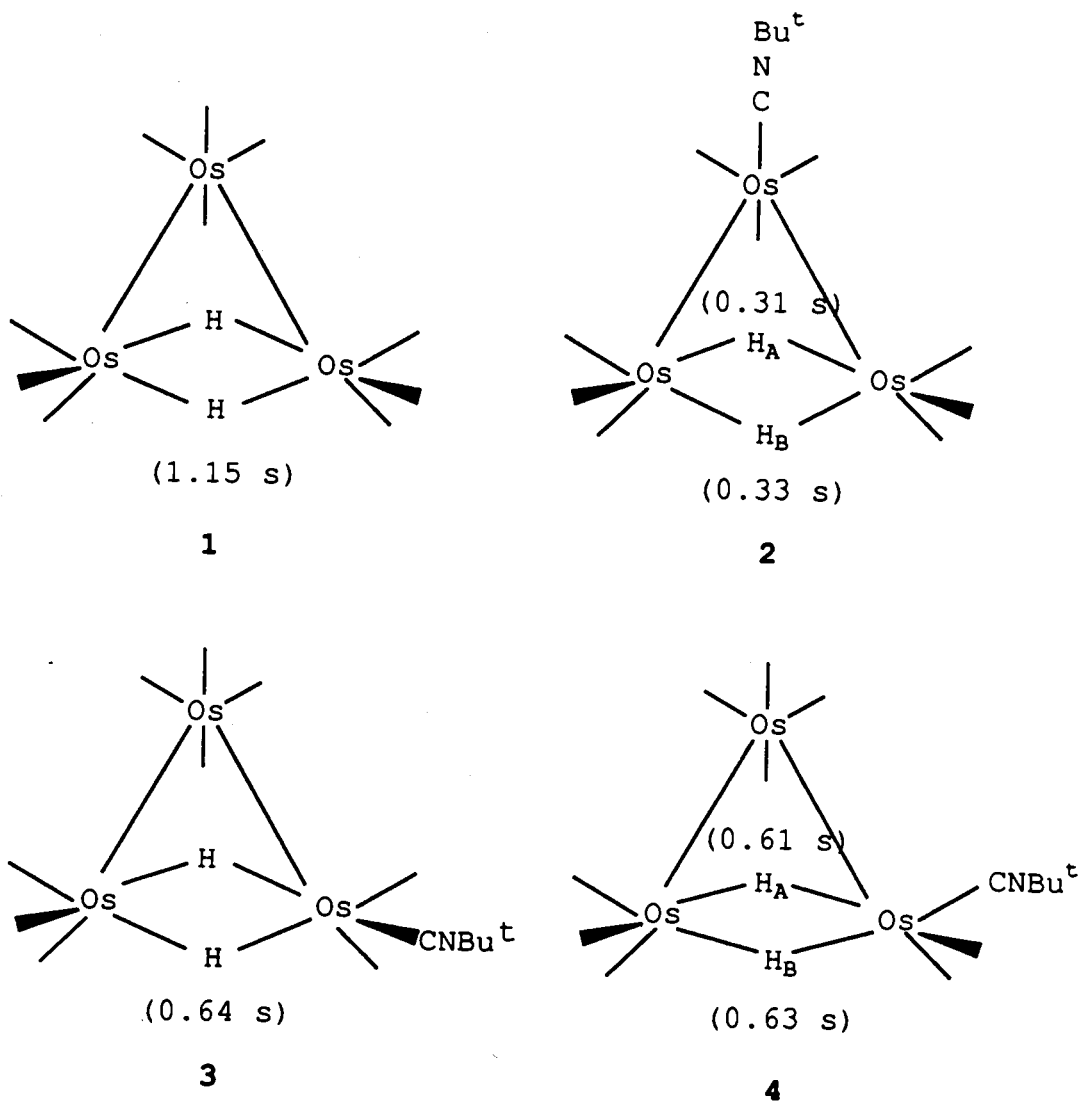


Fig. 1.35 The structures and the measured T_1 's of the hydrido-osmium clusters 1 to 4 (carbonyl ligands are omitted for clarity).

T_1 of the hydride of the monodeuterated species of 1, i.e., $\text{Os}_3(\mu\text{-D})(\mu\text{-H})(\text{CO})_{10}$, is 30.2 s when measured at +20 °C.³⁹ Deuterium possesses a smaller magnetic moment (1.2126 m²A) than hydrogen (4.83724 m²A), and therefore is a less effective relaxation species for dipole-dipole relaxation. The dramatic increase of the T_1 value of the hydride in $\text{Os}_3(\mu\text{-D})(\mu\text{-H})(\text{CO})_{10}$ compared to that in $\text{Os}_3(\mu\text{-H})_2(\text{CO})_{10}$ is a good indication that the main relaxation pathway of the hydrides of 1 is through dipole-dipole interaction between the two bridging hydride ligands. The distance of the two hydrides of 1 from the neutron diffraction study is 2.38 Å.⁴⁰ The correlation time of 1 was calculated to be about 33 ps at 20 °C (from Eqn. 1.5). Furthermore, the viscosity of the solvent, CD_2Cl_2 , at -70 °C is about 3.5 times more viscous than that at 20 °C,⁴¹ the correlation time will, therefore, be about five times longer at -70 °C (from Eqn. 1.6). The τ_c is, therefore, in the range of 10^{-10} to 10^{-9} s, which is in the fast correlation time limit. This implies that the tumbling of the molecule is isotropic and the extreme narrowing condition can be assumed for 1. Although the sizes of the cluster compounds studied were slightly larger than 1 the extreme narrowing condition was also assumed in each case.

The cluster $\text{Os}_3(\mu\text{-H})_2(\text{CO})_9(\text{CNBu}^t)$ has three isomers in solution at equilibrium: 2, 3 and 4 as shown in Fig. 1.35. They are structurally similar to 1 in having $\text{Os}(\mu\text{-H})_2\text{Os}$

linkages (see Chapter 4 for details). The hydrides, however, exhibit much shorter T_1 's at -70°C than those of 1. The shorter T_1 's in these hydrides are attributed to dipole-dipole interactions of the hydrides with the methyl hydrogens. The bridging hydride H_A in 2 is closer to the tert-butyl group than hydride H_B and H_A is therefore expected to have a shorter T_1 (the distance of H_A to the closest methyl hydrogen in the solid state is about 3.0 \AA). This argument was used in the assignment of the hydride signals in the ^1H NMR spectrum of 2: the signal which exhibits a T_1 of 0.31 s is tentatively assigned to H_A since the T_1 is slightly shorter than the T_1 of the other signal (0.33 s) (details of the assignment will be discussed in Chapter 4). The T_1 's of the hydrides were also measured by the exponential method (Fig. 1.31 and 1.32). However, longer T_1 's of $0.53 \pm 0.06\text{ s}$ and $0.54 \pm 0.06\text{ s}$ were obtained respectively for the signals which were tentatively assigned to the hydrides H_A and H_B . The most likely explanation for the deviation of the T_1 values between the two methods may be due to the error in the applied π pulse in the inversion-recovery pulse sequence. Since the T_1 of the hydrides of $\text{Os}_3(\mu\text{-H})_2(\text{CO})_{10}$ is in consistent with the literature value, this may indicate that there is errors both in the literature T_1 values and the T_1 values reported here.

The T_1 's of the two hydrides of 3 and 4 are all longer than those in 2. This is attributed to the decreased

(but not negligible) contribution of dipole-dipole interaction between the methyl hydrogens and the hydrides. The tert-butyl group in both clusters are remote from the bridging hydrides at a distance of about 4 Å. It is noted that the magnitude of the dipolar interaction is inversely proportional to the sixth power of the distance of the nuclei in question (see the NOE section).

Two isomers of $\text{HOs}_3(\mu\text{-H})(\text{CO})_{10}(\text{CNBu}^t)$ are present in solution (5 and 6, major and minor isomers, respectively, as shown in Fig. 1.36). A stack plot of the NMR spectra for the T_1 determinations for 5 and 6 is shown in Fig. 1.34. The T_1 's for the terminal and the bridging hydrides are essentially the same in each isomer (0.75 s for 5 and 0.79 s for 6). The distance between the two hydrides in 5 and 6 is 2.4 Å which is similar to that in 1. On the other hand, the T_1 's of the hydrides in 5 and 6 are shorter than that of 1 (1.2 s). This indicates that the hydrides in 5 and 6 relax also through interaction with the tert-butyl group, similar to the hydrides in the three isomers of $\text{Os}_3(\mu\text{-H})_2(\text{CO})_9(\text{CNBu}^t)$.

The cluster $\text{HOs}_3(\mu\text{-H})(\text{CO})_{10}(\text{PMe}_3)$ (7) has a similar structure as 5 and 6 except that the PMe_3 ligand is located in an equatorial position. The T_1 for the hydrides were determined at -100°C (the lower temperature was necessary in order to stop the H-H exchange in the cluster, see the NOE section). The T_1 values of both hydrides are shorter

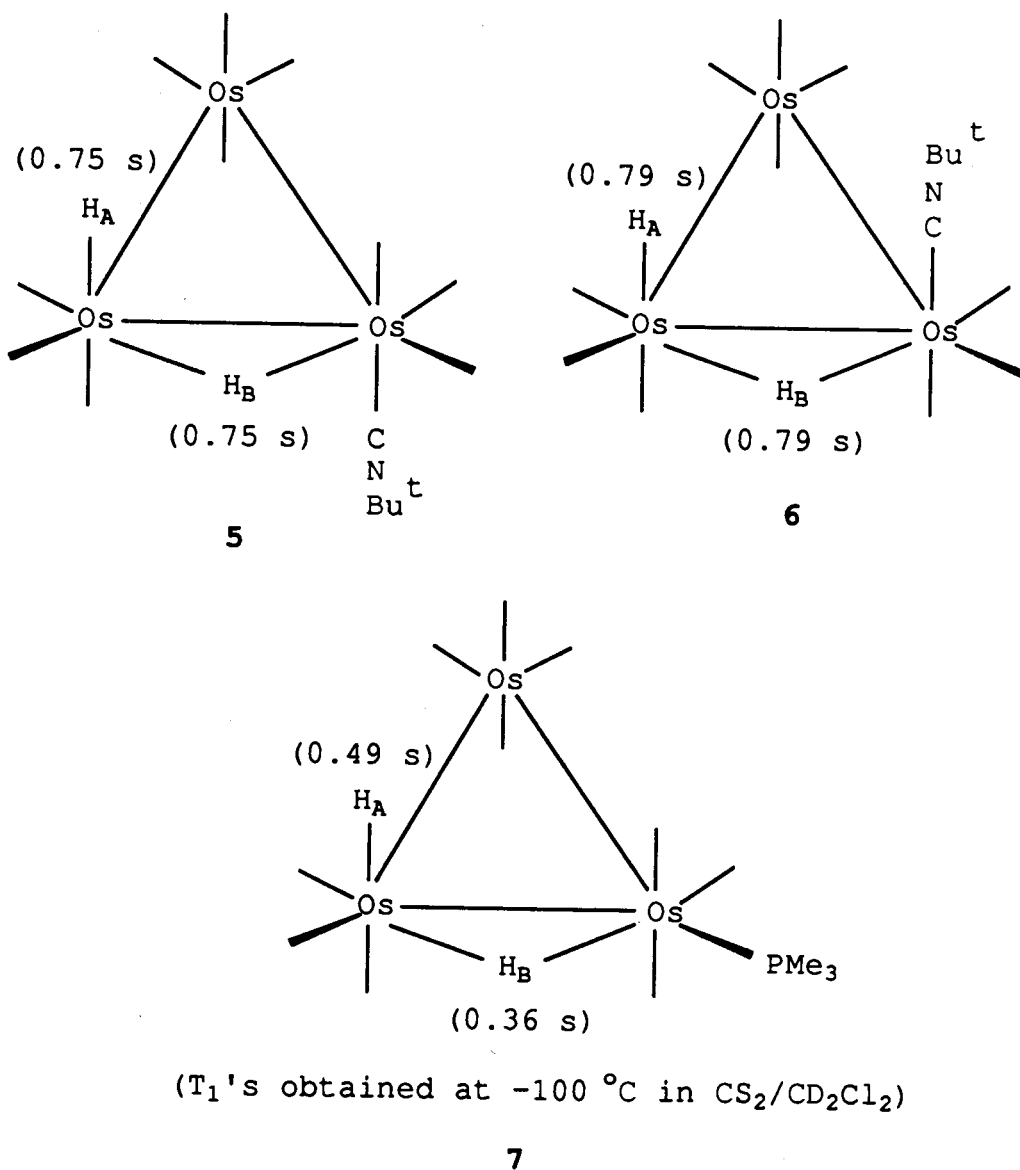
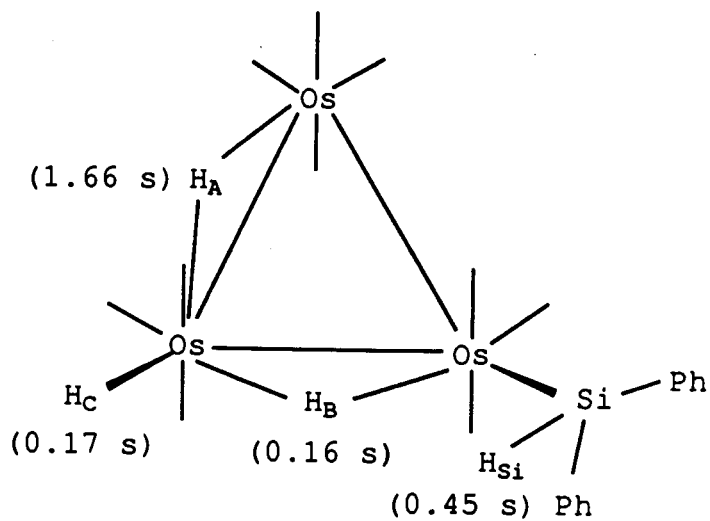


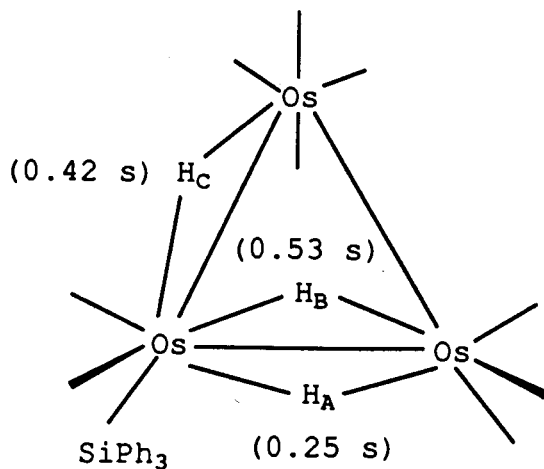
Fig. 1.36 The structures and the measured T_1 's of the hydrido-osmium clusters 5 to 7 (carbonyl ligands are omitted for clarity).

compared to the same hydrides in 5 and 6. This is due to the low temperature condition when the T_1 's were measured. The T_1 for the bridging hydride H_B (0.36 s) is shorter than that for the terminal hydride H_A (0.49 s). This is attributed to additional dipole-dipole interaction of H_B to both the phosphorus atom (H_B is about 3 Å away from the phosphorus atom in the solid state) and the hydrogen atoms of the methyl groups.

The hydride ligands of $\text{HOS}_3(\mu\text{-H})_2(\text{CO})_{10}(\text{SiHPh}_2)$ (8, Fig. 1.37), exhibit both short and long T_1 's. The bridging hydride H_A is surrounded by six carbonyl ligands and it is remote from other hydrogen atoms in the structure (it is more than 3 Å from the other two hydride ligands in the molecule). The lack of effective interaction with other relaxation sources is, therefore, believed the reason for the long T_1 of 1.66 s for H_A . This is a good indication that direct dipole-dipole interactions of H_A with the other hydrides, H_B and H_C , are small. The assumption of a negligible interaction of H_A with H_B and H_C used in the calculation of the NOE in $\text{HOS}_3(\mu\text{-H})_2(\text{CO})_{10}(\text{SiHPh}_2)$ was, therefore, probably justified. The short T_1 of H_B is probably the result of interaction of this hydride with H_C , $\text{H}(\text{Si})$ and, possibly, with the hydrogen atoms of the phenyl groups. It will be shown later that phenyl hydrogen atoms are an effective relaxation source for hydrides when present in clusters. The terminal hydride H_C also exhibits a short



8



9

Fig. 1.37 The structures and the measured T_1 's of the hydrido-osmium clusters 8 to 9 (carbonyl ligands are omitted for clarity).

T_1 of 0.17 s. This is attributed to the interaction of H_C with hydride H_B with which it is in close proximity.

The T_1 relaxation times of hydrides, as mentioned before, can be helpful in the assignment of 1H NMR signals. This is demonstrated for $Os_3(\mu-H)_3(CO)_9(SiPh_3)$ (9). The X-ray crystal structure and the 1H NMR spectrum of 9 are shown in Fig. 1.38. From the observed Os-H coupling constants the 1H NMR resonance at δ -12.45 was assigned to the hydride H_C .³⁵ The other two hydride signals at δ -8.56 and -12.56, however, could not be assigned. The X-ray crystal structure of 9 shows that the triphenylsilyl ligand is at a pseudoaxial position of Os(1) and, therefore, is closer to H_A than to H_B . Due to a better interaction of H_A with the phenyl hydrogen atoms, the relaxation of H_A is expected to be more efficient than that of H_B and should, therefore, lead to a shorter T_1 for H_A . For this reason, the 1H NMR resonance at δ -12.56, which exhibited a T_1 of 0.25 s, was assigned to hydride H_A whereas the resonance at δ -8.56, with a significantly longer T_1 of 0.53 s, was assigned to hydride H_B . Only the interactions of the hydrides and the phenyl hydrogen atoms should vary the T_1 's since the distances between the three hydrides in 9 are almost the same (see the NOE section), and, therefore, the dipolar interactions should be similar. The T_1 of H_A is also similar to the T_1 (of 0.30 s) for the bridging hydride H_{13} in $Os_3(\mu-H)_3(CO)_9(SiPh_3)_3$ (13, Fig. 1.40) which has a

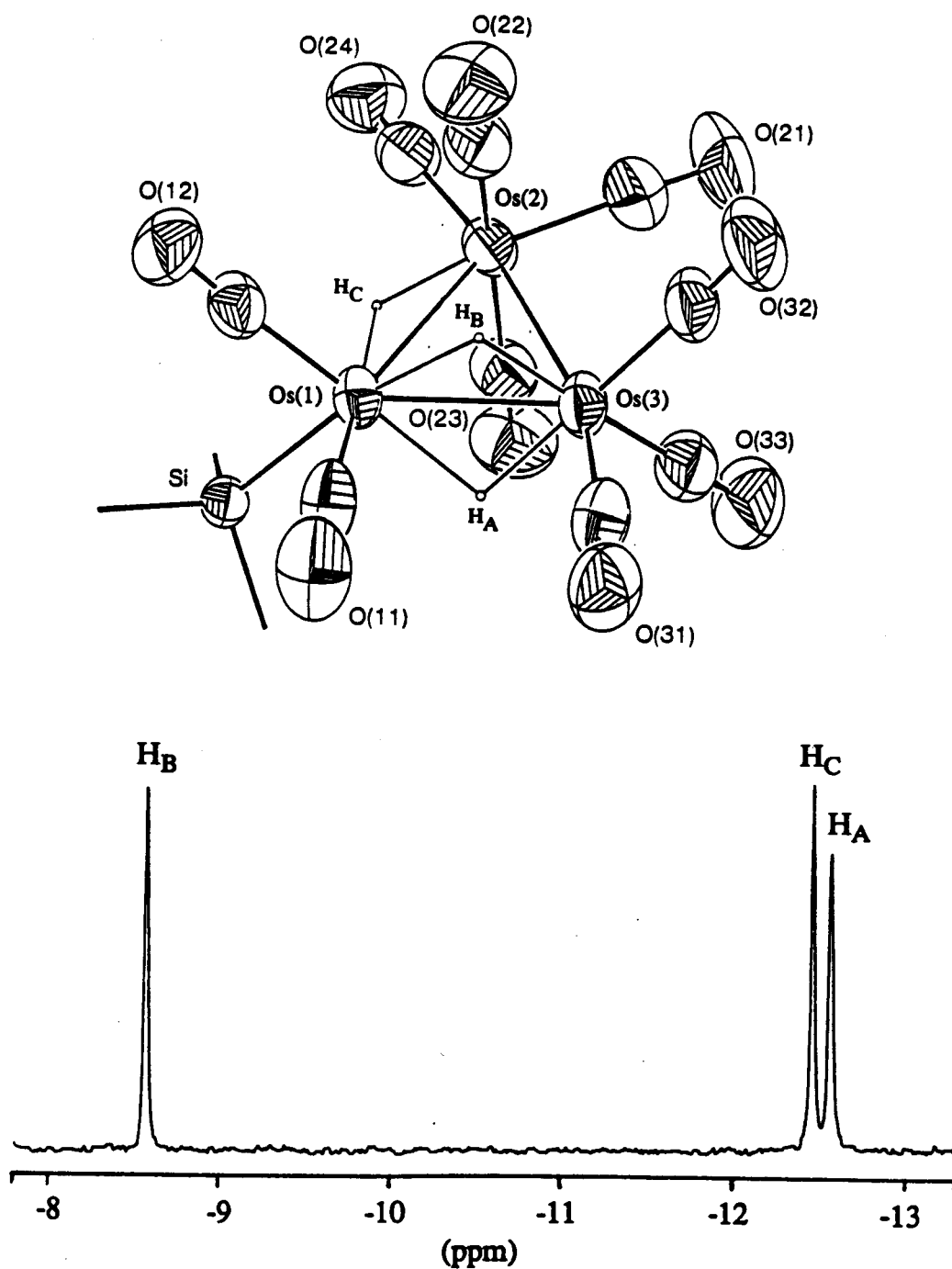


Fig. 1.38 The molecular structure and the ^1H NMR spectrum (hydride region, at -70°C) of $\text{Os}_3(\mu\text{-H})_3(\text{CO})_9(\text{SiPh}_3)$.

similar distance between the hydride and the SiPh₃ group as in 9. Furthermore, the T₁ of the hydride H_C of Os₃(μ-H)₃(CO)₉(SiPh₃) is also of the same order of magnitude as those of H_A and H_B. The H_C···SiPh₃ distance is longer than that of H_A···SiPh₃, but shorter than that of H_B···SiPh₃. Accordingly, the T₁ of H_C (0.42 s) lies between those of H_A and H_B.

The cluster Os₃(μ-H)₂(CO)₁₀(SnMe₃)₂ exists as two isomers in solution. Only one of the isomers, i.e. 10, has been characterized by X-ray crystallography (Fig. 1.39).³⁰ A T₁ of 1.40 s was measured for the two hydride ligands of 10 which indicates that the hydrides have similar arrangements of neighbouring groups which is consistent with the structure found in the solid state. Very different T₁ values were, however, observed for the hydrides of other isomer, 11. (Isomer 11 only exists in solution.) From the results of the NOE experiment and the Sn-H couplings observed in the ¹H NMR spectrum of Os₃(μ-H)₂(CO)₁₀(SnMe₃)₂, the structure 11 was proposed (refer to the NOE section). The structure is also supported by the T₁ measurements for the hydride ligands. The ¹H NMR resonance at δ -16.7 (Fig. 1.19) which shows no couplings to the Sn atoms exhibits a T₁ of 2.2 s. The long T₁ indicates that this hydride is remote from any effective relaxation source. This is, therefore, assigned to a hydride H_C in 11. This is similar to hydride H_A in 8. On the other hand, the ¹H NMR

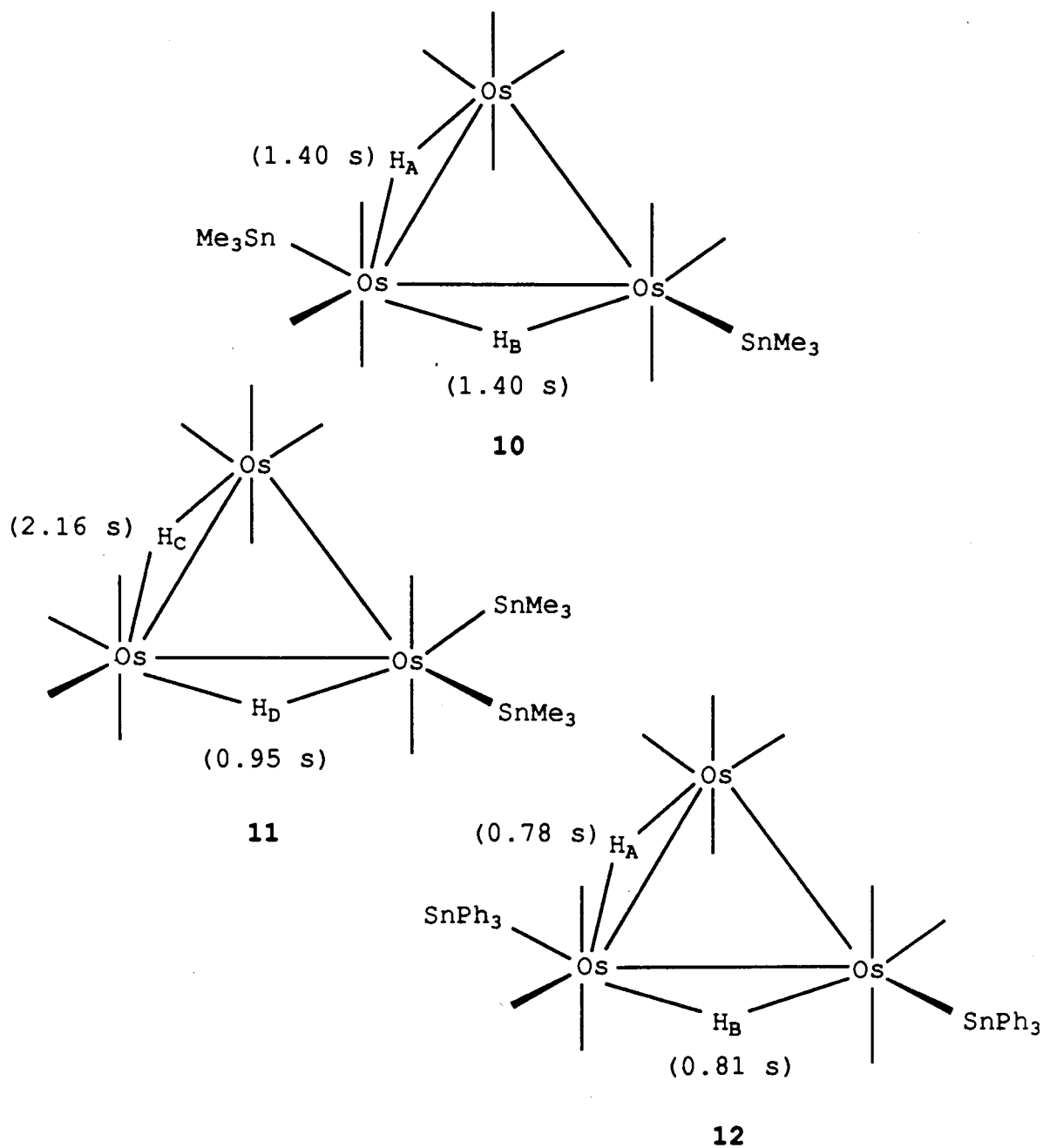


Fig. 1.39 The structures and the measured T_1 's of the hydrido-osmium clusters 10 to 12 (carbonyl ligands are omitted for clarity).

signal at δ -18.7 which shows two Sn-H couplings (assigned to H_D) has a T_1 of 0.95 s which is shorter than those of the hydrides H_A and H_B of 10. This may be due to the steric crowding of the two SnMe_3 groups (both in equatorial positions) such that one of the SnMe_3 groups is much closer to the hydride H_D than in isomer 10. This in turn will result in larger dipolar interactions between the hydride and the methyl hydrogens and, therefore, a shorter T_1 for H_D .

The cluster $\text{Os}_3(\mu\text{-H})_2(\text{CO})_{10}(\text{SnPh}_3)_2$ (12) is an analogue of 10. The T_1 's of the hydrides, H_A and H_B , are shorter than those measured in the trimethyltin cogener. This is attributed to more efficient interaction of the hydrides with the phenyl groups in 12 than the hydrides with the methyl groups in 10. This was also found for the clusters 13, 14 and 15 reported below.

The more effective relaxation induced by phenyl groups is observed in the silyl-substituted Os_3 clusters $\text{Os}_3(\mu\text{-H})_3(\text{CO})_9(\text{SiR}_3)_3$, where $R_3 = \text{Ph}_3$ (13), $(\text{CH}_3)\text{Cl}_2$ (14) and Cl_3 (15) (Fig. 1.40). The structures of 14⁴² and 15⁴³ have been established by X-ray crystallography. (The structure of 13 was not determined but is assumed to be similar to 14 and 15 on the basis of their similar IR and ^1H NMR spectra.) The molecules have C_3 symmetry with a hydride bridging each Os-Os bond. Each osmium has a silyl ligand bound in an equatorial site. The three bridging hydrides in

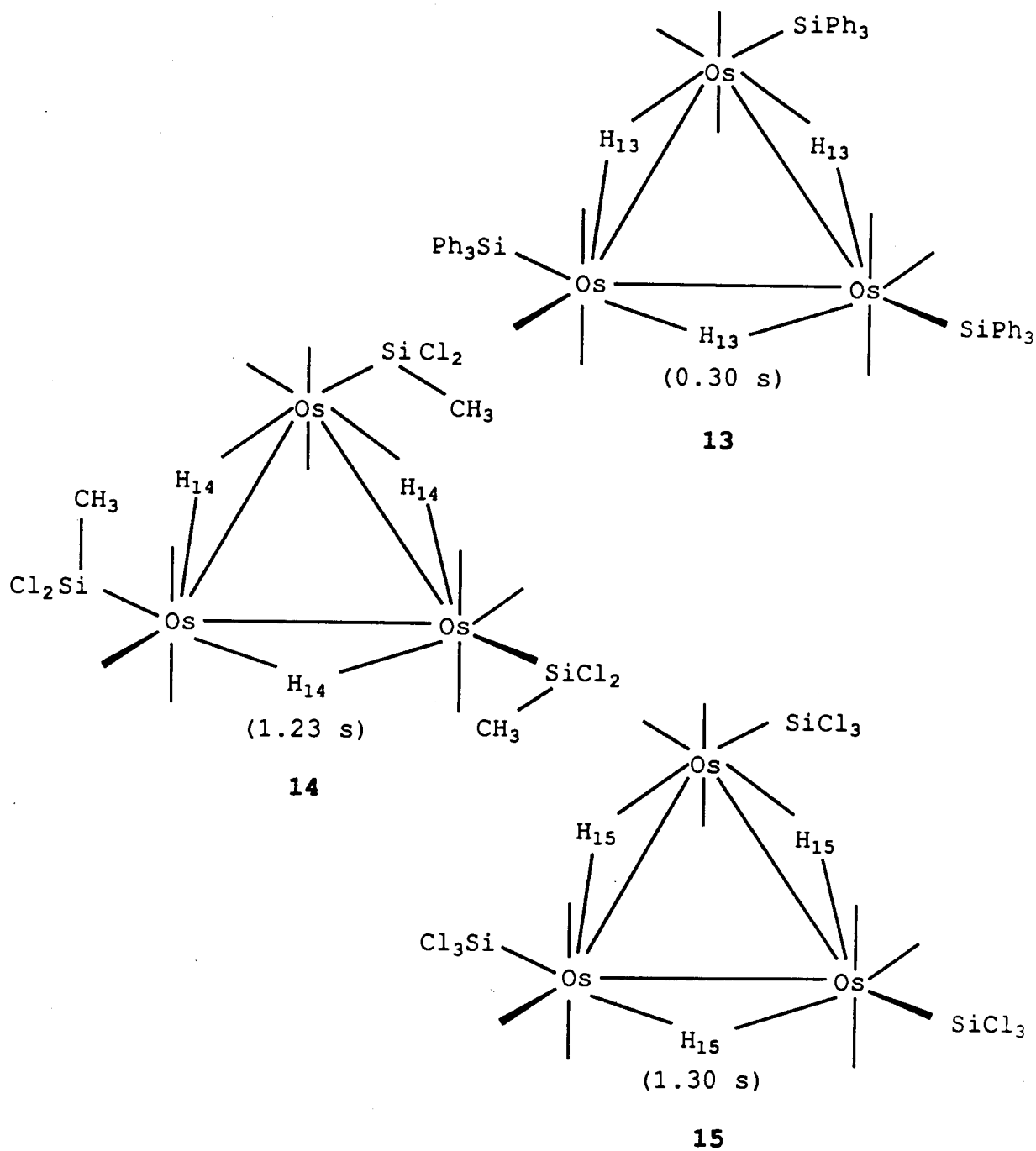


Fig. 1.40 The structures and the measured T₁'s of the hydrido-osmium clusters 13 to 15 (carbonyl ligands are omitted for clarity).

each of the clusters are equivalent. A silyl ligand is in a cis arrangement with a given hydride ligand.

The hydrides H₁₃ of the triphenylsilyl derivatives, **13**, exhibits the shortest T₁ of 0.30 s of the three clusters. The hydrides H₁₅ of the trichlorosilyl derivative show the longest T₁ of 1.30 s. This is because the chloro ligands are not an efficient relaxation source for the hydrides. When one of the chloro ligands of **15** was replaced by a methyl group, i.e., the dichloromethyl derivative (**14**), the hydrides H₁₄ exhibit a shorter T₁ of 1.23 s due to the interaction with the methyl group.

1B.4 Conclusion

It was originally thought that transition metal hydrides had long T₁'s³⁸ but these results agree with other recent studies that show that the T₁'s are short and comparable to the T₁'s of organic molecules.^{38,39} This study also shows that T₁ measurements can provide valuable information on the structure of hydridoosmium clusters and be useful in the assignment of ¹H NMR resonances of such compounds.

Chapter 2

Nonrigidity of $\text{Os}_3(\text{CO})_{11}(\text{ER}_3)$ and the Donor Ability of Group 15 Ligands.

2.1 Introduction

One of the fascinating properties exhibited by metal carbonyl cluster compounds is the stereochemical nonrigidity they often exhibit.¹⁻⁵ This is no better illustrated than with the carbonyl cluster compounds of the group 8 metals. The trinuclear binary carbonyls of iron and ruthenium, $\text{Fe}_3(\mu\text{-CO})_2(\text{CO})_{10}$ and $\text{Ru}_3(\text{CO})_{12}$ respectively, exhibit a single ^{13}C NMR resonance in solution even at very low temperatures.^{44,45} This is indicative of rapid carbonyl exchange such that they become equivalent on the NMR time scale. On the other hand, the osmium analogue, $\text{Os}_3(\text{CO})_{12}$, exhibits two ^{13}C NMR resonances in solution at room temperature attributable to the axial and equatorial carbonyl ligands. Warming the solution to above $\approx 70^\circ\text{C}$ causes coalescence of the two signals. An activation barrier of $16.7\text{ kcal mol}^{-1}$ has been estimated for the axial-equatorial carbonyl exchange.⁴⁵

Because of the high symmetry of $\text{Os}_3(\text{CO})_{12}$ there are several possible mechanisms that can account for the carbonyl exchange. The carbonyls of $\text{Os}_3(\text{CO})_{11}(\text{PEt}_3)$ also undergo exchange.⁴⁶ The pattern of collapse of the ^{13}C NMR resonances is consistent with terminal-bridge carbonyl

exchange in the vertical plane cis to the phosphine ligand (see Discussion section). A similar pattern of collapse was observed in $\text{Os}_3(\text{CO})_{11}[\text{P}(\text{OMe})_3]$ where a barrier to the exchange of $12.4 \pm 0.4 \text{ kcal mol}^{-1}$ was estimated.⁴⁷ The lower barrier to the exchange compared to that in $\text{Os}_3(\text{CO})_{12}$ was rationalized in terms of the relative energies needed to form the intermediate with bridging carbonyls in the two cases. This is discussed in more detail below.

In the study reported here, the effect on the CO exchange processes in some $\text{Os}_3(\text{CO})_{11}(\text{ER}_3)$ clusters has been investigated as the electronic properties of ER_3 are changed. It is well-known that changing the substituents (R) on a phosphorus ligand PR_3 causes changes to its properties when it acts as a ligand to a transition metal. This has been rationalized in terms of both the electronic and steric effects of the ligand.⁴⁸ The electronic factor of the phosphorus ligands was measured by the A_1 stretching frequency of CO in the infrared spectrum of the appropriate $\text{Ni}(\text{CO})_3(\text{PR}_3)$ complex. The steric factor was measured by the cone angle of the ligand.⁴⁸ Bodner later demonstrated that the electronic effect parameter of group 15 ligands (ER_3) could be measured by the ^{13}C chemical shifts of the cis carbonyls in $\text{M}(\text{CO})_5(\text{ER}_3)$ ($\text{M} = \text{Cr}, \text{Mo}$), $\text{Ni}(\text{CO})_3(\text{ER}_3)$ and $(\eta^6\text{-C}_6\text{H}_6)\text{Cr}(\text{CO})_2(\text{ER}_3)$ compounds.⁴⁹ There is some preference to use the NMR parameters since the ^{13}C chemical shifts could be measured more precisely than the carbonyl

stretching frequencies. (For most ligands there is a linear relationship between the two parameters.) Both the IR and NMR parameters are believed to characterize the ratio of the σ basicity to π acidity, i.e., the donor/acceptor ratio of the ligand ER_3 .

2.2 Experimental Section

2.2.1 General Procedure

Unless otherwise stated, purification of solvents, reactions, and manipulation of compounds were carried out under a nitrogen atmosphere with use of standard Schlenk techniques. Hydrocarbon solvents and methanol were refluxed over potassium and magnesium respectively, distilled, and stored over type 4A molecular sieves before use. Dichloromethane was dried similarly except that P_2O_5 was used as the drying agent. Before use, trimethyl phosphite and trimethylphosphine as obtained commercially were transferred under nitrogen to 100-mL round-bottom flasks (fitted with a Teflon valve); they were pure by $^{31}P\{^1H\}$ NMR spectroscopy. Other group 15 ligands and acetonitrile were used as received from the manufacturers. Trimethylamine oxide (Me_3NO), as obtained commercially, was sublimed at room temperature under reduced pressure onto a probe cooled to -78 °C. The sublimed product was then dissolved in methanol (ca. 4 mg/mL) and stored under dry N_2 for future

use. Dodecacarbonyltriosmium was prepared by a literature method.⁵⁰ The ^{13}C -enriched $\text{Os}_3(\text{CO})_{12}$ ($\approx 35\%$ ^{13}C) was prepared by heating $\text{Os}_3(\text{CO})_{12}$ in toluene at 125°C under ≈ 1.5 atm of ^{13}CO (99% ^{13}C) for 3 days. Column chromatography was performed with use of silica-gel.

Infrared spectra were recorded on a Perkin-Elmer 983 spectrometer; the internal calibration of the instrument was periodically checked against the known absorption frequencies of gaseous CO.

2.2.2 NMR Studies

NMR spectra were obtained with a Bruker SY-100 spectrometer (operating frequencies: ^1H , 100.0 MHz; ^{13}C , 25.18 MHz), and a Bruker WM400 spectrometer (operating frequencies: ^1H , 400.13 MHz; ^{13}C , 100.6 MHz). The temperatures of the samples whose spectra were recorded on the WM400 spectrometer were obtained from the temperature controller of the spectrometer. The thermocouple of the temperature controller had been previously calibrated and shown to be accurate to $\pm 2^\circ\text{C}$ in the temperature range concerned. The NMR line-shape simulations were carried out with a computer program written by Professor R. E. D. McClung of the University of Alberta; the program is capable of simulating the spectra expected for the exchange of up to ten, uncoupled, spin $1/2$ nuclei. One of the input parameters for the spectrum simulations is the natural

linewidth of the ^{13}C NMR resonances. The linewidth was measured from the ^{13}C NMR signal which was not involved in any exchange processes at the temperature where the lineshape was simulated. The free energies of activation, ΔG^\ddagger , were calculated from the Eyring equation given in Eqn. 2.1.51

$$k_r = \frac{\kappa kT}{h} \exp\left(\frac{-\Delta G^\ddagger}{RT}\right)$$

... Eqn. 2.1

κ = Transmission coefficient = 1;

k_r = Rate of carbonyl exchange (Hz) at temperature T;

k = Boltzmann constant;

h = Planck's constant;

R = Gas constant.

It is realized that ΔG^\ddagger is related to the entropy factor, ΔS^\ddagger :⁵¹

$$\Delta G^\ddagger = \Delta H^\ddagger - T\Delta S^\ddagger$$

Detailed lineshape analysis were not carried out for the $\text{Os}_3(\text{CO})_{11}(\text{ER}_3)$ clusters. The entropy factors may not be negligible although they are expected to be small. A ΔS^\ddagger value of $-3.1 \text{ cal mol}^{-1} \text{ K}^{-1}$ was found for $\text{Os}_3(\text{CO})_{12}$ ³² where a similar nondissociative CO exchange process was proposed. Thus the error in the neglecting the entropy factor would be about $0.2 \text{ kcal mol}^{-1}$ for $\text{Os}_3(\text{CO})_{11}(\text{ER}_3)$ given that the ΔG^\ddagger

determinations were carried out over an approximate 50 °C. The uncertainty of ΔG^\ddagger reported in this thesis were estimated from the errors in the rate constants ($\pm 10\%$) and the temperatures (± 2 °C) (Eqn. 2.1) as mentioned before.

2.2.3 Preparation of $\text{Os}_3(\text{CO})_{11}(\text{ER}_3)$ ($\text{ER}_3 = \text{PMe}_3, \text{PPh}_3, \text{SbPh}_3, \text{AsPh}_3, \text{P}(p\text{-tolyl})_3, \text{P}(\text{OPh})_3, \text{P}(\text{OMe})_3, \text{P}(\text{OCH}_2)_3\text{CCH}_3$)

All derivatives of $\text{Os}_3(\text{CO})_{11}(\text{ER}_3)$ were synthesized by the method reported in the literature.⁵² To a solution of $\text{Os}_3(\text{CO})_{12}$ (50 mg, 0.055 mmol) in CH_2Cl_2 (50 mL) and CH_3CN (1 mL), Me_3NO in methanol (ca. 4 mg/mL) was added dropwise over 30 min (ca. 1.2 mL used). The mixture was stirred for another 2 hrs. An infrared spectrum (CO region) of the solution at this stage showed no absorptions due to $\text{Os}_3(\text{CO})_{12}$. Excess ER_3 was added to the solution which was stirred for another 2 hrs. The solvent and volatile materials were removed under reduced pressure. The yellow residue was redissolved in hexane/ CH_2Cl_2 (9:1) and chromatographed on a silica-gel column (20 x 1.5 cm) with hexane/ CH_2Cl_2 (9:1) as eluent. The first yellow band was identified as the desired product by infrared spectroscopy. The solvent was then removed under vacuum; recrystallization of the residue from the minimum amount of hexane yielded air-stable, yellow crystals of $\text{Os}_3(\text{CO})_{11}(\text{ER}_3)$ [orange crystals for $\text{Os}_3(\text{CO})_{11}(\text{PMe}_3)$]. A yield of 45 - 60% was obtained. The second band on the column was collected with

the use of hexane/CH₂Cl₂ (1:1) as eluent and was identified as the bis-substituted derivative, Os₃(CO)₁₀(ER₃)₂ by IR spectroscopy. A typical IR spectrum of a Os₃(CO)₁₁(ER₃) derivative is shown in Fig. 2.1. The infrared and NMR data for Os₃(CO)₁₁(ER₃) complexes are reported in Tables 2.1 and 2.2, respectively.

2.2.4 Preparation of Os₃(CO)₁₁(PF₃)

A round-bottom flask (fitted with a Teflon valve) was charged with Os₃(CO)₁₁(NCCH₃) (40 mg, 0.043 mmol) (prepared as reported in literature⁵²) and CH₂Cl₂ (60 mL) and evacuated at -196 °C. The solution was degassed with three freeze-pump-thaw cycles. The flask was then pressurized with 1.5 atm of PF₃ (6 mmol). The mixture was stirred at room temperature for 15 hrs. Excess PF₃ and solvent were removed under reduced pressure to yield a yellow solid. Recrystallization of the solid from a minimum amount of hexane afforded Os₃(CO)₁₁(PF₃) (11 mg, 0.011 mmol, 25% yield) as air-stable, bright-yellow crystals. Purification of the product by column chromatography (as in the syntheses of other Os₃(CO)₁₁(ER₃) derivatives) was unsuccessful. The infrared and NMR data are reported in Tables 2.1 and 2.2, respectively. The sample as obtained contained more CO stretching bands and ¹³C NMR resonances than expected for pure Os₃(CO)₁₁(PF₃) (where PF₃ is in equatorial site). The extra signals were, however, weak.

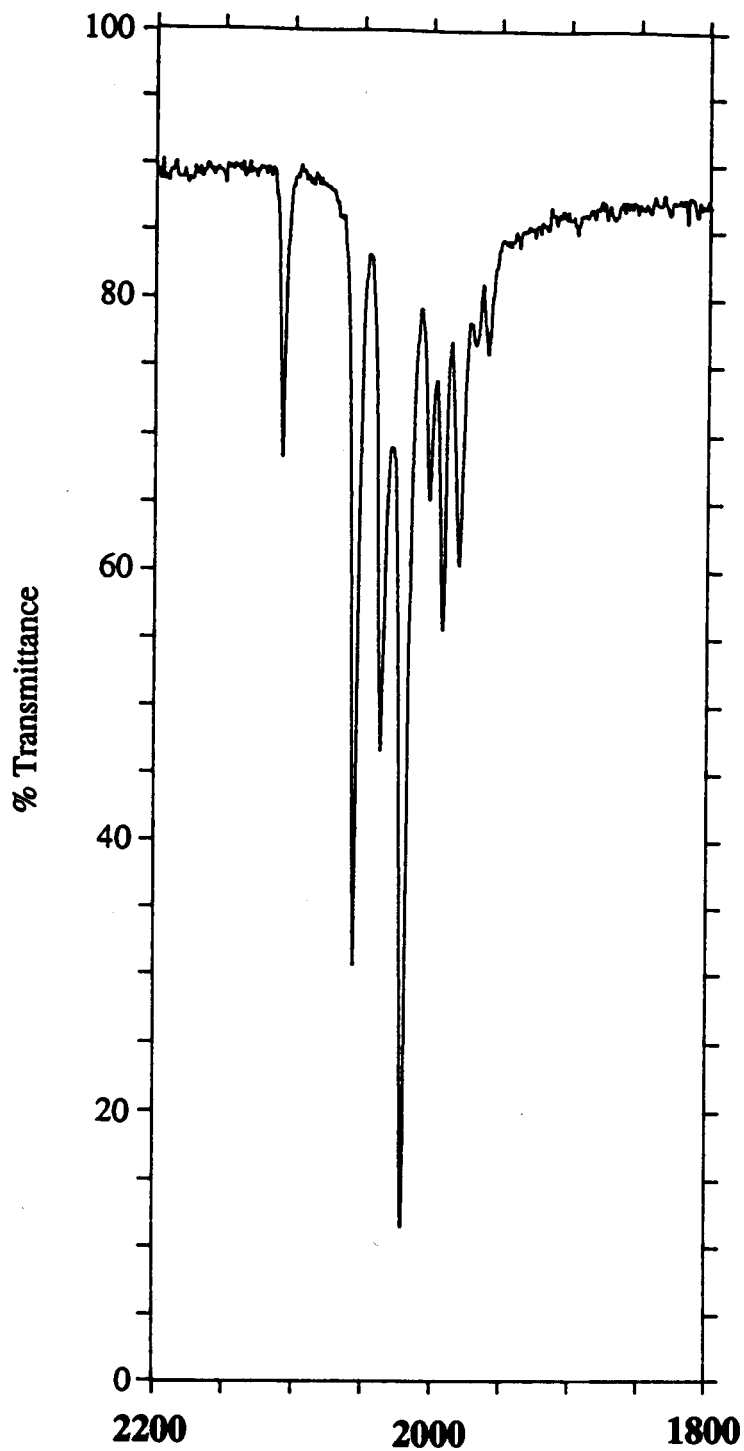


Fig. 2.1 IR spectrum (CO stretching region) of $\text{Os}_3(\text{CO})_{11}(\text{PPh}_3)$ in hexane.

Table 2.1 The IR frequencies of terminal carbonyls of $\text{Os}_3(\text{CO})_{11}(\text{ER}_3)$ derivatives.

ER_3	$\nu(\text{CO}) \text{ cm}^{-1}$ (in hexane)
CO^{a}	2068(s), 2034(s), 2012(m), 2000(m)
PMe_3	2107(w), 2053(m), 2031(m), 2019(s), 2001(w), 1988(mw), 1972(mw), 1967(sh), 1957(w)
PPh_3	2106(w), 2054(ms), 2035(m), 2019(s), 2001(w), 1989(mw), 1979(w), 1968(vw), 1957(vw)
P(p-totyl)_3	2107(w), 2054(ms), 2035(m), 2019(s), 2000(w), 1990(mw), 1979(mw), 1958(vw)
$\text{P(OMe)}_3^{\text{b}}$	2111(w), 2056(s), 2040(m), 2022(s), 2003(w), 1993(m), 1983(w), 1970(w)
$\text{P(OCH}_2)_3\text{CCH}_3$	2114(w), 2058(s), 2047(m), 2026(s), 2003(mw), 1994(m), 1982(sh.), 1977(w)
$\text{P(OPh)}_3^{\text{a}}$	2113(w), 2060(s), 2045(m), 2025(s), 2005(mw), 1996(m), 1991(sh.), 1978(w)
AsPh_3	2108(w), 2055(s), 2036(m), 2020(s), 2002(w), 1992(mw), 1978(w), 1965(vw), 1958(vw)
SbPh_3	2108(w), 2057(ms), 2034(m), 2021(s), 2003(w), 1992(mw), 1978(w), 1965(vw), 1957(vw)
PF_3^{c}	2123(vw), 2100(vw), 2080(w), 2069(s), 2058(m), 2036(s), 2016(m), 2010(m), 2005(m), 1993(w)

a. IR in CH_2Cl_2 .

b. Reference 47.

c. Extra bands are weak (see text).

Table 2.2 ^{13}C O chemical shifts of $\text{Os}_3(\text{CO})_{11}(\text{ER}_3)$ clusters at $-53\text{ }^\circ\text{C}$ in $\text{CD}_2\text{Cl}_2/\text{CH}_2\text{Cl}_2$ (1:4 ratio).

ER_3	$\delta(\text{ax-CO})$ ppm	$\delta(\text{eq-CO})$ ppm
$\text{P}(\text{p-tolyl})_3$	193.2 ($J_{\text{CP}} = 5.9$ Hz), 186.2, 183.9	177.1, 175.0, 172.5, 172.0, 169.9
PMe_3	192.9 ($J_{\text{CP}} = 7.4$ Hz), 185.3, 184.4	177.5, 176.4, 173.3, 172.5, 170.7
PPh_3	192.8 ($J_{\text{CP}} = 7.5$ Hz), 185.9, 183.7	176.9, 174.9, 172.1, 171.8, 169.7
AsPh_3	192.1, 185.8, 183.3	177.0, 175.1, 171.4, 171.1, 169.8
SbPh_3	190.1, 185.1, 183.2	177.4, 174.9, 171.1, 171.0, 169.8
$\text{P}(\text{OMe})_3^{\text{a}}$	189.8 ($J_{\text{CP}} = 12.3$ Hz), 185.1, 184.2	176.0, 174.5, 172.9, 171.8, 170.8
$\text{P}(\text{OPh})_3$	188.1 ($J_{\text{CP}} = 11.3$ Hz), 184.2, 183.7	174.7, 172.7, 171.8, 171.4, 170.2
$\text{P}(\text{OCH}_2)_3\text{CCH}_3$	188.0 ($J_{\text{CP}} = 12.4$ Hz), 184.5, 184.3	174.5, 173.8, 172.7, 172.0, 171.3
PF_3	183.3 ($J_{\text{CP}} = 13.4$ Hz), 182.5, 182.0	171.0, 170.7, 170.4, 169.8, 169.5
CO	182.9	170.7

a. Reference 47.

All the ^{13}C -enriched $\text{Os}_3(\text{CO})_{11}(\text{ER}_3)$ derivatives used in the NMR studies were prepared in the same way as the $\text{Os}_3(\text{CO})_{11}(\text{ER}_3)$ complexes except that ^{13}C -enriched $\text{Os}_3(\text{CO})_{12}$ was used as starting material.

2.3 Results and Discussion

2.3.1 Nonrigidity of $\text{Os}_3(\text{CO})_{11}(\text{ER}_3)$

The solid state structure of $\text{Os}_3(\text{CO})_{11}[\text{P}(\text{OMe})_3]$ has been reported.⁵³ The cluster adopts a triangular osmium framework with the $\text{P}(\text{OMe})_3$ ligand in an equatorial site on one of the osmium centres (Fig. 2.2). This is in agreement with other studies^{24,27,54,55} that bulky ligands generally adopt equatorial positions in trinuclear clusters. (Small ligands such as H ,^{9,22,24} CH_3CN ⁵⁶ and CNR ^{22,57} are usually found in axial sites in such clusters.) The solution structure of the $\text{Os}_3(\text{CO})_{11}(\text{ER}_3)$ derivatives reported in this thesis is believed similar to that of the $\text{P}(\text{OMe})_3$ congener in the solid state (Fig. 2.2) according to their infrared and ^{13}C NMR spectra. There were, however, weak peaks in the ^{13}C NMR and infrared spectra of the PF_3 derivative that may have been due to small amounts of the axial isomer.

The ^{13}C NMR spectra of all the $\text{Os}_3(\text{CO})_{11}(\text{ER}_3)$ derivatives in $\text{CD}_2\text{Cl}_2/\text{CH}_2\text{Cl}_2$ (1:4) at -53°C are similar: three signals of intensity two at low field of 180 ppm which are assigned to the axial carbonyls, and five signals of

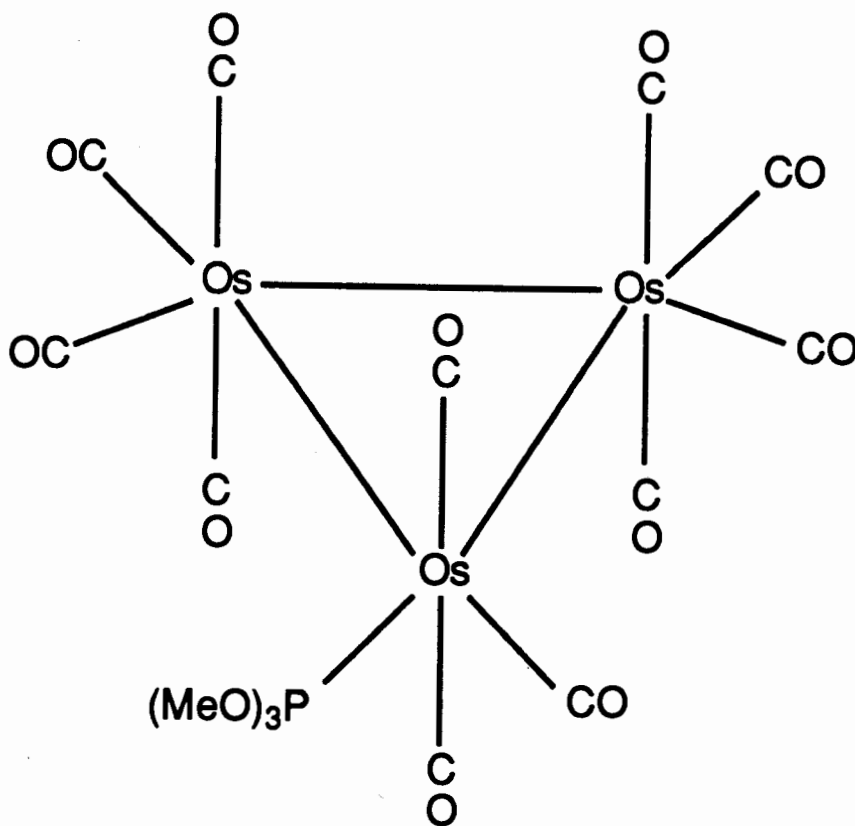


Fig. 2.2 Structure of $\text{Os}_3(\text{CO})_{11}[\text{P}(\text{OMe})_3]$.⁵³

intensity one to high field of 180 ppm which are assigned to the equatorial carbonyls (Table 2.2). These spectra are consistent with the structure proposed, i.e., the structure similar to that of $\text{Os}_3(\text{CO})_{11}[\text{P}(\text{OMe})_3]$ (Fig. 2.2). The resonance at lowest field of the spectra, which exhibits ^{13}C - ^{31}P coupling when $\text{ER}_3 = \text{PR}_3$ and $\text{P}(\text{OR})_3$ is, therefore, assigned to the axial carbonyls of the $\text{Os}(\text{CO})_3(\text{ER}_3)$ group. As observed previously, no coupling was observed from the phosphorus atom to the equatorial carbonyl of the $\text{Os}(\text{CO})_3(\text{PR}_3)$ grouping.⁴⁶ The ^{13}C - ^{31}P coupling constants measured in $\text{Os}_3(\text{CO})_{11}(\text{ER}_3)$ clusters varied depending on the substituent ER_3 : they were larger when ER_3 was a phosphite (11.3 - 12.4 Hz) and smaller when ER_3 was a phosphine (5.9 - 7.5 Hz). However, the largest ^{13}C - ^{31}P coupling constant observed was when $\text{ER}_3 = \text{PF}_3$ (13.4 Hz) which is the weakest σ -donor ligand among the different substituents used.

The mode of collapse of signals in the ^{13}C NMR spectra of $\text{Os}_3(\text{CO})_{11}(\text{ER}_3)$ clusters are similar. The details of the nonrigidity of $\text{Os}_3(\text{CO})_{11}(\text{PMe}_3)$ are reported below. The structure and the labelling of carbonyl ligands of $\text{Os}_3(\text{CO})_{11}(\text{PMe}_3)$ is shown diagrammatically in Fig. 2.3. As mentioned before, the ^{13}C resonances to low field of 180 ppm are assigned to the axial carbonyls on the basis of intensity. The signal which exhibits ^{13}C - ^{31}P coupling at δ 192.9 is assigned to the axial carbonyls a of the $\text{Os}(\text{CO})_3(\text{PMe}_3)$ unit (Fig. 2.3). The other two signals of

intensity two in the axial carbonyl region, at δ 185.3 and 184.4, are assigned to carbonyls f and c, respectively, from the mode of collapse of the signals at higher temperatures (discussed below). The ^{13}C O resonances of intensity one are therefore assigned to the five equatorial carbonyls. The signal at δ 172.5 is assigned to carbonyl e because this carbonyl does not exchange with other carbonyl ligands until higher temperatures and therefore remains sharp (discussed below). The pairs of signals at δ 177.5/173.3 and 176.4/170.7 are assigned to the carbonyls h/d and b/g respectively from the rate of collapse of the signals and the proposed mechanisms. A definite assignment of the pairs of signals cannot be made at this time. In the assignment of the signals of the axial carbonyls it is, however, observed that the resonance of the carbonyl ligands which are bonded to the metal atom that is bound to the ER_3 group appears at lower field. Since carbonyl b is closer to PMe_3 than carbonyl g, the low field signal at δ 176.4 is tentatively assigned to carbonyl b and, therefore, that at δ 170.7 to carbonyl g. Accordingly, the signals at δ 177.5 and 173.3 are assigned to carbonyls h and d respectively.

The variable temperature ^{13}C NMR spectrum of $\text{Os}_3(\text{CO})_{11}(\text{PMe}_3)$ and the assignment of the signals (spectrum at -53°C) are shown in Fig. 2.4. When the sample was warmed to -35°C , two axial and two equatorial signals

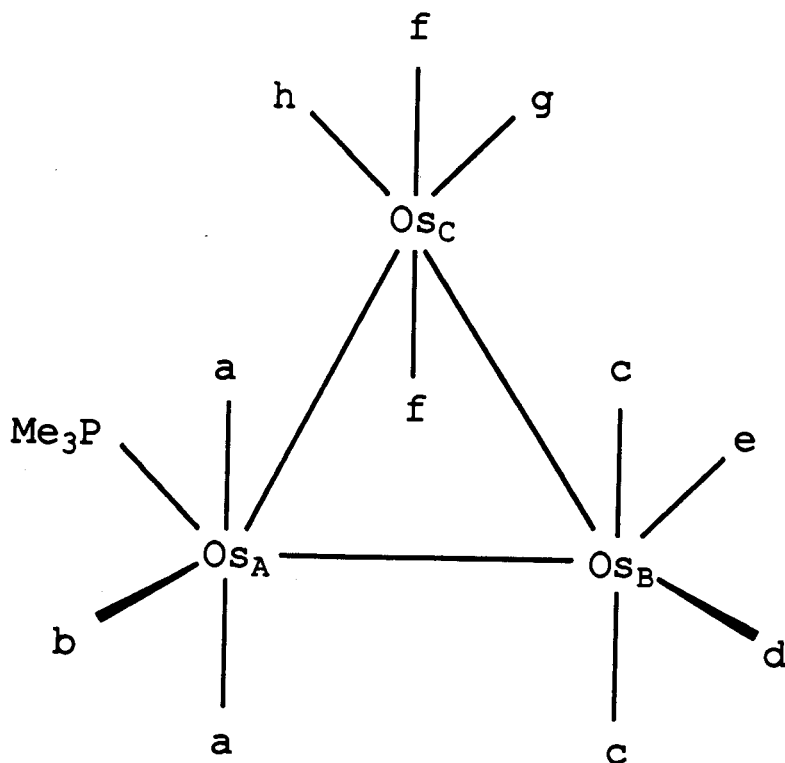


Fig. 2.3 Diagrammatic presentation of the structure and the labelling scheme of carbonyl ligands in $Os_3(CO)_{11}(PMe_3)$.

(labelled a, f and b, g respectively) broadened and collapsed to the base line by $-11\text{ }^{\circ}\text{C}$. The mode of collapse is similar to that observed for $\text{Os}_3(\text{CO})_{11}(\text{PEt}_3)$,⁴⁶ $\text{Os}_3(\text{CO})_{11}[\text{P}(\text{OMe})_3]$ ⁴⁷ and in tetraosmium clusters $\text{Os}_3(\text{CO})_{11}[\text{Os}(\text{CO})_4(\text{PMe}_3)]$ ³⁷ and $\text{Os}_3(\text{CO})_{11}[\text{Os}(\text{CO})_{5-x}(\text{CNBu}^t)_x]$ ($x = 1, 2$).^{70, a} The most reasonable mechanism to account for this collapse is that first proposed by Lewis and co-workers: namely the pairwise terminal-bridge carbonyl exchange.⁴⁶ Since one of the signals that collapsed is due to the axial carbonyls of the $\text{Os}(\text{CO})_3(\text{PMe}_3)$ group (that is labelled a in Fig. 2.3), the vertical plane that the carbonyl exchange occurs is thought to be the plane that is perpendicular to the PMe_3 ligand, i.e., the AC plane in Fig. 2.5. This exchange, if viewed directly along the side of the $\text{Os}_A\text{-Os}_C$ bond, is shown in Fig. 2.6. A line shape analysis of the ^{13}C NMR spectrum of $\text{Os}_3(\text{CO})_{11}(\text{PMe}_3)$ at $-35\text{ }^{\circ}\text{C}$ (Fig. 2.7) indicates that the proposed exchange process is consistent with the observed spectrum. The calculation yielded a first-order rate constant for the process of 15 s^{-1} which corresponds to a ΔG_1^\ddagger of $12.4 \pm 0.3\text{ kcal mol}^{-1}$.

a. The nonrigidity of $\text{Os}_3(\text{CO})_{11}[\text{Os}(\text{CO})_{5-x}(\text{CNBu}^t)_x]$ ($x = 1, 2$) is reported in Chapter 3 of this thesis.

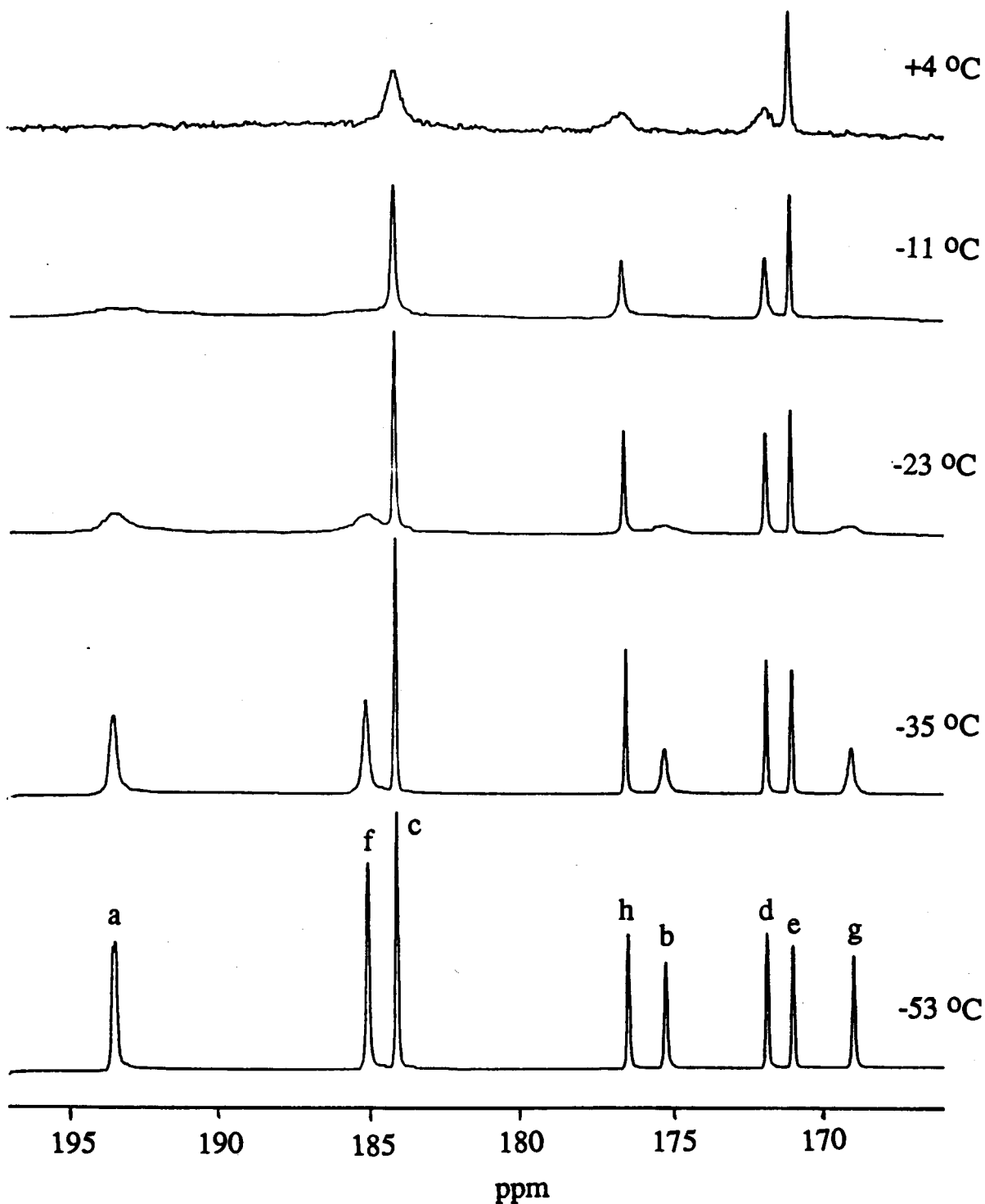


Fig. 2.4 Variable temperature ^{13}C NMR spectra for $\text{Os}_3(\text{CO})_{11}(\text{PMe}_3)$ (^{13}C -enriched; in $\text{CH}_2\text{Cl}_2/\text{CD}_2\text{Cl}_2$). The assignment of the signals follows that in Fig. 2.3.

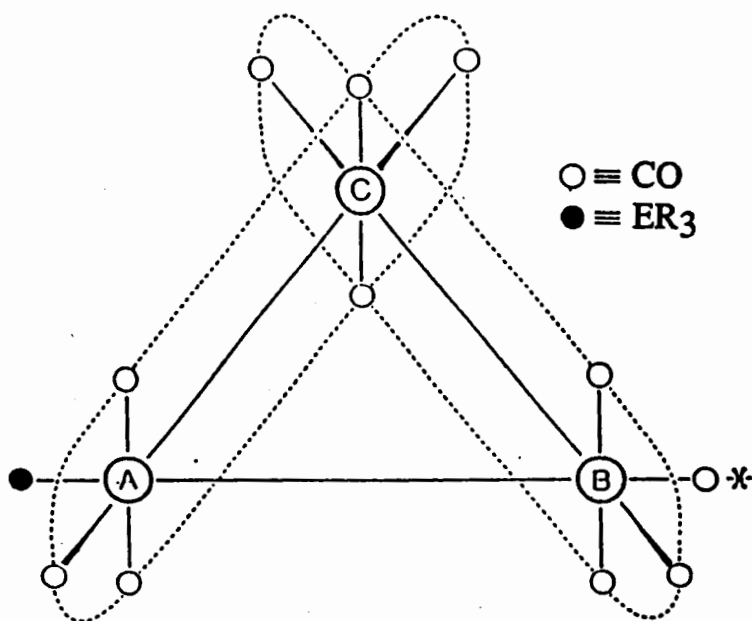


Fig. 2.5 Allowed planes of pairwise terminal-bridge carbonyl exchange in $\text{Os}_3(\text{CO})_{11}(\text{ER}_3)$.

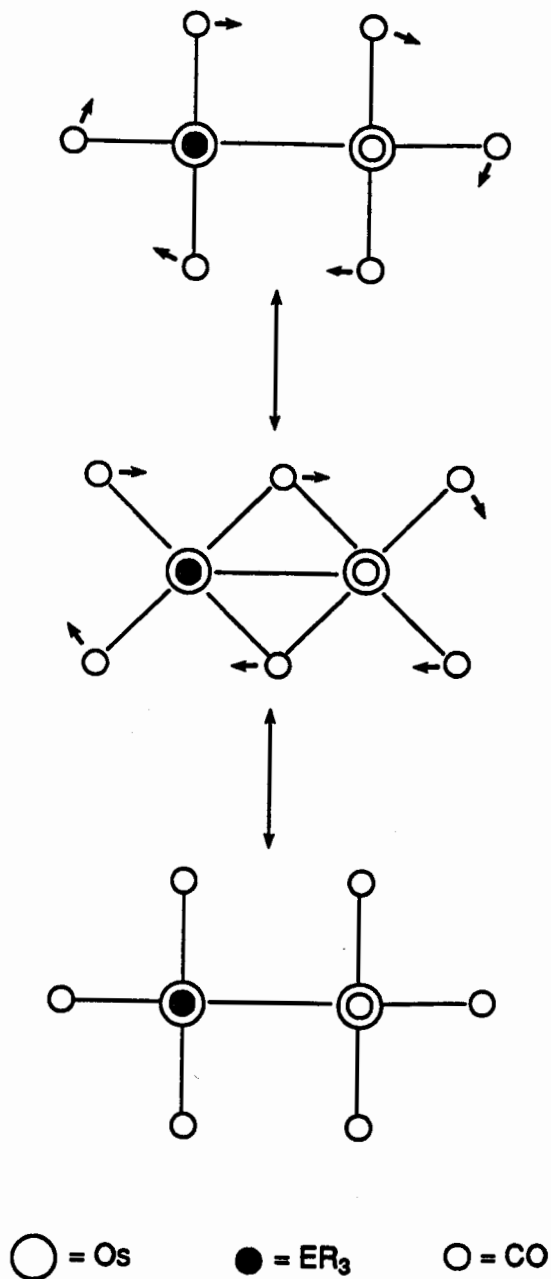


Fig. 2.6 Terminal-bridge carbonyl exchange in $\text{Os}_3(\text{CO})_{11}(\text{ER}_3)$ when viewed directly along the edge of the $\text{Os}_A\text{-Os}_C$ bond.

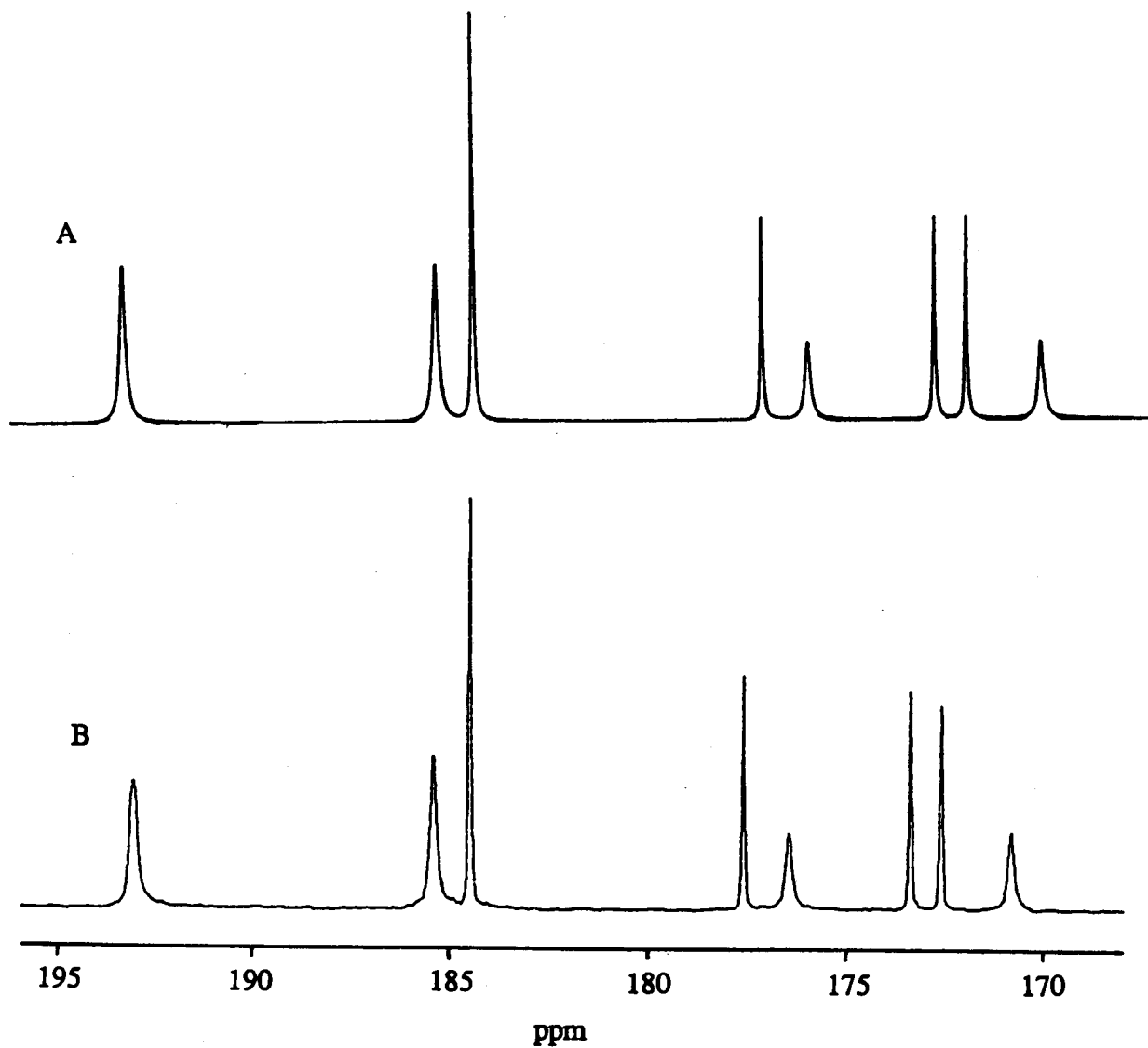


Fig. 2.7 Calculated (A) and experimental (B) ^{13}C NMR spectra of $\text{Os}_3(\text{CO})_{11}(\text{PMe}_3)$ at -35°C .

As previously noted for $\text{Os}_3(\text{CO})_{11}(\text{PEt}_3)$,⁴⁶ the phosphorus containing ligand lowers the barrier to axial-equatorial carbonyl exchange compared to the parent binary cluster $\text{Os}_3(\text{CO})_{12}$. It was reasoned⁴⁷ that substitution of a carbonyl ligand in $\text{Os}_3(\text{CO})_{12}$ by a phosphorus-donor ligand would increase the electron density at the osmium atom where substitution had occurred. The electron density would cause expansion of the 5d orbitals on the osmium atom. This in turn could result in better overlap of these orbitals with the π^* orbitals of the axial carbonyls on the adjacent osmium atom as shown in Fig. 2.8. This, therefore, would be expected to lower the activation energy for the formation of the intermediate with bridging carbonyls. It is known that phosphorus-donor ligands can stabilize ground-state structures with bridging carbonyls. For example, $\text{Ru}_3(\mu\text{-CO})_2(\text{CO})_6[\text{P}(\text{OMe})_2\text{Ph}]_4$ ⁵⁸ and $\text{Ir}_4(\mu\text{-CO})_3(\text{CO})_6(\text{PPh}_3)_3$ ⁵⁹ have bridging carbonyls, but the parent carbonyls, $\text{Ru}_3(\text{CO})_{12}$ ⁶⁰ and $\text{Ir}_4(\text{CO})_{12}$ ⁶¹, do not. Furthermore, although $\text{Ru}_3(\mu\text{-CO})_2(\text{CO})_6[\text{P}(\text{OMe})_2\text{Ph}]_4$ ⁵⁸ has bridging carbonyls in the solid state, the less substituted derivative $\text{Ru}_3(\text{CO})_{10}[\text{P}(\text{OMe})_3]_2$ ⁵⁴ does not.

During the collapse of the four ^{13}CO signals at -23°C , three other signals (labelled c, h and d) start to broaden at a slower rate. This collapse is best rationalized in terms of a second terminal-bridge carbonyl exchange (with slightly higher energy barrier than the first

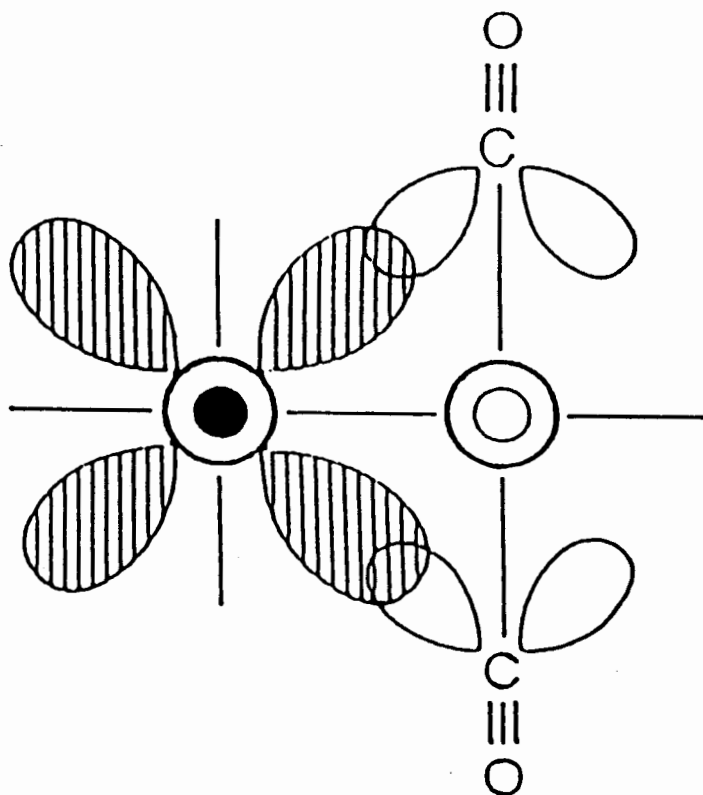


Fig. 2.8 Diagram that shows the overlap of the expanded 5d orbitals on osmium with the π^* orbitals of the axial carbonyls on the adjacent osmium atom.

exchange) that occurs in the other vertical plane that does not contain the phosphine ligand, i.e., the BC plane in Fig. 2.5. The axial carbonyls f are involved in the exchange processes that occur in both the AC and BC planes. A calculation from the line shape analysis yields an energy barrier for the CO-exchange process, ΔG_2^\ddagger of 14.5 ± 0.3 kcal mol⁻¹. As proposed for Os₃(CO)₁₁[P(OMe)₃],⁴⁷ bridge-terminal carbonyl exchange in the vertical plane that contains the phosphorus-donor ligand [i.e., the plane that passes through Os(A) and Os(B)] would result in the phosphorus-donor ligand in an axial position in the cluster. Models show there would be severe steric interactions of the phosphorus ligand with the neighbouring axial carbonyls in the cluster.

The signal that remains sharp in the ¹³C NMR spectrum at -11 °C may be assigned to the carbonyl in the trans two bond position to the phosphine ligand, namely, carbonyl e in Fig. 2.3 (and that marked with an asterisk in Fig. 2.5). The ¹³C NMR spectrum at +4 °C shows that this signal also broadens. There are a number of processes that could account for this observation. One process involves a restricted trigonal twist at Os(A) that rotates the phosphine ligand from one equatorial position to the other (Fig. 2.9). This type of trigonal twist mechanism has been proposed for the high energy carbonyl scrambling process in Os₃(CO)₁₀[P(OMe)₃]₂ and Os₃(CO)₇[P(OMe)₃]₅.⁴⁷ When this

process occurs in $\text{Os}_3(\text{CO})_{11}(\text{PMe}_3)$, the terminal-bridge CO exchange in the AB vertical plane, which is considered a forbidden plane for CO exchange, will equilibrate carbonyl e with carbonyls a, b and c. Another possible process is a trigonal twist mechanism that takes place at Os(B). This simple axial-equatorial CO exchange will equilibrate the carbonyls at Os(B). A similar mechanism has been proposed for the equilibration of the axial-equatorial carbonyls of the $\text{Ru}(\text{CO})_4$ group in $\text{Ru}_3(\text{CO})_{10}(\text{NO})_2$,⁶² and has been suggested as one of the possible mechanisms of carbonyl scrambling in $\text{Os}_3(\text{CO})_{12}$.⁶² Both trigonal twist processes at different osmium centres of $\text{Os}_3(\text{CO})_{11}(\text{PMe}_3)$ will eventually scramble all carbonyl ligands in the cluster. Due to the collapse of all carbonyl signals in the ^{13}C NMR spectrum, the various mechanisms cannot be distinguished.

The variable temperature ^{13}C NMR spectra of other $\text{Os}_3(\text{CO})_{11}(\text{ER}_3)$ derivatives are shown in Fig. 2.10 to 2.17. The modes of collapse of the signals in the spectra of each derivative are similar and, therefore, are rationalized in the same manner as for $\text{Os}_3(\text{CO})_{11}(\text{PMe}_3)$, i.e., in terms of two terminal-bridge carbonyl exchange processes and a restricted trigonal twist process. In some cases two of the processes had similar energy barriers. For example, the activation energies of the two terminal-bridge CO-exchange processes were similar in $\text{Os}_3(\text{CO})_{11}[\text{P}(\text{OCH}_2)_3\text{CCH}_3]$ (14.8 and 15.1 kcal mol⁻¹). The activation energies, ΔG_1^\ddagger and ΔG_2^\ddagger ,

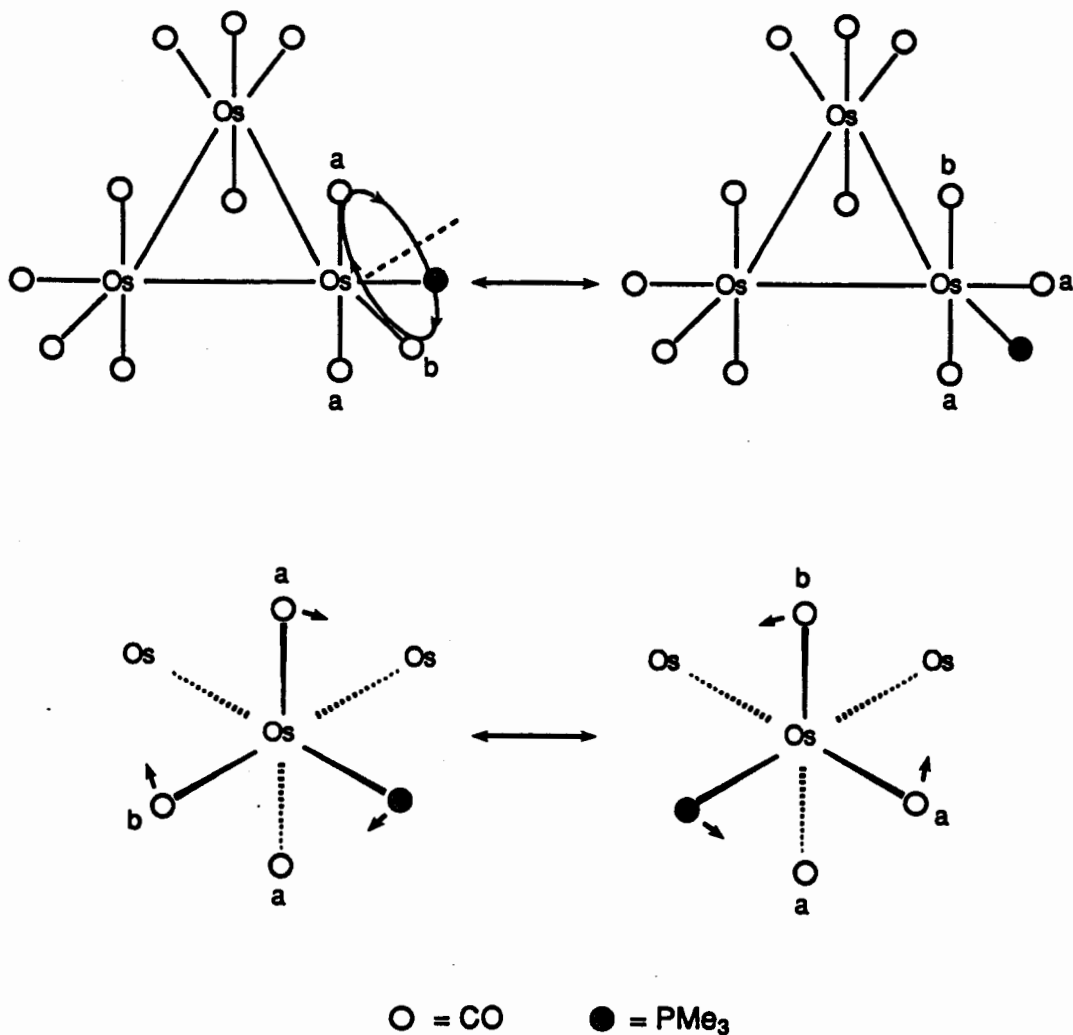


Fig. 2.9 Diagrammatic presentation of the partially restricted rotation that brings the PMe_3 group from one equatorial site to the other.

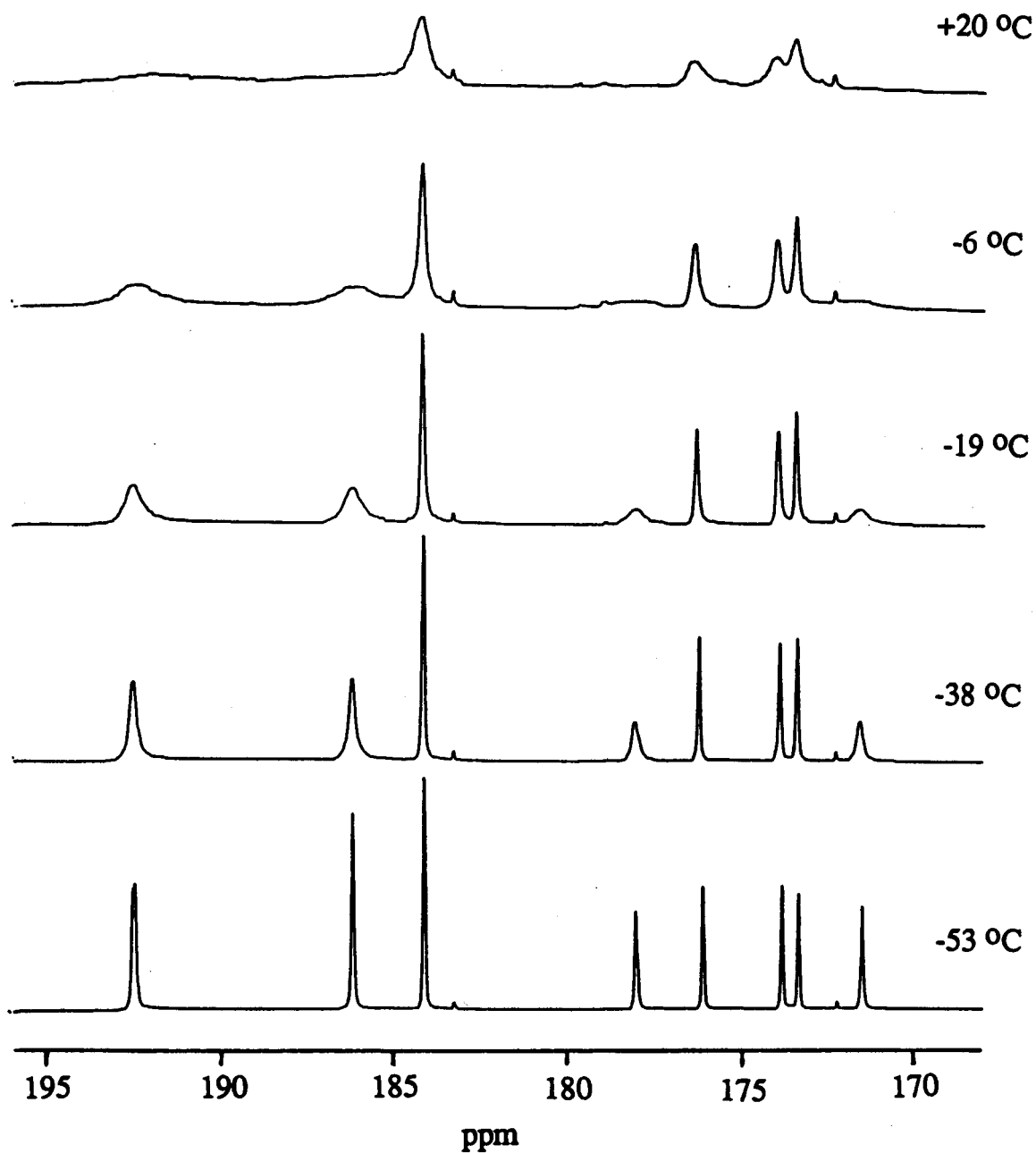


Fig. 2.10 Variable temperature ^{13}C NMR spectra of $\text{Os}_3(\text{CO})_{11}[\text{P}(\text{p-tolyl})_3]$ (^{13}CO -enriched; in $\text{CH}_2\text{Cl}_2/\text{CD}_2\text{Cl}_2$).

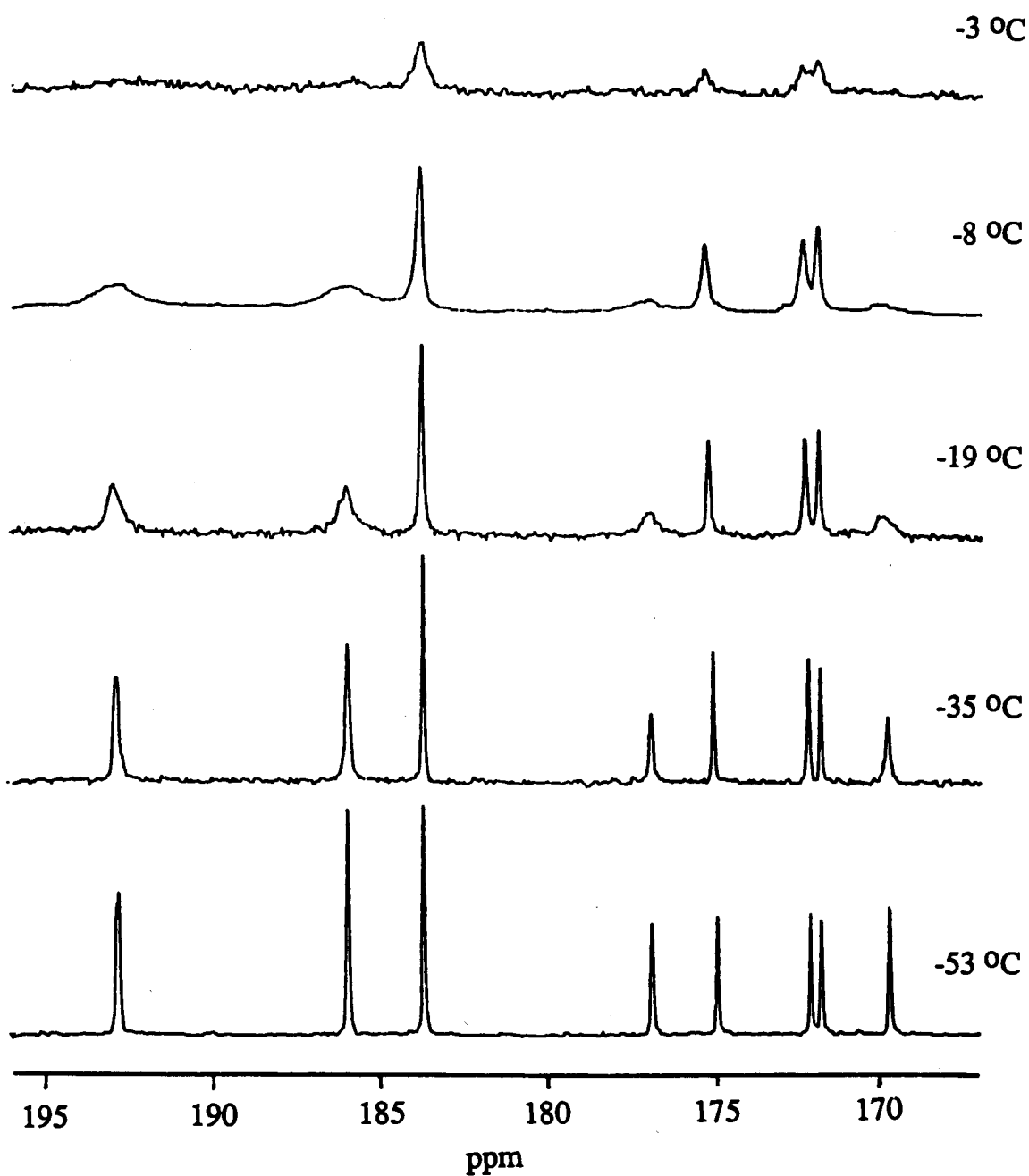


Fig. 2.11 Variable temperature ^{13}C NMR spectra of $\text{Os}_3(\text{CO})_{11}(\text{PPh}_3)$ (^{13}C -enriched; in $\text{CH}_2\text{Cl}_2/\text{CD}_2\text{Cl}_2$).

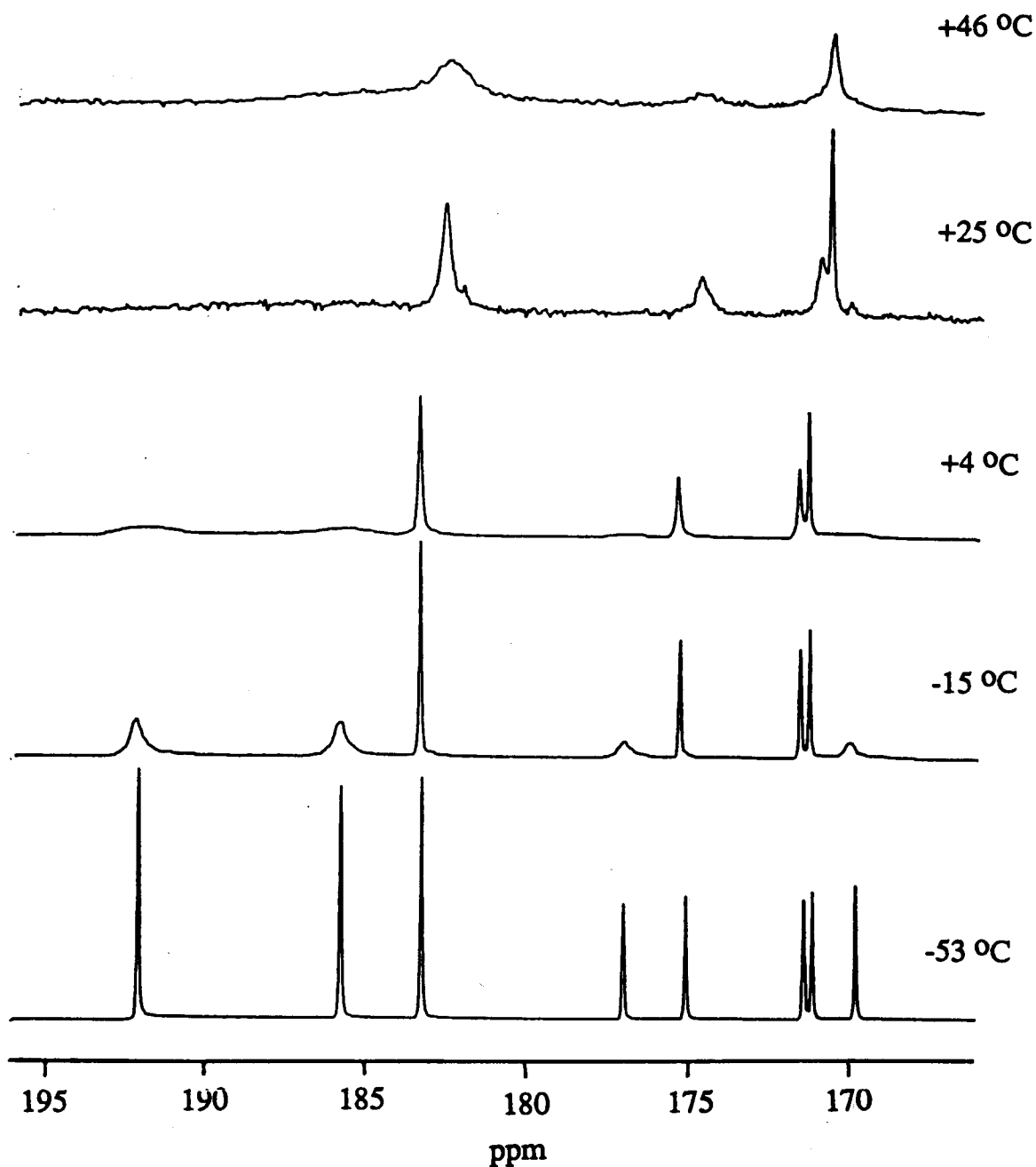


Fig. 2.12 Variable temperature ^{13}C NMR spectra of $\text{Os}_3(\text{CO})_{11}(\text{AsPh}_3)$ (^{13}C -enriched; in $\text{CH}_2\text{Cl}_2/\text{CD}_2\text{Cl}_2$ for spectra from -53 °C to +4 °C; in toluene/toluene- d_8 for spectra at +25 °C and +46 °C).

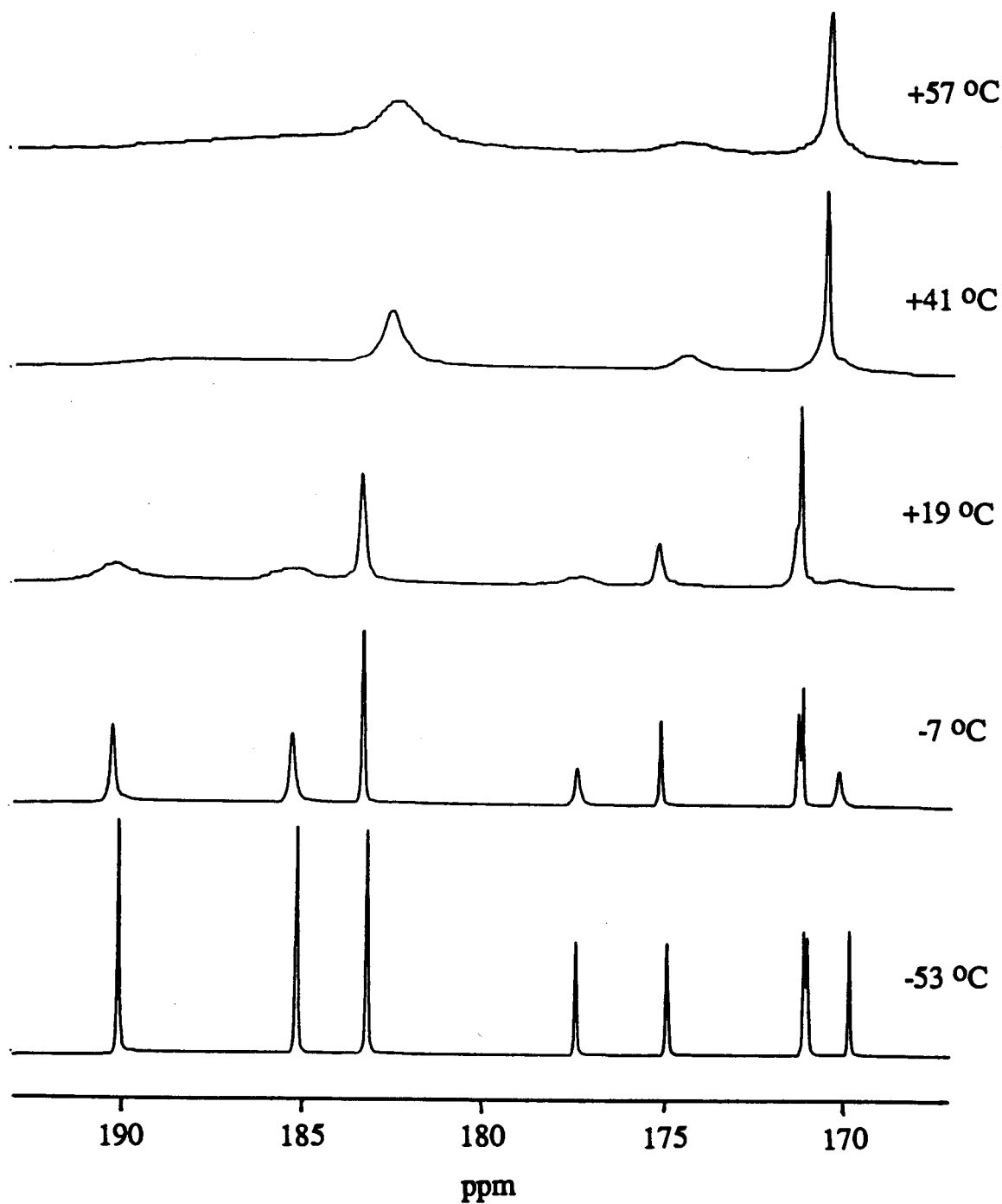


Fig. 2.13 Variable temperature ^{13}C NMR spectra of $\text{Os}_3(\text{CO})_{11}(\text{SbPh}_3)$ (^{13}C -enriched; in $\text{CH}_2\text{Cl}_2/\text{CD}_2\text{Cl}_2$ for spectra from -53 °C to +19 °C; in toluene/toluene- d_8 for spectra at +41 °C and +57 °C).

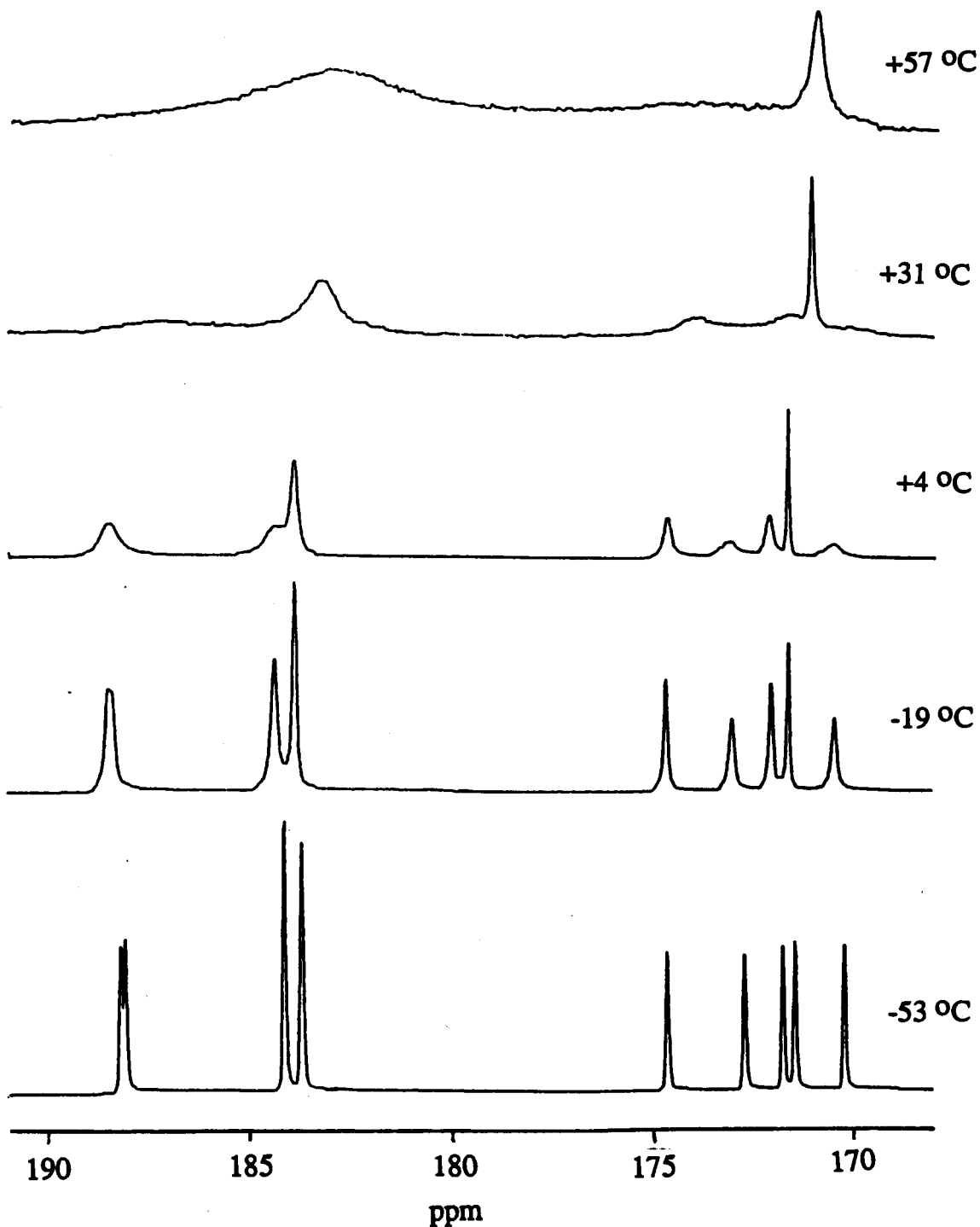


Fig. 2.14 Variable temperature ^{13}C NMR spectra of $\text{Os}_3(\text{CO})_{11}[\text{P}(\text{OPh}_3)]$ (^{13}C -enriched; in $\text{CH}_2\text{Cl}_2/\text{CD}_2\text{Cl}_2$ for spectra from -53 °C to +4 °C; in toluene/toluene- d_8 for spectra at +31 °C and +57 °C).

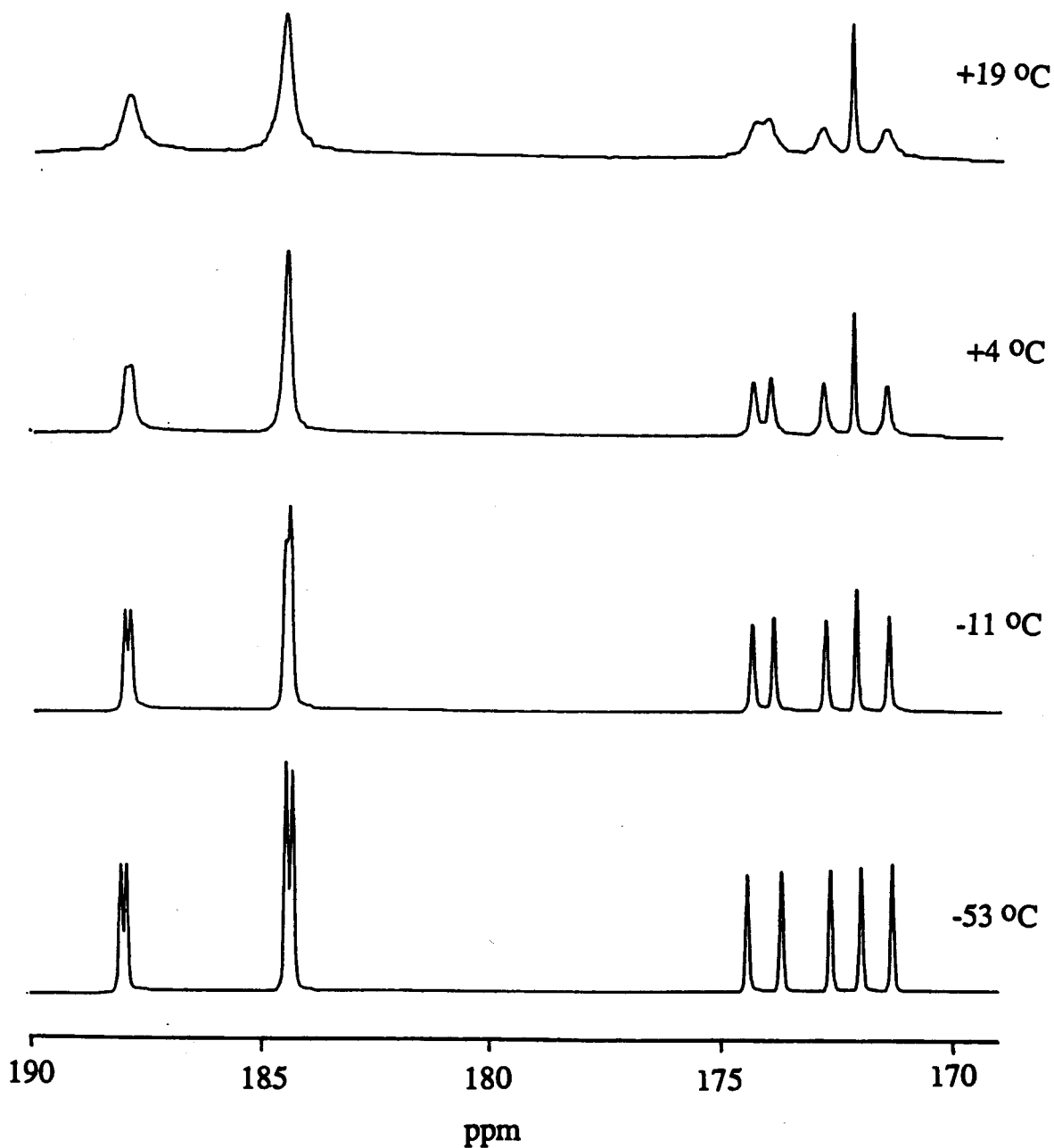


Fig. 2.15 Variable temperature ^{13}C NMR spectra of $\text{Os}_3(\text{CO})_{11}[\text{P}(\text{OCH}_2)_3\text{CCH}_3]$ (^{13}CO -enriched; in $\text{CH}_2\text{Cl}_2/\text{CD}_2\text{Cl}_2$).

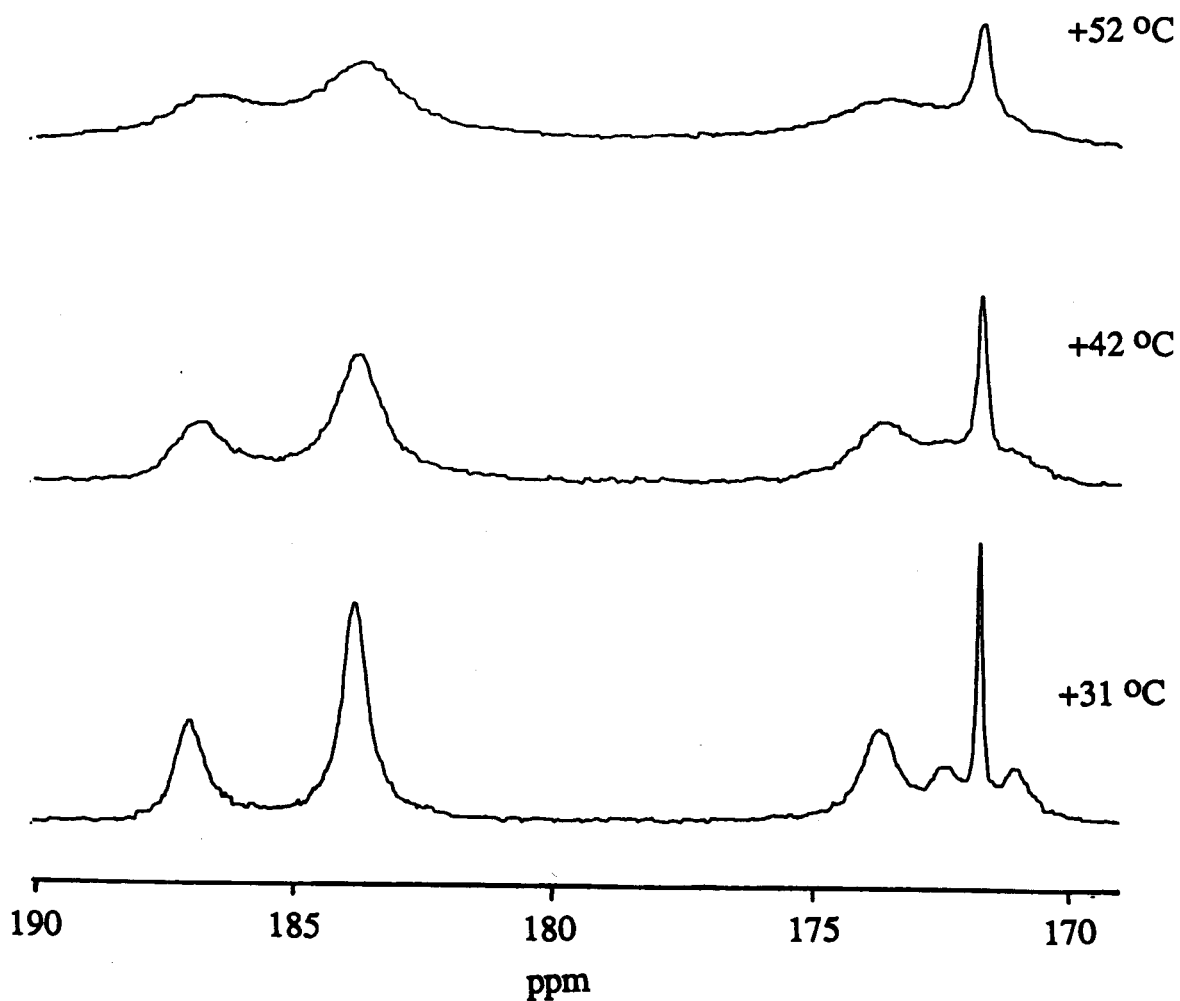


Fig. 2.16 Variable temperature ^{13}C NMR spectra of $\text{Os}_3(\text{CO})_{11}[\text{P}(\text{OCH}_2)_3\text{CCH}_3]$ (^{13}C -enriched; in toluene/toluene- d_8).

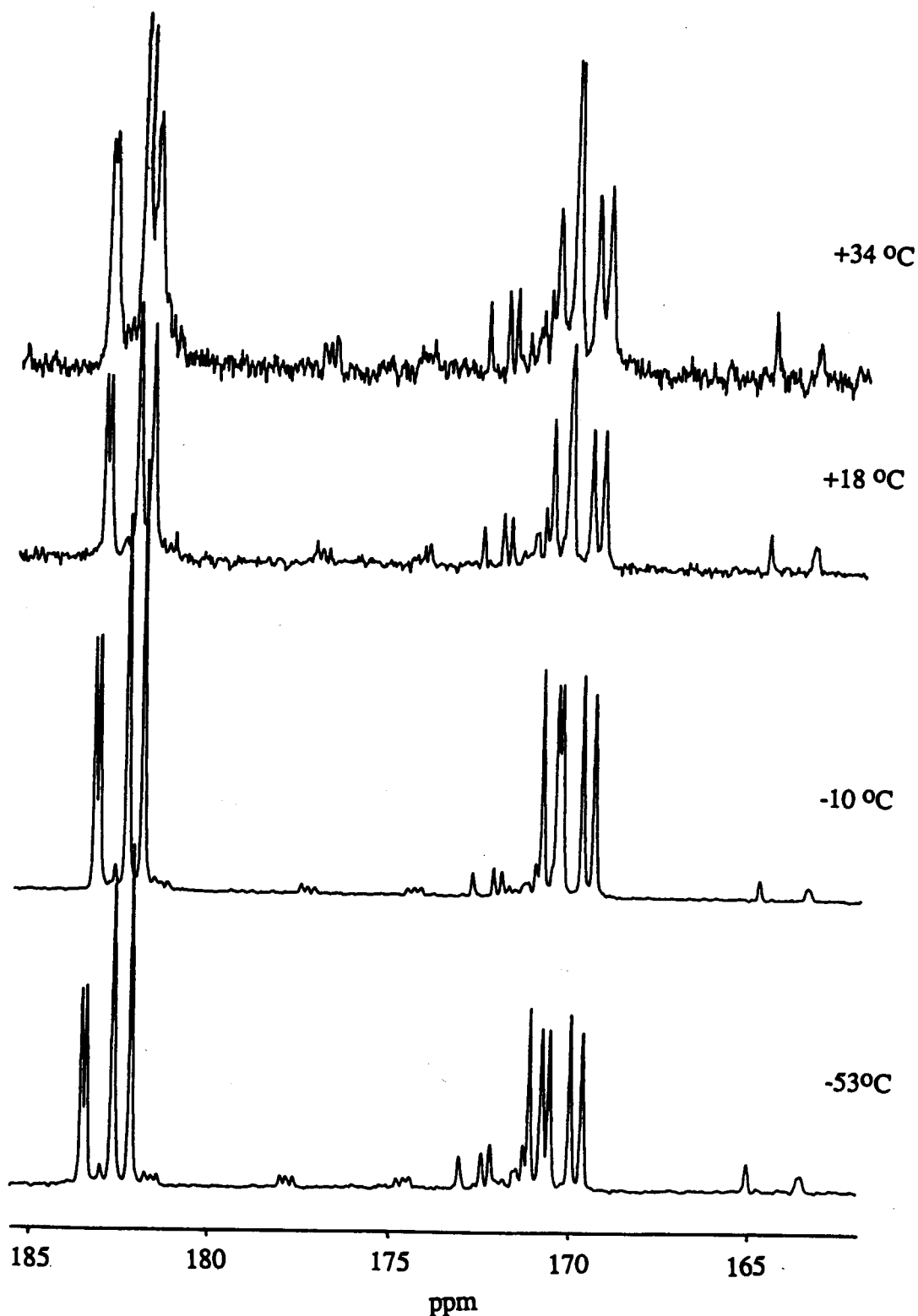


Fig. 2.17 Variable temperature ^{13}C NMR spectra of $\text{Os}_3(\text{CO})_{11}(\text{PF}_3)$ (^{13}C -enriched; in $\text{CH}_2\text{Cl}_2/\text{CD}_2\text{Cl}_2$).

found for these exchanges in the $\text{Os}_3(\text{CO})_{11}(\text{ER}_3)$ compounds are reported in Table 2.3.

Table 2.3 The chemical shift difference between the axial carbonyls of the $\text{Os}(\text{CO})_3(\text{ER}_3)$ group of $\text{Os}_3(\text{CO})_{11}(\text{ER}_3)$ and that in $\text{Os}_3(\text{CO})_{12}$, and the activation energies of the two terminal-bridge CO exchange processes in $\text{Os}_3(\text{CO})_{11}(\text{ER}_3)$.

Ligand (ER_3)	Chemical Shift Difference ($\Delta\delta$)	ΔG_1^\ddagger (kcal mol ⁻¹)	ΔG_2^\ddagger (kcal mol ⁻¹)
P(p-totyl) ₃	10.27	12.4 ± 0.4	13.4 ± 0.4
PMe ₃	9.99	12.4 ± 0.3	14.5 ± 0.3
PPh ₃	9.88	13.0 ± 0.4	14.0 ± 0.4
AsPh ₃	9.18	13.1 ± 0.4	15.4 ± 0.3
SbPh ₃	7.16	14.0 ± 0.4	15.7 ± 0.3
P(OMe) ₃ ^a	6.91	14.0 ± 0.4	14.9 ± 0.4
P(OPh) ₃	5.25	13.7 ± 0.4	14.5 ± 0.4
P(OCH ₂) ₃ CCH ₃	5.09	14.8 ± 0.4	15.1 ± 0.3
PF ₃	0.46	16.5 ± 0.5	b
CO	0.00	16.8 ± 0.5	c

a. Reference 47.

b. The two processes have indistinguishable activation barriers;

c. The two processes are equivalent.

2.3.2 Correlation of the Activation Barriers to CO-Exchange with the Properties of the Group 15 Ligand.

The group 15 ligand does not only affect the low energy CO exchange process in $\text{Os}_3(\text{CO})_{11}(\text{ER}_3)$ but also affects the ^{13}C chemical shifts of the axial carbonyls of the $\text{Os}(\text{CO})_3(\text{ER}_3)$ group and, to some extent, the chemical shifts of the other carbonyls in the cluster (see Table 2.3). From Table 2.2, it is apparent that the better donor ligands cause a deshielding of the CO resonances of the carbonyls associated with the $\text{Os}(\text{CO})_3(\text{ER}_3)$ grouping. This is contrary to simple electron density arguments used in organic chemistry, that a shielding effect should be observed. Since the extent of transition metal to carbonyl π back-bonding is increased with increasing electron density on the transition metal, Bodner^{51,63} and Braterman⁶⁴ have attributed the deshielding of the carbonyl resonances in these complexes to a decrease in the magnitude of the separation between the electronic ground state and the lowest lying excited state (ΔE). The ΔE parameter makes a major contribution to the paramagnetic term (σ_p) of the chemical shift. The expression of σ_p is given in Eqn. 2.2.

$$\sigma_p = \frac{-\mu_0 e^2 h^2}{6\pi m^2} \left[\frac{1}{\Delta E} \right] \left[\langle r^{-3} \rangle_{npP_i} + \langle r^{-3} \rangle_{ndD_i} \right]$$

... Eqn. 2.2

where n_p and n_d refer to the valence p and d electrons respectively; P_i and D_i represent the p and d electron imbalance about the nucleus, respectively; r is the average radius of the valence term; $\langle r^{-3} \rangle$ is usually called the radial term. The other symbols have their usual meaning.

As mentioned previously, Bodner has taken the downfield shift of the resonance due to the cis carbonyls in $\text{Ni}(\text{CO})_3(\text{ER}_3)$ compared to that in $\text{Ni}(\text{CO})_4$ as a measure of the electronic property of ER_3 .⁴⁹ A similar treatment may be carried out with the $\text{Os}_3(\text{CO})_{11}(\text{ER}_3)$ clusters, that is, the downfield shift of the resonance due to the axial carbonyls of the $\text{Os}(\text{CO})_3(\text{ER}_3)$ group compared to that of the axial carbonyls in $\text{Os}_3(\text{CO})_{12}$, may be taken as a measure of the electronic property of ER_3 in these compounds.

The plot of the difference of chemical shifts ($\Delta\delta_{\text{Os}}$) and the activation energies (ΔG_1^\ddagger) is shown in Fig. 2.18. An excellent linear correlation was obtained (correlation coefficient $r = 0.97$). The strong correlation suggests that the low energy CO exchange process in $\text{Os}_3(\text{CO})_{11}(\text{ER}_3)$ is strongly governed by the electronic effect of the ligand ER_3 . That there is a correlation of ΔG_1^\ddagger with $\Delta\delta_{\text{Os}}$ is also consistent with the explanation of Alex and Pomeroy of why the ER_3 ligands lower the barrier to exchange compared to that in $\text{Os}_3(\text{CO})_{12}$.⁴⁷

The y -intercept on the plot of ΔG^\ddagger vs. $\Delta\delta_{\text{Os}}$ corresponds to the activation energy of the CO exchange

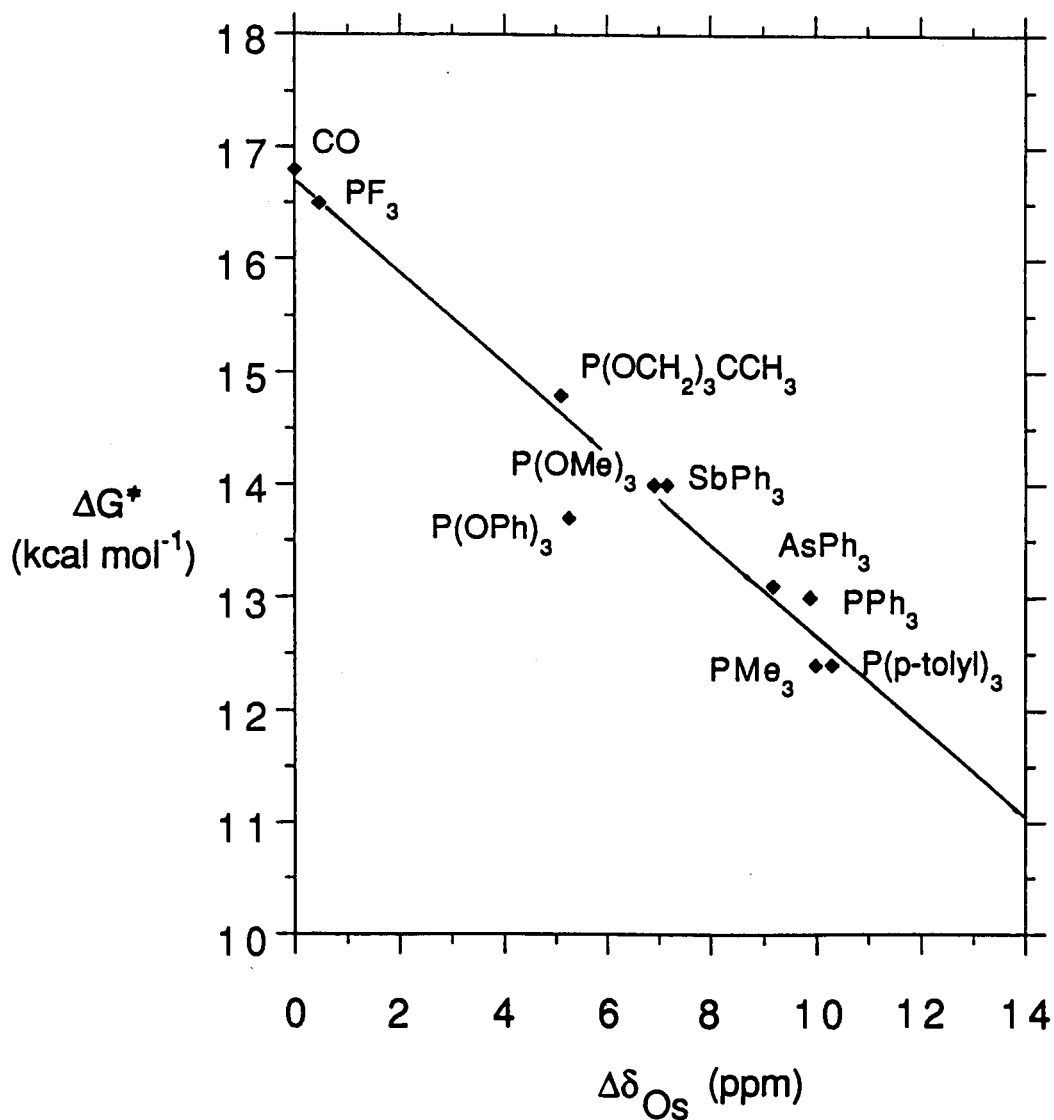


Fig. 2.18 A plot that shows the linear correlation between the $\Delta\delta_{Os}$ and the activation energy, ΔG_1^\ddagger , for the first CO-exchange process in $Os_3(CO)_{11}(ER_3)$ (see text).

process in the parent $\text{Os}_3(\text{CO})_{12}$ cluster. This is extrapolated to be $16.6 \text{ kcal mol}^{-1}$ which is in excellent agreement with the value of $16.7 \text{ kcal mol}^{-1}$ reported in the literature.⁶² This provides strong support for the view that CO-exchange in $\text{Os}_3(\text{CO})_{12}$ is bridge-terminal CO exchange in the vertical planes that contain two of the Os atoms. This mechanism, first proposed by Adams and Cotton for $\text{Fe}_3(\text{CO})_{12}$ in 1973, is the widely accepted mechanism for exchange in the Group 8 trinuclear dodecacarbonyls.

It is apparent that the data point for $\text{P}(\text{OPh})_3$ does not lie on the line. This may be due to a ring current effect from the phenyl groups which may deshield the axial carbonyls of the $\text{Os}(\text{CO})_3[\text{P}(\text{OPh})_3]$ grouping, i.e., one or more phenyl rings come close to the axial carbonyls as the $\text{P}(\text{OPh})_3$ rotates. It has been reported that, in the X-ray structure determinations of a wide range of different $\text{P}(\text{OCH}_3)_3$ complexes, a "two down, one up" arrangement of methyl groups is observed. This is illustrated in Fig. 2.19 for $\text{Ru}(\text{CO})_4[\text{P}(\text{OMe})_3]$.⁶⁵ This arrangement is also maintained, on the infrared time scale, in solution. The result suggests that a similar arrangement of phenyl groups of $\text{P}(\text{OPh})_3$ (i.e., "two down, one up") may exist in $\text{Os}_3(\text{CO})_{11}[\text{P}(\text{OPh})_3]$ so that the phenyl rings are close to the axial carbonyls.

A plot of chemical shift parameter, $\Delta\delta_{\text{Ni}}$, of $\text{Ni}(\text{CO})_3(\text{ER}_3)$ ⁴⁹ versus that of $\text{Os}_3(\text{CO})_{11}(\text{ER}_3)$ is shown in

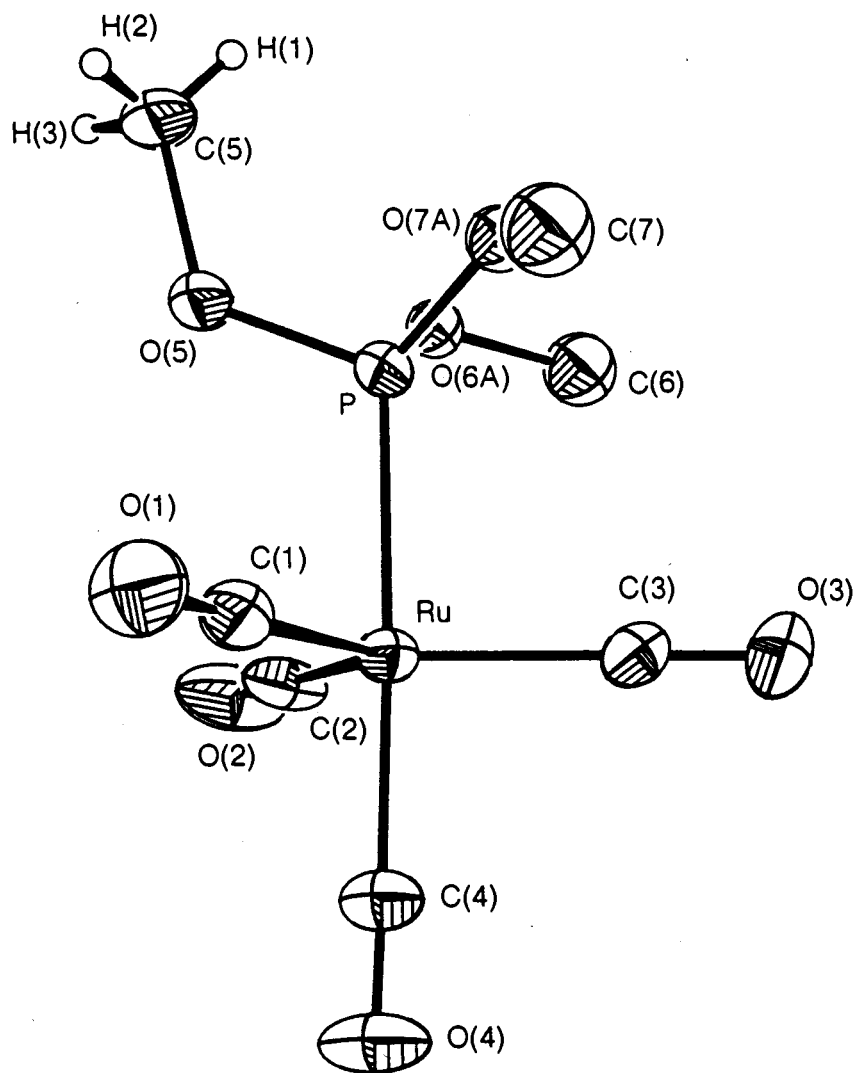


Fig. 2.19 Molecular structure of $\text{Ru}(\text{CO})_4[\text{P}(\text{OCH}_3)_3]$.⁶⁵

Fig. 2.20. A straight line with good correlation coefficient is obtained for the parameters of the phosphorus donor ligands. (It is noted that if ring current effect, as mentioned before, is taken into account in both complexes, the data point for $P(OPh)_3$ will be close to the line.) A similar line is also obtained when the $\Delta\delta_{Os}$ parameter is plotted against the $\nu(CO)$, the CO stretching frequency of $Ni(CO)_3(ER_3)^{48}$ (Fig. 2.21). This is an indication that the electronic parameters of a given phosphorus-donor ligand can be transferred from one type of complex to another.

From the results of this study the electronic effect (or the donor/acceptor character) of the group 15 ligands increases in the order: $CO < PF_3 < P(OCH_2)_3CCH_3 < P(OMe)_3 \approx SbPh_3 \approx P(OPh)_3 < AsPh_3 < PPh_3 < PMe_3 < P(p\text{-tolyl})_3$. Among the ligands studied PF_3 has the least donor/acceptor character and is similar in this respect to carbonyl; the donor/acceptor ratio increases from phosphites to phosphines. These results are in accordance with the electronic property of the free ligand.⁶⁶

The donor/acceptor ratio of EPh_3 ($E = P, As, Sb$) is found to increase in the order: $SbPh_3 < AsPh_3 < PPh_3$. This order is consistent with the result found by Pomeroy and co-workers in the study of the $M(CO)_4(L)$ ($M = Fe, Ru, Os$; $L =$ Group 15 ligand) complexes.⁶⁷ It is also in accordance with the enthalpy data for the gas-phase reaction of the group 15 ligand with BX_3 Lewis acids and the photoelectron spectra of

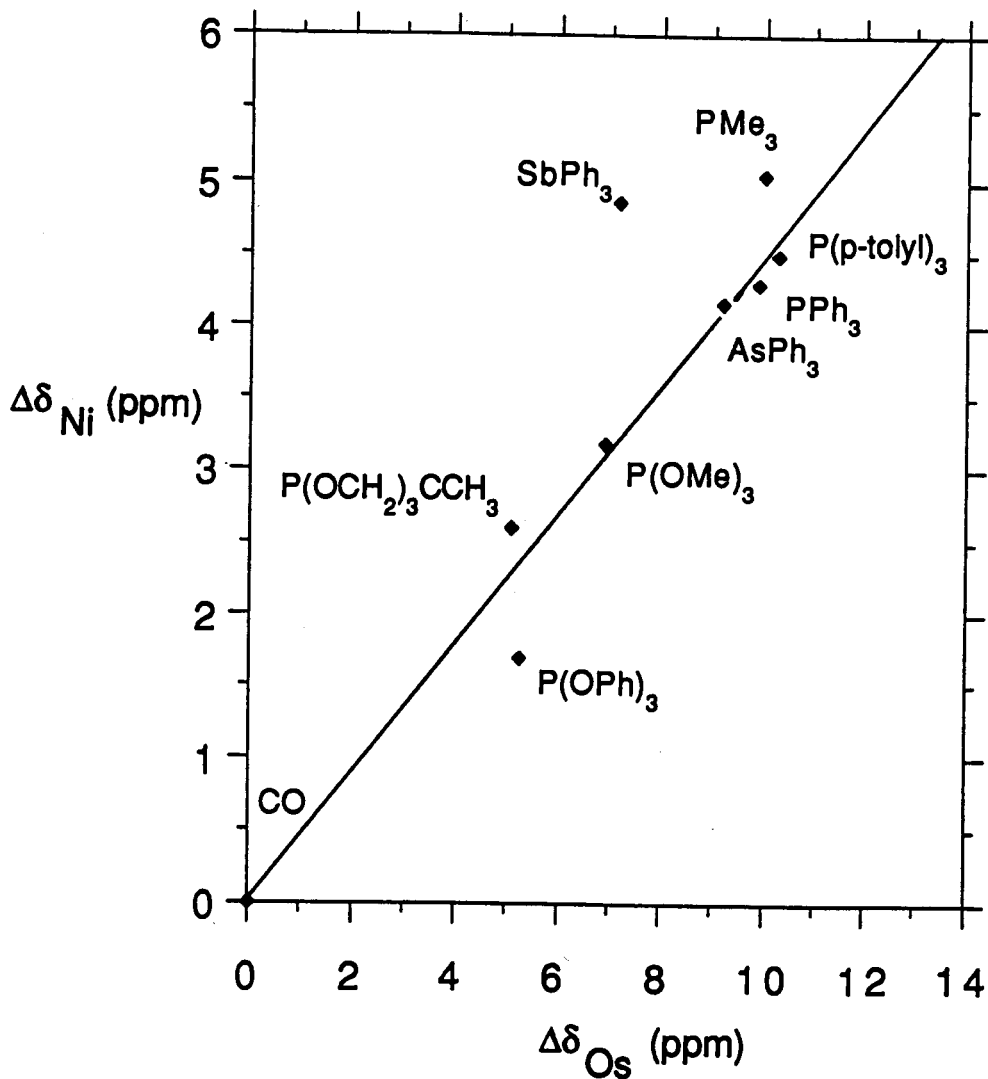


Fig. 2.20 Comparison of the $\Delta\delta$ parameter in $\text{Ni}(\text{CO})_3(\text{ER}_3)$ ($\Delta\delta_{\text{Ni}}$) and $\text{Os}_3(\text{CO})_{11}(\text{ER}_3)$ ($\Delta\delta_{\text{Os}}$).

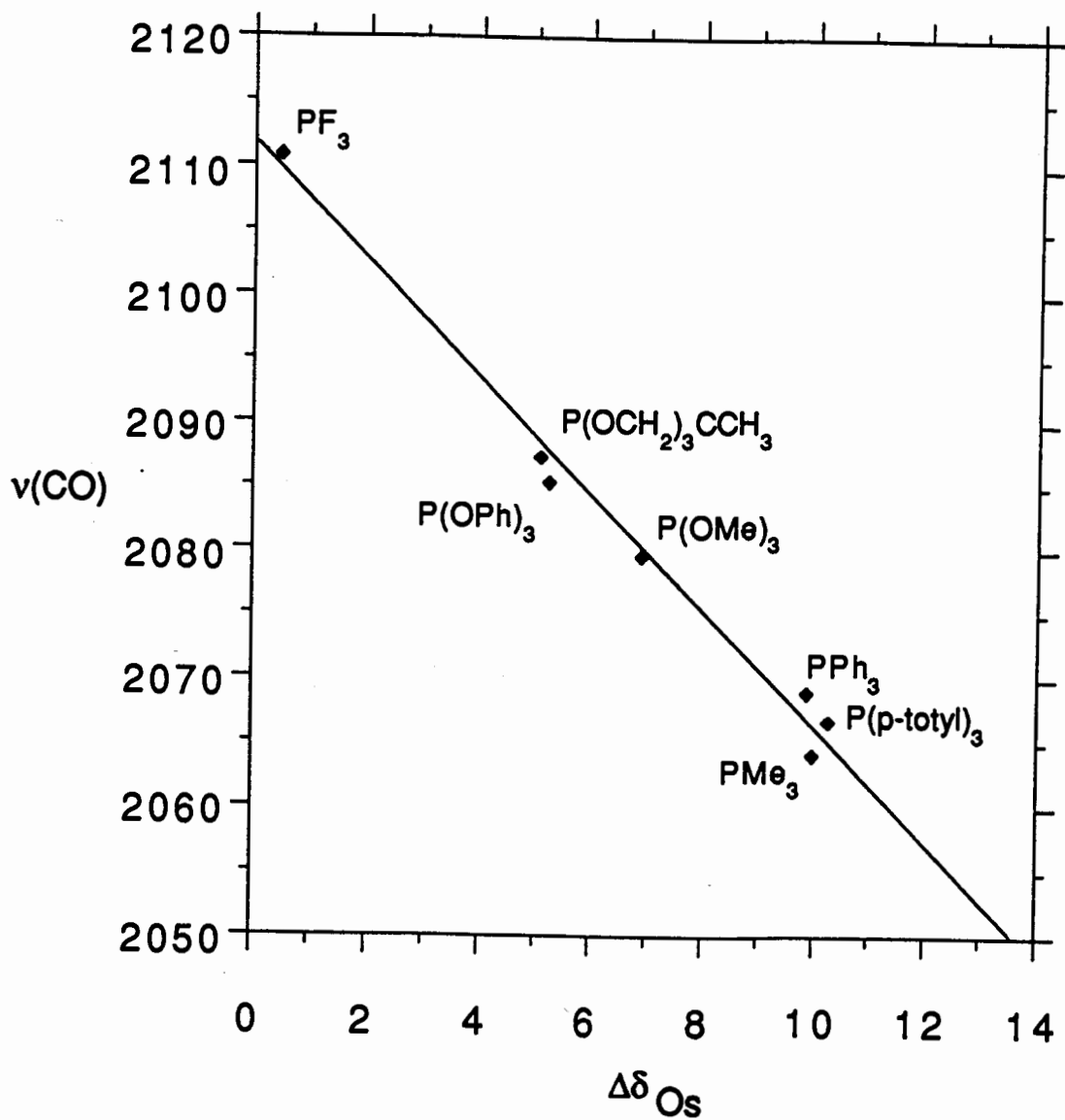


Fig. 2.21 Plot of the $\nu(CO)$ in $Ni(CO)_3(ER_3)$ and $\Delta\delta_{Os}$ parameter in $Os_3(CO)_{11}(ER_3)$.

the free ligands.⁶⁸ Bodner has measured the electronic effect parameter of these group 15 ligands from the ¹³C NMR carbonyl chemical shifts in $M(\text{CO})_5(\text{ER}_3)$ ($M = \text{Cr}, \text{Mo}$), $\text{Ni}(\text{CO})_3(\text{ER}_3)$ and $(\eta^6\text{-C}_6\text{H}_6)\text{Cr}(\text{CO})_2(\text{ER}_3)$.⁴⁹ His results, however, indicated that the donor/acceptor ratio of EPh_3 increases in the order: $\text{AsPh}_3 < \text{PPh}_3 < \text{SbPh}_3$ in these complexes, i.e., the stibine has the largest donor/acceptor property in the group. In the plot of $\Delta\delta_{\text{Os}}$ vs. $\Delta\delta_{\text{Ni}}$ (Fig. 2.20) the point for SbPh_3 does not lie on the line. This suggests that, unlike the phosphorus ligands studied here, the SbPh_3 ligand changes its electronic character towards the metal atom on going from $\text{Ni}(\text{CO})_3(\text{SbPh}_3)$ to $\text{Os}_3(\text{CO})_{11}(\text{SbPh}_3)$. Bodner finds that in some compounds the PPh_3 , AsPh_3 , SbPh_3 order was different. He attributed the large donor/acceptor ratio for the stibine ligand in the Ni complexes to the strength of the σ interaction between the group 15 element and the transition metals studied.⁴⁹

The barriers to the second CO exchange in the $\text{Os}_3(\text{CO})_{11}(\text{ER}_3)$ clusters although higher than those of the first are still lower than that in $\text{Os}_3(\text{CO})_{12}$. This must be attributable to an electronic effect of the ER_3 ligand. However, in contrast to what is found for the first CO-exchange process, there appears to be no direct correlation of the electronic properties of the ER_3 ligands and the activation barrier for the second CO exchange in these clusters.

Chapter 3

Stereochemical Nonrigidity of Tetraosmium Clusters

3.1 Introduction

A number of tetranuclear osmium clusters have recently been synthesized by Pomeroy and co-workers that have been shown by X-ray crystallography to have novel structures. They have a range of metal skeletons, namely, tetrahedral,³⁷ butterfly,²⁸ kite-shaped,^{36,37,69} spiked-triangular^{37,70,71} and puckered-square.⁷⁰ As mentioned in Chapter 2, one of the fascinating properties of metal cluster compounds is the stereochemical nonrigidity they often exhibit,^{72,73} and these tetranuclear osmium clusters are no exception. In this chapter details of the study of the nonrigidity in some of these clusters by ¹³C NMR spectroscopy are discussed.

3.2 Spiked-triangular Os₄ Clusters

Os₄(CO)₁₅(CNBu^t)

The X-ray crystal structure of Os₄(CO)₁₅(CNBu^t) revealed a spiked-triangular metal framework (Fig. 3.1).⁷⁰ The 18-electron species, Os(CO)₄(CNBu^t), acts as a two-electron donor ligand to the Os₃(CO)₁₁ fragment via an unbridged dative Os-Os bond. This is structurally similar to the clusters Os₄(CO)₁₅(PR₃) (PR₃ = P(OCH₂)₃CCH₃,⁶⁹ PMe₃).³⁷ The CNBu^t ligand of the Os(CO)₄(CNBu^t) fragment

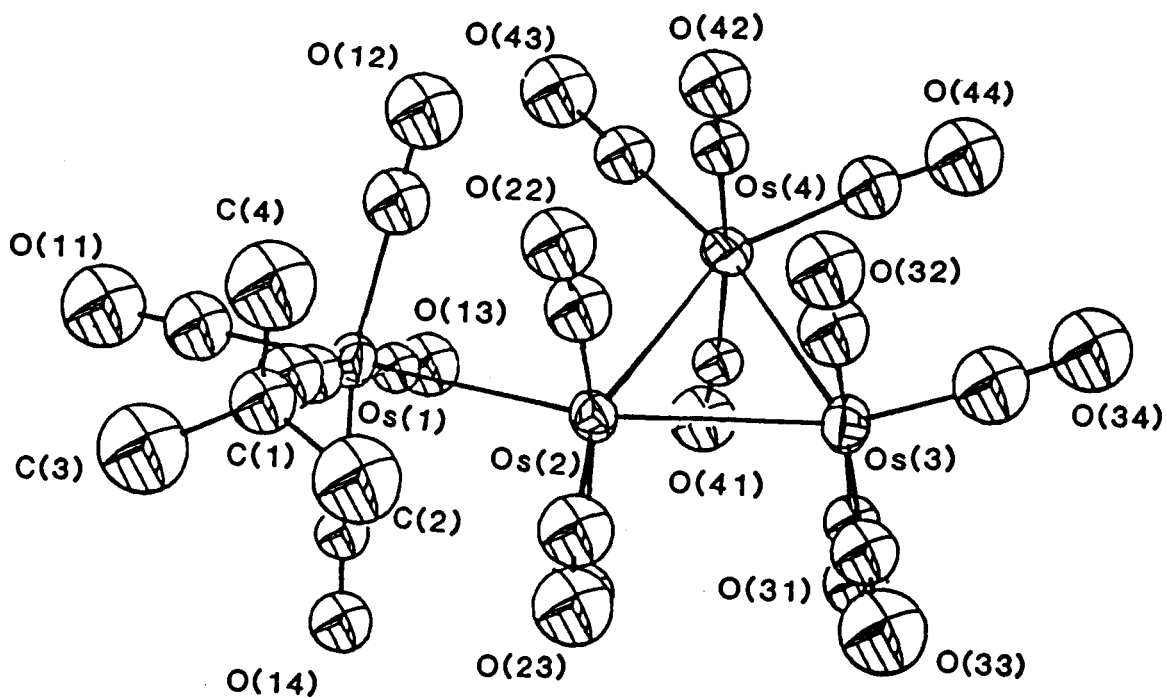


Fig. 3.1 Molecular structure of $\text{Os}_4(\text{CO})_{15}(\text{CNBut}) \cdot 70$
 Important bond lengths (Å) are: $\text{Os}(1)\text{-Os}(2) = 2.918(2)$; $\text{Os}(2)\text{-Os}(3) = 2.853(2)$; $\text{Os}(2)\text{-Os}(4) = 2.929(2)$; $\text{Os}(3)\text{-Os}(4) = 2.890(2)$.

occupies a radial position cis to the dative Os-Os bond. This is in contrast to the position of the PR_3 ligands in the $\text{Os}_4(\text{CO})_{15}(\text{PR}_3)$ cluster where the PR_3 ligand is trans to the dative bond, i.e., the axial position.^a It is known that when two carbonyls are trans to each other there is a considerable competition for back donation of electron density from the filled d-orbitals of the Os atom to the empty π^* orbitals of the carbonyls.⁷² The CNBu^t group may therefore be in the electronically preferred radial (equatorial) position so as to reduce this effect since CNBu^t is a poorer π -acceptor than the carbonyls.⁷³ Although the PR_3 ligand is a better σ -donor than CNBu^t , it is a more bulky ligand and may adopt the site which is trans to the dative bond for steric reasons. There is spectroscopic evidence that the cis isomer of the $\text{Os}(\text{CO})_4(\text{PMe}_3)$ derivative is present in solution.³⁷ It is interesting that in triosmium carbonyl clusters the phosphorus ligands also usually adopt equatorial sites^a while the isocyanide ligands are usually found in axial positions.^{22,57,74,75}

a. In trinuclear clusters the axial positions are cis to the metal-metal bonds whereas in dinuclear compounds the axial positions are trans to the metal-metal bond. Because of this, there is an ambiguity when labelling the positions in spiked-triangular clusters in that the site trans to the dative metal-metal bond is deemed an axial site even though it lies in the equatorial plane of the Os_3 unit.

The ^{13}C NMR spectrum of $\text{Os}_4(\text{CO})_{15}(\text{CNBu}^t)$ (^{13}C -enriched) in $\text{CH}_2\text{Cl}_2/\text{CD}_2\text{Cl}_2$ at -119°C exhibits 14 carbonyl resonances in the terminal carbonyl region at δ 199.2, 198.7, 188.2, 187.8, 184.6, 184.3, 179.9, 178.8, 177.0, 174.9, 173.4, 171.9, 171.0, 160.4 (Fig. 3.2). All signals are of approximate intensity one except the resonance at δ 184.6 which has an intensity of two. The spectrum at -108°C indicates that this signal is comprised of two signals. Fifteen resonances are consistent with the solid-state structure if the isocyanide group remains locked to one side of the Os_4 plane in solution (this is discussed below). From the spectrum obtained at -119°C , it can be seen that there is no real evidence for a second isomer of $\text{Os}_4(\text{CO})_{15}(\text{CNBu}^t)$ with the CNBu^t group trans to the dative Os-Os bond, or with the CNBu^t occupying a site on the Os_3 triangle. This latter observation probably means the CNBu^t ligand does not migrate across the dative Os-Os bond as CO does (see below).

The assignments of the signals shown in Fig. 3.2 follow the labelling scheme in Fig. 3.1. The assignment is based on the following: The resonance of a carbonyl with a chemically different carbonyl trans to it is expected to show C-C coupling;^{76,77} the resonances of axial carbonyls appear to lower field than those of the corresponding equatorial carbonyls of $\text{Os}(\text{CO})_4$ or $\text{Os}(\text{CO})_3(\text{L})$ units in osmium clusters;^{47,78,79} the resonances of $\text{Os}(\text{CO})_3(\text{L})$ groups

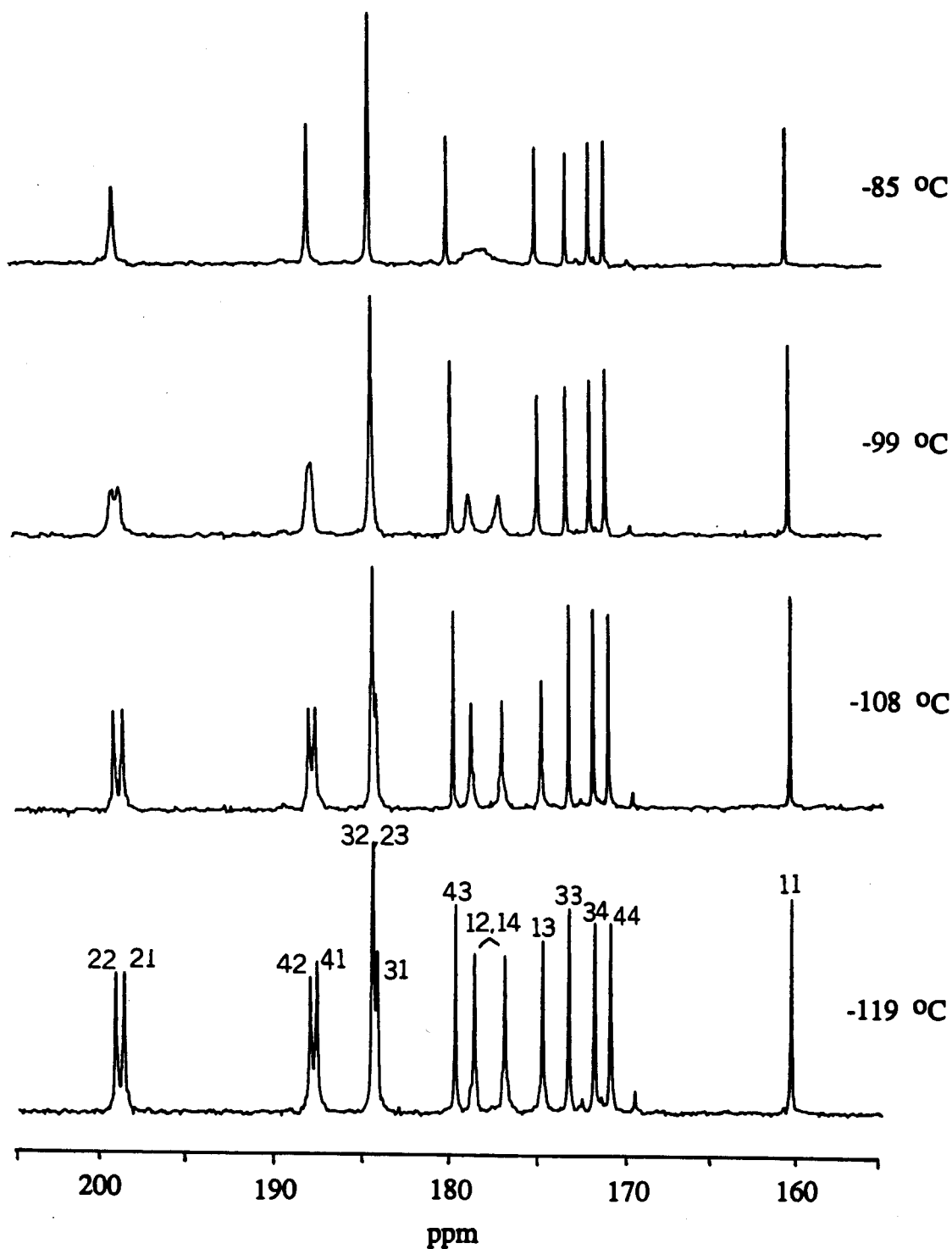


Fig. 3.2 Variable temperature ^{13}C NMR spectra for $\text{Os}_4(\text{CO})_{15}(\text{CNBu}^t)$ (^{13}C -enriched sample; in $\text{CH}_2\text{Cl}_2/\text{CD}_2\text{Cl}_2$ except for the spectrum at -119°C which was taken in $\text{CHCl}_2/\text{CD}_2\text{Cl}_2$).

are shifted to lower field than the corresponding resonances of $\text{Os}(\text{CO})_4$ groups;^{47,78,79} the resonance of the carbonyl trans to the dative metal-metal bond appears at characteristic high fields;^{80,81} the mode of collapse of the signals at higher temperatures and the proposed mechanism for the CO exchange (discussed below).

As mentioned, the spectrum of $\text{Os}_4(\text{CO})_{15}(\text{CNBu}^t)$ at low temperature indicates the CNBu^t is locked in a position out of the Os_4 plane, that is, the rotation about the $\text{Os}(1)$ - $\text{Os}(2)$ bond is slow on the NMR time scale. Fig. 3.3 is a diagrammatic representation of the various staggered conformers that result from rotation about the $\text{Os}(1)$ - $\text{Os}(2)$ bond. Models show there is a severe steric interaction between the isocyanide ligand and the vicinal equatorial

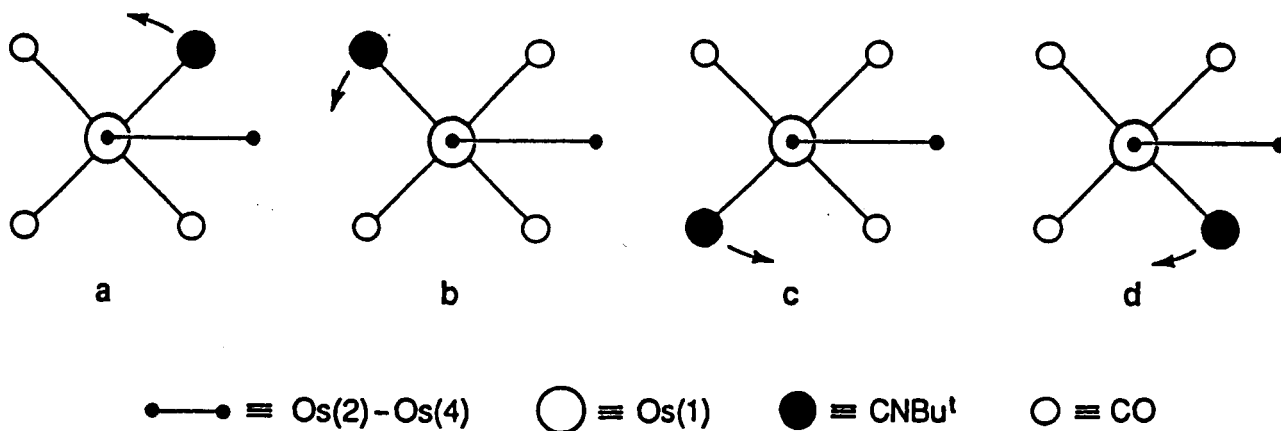


Fig. 3.3 Diagrammatic representation of the different conformations resulted when the $\text{Os}(\text{CO})_4(\text{CNBu}^t)$ group oscillates about the Os - Os bond in $\text{Os}_4(\text{CO})_{15}(\text{CNBu}^t)$.

carbonyl on Os(4) (i.e., CO(43)) when the Os(1)-Os(2) bond is rotated (Fig. 3.4). The estimated distance of the quaternary carbon of the tert-butyl group, C(1), from the oxygen atom of the carbonyl, O(43), is about 1.05 Å.⁶⁹ It is easy to visualize that this interaction could prevent the direct conversion of the conformers represented as **a** and **d**. This is, however, not sufficient to account for the inequivalencies in the low-temperature ¹³C NMR spectrum of Os₄(CO)₁₅(CNBu^t) since rapid oscillation back and forth between conformers **a** and **d** via conformers **b** and **c** (i.e., without the CNBu^t ligand passing CO(43)) would result in the pairs of carbonyls above and below the Os₄ plane becoming equivalent (which is observed at high temperatures). If the barrier to rotation is steric in origin, there must be a second point of severe interaction to cause the inequivalencies. This could be due to either the CNBu^t ligand passing a second carbonyl (CO(21), CO(22), or CO(23)) or to a radial carbonyl of Os(CO)₄(CNBu^t) passing the vicinal carbonyl CO(43). Models show that it is probably the latter interaction that gives rise to the barrier (Fig. 3.5).

If the barrier to rotation or oscillation is due to a carbonyl of the Os(CO)₄(L) ligand passing a vicinal equatorial carbonyl of the Os₃(CO)₁₁ unit, then a similar barrier should be present in (Me₃P)(OC)₄OsOs₃(CO)₁₁. Such a barrier would be detectable since the inequivalent radial

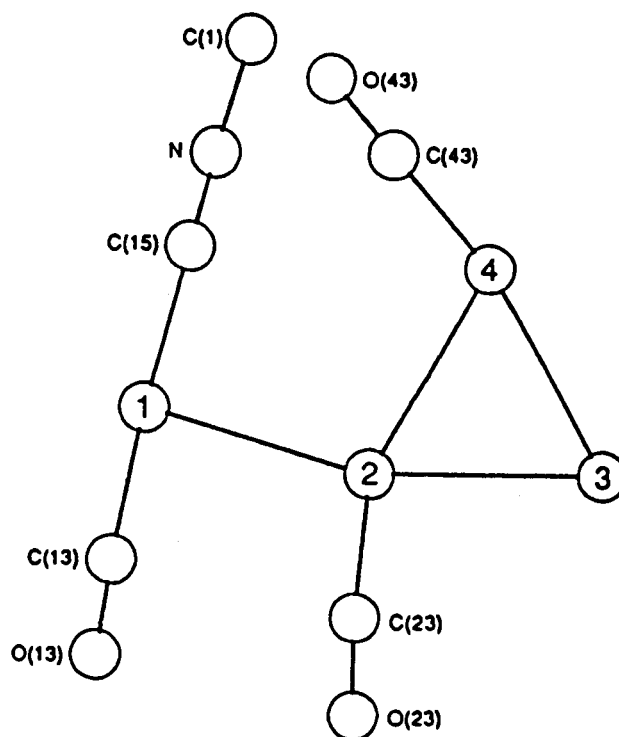


Fig. 3.4 Calculated model showing the steric hindrance between the CNBu^t ligand and its vicinal carbonyl during the rotation of the $\text{Os}(\text{CO})_4(\text{CNBu}^t)$ group about the $\text{Os}(1)\text{-Os}(2)$ bond.

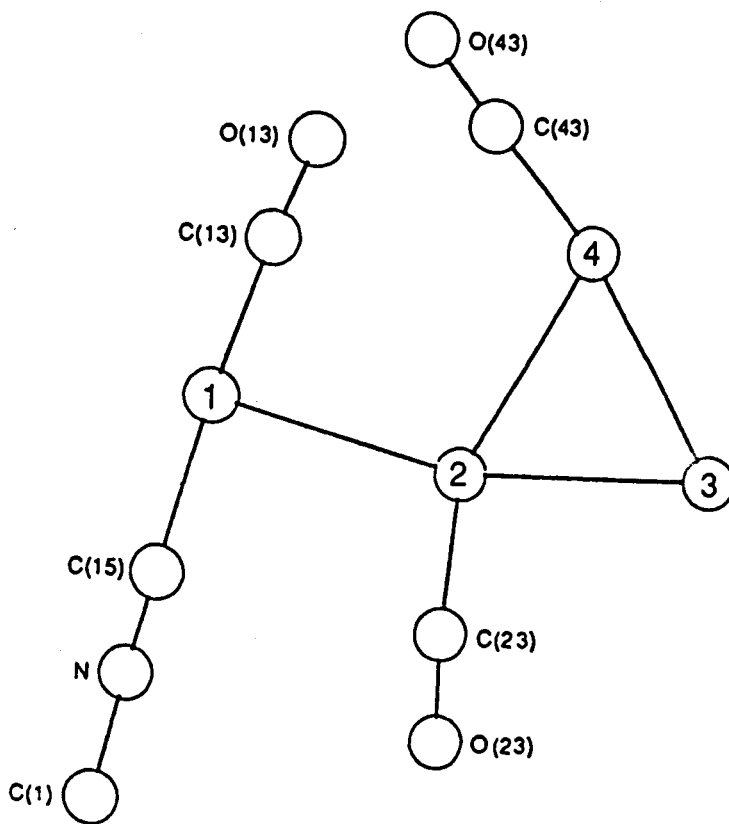


Fig. 3.5 Calculated model showing the steric hindrance between CO(13) and its vicinal carbonyl CO(43) during the rotation of the $\text{Os}(\text{CO})_4(\text{CNBu}^t)$ group about the Os(1)-Os(2) bond.

carbonyls should give two resonances due to inner (near the Os₃ triangle) and outer pairs. The results of the investigation of the ¹³C NMR spectrum of (Me₃P)(OC)₄Os-Os₃(CO)₁₁ at low temperature, however, were inconclusive. At -90 °C the signal assigned to the radial carbonyls of the Os(CO)₄(PMe₃) unit was slightly broadened which might have indicated the onset of restricted rotation about the Os-Os dative bond. Studies at still lower temperatures were prevented by the low solubility of the compound. It might be expected that the barrier to this rotation in Os₃(CO)₁₁-Os(CO)₄(PMe₃) would be lower than the corresponding barrier in Os₄(CO)₁₅(CNBu^t) since the dative Os-Os bond length in Os₃(CO)₁₁Os(CO)₄(PMe₃) is somewhat longer than that in Os₄(CO)₁₅(CNBu^t).

On warming the sample of Os₄(CO)₁₅(CNBu^t) from -115 °C to -50 °C, four pairs of signals each coalesce to a singlet (Fig. 3.2 and 3.6). This behaviour is consistent with the onset of oscillation of the CNBu^t group about the Os₄ plane. Given the severity of the interaction between the CNBu^t ligand with CO(43) (Fig. 3.4), it is probable that there is never completely free rotation about the Os(1)-Os(2) bond. Simulation of the spectrum at -85 ± 2 °C (Fig. 3.7) yielded a first-order rate constant for the process of 350 ± 35 s⁻¹ which corresponds to a ΔG[‡] of 8.7 ± 0.2 kcal mol⁻¹. Other compounds which show restricted rotation about unbridged, single bonds between transition metals are those in

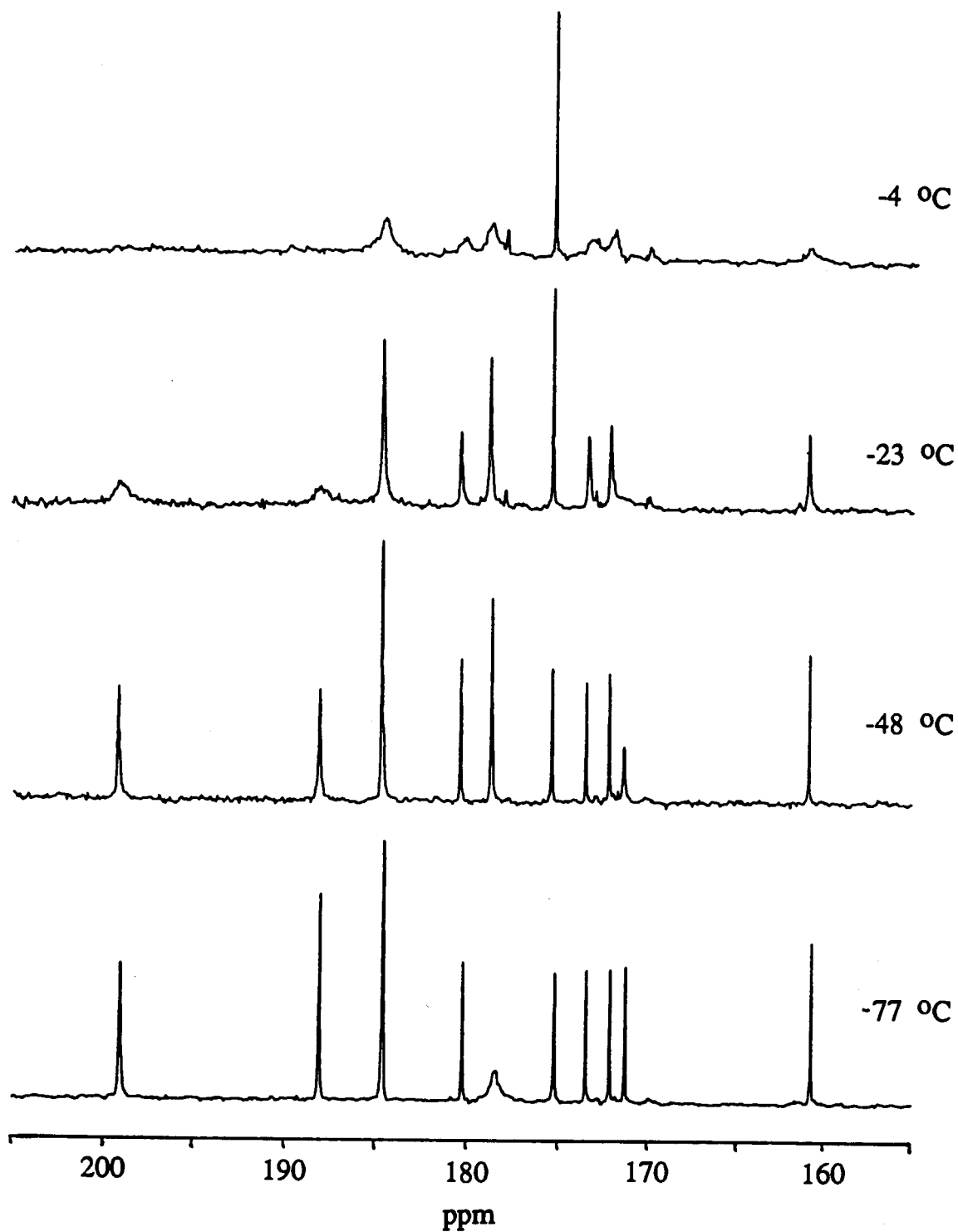


Fig. 3.6 Variable temperature ^{13}C NMR spectra for $\text{Os}_4(\text{CO})_{15}(\text{CNBu}^t)$ (^{13}C O-enriched sample; in $\text{CH}_2\text{Cl}_2/\text{CD}_2\text{Cl}_2$).

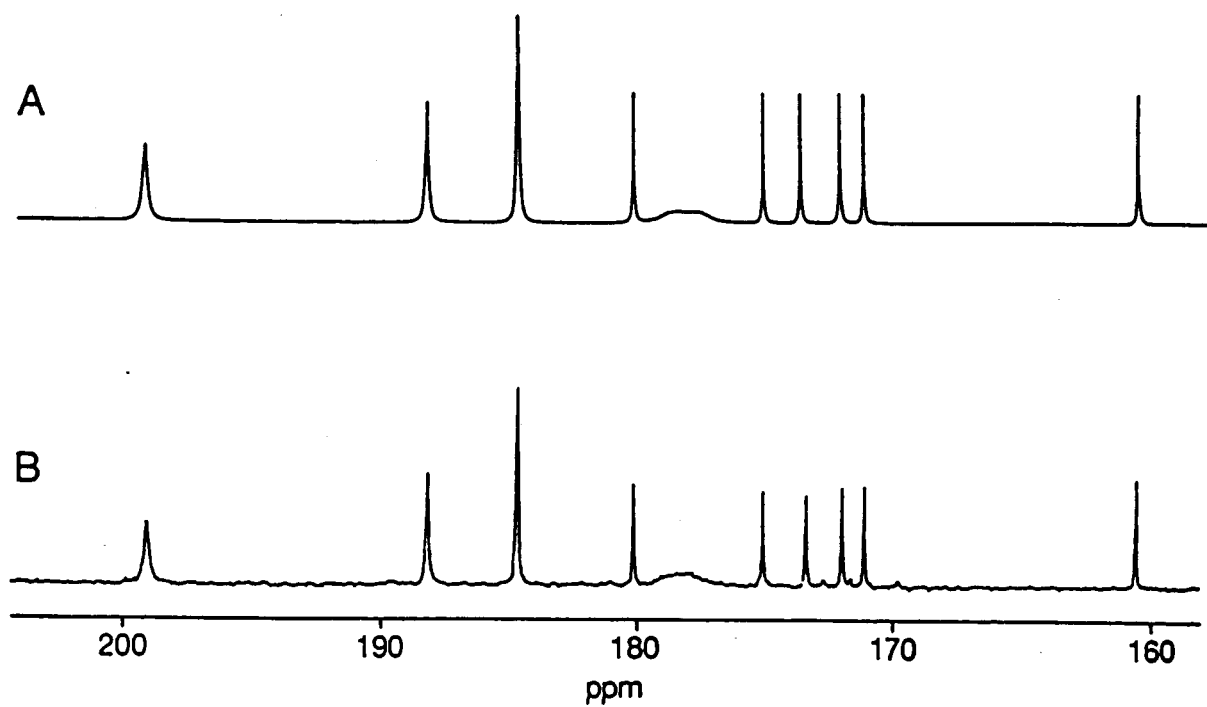


Fig. 3.7 Calculated (A) and experimental (B) ^{13}C NMR spectra of $\text{Os}_4(\text{CO})_{15}(\text{CNBu}^t)$ at -85°C .

molecules of the type $[(\eta^5\text{-C}_5\text{H}_5)\text{M}(\text{CO})_3]_2$ (M = Cr, Mo, W) and the related compound $(\eta^5\text{-C}_5\text{H}_5)_2\text{Mo}_2(\text{CO})_5(\text{CNMe})$ observed by Cotton and co-workers.¹

From about -50 °C to -20 °C, two signals assigned to equatorial carbonyls and two signals assigned to axial carbonyls of the $\text{Os}_3(\text{CO})_{11}$ unit collapse to the base line (Fig. 3.2; one of the resonances is degenerated with a signal at δ 184.6 that does not collapse). Of the latter two signals, one is due to the axial carbonyls attached to the osmium atom to which the $\text{Os}(\text{CO})_4(\text{CNBu}^t)$ group is bound. This pattern of collapse has been observed previously in $(\text{Me}_3\text{P})(\text{OC})_4\text{OsOs}_3(\text{CO})_{11}$ ³⁷ and other $\text{Os}_3(\text{CO})_{11}(\text{L})$ derivatives;^{46,47,a} it has been rationalized in terms of the well-known, terminal-bridge carbonyl exchange in the axial plane that is cis perpendicular to L as shown in Fig. 3.8 (L = $\text{Os}(\text{CO})_4(\text{CNBu}^t)$). Simulation of the spectrum at -48 ± 2 °C gave a first-order rate constant for this process of 11 ± 1 s⁻¹ and hence a ΔG^\ddagger of 12.0 ± 0.2 kcal mol⁻¹ (Fig. 3.9).

Between -20 and -4 °C all the remaining signals except that at δ 174.9 collapsed to the base line (Fig. 3.6). Spectra at higher temperatures were not investigated because of appreciable decomposition of the sample in solution at

a. Other examples have been described in Chapter 2 of this thesis.

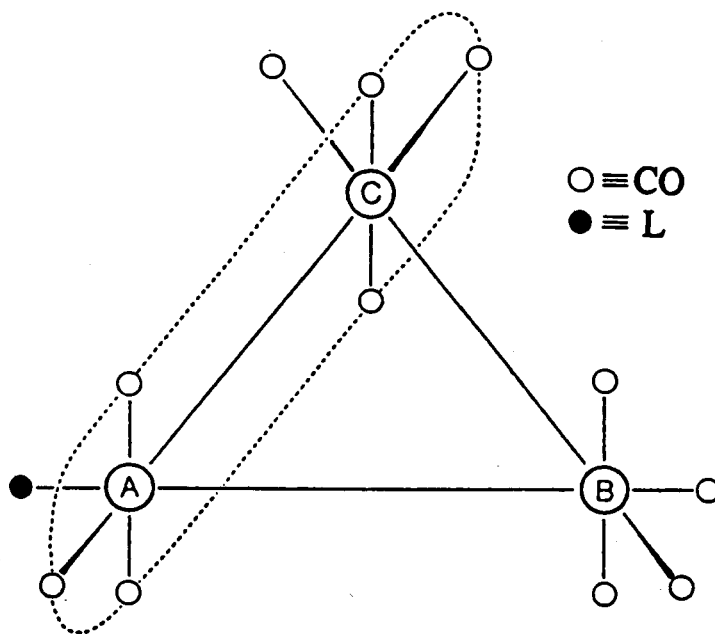


Fig. 3.8 Terminal-bridge carbonyl exchange process that takes place in the axial plane that is cis perpendicular to L of $\text{Os}_3(\text{CO})_{11}(\text{L})$ cluster.

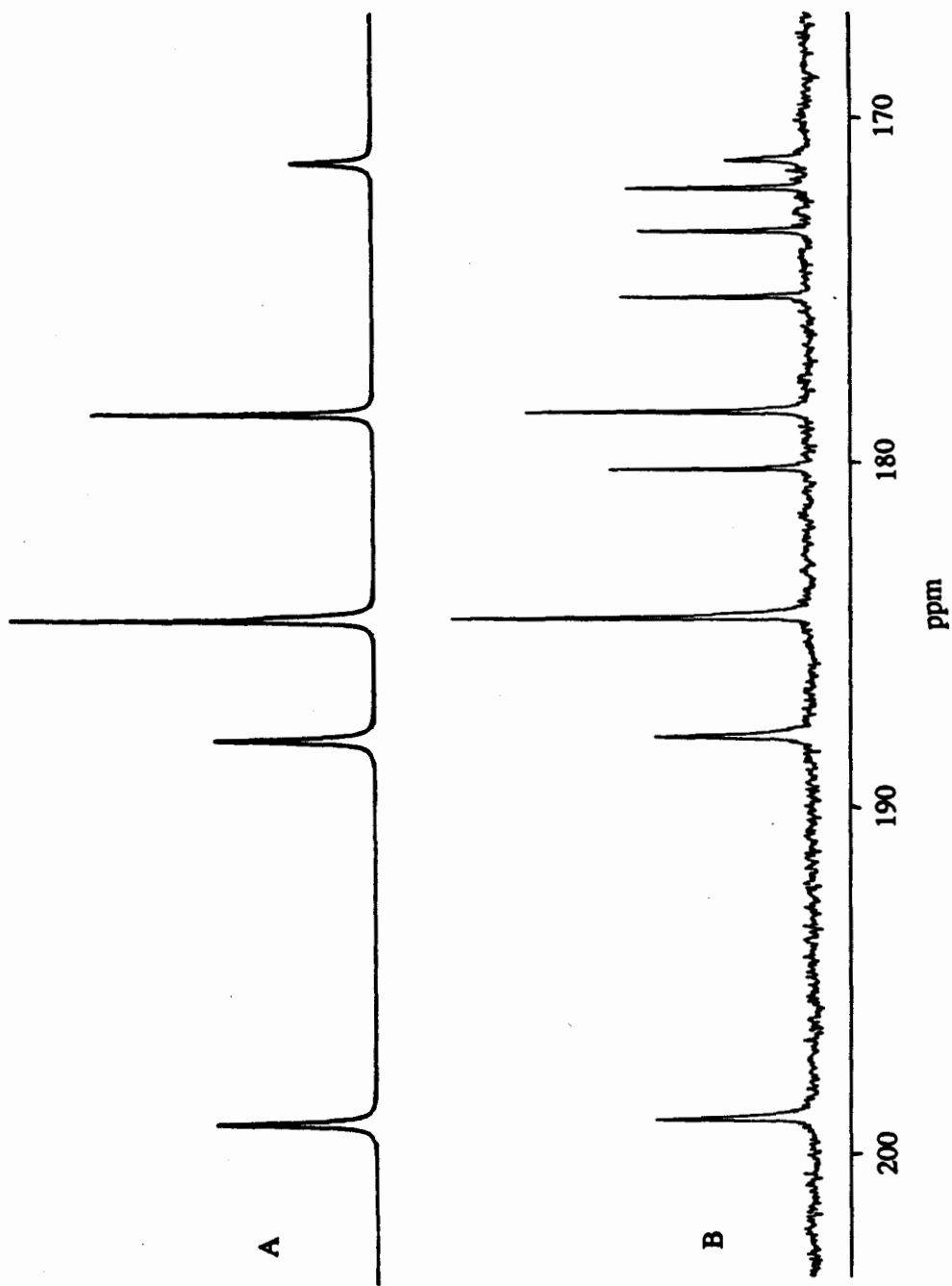


Fig. 3.9 Calculated (A) and observed (B) ^{13}C NMR spectra of $\text{Os}_4(\text{CO})_{15}(\text{CNBu}^t)$ at -48°C . (only the signals of the carbonyls involved in the exchange processes were simulated due to the limit of 10 spins of the EXCHANGE program; the high field signal of carbonyl 11 is not shown.)

these temperatures. The collapse is best rationalized in terms of terminal-bridge carbonyl exchanges, with approximately equal activation energies, in the other two planes that are perpendicular to the Os_4 plane and pass through two of the osmium atoms of the Os_3 triangle. Furthermore, three of the four carbonyls of the $Os(CO)_4(CNBU^t)$ grouping are believed to take part in the exchange in the plane that contains $Os(2)$ and $Os(3)$; this is shown in Fig. 3.10 (positions 1, 2, and 3 occupied by CO). The sharp signal in the spectrum of the sample at $-4^\circ C$ is therefore assigned to the carbonyl trans to the $CNBU^t$ ligand (i.e., $CO(13)$) which is not involved in any of these processes.

A similar exchange was proposed for $(Me_3P)(OC)_4Os-Os_3(CO)_{11}$.³⁷ However, the noncarbonyl ligand in this molecule is initially trans to the metal-metal bond (i.e., in position 2), and isomerization occurs with the terminal-bridge carbonyl exchange. This isomerization results in all the carbonyls of $(Me_3P)(OC)_4OsOs_3(CO)_{11}$ becoming involved in the exchange and all the signals of the $Os(CO)_4(PMe_3)$ unit collapse, as observed. That one of the signals of the $Os(CO)_4(CNBU^t)$ unit remains sharp probably indicates that the isomer of $Os_4(CO)_{15}(CNBU^t)$ with the $CNBU^t$ trans to the $Os(1)-Os(2)$ bond is not present in solution. Strong support for this view is provided by the fluxional processes exhibited by $[(OC)_3(BU^tNC)_2Os]Os_3(CO)_{11}$ reported below.

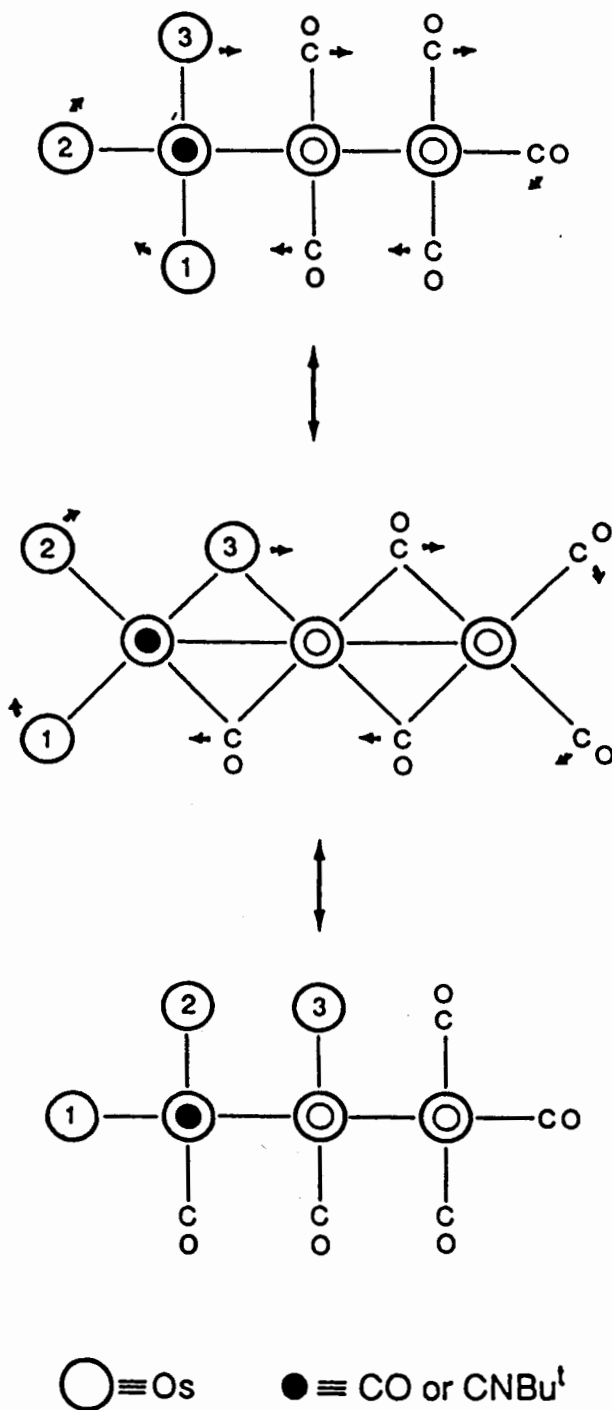


Fig. 3.10 Proposed mechanism that exchanges three carbonyls of the $\text{Os}(\text{CO})_4(\text{CNBU}^t)$ group with those of the $\text{Os}_3(\text{CO})_{11}$ fragment.

It is pointed out here that in $\text{Os}_3(\text{CO})_{11}[\text{P}(\text{OMe})_3]$ terminal-bridge carbonyl exchange occurs in only two of the axial planes as shown in Fig. 3.11 ($L = \text{P}(\text{OMe})_3$). This results in all the ^{13}C NMR signals except one (that marked with an asterisk) of the $\text{Os}_3(\text{CO})_{11}$ unit collapsing to the base line.⁴⁷ (The low temperature ^{13}C NMR spectrum of $\text{Ru}_3(\text{CO})_{11}[\text{P}(\text{OMe})_3]$ exhibits two signals in a 10:1 ratio; this indicates the same processes are probably occurring but at a faster rate.⁵) That a similar situation could be taking place in $\text{Os}_4(\text{CO})_{15}(\text{CNBu}^t)$ was therefore considered, that is, the sharp signal in the spectrum recorded with the sample at -4°C is due to the carbonyl in the trans, three-bond position to the $\text{Os}(\text{CO})_4(\text{CNBu}^t)$ ligand (i.e., Fig. 3.11, $L = \text{Os}(\text{CO})_4(\text{CNBu}^t)$). This was, however, rejected as improbable. If the mechanism shown in Fig. 3.11 is applied to $\text{Os}_4(\text{CO})_{15}(\text{CNBu}^t)$ (i.e., no exchange in the axial $\text{Os}(1)\text{-Os}(2)\text{-Os}(3)$ plane so that $\text{CO}(34)$ remains rigid), it would require all three different types of carbonyls of the $\text{Os}(\text{CO})_4(\text{CNBu}^t)$ unit to simultaneously exchange with some of the carbonyls attached to $\text{Os}(4)$, an atom that is not directly bound to the $\text{Os}(\text{CO})_4(\text{CNBu}^t)$ fragment. This is considered most unlikely.

Further support for the mechanism shown in Fig. 3.10 over that shown in Fig. 3.11 comes from the fluxional processes exhibited by $[(\text{OC})_3(\text{Bu}^t\text{NC})_2\text{Os}]\text{Os}_3(\text{CO})_{11}$ discussed in detail below. The mechanism in Fig. 3.10 also leads to

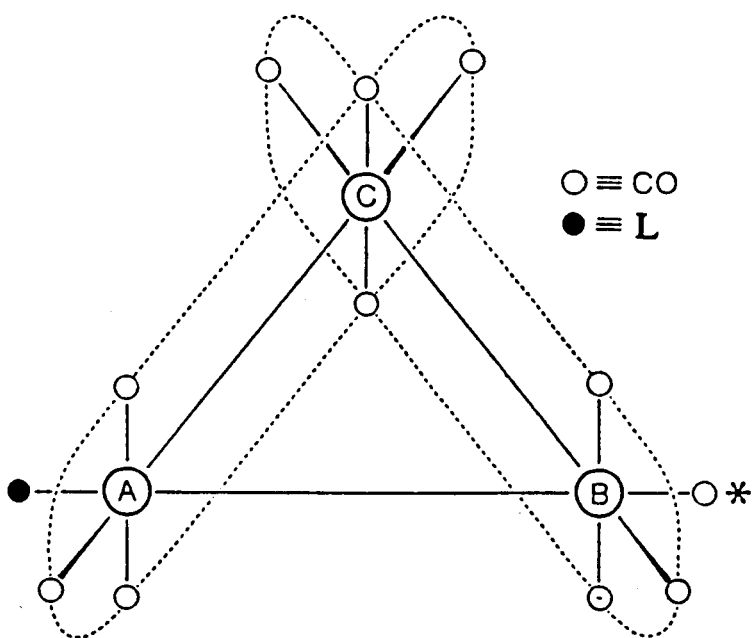


Fig. 3.11 The two proposed terminal-bridge carbonyl exchange processes that take place in the perpendicular plane of the Os₃(CO)₁₁(L) cluster.

the assignment of the carbonyl resonance trans to the CNBu^t ligand ($\text{CO}(13)$) as upfield rather than downfield to the signal due to the carbonyls cis to the isocyanide ligand ($\text{CO}(12)$ and $\text{CO}(14)$). In $(\text{OC})_4(\text{Bu}^t\text{NC})\text{OsM}(\text{CO})_5$ ($\text{M} = \text{Cr}, \text{Mo}, \text{W}$), recently prepared by Shipley and Pomeroy, the assignment of the ^{13}C NMR resonances is unambiguous,⁸¹ and the signal of the carbonyl trans to CNBu^t is to higher field than the resonances of the carbonyls cis to the CNBu^t ligand (but not trans to the dative Os-Cr bond).

If the process in Fig. 3.10 is operative in $\text{Os}_4(\text{CO})_{15}(\text{CNBu}^t)$, then exchange must also occur in the axial plane containing the Os(3) and Os(4) atoms in order that all the signals due to the carbonyls of the $\text{Os}_3(\text{CO})_{11}$ moiety collapse. This, however, is expected: the corresponding exchanges in the allowed planes of $\text{Os}_3(\text{CO})_{12-x}[\text{P}(\text{OMe})_3]_x$ ($x = 1, 2, 4$)⁴⁷ and in $\text{Os}_3(\text{CO})_{12-x}(\text{PEt}_3)_x$ ($x = 1, 2$)⁴⁶ have similar activation energies.

$\text{Os}_4(\text{CO})_{14}(\text{CNBu}^t)_2$

The X-ray structure of $\text{Os}_4(\text{CO})_{14}(\text{CNBu}^t)_2$ has not been determined. The ^{13}C NMR spectrum of this cluster at -101°C , however, is consistent with the structure shown in Fig. 3.12.⁷⁰ The two CNBu^t ligands of the $\text{Os}(\text{CO})_3(\text{CNBu}^t)_2$ group are in a cis arrangement in radial positions. This arrangement of isocyanide ligands was found in the crystal structure of $(\text{OC})_3(\text{Bu}^t\text{NC})_2\text{OsCr}(\text{CO})_5$.⁸¹ This configuration

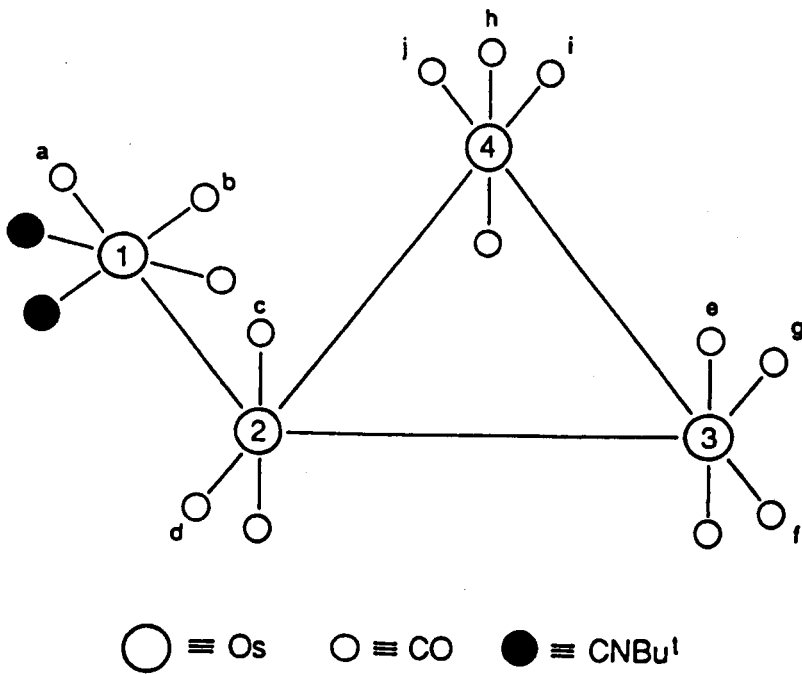


Fig. 3.12 Proposed structure and the labelling scheme of $\text{Os}_4(\text{CO})_{14}(\text{CNBu}^t)_2$.⁷⁰

in $\text{Os}_4(\text{CO})_{14}(\text{CNBu}^t)_2$ probably avoids the steric interactions of the CNBu^t ligands with the vicinal carbonyl on the adjacent Os atom (i.e., carbonyl j in Fig. 3.12) in a similar manner to that discussed for $\text{Os}_4(\text{CO})_{15}(\text{CNBu}^t)$. It may also be the electronically preferred arrangement since it reduces the competition for π -electron density by the carbonyl ligands on the same metal centre. That two infrared $\text{C}\equiv\text{N}$ stretches, at 2220.5 and 2201.5 cm^{-1} , observed for $\text{Os}_4(\text{CO})_{14}(\text{CNBu}^t)_2$ in hexane solution is also consistent with a cis arrangement of the two CNBu^t ligands.⁸¹ For the $(\text{OC})_3(\text{Bu}^t\text{NC})_2\text{OsM}(\text{CO})_5$ ($\text{M} = \text{Cr}, \text{Mo}, \text{W}$) complexes, there was evidence in solution for the isomer with the isocyanide ligands in radial positions but in a trans arrangement to one another. There was, however, no spectroscopic evidence for this isomer for $\text{Os}_4(\text{CO})_{14}(\text{CNBu}^t)_2$.

The ^{13}C NMR spectrum of $\text{Os}_4(\text{CO})_{14}(\text{CNBu}^t)_2$ (^{13}CO -enriched) in $\text{CH}_2\text{Cl}_2/\text{CD}_2\text{Cl}_2$ at -101°C exhibits ten carbonyl resonances at δ 200.4 (2C), 188.7 (2C), 186.2 (1C), 185.5 (2C), 180.5 (1C), 179.6 (2C), 175.2 (1C), 172.9 (1C), 171.3 (1C), 161.7 (1C) (Fig. 3.13). The assignments of the signals shown in Fig. 3.13 follows arguments similar to those used for $\text{Os}_4(\text{CO})_{15}(\text{CNBu}^t)$. The assignments of the signals due to carbonyls f, g, and j are not as definitive as those for the other carbonyls. These are assigned based on the assumption that peaks due to carbonyls in similar chemical environments should have similar chemical shifts.

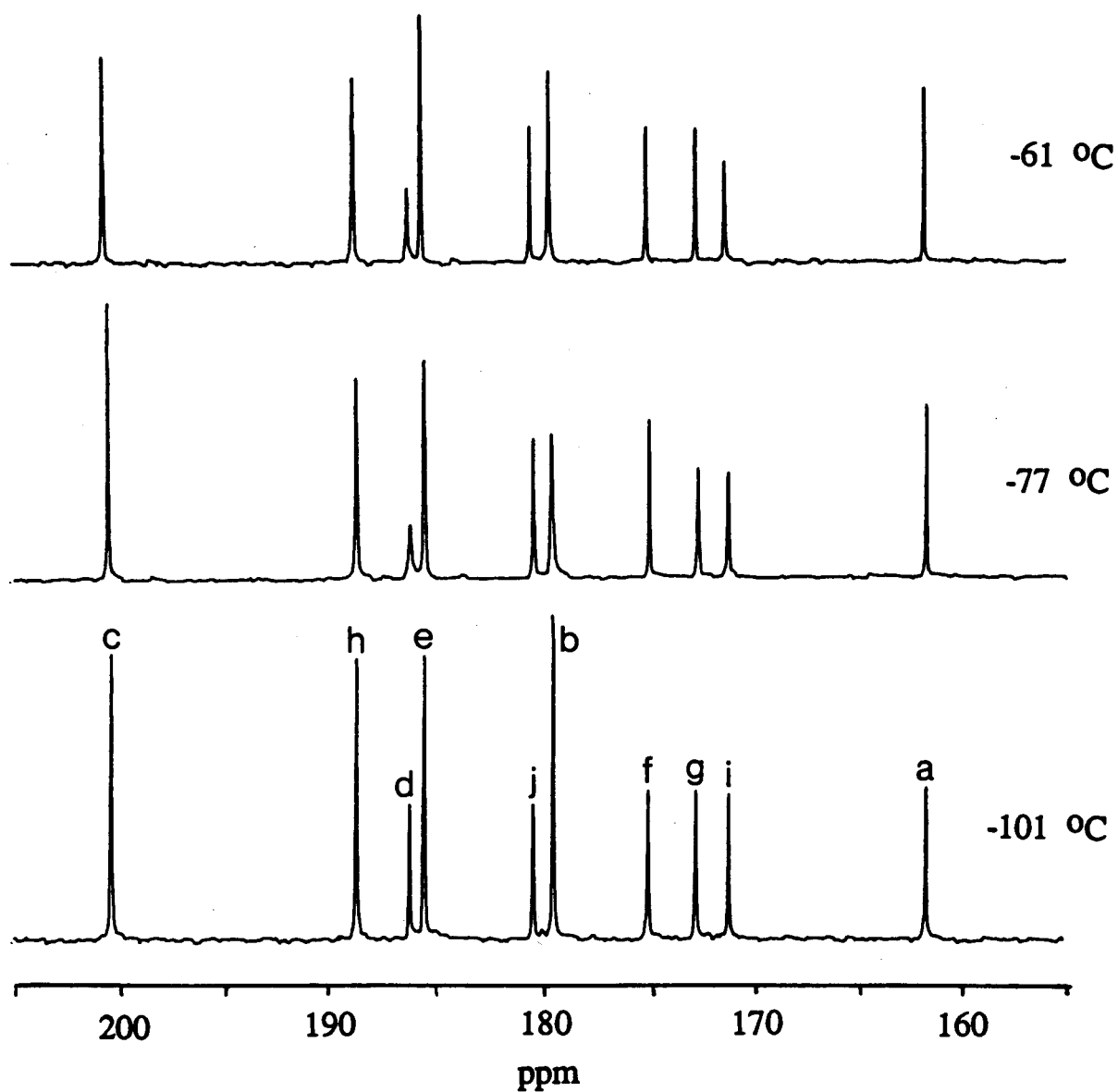


Fig. 3.13 Variable temperature ^{13}C NMR spectra for $\text{Os}_4(\text{CO})_{14}(\text{CNBu}^t)_2$ (^{13}C O-enriched sample; in $\text{CH}_2\text{Cl}_2/\text{CD}_2\text{Cl}_2$ solution). The assignment of the signals follows that in Fig. 4.12.

On warming the sample from $-101\text{ }^{\circ}\text{C}$ to about $-70\text{ }^{\circ}\text{C}$ a general loss of intensity of all carbonyl signals, with respect to the intensity of the signal at $\delta\ 161.7$ assigned to carbonyl a, was observed in the ^{13}C NMR spectrum (Fig. 3.13). The distinct high field signal of carbonyl a is used as a reference peak because it does not exchange with other carbonyls in the cluster up to $19\text{ }^{\circ}\text{C}$ and because it would be less affected by any type of restricted rotation about the Os-Os dative bond. A possible explanation for this observation is as follows. In solution there is a second conformer present due to restricted rotation about the Os-Os dative bond. This would most probably be b (or b') as shown in Fig. 3.14. The concentration of this second isomer is so low that its presence is not detected. On warming the sample to $-70\text{ }^{\circ}\text{C}$ oscillation about the Os-Os dative bond becomes rapid which thus equilibrates the two conformers a and b (Fig. 3.14). The chemical shifts of a given carbonyl in each conformer are expected to be similar because of the similarity of the two conformers. Hence the loss of intensity in the signal due to a given carbonyl in each conformer would be small because of their small chemical shift difference. The exception to this would be the signals due to carbonyls b and d because they are most affected by the change in the environments of the isocyanide ligands, i.e., the chemical shift difference between signals

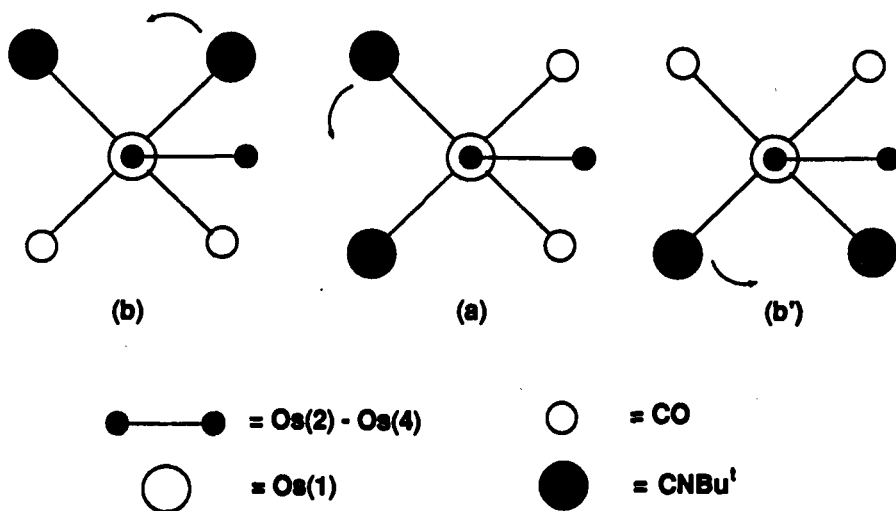


Fig. 3.14 Schematic presentation of different conformations resulted when $\text{Os}(\text{CO})_3(\text{CNBu}^t)_2$ group oscillates about the Os(1)-Os(2) bond.

due to carbonyls b and d would be large in the two conformers. Consequently, as the equilibration of the two conformers becomes rapid these signals should broaden the most, as is observed. This is shown diagrammatically in Fig. 3.15.⁵¹

On warming the sample from $-60\text{ }^\circ\text{C}$ to $-35\text{ }^\circ\text{C}$, the now familiar mode of collapse of signals was observed: two signals assigned to four axial carbonyls and two signals assigned to two equatorial carbonyls collapsed to the base line at the same rate (Fig. 3.16). This is, once again, rationalized in terms of terminal-bridge carbonyl exchange

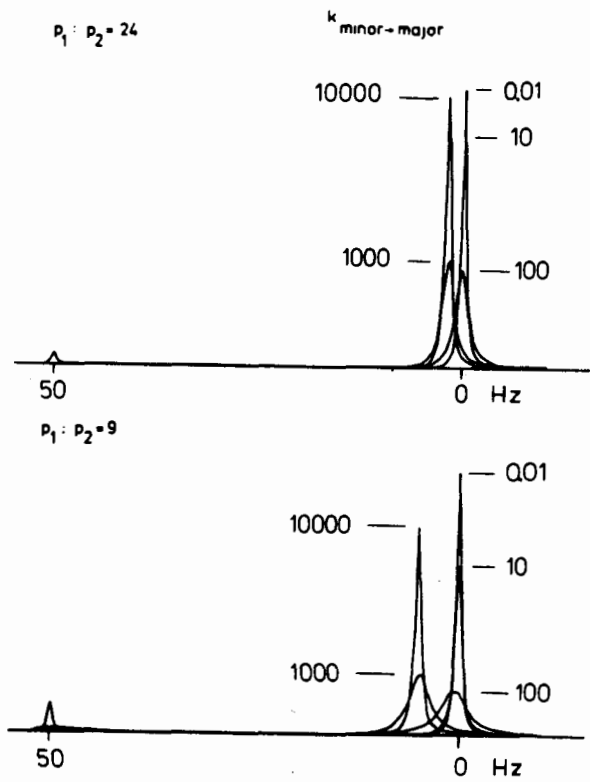


Fig. 3.15 Diagrammatic presentation of the coalescence of two unequally populated signals when the two signals are close and far apart.⁵¹

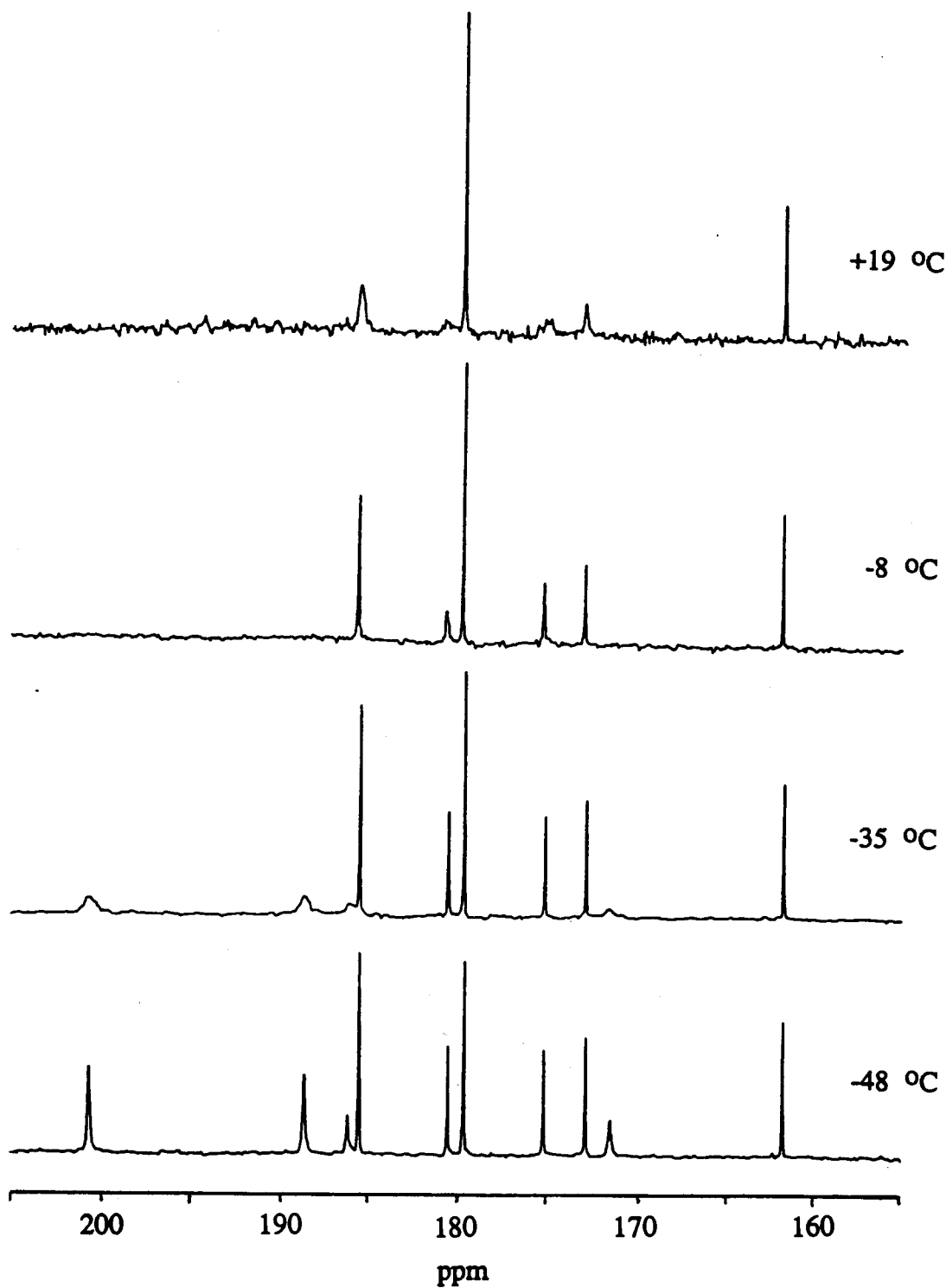


Fig. 3.16 Variable temperature ^{13}C NMR spectra for $\text{Os}_4(\text{CO})_{14}(\text{CNBu}^t)_2$ (^{13}C O-enriched sample; in $\text{CH}_2\text{Cl}_2/\text{CD}_2\text{Cl}_2$ solution).

which takes place in the vertical plane cis to the $\text{Os}(\text{CO})_3(\text{CNBu}^t)_2$ grouping that contains the Os(2) and Os(4) atoms. The simulation of the ^{13}C NMR spectrum at -48°C (Fig. 3.17) yielded a first-order rate constant of $14 \pm 2 \text{ s}^{-1}$ and hence a ΔG^\ddagger value of $11.9 \pm 0.3 \text{ kcal mol}^{-1}$. It is noted that the activation energy of this carbonyl exchange process for $\text{Os}_4(\text{CO})_{14}(\text{CNBu}^t)_2$ is similar to that found in $\text{Os}_4(\text{CO})_{15}(\text{CNBu}^t)$ ($12.0 \pm 0.2 \text{ kcal mol}^{-1}$) and in $\text{Os}_4(\text{CO})_{15}(\text{PMe}_3)$ ($11.6 \pm 0.2 \text{ kcal mol}^{-1}$) for the same process.

Warming the sample to about -10°C caused four more signals to broaden and collapse to the base line. In a manner similar to the carbonyl exchange process proposed for $\text{Os}_3(\text{CO})_{11}(\text{ER}_3)$ (discussed in Chapter 2), terminal-bridge carbonyl exchange in the vertical plane that contains Os(3) and Os(4) can account for the collapse of the signals which are assigned to carbonyls e, f and j (Fig. 3.16). The collapse of the signal assigned to carbonyl g is rationalized in terms of a trigonal twist mechanism at Os(3) that exchanges carbonyls e, f and g. This type of exchange has been proposed for $\text{Os}_3(\text{CO})_{11-x}[\text{P}(\text{OMe})_3]_x$ ($x = 1 - 5$)^{47,82} and $\text{HOs}_3(\text{CO})_{10}(\text{COEt})$.⁸³ It was observed in the ^{13}C NMR spectrum at -8°C that the signal assigned to carbonyl j collapsed to the base line at a rate faster than it should do if this carbonyl were only involved in the CO exchange in the vertical plane containing Os(3) and Os(4). It is

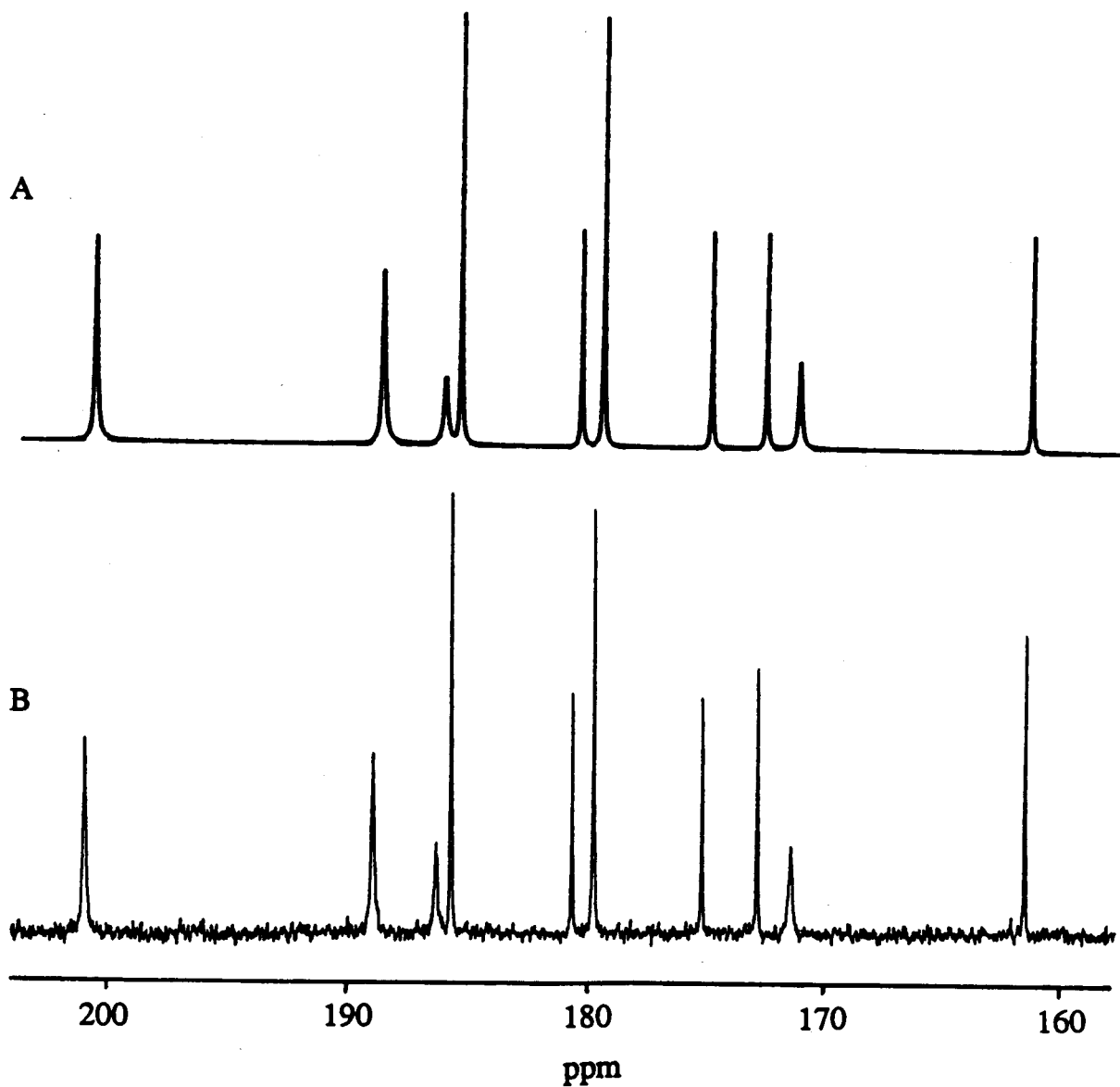


Fig. 3.17 Calculated (A) and observed (B) ^{13}C NMR spectra of $\text{Os}_4(\text{CO})_{14}(\text{CNBu}^t)_2$ at -48°C .

believed that a trigonal twist process at Os(4) that exchanges carbonyls i, h and j also occurs thus increasing the rate of broadening of the signal due to carbonyl j.

Two signals remain sharp in the spectrum recorded at +19 °C. These signals are assigned to carbonyls a and b of the Os(CO)₃(CNBu^t)₂ grouping. This indicates that, at this temperature, they do not exchange with the carbonyls of the Os₃(CO)₁₁ fragment. The exchange of the carbonyls of the Os(CO)₄(CNBu^t) units with those of the Os₃(CO)₁₁ fragment occurs in Os₄(CO)₁₅(CNBu^t) was rationalized in terms of a terminal-bridge CO exchange in the vertical plane that contains Os(1), Os(2) and Os(3). This involves an intermediate with two bridging carbonyls across the Os(1)-Os(2) dative bond as shown in Fig. 3.12. When position 1 in Fig. 3.12 is occupied by a CNBu^t ligand, the exchange would require the CNBu^t ligand to move to the axial position (i.e., trans to the Os(1)-Os(2) dative bond). That this apparently does not occur may indicate there is a strong electronic preference for the CNBu^t ligand to stay in a radial position. When position 3 is occupied by a CNBu^t ligand, the exchange would require the CNBu^t ligand (and one carbonyl) to move to a bridging position. That this also does not occur probably indicates that such an intermediate may have a higher energy than the corresponding intermediate with two bridging carbonyls. It may be that the π* orbitals of CNBu^t are higher in energy than those of CO (since the

NBu^t unit is less electronegative than oxygen) and this results in a less favoured overlap of these orbitals with the filled d orbitals on the adjacent osmium atom; in turn, the intermediate with a bridging CNBu^t is less readily formed. It is known that CNBu^t is not as good a bridging species as other isocyanide ligands such as methylisocyanide, phenylisocyanide and benzylisocyanide.⁸⁴

3.3 Puckered-square Os₄ Cluster

Os₄(CO)₁₅(PF₃)

The X-ray crystal structure of Os₄(CO)₁₅(PF₃) revealed that it has a puckered-square Os₄ framework (Fig. 3.18)⁷¹ similar to that of the parent binary carbonyl cluster Os₄(CO)₁₆,⁸⁵ and to the carbon framework in cyclobutane C₄H₈.⁸⁶ The dihedral angle between the planes Os(1)-Os(2)-Os(4) and Os(2)-Os(3)-Os(4) in Os₄(CO)₁₅(PF₃) is 151.7° (the corresponding angle in Os₄(CO)₁₆ is 159.0°). Because of this arrangement, the two axial carbonyls at each osmium centre are chemically nonequivalent. As in trinuclear carbonyl clusters of osmium, the phosphine ligand occupies an equatorial position.^{24,46,53,87} The average Os-Os bond length is about 3.0 Å which is much longer than that found in saturated triosmium clusters. For example, in Os₃(CO)₁₂ the average Os-Os bond length is 2.877 Å.⁹

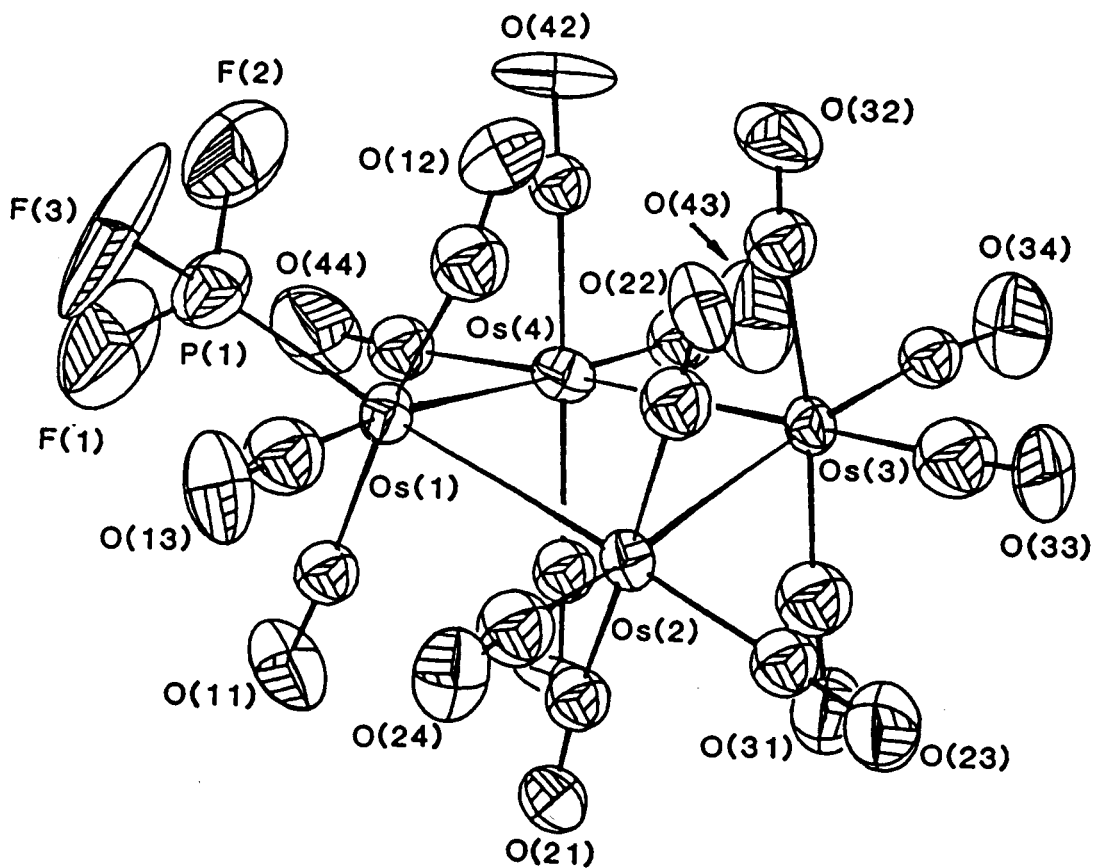


Fig. 3.18 Molecular structure of $\text{Os}_4(\text{CO})_{15}(\text{PF}_3) \cdot 71$
 Important bond lengths (Å) are: $\text{Os}(1)\text{-Os}(2) = 3.005(2)$; $\text{Os}(1)\text{-Os}(4) = 3.000(2)$; $\text{Os}(2)\text{-Os}(3) = 2.977(2)$; $\text{Os}(3)\text{-Os}(4) = 2.994(2)$. Dihedral angle between the planes $\text{Os}(1)\text{-Os}(2)\text{-Os}(4)$ and $\text{Os}(2)\text{-Os}(3)\text{-Os}(4)$ is 151.7° .

The puckered-square Os_4 arrangement found for $\text{Os}_4(\text{CO})_{15}(\text{L})$ ($\text{L} = \text{CO}, \text{PF}_3$) is in contrast to $\text{Os}_4(\text{CO})_{15}(\text{CNBu}^t)$ described above, and $\text{Os}_4(\text{CO})_{15}(\text{L}')$ ($\text{L}' = \text{PMe}_3$,³⁷ $\text{P}(\text{OCH}_2)_3\text{CMe}^{69}$) which have a spiked-triangular array of metal atoms. This difference has been attributed to the electronic rather than steric properties of the noncarbonyl ligand in these clusters.

The ^{13}C NMR spectrum of $\text{Os}_4(\text{CO})_{15}(\text{PF}_3)$ (^{13}C -enriched) in $\text{CH}_2\text{Cl}_2/\text{CD}_2\text{Cl}_2$ at -56°C (Fig. 3.19) exhibits ten resonances at δ 177.3 (2C, $J_{\text{P-C}} = 11.2$ Hz), 176.7 (broad, 4C), 176.3 (2C), 169.6 (1C, $J_{\text{P-C}} = 6.4$ Hz), 169.3 (1C), 169.0 (1C), 168.8 (1C), 168.7 (1C), 168.3 (1C), 168.0 (1C). It has been observed in saturated triosmium clusters that the ^{13}C NMR resonances of axial carbonyls usually appear to low field to those due to the equatorial carbonyls.^{47,78,79} The seven signals to high field of 170 ppm are therefore assigned to the seven equatorial carbonyls in $\text{Os}_4(\text{CO})_{15}(\text{PF}_3)$. The resonance at δ 169.6 which exhibits a partly resolved coupling of ≈ 6.4 Hz to the phosphorus atom of PF_3 is probably due to carbonyl 13. It is curious that a cis coupling of the phosphorus atom of PF_3 with an equatorial carbonyl of $\text{Os}(\text{CO})_3(\text{PF}_3)$ unit is observed in $\text{Os}_4(\text{CO})_{15}(\text{PF}_3)$ but not in $\text{Os}_3(\text{CO})_{11}(\text{PR}_3)$ clusters (see Chapter 2). It is possible, however, that the coupling is a trans, three-bond coupling and therefore the signal is due to carbonyl 23. It has been observed in $\text{Os}_3(\text{CO})_{10}[\text{P}(\text{OMe})_3]_2$

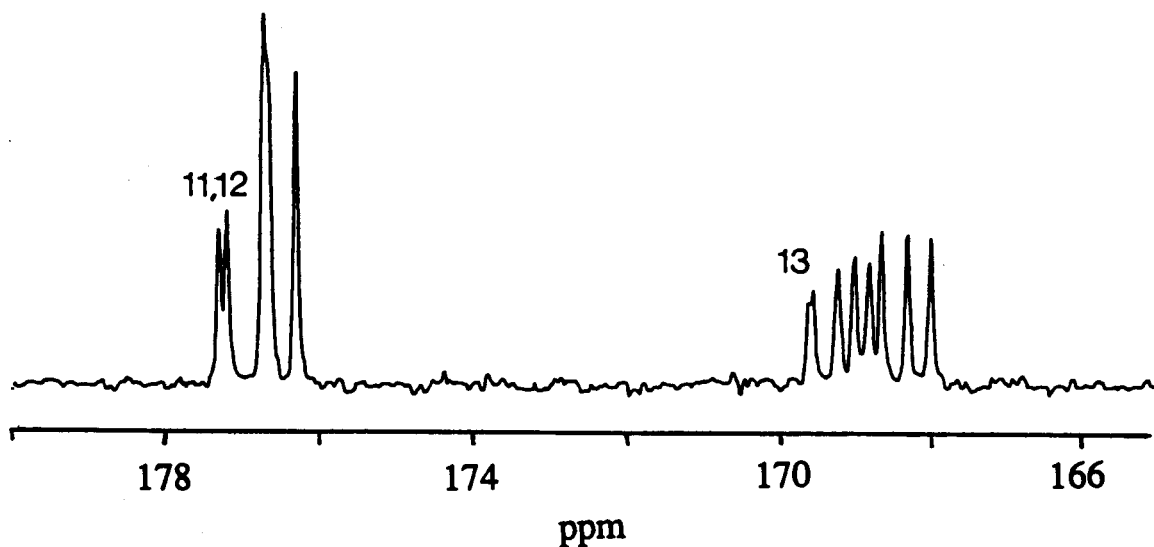


Fig. 3.19 ^{13}C NMR spectrum of $\text{Os}_4(\text{CO})_{15}(\text{PF}_3)$ (^{13}C -enriched, in $\text{CH}_2\text{Cl}_2/\text{CD}_2\text{Cl}_2$) at -56°C .

that the corresponding trans, three-bond coupling is larger than the cis two-bond coupling.⁴⁷ Three-bond F-C couplings from the carbonyls to the fluorine atoms were not observed in the ^{13}C NMR spectrum of $\text{Os}_4(\text{CO})_{15}(\text{PF}_3)$. In the axial carbonyl region (i.e., to low field of 170 ppm), the doublet at δ 177.3 which shows a coupling of 11.2 Hz to the phosphorus atom of the PF_3 ligand is assigned to the axial carbonyls 11 and 12 of the $\text{Os}(\text{CO})_3(\text{PF}_3)$ unit. The P-C coupling constant is close to that observed in $\text{Os}_3(\text{CO})_{11}(\text{PF}_3)$ where $J_{\text{P-C}} = 13.3$ Hz (see Chapter 2). (The three-bond F-C couplings were not observed in either compound.) The broad signal at δ 176.7 is attributed to two unresolved resonances each of relative intensity two.

Further assignment of the signals is, however, not possible. The ^{13}C NMR spectrum of $\text{Os}_4(\text{CO})_{16}$ exhibits two signals at δ 176.6 and 168.8 which are assigned to the axial and equatorial carbonyls, respectively.⁷¹ The similarity of the chemical shifts of the ^{13}C signals of $\text{Os}_4(\text{CO})_{15}(\text{PF}_3)$ and $\text{Os}_4(\text{CO})_{16}$ suggests that the electronic effects of CO and PF_3 are similar in these clusters. It is well known that the CO and PF_3 ligands have similar electronic effects in transition metal complexes.⁸⁸

For a completely rigid molecule of $\text{Os}_4(\text{CO})_{15}(\text{PF}_3)$, eight ^{13}C NMR resonances would be expected for the eight axial carbonyls. However, only four were observed at -56 °C. This is best interpreted in terms of a rapid ring inversion process as proposed for $\text{Os}_4(\text{CO})_{16}$.⁸⁵ The ^{13}C NMR spectrum of $\text{Os}_4(\text{CO})_{15}(\text{PF}_3)$ at -122 °C, however, exhibited an invariant spectrum except that a general broadening of the signals was observed. There was no indication of broadening due to a slowing down of the ring inversion which suggests that the process has a very low energy barrier. Because of its thermal instability in solution above -20 °C, ^{13}C NMR spectra of $\text{Os}_4(\text{CO})_{15}(\text{PF}_3)$ at higher temperatures were not investigated.

3.4 Kite-shaped Os₄ Clusters

Os₄(CO)₁₅

Among the transition metals, osmium forms the most binary carbonyls. The crystal structures of Os₃(CO)₁₂,⁹ Os₅(CO)₁₆,⁸⁹ Os₅(CO)₁₉,⁹⁰ Os₆(CO)₁₈,⁹¹ Os₇(CO)₂₁,⁹² and Os₈(CO)₂₃⁹³ have been determined. The first tetraosmium binary carbonyl, Os₄(CO)₁₅, was synthesized and its structure determined by X-ray crystallography at Simon Fraser University.³⁶ It is the missing link between Os₃(CO)₁₂ and the higher nuclearity osmium clusters mainly synthesized by Lewis and Johnson and co-workers. The crystal structure of Os₄(CO)₁₅, shown in Fig. 3.20, reveals that the metal framework is composed of a planar, kite-shaped Os₄ unit with adjacent long and short Os-Os bonds that have been assigned a bond order of 0.5 and 1.5, respectively.^{36,94} A similar configuration of metal atoms had been previously observed in Os₄(CO)₁₄(PMe₃) and rationalized in terms of three-center, two-electron metal-metal bonds.³⁷

If Os₄(CO)₁₅ is rigid in solution seven carbonyl signals would be expected (Fig. 3.21) in the ¹³C NMR spectrum. The low temperature ¹³C NMR spectra of Os₄(CO)₁₅ (¹³CO enriched sample) in CHFCl₂/CD₂Cl₂, however, only exhibit three signals, at δ 190.5, 189.0 and 171.4. These signals have varying intensities between -6 °C and -119 °C

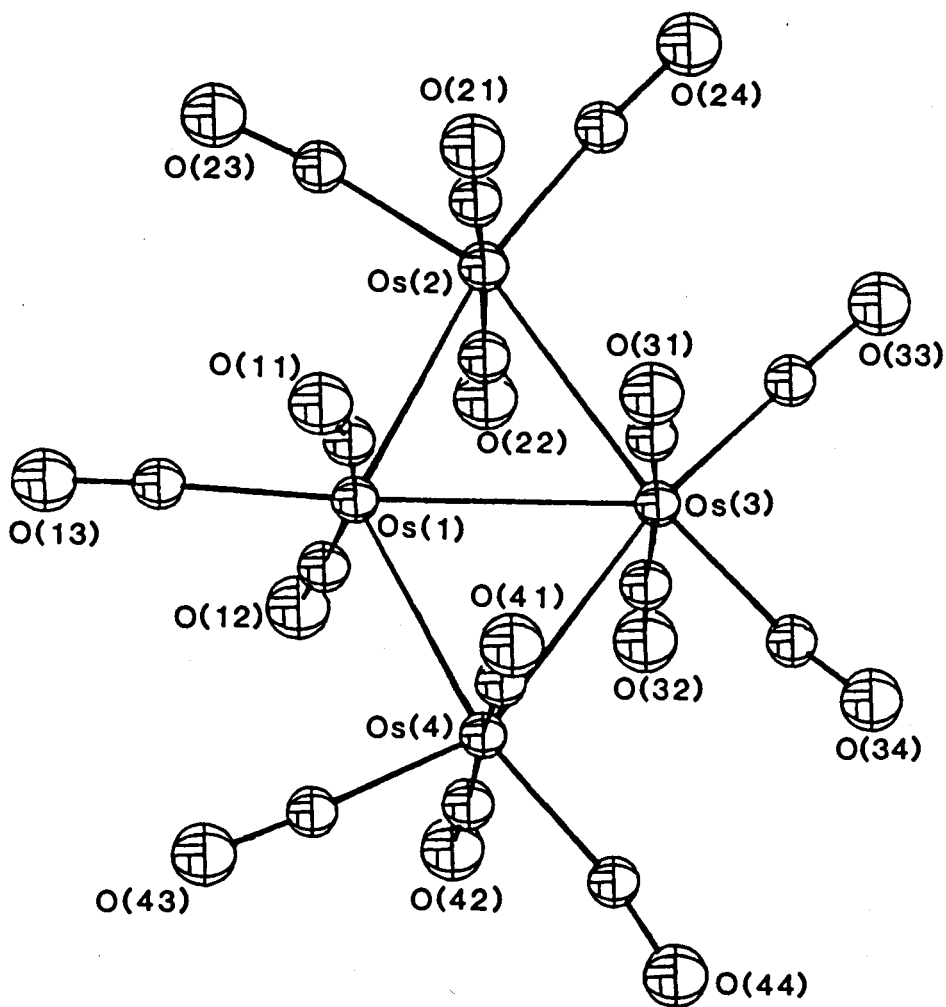


Fig. 3.20 Molecular structure of $\text{Os}_4(\text{CO})_{15.36}$.³⁶ Important bond lengths (Å) are as follows: $\text{Os}(1)\text{-Os}(3) = 2.772(1)$; $\text{Os}(1)\text{-Os}(4) = 2.772(1)$; $\text{Os}(2)\text{-Os}(3) = 2.997(1)$; $\text{Os}(2)\text{-Os}(4) = 2.997(1)$. The dihedral angle between the planes $\text{Os}(1)\text{-Os}(2)\text{-Os}(3)$ and $\text{Os}(1)\text{-Os}(2)\text{-Os}(4)$ is 179.0° .

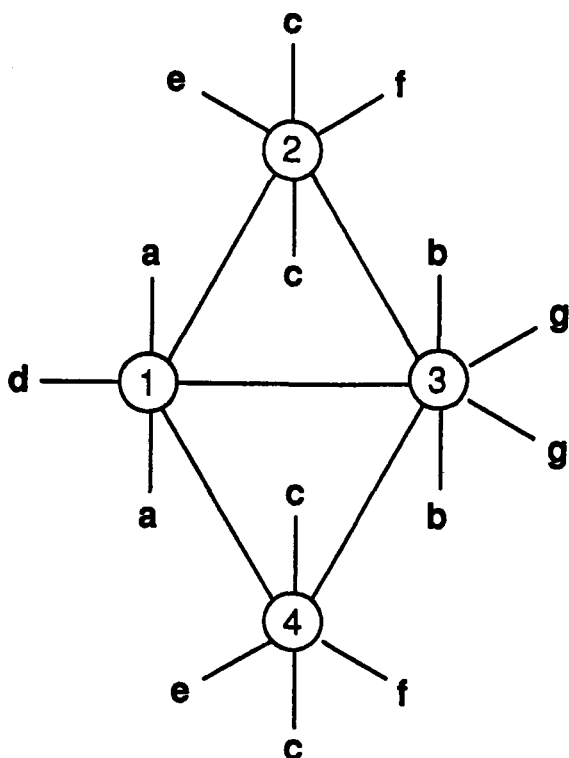


Fig. 3.21 Labels indicating nonequivalent carbonyls in $\text{Os}_4(\text{CO})_{15}$.

(Fig. 3.22). In saturated triosmium clusters such as $\text{Os}_3(\text{CO})_{11}(\text{ER}_3)$ (ER_3 = group 15 ligand) discussed in Chapter 2, the ^{13}C NMR resonances of axial carbonyls are to low field to those of equatorial carbonyls of the same group.^{76,78,79} The two ^{13}C NMR resonances at low field are therefore tentatively assigned to axial carbonyls **a**, **b** and **c** (Fig. 3.21) and that at high field is assigned to the seven equatorial carbonyls (**d** - **g**). This assignment is supported by the integration of the ^{13}C NMR signals of the spectrum obtained at -56°C which gives a ratio of 4:4:7. Given this assignment, the observed pattern of the spectra is

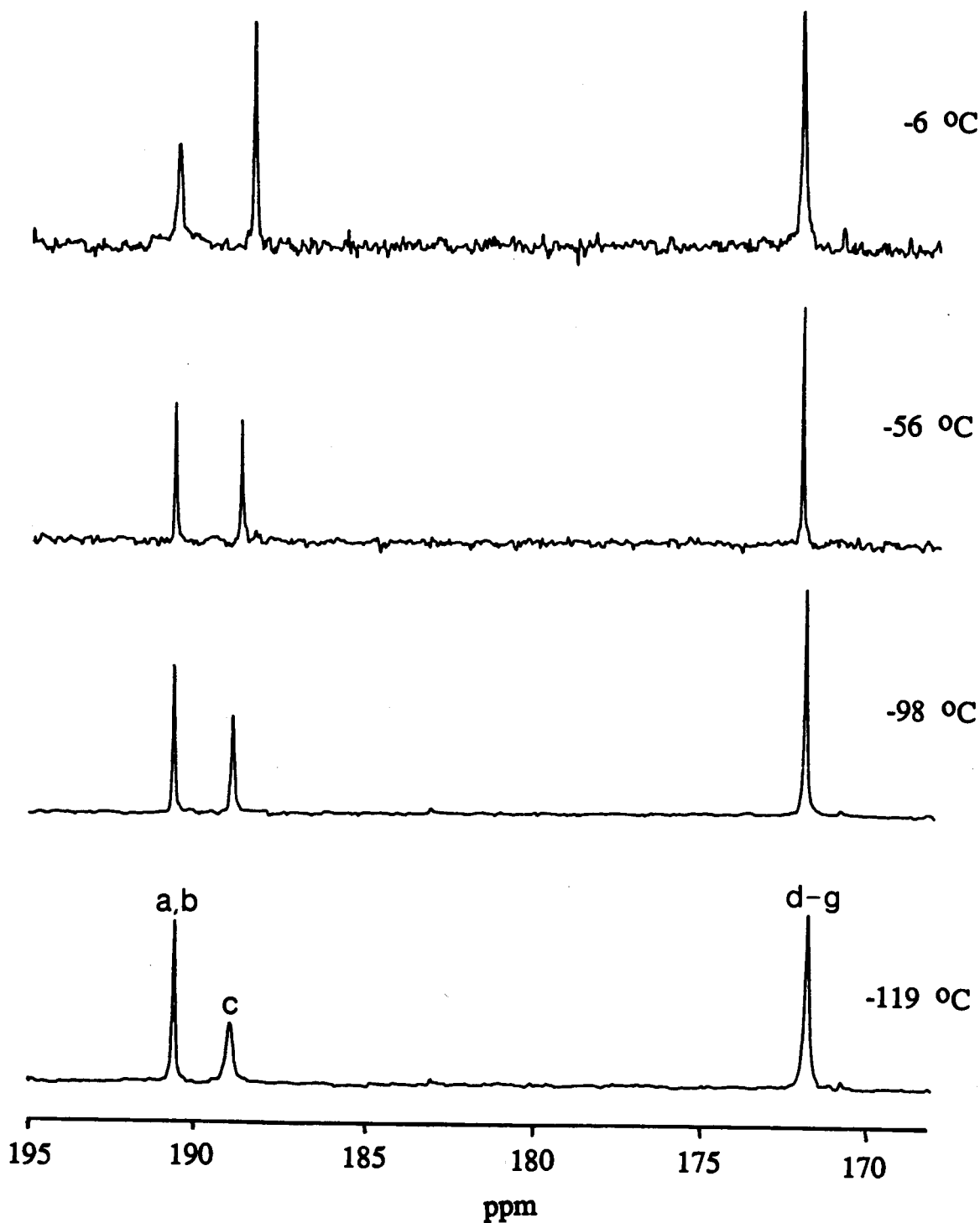


Fig. 3.22 Variable temperature ^{13}C NMR spectra of $\text{Os}_4(\text{CO})_{15}$ (^{13}CO enriched; in $\text{CH}_2\text{Cl}_2/\text{CD}_2\text{Cl}_2$ except for the spectrum at $-119\text{ }^\circ\text{C}$ which was taken in $\text{CHFCl}_2/\text{CD}_2\text{Cl}_2$).

consistent with a low energy in-plane merry-go-round equatorial carbonyl exchange process as shown in Fig. 3.23. This CO exchange process also equilibrates the axial carbonyls of the hinge osmium atoms Os(1) and Os(3) but not with the axial carbonyls of the apical (wingtip) osmium atoms.

At -119 °C the ^{13}C O signal at high field assigned to the seven equatorial carbonyls and the signal at δ 189.0 broaden simultaneously; this indicates that the CO exchange process is slowing down on the NMR time scale. This observation allows further assignment of the low field signals at δ 190.5 and 189.0 to the axial carbonyls on the wingtip and the hinge osmium atoms, respectively.

The difference in chemical shifts of the axial carbonyls on the hinge osmium atoms has been estimated to be about 40 ppm in the absence of CO exchange (or about 4000 Hz for an operating frequency of 100.6 MHz). This value was estimated from two closely related clusters, $\text{Os}_4(\text{CO})_{14}(\text{PMe}_3)^{36}$ and $\text{Os}_4(\text{CO})_{13}(\text{PMe}_3)[\text{P}(\text{OMe})_3]$ (to be discussed later), which show a chemical shift difference of 39.9 ppm and 41.8 ppm, respectively. For the case of fast two-site exchange, the linewidth, $\Delta\nu_{1/2}$, can be expressed as:^{15,51}

$$\Delta\nu_{1/2} = \frac{1}{2}\pi(\Delta\delta)^2 k_r^{-1}$$

where k_r is the first-order rate constant of the carbonyl exchange, and $\Delta\delta$ (in Hz) is the separation of the two signals

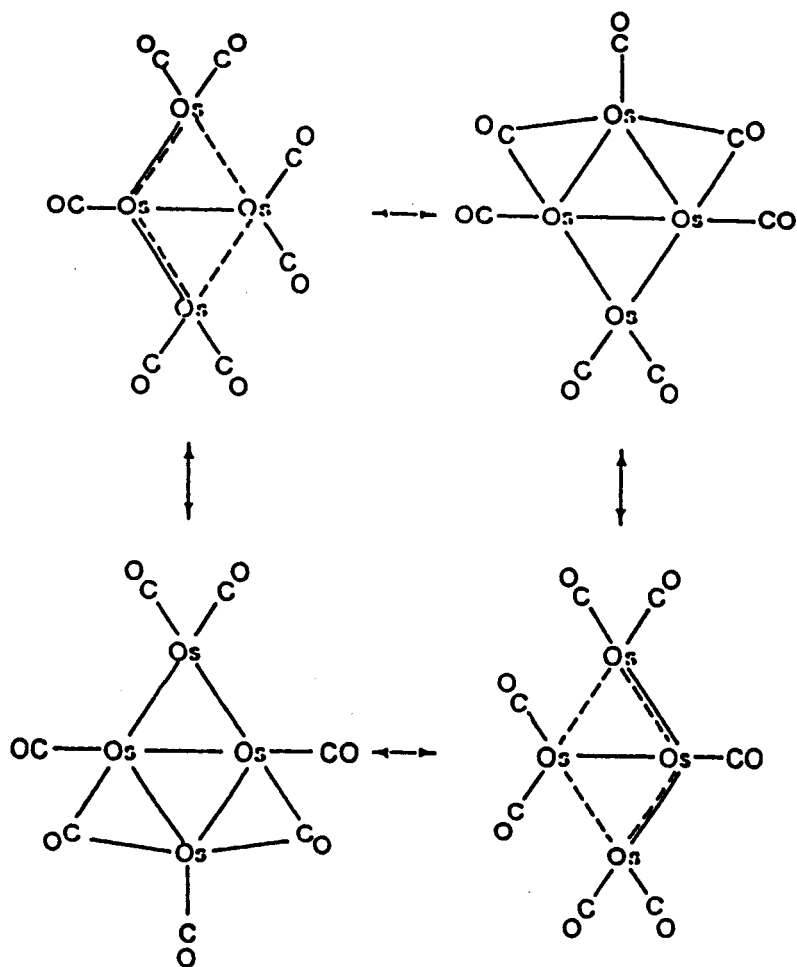


Fig. 3.23 Proposed mechanism of in-plane merry-go-round equatorial CO exchange process for $\text{Os}_4(\text{CO})_{15}$.

involved in the exchange process. For a broadening of 10 Hz due to slowing down of the process, k_T is therefore given by $\frac{1}{20}(\pi)(\Delta\delta)^2$. Accordingly, the rate of the in-plane, all-equatorial merry-go-round CO exchange in $\text{Os}_4(\text{CO})_{15}$ is estimated to be about $2.5 \times 10^6 \text{ s}^{-1}$ at -56°C and hence have an energy barrier of about 6 kcal mol^{-1} .

The ^{13}C NMR spectrum at -6°C , on the other hand, shows broadening of the resonances at δ 190.5 and 171.4 while that at δ 189.0 remains reasonably sharp. This is rationalized in terms of a trigonal twist mechanism at the wingtip osmium atoms that scrambles the equatorial and axial carbonyls of the $\text{Os}(\text{CO})_4$ groups. The nonrigidity of $\text{Os}_4(\text{CO})_{15}$ at higher temperatures was, however, not investigated.

$\text{Os}_4(\text{CO})_{13}(\text{PMe}_3)[\text{P}(\text{OMe})_3]$

The X-ray crystal structure of $\text{Os}_4(\text{CO})_{13}(\text{PMe}_3)[\text{P}(\text{OMe})_3]$ (Fig. 3.24) reveals a metal core of Os_4 in an almost planar kite arrangement with long and short Os-Os bonds⁴ similar to those found in $\text{Os}_4(\text{CO})_{15}$,³⁶ $\text{Os}_4(\text{CO})_{14}(\text{PMe}_3)$ ³⁷ and $\text{Os}_4(\text{CO})_{14}(\text{CNBu}^t)$ (discussed later).³⁶ The PMe_3 and $\text{P}(\text{OMe})_3$ ligands are each located in an equatorial position at one of the wingtip osmium centres, which are the least sterically hindered positions, on the same side of the Os_4 skeleton as the $\text{Os}(\text{CO})_3$ group.

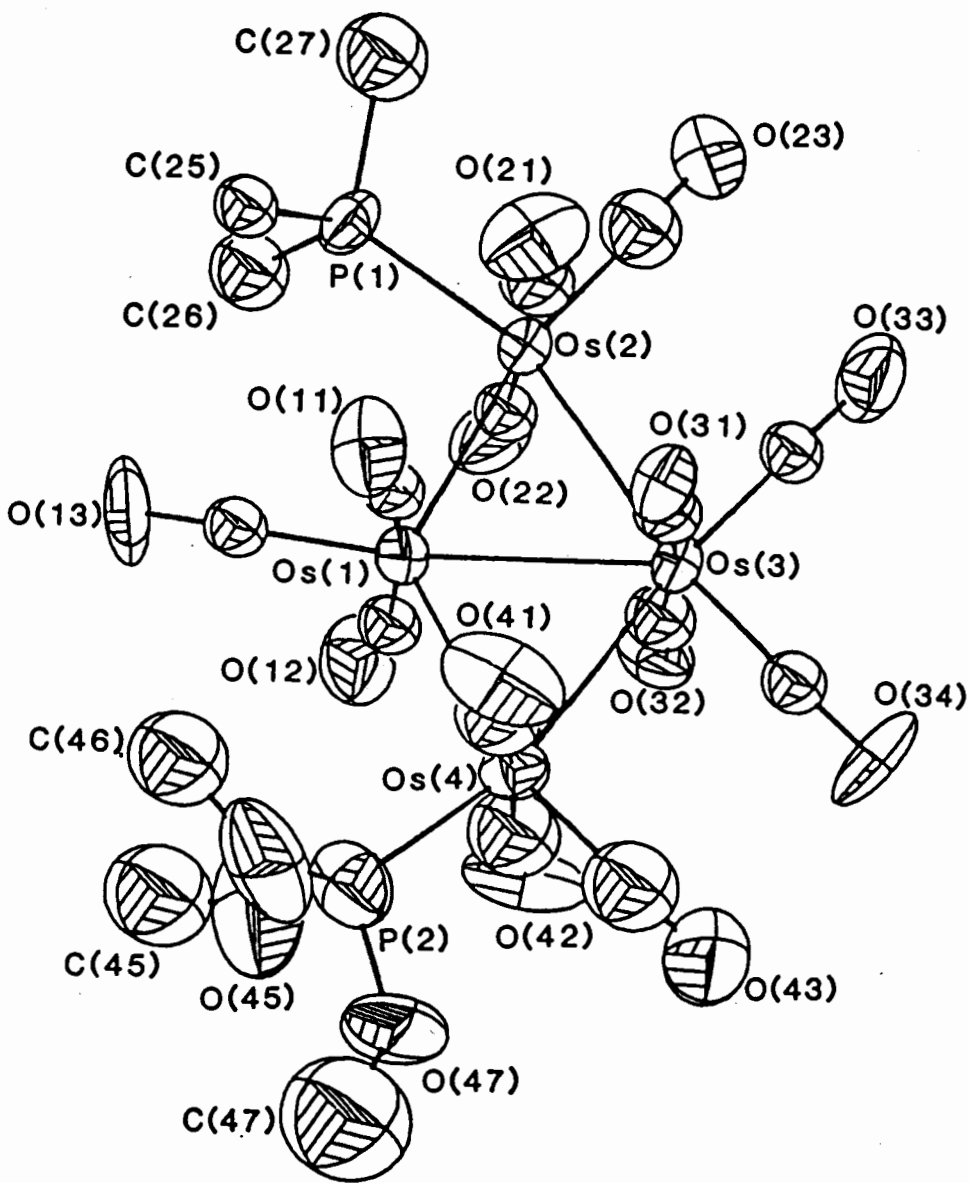


Fig. 3.24 Molecular structure of $\text{Os}_4(\text{CO})_{13}(\text{PMe}_3)[\text{P}(\text{OMe})_3]$.⁶⁹
 Important bond lengths (Å) are: $\text{Os}(1)-\text{Os}(2) = 2.783$ (3); $\text{Os}(1)-\text{Os}(4) = 2.792$ (2); $\text{Os}(1)-\text{Os}(3) = 2.937$ (2); $\text{Os}(2)-\text{Os}(3) = 2.978$ (2); $\text{Os}(3)-\text{Os}(4) = 3.019$ (2).

The ^1H NMR spectrum of $\text{Os}_4(\text{CO})_{13}(\text{PMe}_3)[\text{P}(\text{OMe})_3]$ in toluene- d_8 at room temperature exhibits two resonances at δ 3.65 (d, $J_{\text{P-H}} = 12$ Hz) and 1.83 (d, $J_{\text{P-H}} = 11$ Hz) which are assigned to the methyl hydrogens of $\text{P}(\text{OMe})_3$ and PMe_3 , respectively. These resonances are in regions of the spectrum that are typical for these ligands. The assignments are based on the chemical environments of the methyl groups: methyl groups that are directly attached to an electron withdrawing atom such as oxygen are shifted downfield.⁹⁵ There was no evidence for other isomers in the spectrum.

The variable temperature ^{13}C NMR spectra are shown in Fig. 3.25. At -44 °C the ^{13}C NMR spectrum exhibits nine resonances in the terminal carbonyl region at δ 214.8 (s, 2C), 203.7 (d, $J_{\text{P-C}} = 9.0$ Hz, 2C), 201.6 (d, $J_{\text{P-C}} = 12.3$ Hz, 2C), 195.4 (s, 1C), 178.0 (s, 1C), 176.4 (s, 1C), 173.3 (s, 1C), 173.1 (s, 1C), 173.0 (s, 2C). The assignments are consistent with the mode of collapse of the signals and the proposed CO exchange processes, as discussed below. Note that there is a chemical shift difference of 41.8 ppm between the axial carbonyls at the hinge osmium atoms. In $\text{Os}_4(\text{CO})_{14}(\text{PMe}_3)$ this difference was 39.9 ppm.³⁷ This difference is outside the normal range found in osmium carbonyl clusters and no doubt reflects the unusual bonding in these clusters. The resonance at δ 195.4 of intensity one is assigned to equatorial carbonyl 13 of the $\text{Os}(\text{CO})_3$

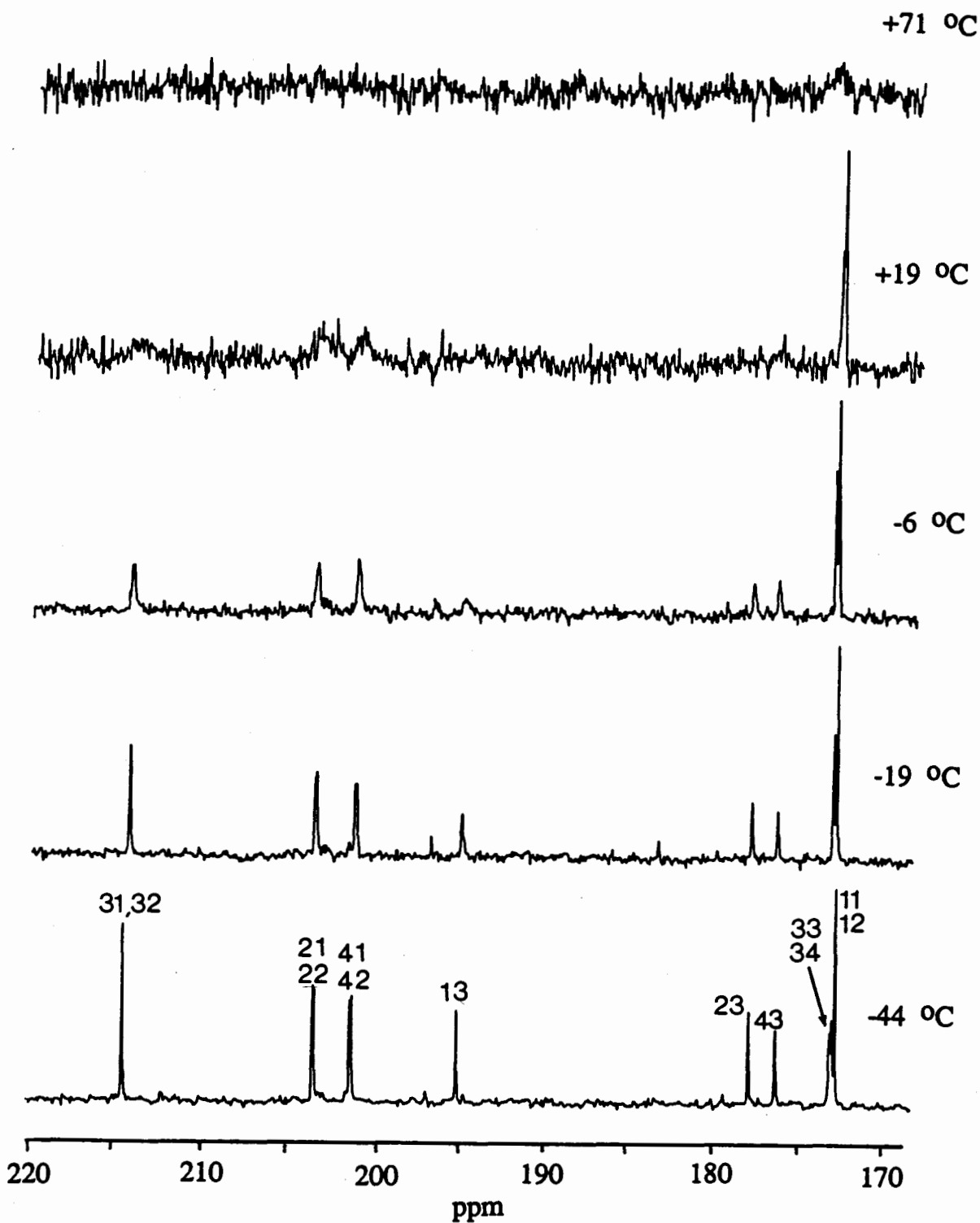


Fig. 3.25 Variable temperature ^{13}C NMR spectra of $\text{Os}_4(\text{CO})_{13}(\text{PMe}_3)[\text{P}(\text{OMe})_3]$ (^{13}C -enriched; in $\text{CH}_2\text{Cl}_2/\text{CD}_2\text{Cl}_2$ except for the spectrum at +71 °C which was taken in toluene/toluene- d_8).

group since it occurs at an unusual position for a CO in an equatorial position. The two signals at δ 173.1 and 173.3 are assigned to carbonyls 33 and 34 since they have similar chemical environments. It has been observed that the $31\text{p}-^{13}\text{C}$ coupling of the axial carbonyls to the equatorial phosphorus atom of a $\text{P}(\text{OR})_3$ ligand in an $\text{Os}(\text{CO})_3[\text{P}(\text{OR})_3]$ group is larger than that to the phosphorus atom of a PR_3 ligand in an $\text{Os}(\text{CO})_3(\text{PR}_3)$ group. Furthermore, the ^{13}C resonance of the axial carbonyls of an $\text{Os}(\text{CO})_3[\text{P}(\text{OR})_3]$ group appears to higher field than that of an $\text{Os}(\text{CO})_3(\text{PR}_3)$ group. For example, this has been observed for $\text{Os}_3(\text{CO})_{11}(\text{PR}_3)$ where $\text{R} = \text{Me}, \text{OMe}; \text{Ph}, \text{OPh}^{\text{a}}$ and $(\text{R}_3\text{P})(\text{OC})_4\text{OsM}(\text{CO})_5$ where $\text{M} = \text{W}, \text{Cr}$ and $\text{R} = \text{Me}, \text{OMe}$.⁹⁶ The ^{13}CO resonance at δ 201.6 with $J_{\text{p-C}} = 12.3$ Hz is therefore assigned to the axial carbonyls 41 and 42 of the $\text{Os}(\text{CO})_3[\text{P}(\text{OMe})_3]$ grouping and that at δ 203.7 with $J_{\text{p-C}} = 9.0$ Hz to the axial carbonyls 21 and 22 of the $\text{Os}(\text{CO})_3(\text{PMe}_3)$ unit. The other two signals at δ 178.0 and 176.4 are assigned to the two equatorial carbonyls 23 and 43 which are adjacent to PMe_3 and $\text{P}(\text{OMe})_3$, respectively. The assignments shown on the spectrum at -44 °C follow the labelling scheme in Fig. 3.19.

On warming the sample from -44 °C to about 0 °C, six resonances to low field of 175 ppm broadened and collapsed

a. The ^{13}CO chemical shifts and $31\text{p}-^{13}\text{C}$ coupling constants of these clusters have been reported in Chapter 2.

to the base line, while the three signals to higher field, assigned to the carbonyls of the $\text{Os}(\text{CO})_4$ grouping, remained sharp. We believe this is best rationalized in terms of two independent terminal-bridge carbonyl exchange processes in two vertical planes, one that contains the Os(1) and Os(2) atoms (process-12), and the other that contains the Os(1) and Os(4) atoms (process-14) as shown in Fig. 3.26. Because of the small chemical shift difference of the signals for carbonyls 33 and 34 the apparent coalescence of the two signals observed in the spectrum at -19°C (and spectra at higher temperatures) is likely caused by a shift of the resonance with temperature such that they become accidentally degenerate rather than coalescence due to an exchange process. This signal remained sharp up to room temperature while the signals due to the other equatorial carbonyls in the cluster collapsed to the base line. This indicates that an all-equatorial merry-go-round CO exchange process is not involved in the process that gives rise to the collapse. Such an exchange process would require one or both of the phosphorus ligands to move to a bridging position which is considered unlikely.⁴⁷ The signal assigned to CO(13) broadens at a much faster rate than the other signals. This is as expected since CO(13) is involved in both processes.

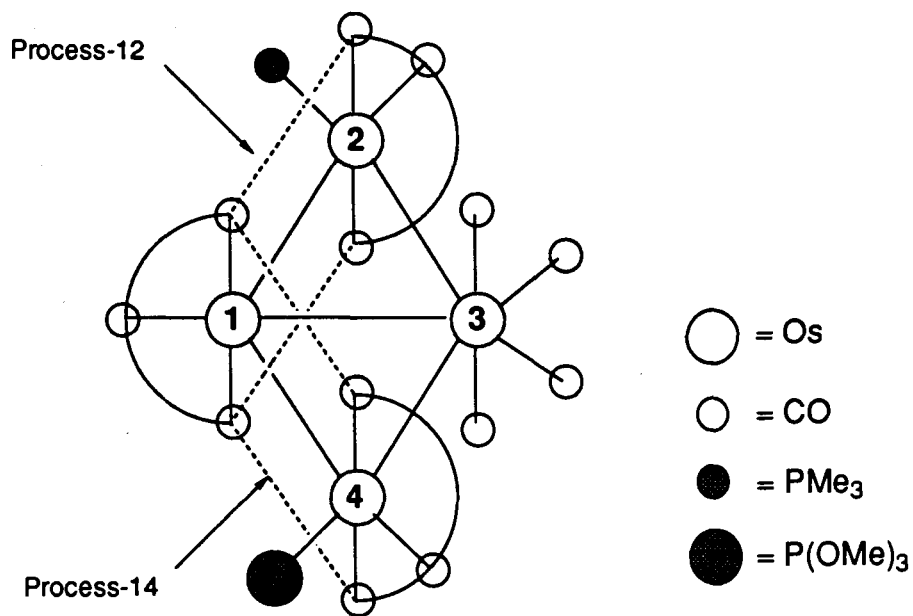


Fig. 3.26 Proposed CO exchange processes in $\text{Os}_4(\text{CO})_{13}(\text{PMe}_3)[\text{P}(\text{OMe})_3]$.

Simulation of the ^{13}C NMR spectrum at -6°C (Fig. 3.27) shows that the first order rate constants of the two CO exchange processes are slightly different: $30 \pm 3 \text{ s}^{-1}$ for process-12 and $25 \pm 3 \text{ s}^{-1}$ for process-14. These yield activation energies, ΔG^\ddagger , of $13.8 \text{ kcal mol}^{-1}$ for process-12 and $13.9 \text{ kcal mol}^{-1}$ for process-14. Because of the similarity of the two exchange processes, the difference in their energy barriers may be related to the electronic properties of the phosphorus ligand associated with each process. This is in consistent with the results in Chapter 2: that the first CO exchange in $\text{Os}_3(\text{CO})_{11}(\text{PMe}_3)$ had a lower

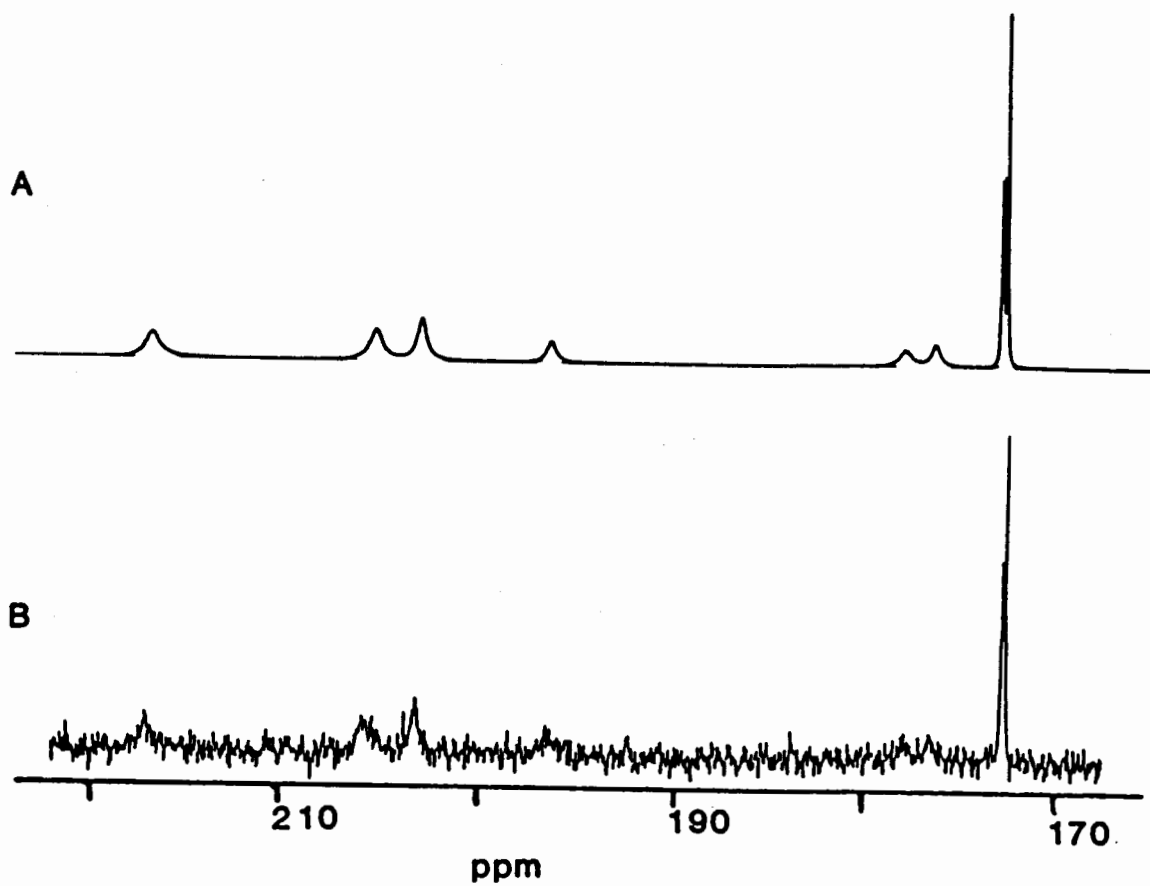


Fig. 3.27 Calculated (A) and observed (B) ^{13}C NMR spectra of $\text{Os}_4(\text{CO})_{13}(\text{PMe}_3)[\text{P}(\text{OMe})_3]$ at $-6\text{ }^\circ\text{C}$.

barrier ($\Delta G_1^\ddagger = 12.4 \text{ kcal mol}^{-1}$) than that in $\text{Os}_3(\text{CO})_{11}[\text{P}(\text{OMe})_3]$ ($\Delta G_1^\ddagger = 14.0 \text{ kcal mol}^{-1}$).

On warming the sample of $\text{Os}_4(\text{CO})_{13}(\text{PMe}_3)[\text{P}(\text{OMe})_3]$ to about 70°C the two high field signals assigned to the carbonyls of the $\text{Os}(\text{CO})_4$ grouping also collapsed to the base line. This indicates that the carbonyls of the $\text{Os}(\text{CO})_4$ group must exchange with the other carbonyls in the cluster. A bridge-terminal CO exchange across the hinge $\text{Os}(1)\text{-Os}(3)$ bond appears most likely. In this case there is no preference in energy barrier for CO(33) and CO(34) to take part in this exchange process.

$\text{Os}_4(\text{CO})_{14}(\text{CNBu}^t)$

The X-ray crystal structure of $\text{Os}_4(\text{CO})_{14}(\text{CNBu}^t)$ revealed a planar Os_4 core with adjacent long and short Os-Os bonds (Fig. 3.28) similar to that found in $\text{Os}_4(\text{CO})_{15}$ ³⁶ and $\text{Os}_4(\text{CO})_{13}(\text{PMe}_3)[\text{P}(\text{OMe})_3]$.⁶⁹ The CNBu^t ligand is located in an axial position on the osmium atom at the hinge which is associated with two equatorial carbonyls. As discussed for $\text{Os}_3(\text{CO})_{11}(\text{ER}_3)$ in Chapter 2 and in this chapter, the CNBu^t ligand prefers axial sites in clusters whereas phosphorus ligands occupy equatorial positions. It is also interesting that the isocyanide ligand is bound to the hinge Os atom that is bounded to four two-electron donor ligands. This may indicate that this osmium center is electron deficient.

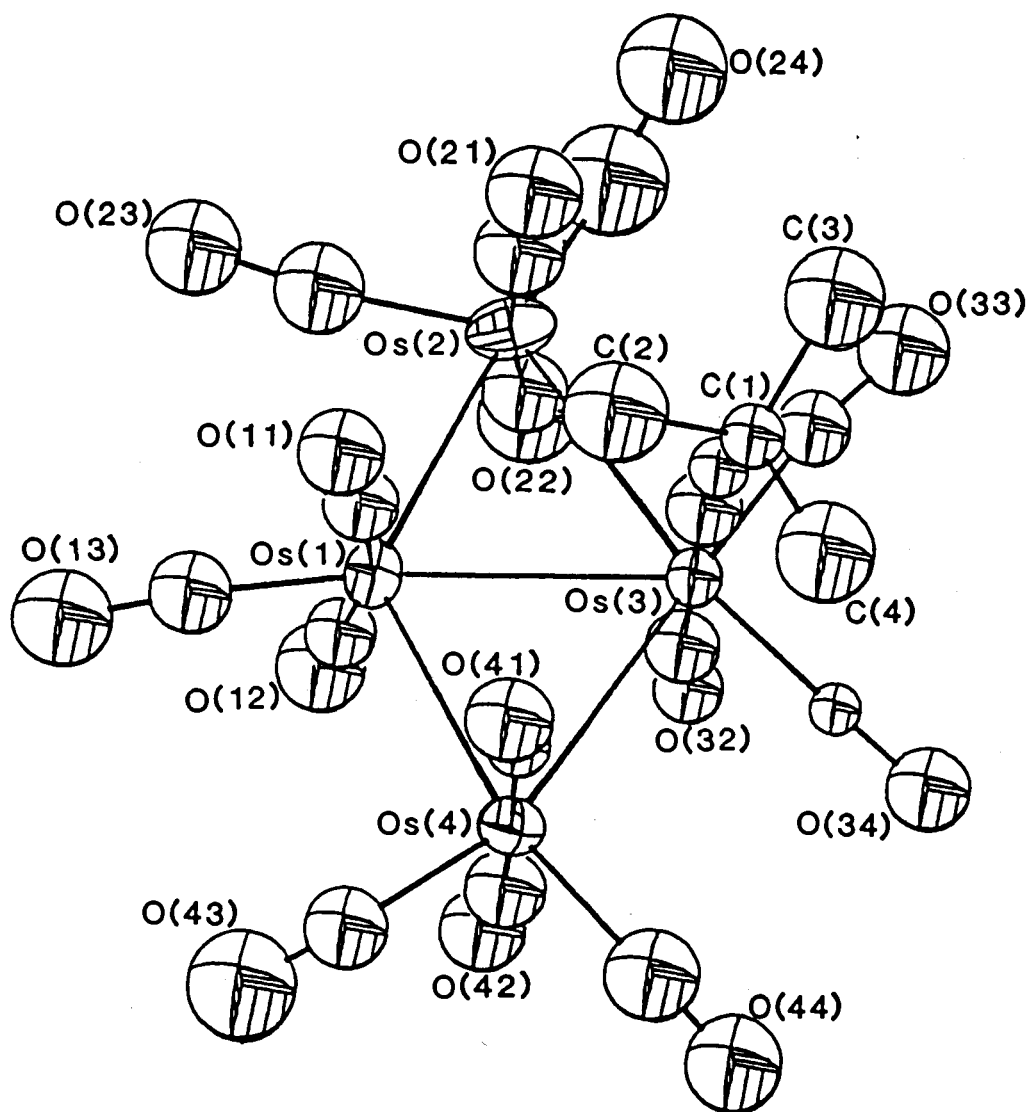


Fig. 3.28 Molecular structure of $\text{Os}_4(\text{CO})_{14}(\text{CNBut}) \cdot 69$
 Hydrogen atoms are omitted for clarity.
 Important bond lengths (Å) are: $\text{Os}(1)\text{-Os}(2) = 2.793$ (2); $\text{Os}(1)\text{-Os}(4) = 2.775$ (2); $\text{Os}(1)\text{-Os}(3) = 2.936$ (2); $\text{Os}(2)\text{-Os}(3) = 2.985$ (2); $\text{Os}(3)\text{-Os}(4) = 2.983$ (2).

The ^1H NMR spectrum of $\text{Os}_4(\text{CO})_{14}(\text{CNBu}^t)$ in toluene- d_8 at ambient temperature exhibited two signals at δ 0.95 and 0.96 of almost equal intensity; these are assigned to the hydrogen atoms of the tert-butyl group of different isomers. The ^1H signal at the higher field (i.e., at δ 0.95) was slightly broader. The same result was obtained on an NMR spectrometer operating at a higher frequency. This indicates that the broader signal is not a result of two close lying signals. Although the X-ray crystal structure revealed only one isomer, two (or more) isomers appear to be present in solution. The reason why one of the ^1H NMR signals was broader is not known. A similar spectrum was obtained at -50 °C which indicates that the broad signal was not due to an exchange process of two isomers that results in coalescence at room temperature.

The ^{13}C NMR spectrum of $\text{Os}_4(\text{CO})_{14}(\text{CNBu}^t)$ at -45 °C exhibited two major resonances in the terminal carbonyl region at δ 174.7 and 174.8 of approximately equal intensity (Fig. 3.29). Unfortunately, the ^{13}C NMR spectrum at -120 °C only exhibited several other small signals in the low field region which were not consistent with the solid state structure. The presence of other isomer(s) of unknown structure makes the interpretation impossible. The result only indicates that $\text{Os}_4(\text{CO})_{14}(\text{CNBu}^t)$ is more fluxional than $\text{Os}_4(\text{CO})_{15}$.

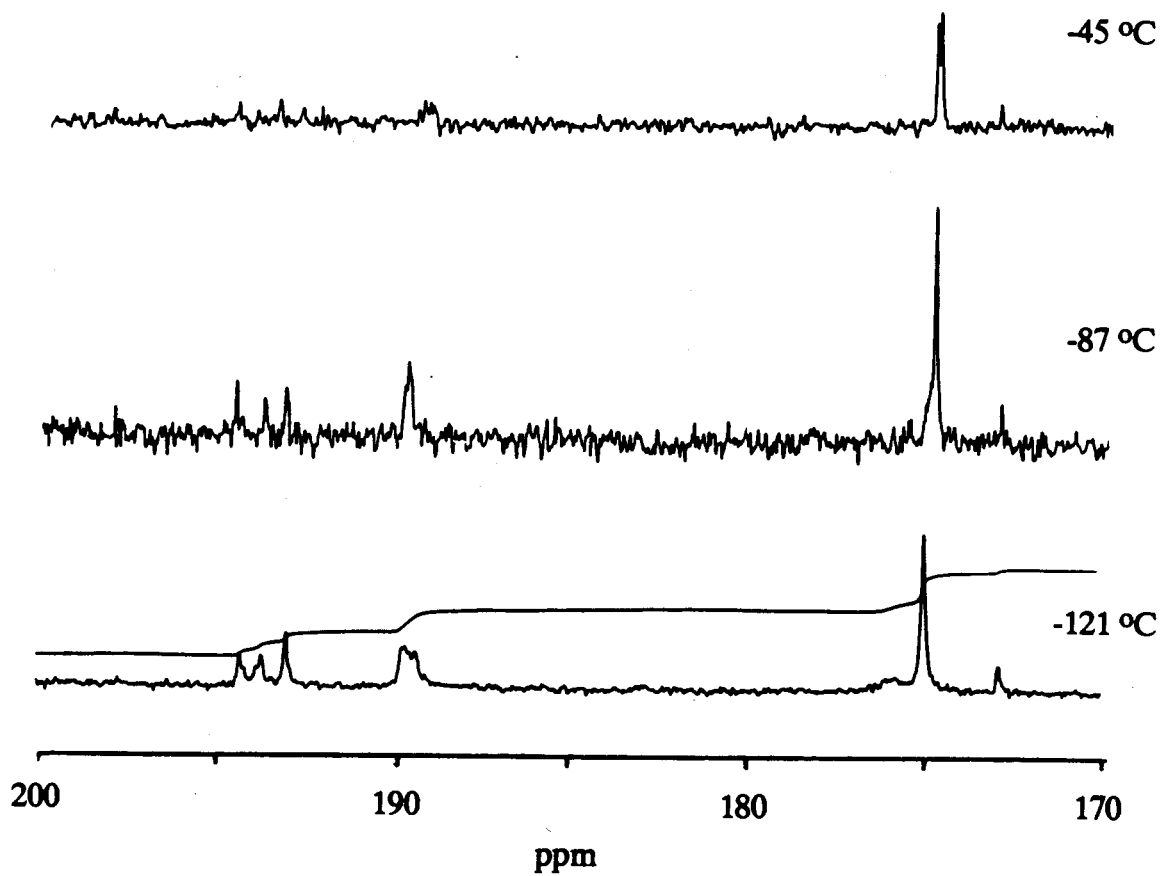


Fig. 3.29 ^{13}C NMR spectra of $\text{Os}_4(\text{CO})_{14}(\text{CNBu}^t)$ (^{13}CO enriched; in $\text{CHCl}_2/\text{CD}_2\text{Cl}_2$).

Chapter 4

Nonrigidity in the Isomers of $\text{Os}_3(\mu\text{-H})_2(\text{CO})_9(\text{CNBu}^t)$.

4.1 Introduction

Metal carbonyl clusters with bridging hydride ligands are ubiquitous. Furthermore, the hydride ligands in these clusters are often stereochemically nonrigid, undergoing exchange that can be detected by ^1H NMR spectroscopy.

In hydrido-osmium clusters, CO exchange processes are sometimes associated with hydride exchange. For example, in the clusters $\text{HOs}_3(\mu\text{-H})(\text{CO})_{10}(\text{L})$ ($\text{L} = \text{CO},^{97} \text{CNBu}^t^{97}, \text{PPh}_3^{79}$), the low energy process involves the oscillation of the $\text{HOs}(\text{CO})_3$ group that allows exchange of the terminal hydride with the adjacent bridging hydride.²⁷

Nonrigidity studies have usually been restricted to hydrido-osmium clusters which have $\text{Os}(\mu\text{-H})\text{Os}$ linkages. Studies of the nonrigidity of hydride ligands in cluster compounds which have the $\text{Os}(\mu\text{-H})_2\text{Os}$ unit are much less common. This may be because these hydrido-osmium clusters are rare,¹⁹ and that the hydride ligands of the $\text{Os}(\mu\text{-H})_2\text{Os}$ group are usually chemically equivalent, as in $\text{Os}_3(\mu\text{-H})_2(\text{CO})_{10}$ ⁴⁰ and $\text{Os}_3(\mu\text{-H})_2(\text{CO})_9(\text{PR}_3)$.⁹⁸ If hydride exchange occurs in these clusters, it cannot be detected by ^1H NMR spectroscopy. Aime and co-workers reported a study of the deuterium kinetic isotope effect on the rate of carbonyl exchange in $\text{Os}_3(\mu\text{-H})_2(\text{CO})_{10}$. It was concluded that

the two bridging hydrides are rigid during the carbonyl exchange process.⁹⁹ On the other hand, in $\text{Os}_3(\mu\text{-H})_3(\text{CO})_9(\text{SiPh}_3)$, the hydrides of the $\text{Os}(\mu\text{-H})_2\text{Os}$ unit undergo mutual exchange and also exchange with the hydride of the $\text{Os}(\mu\text{-H})\text{Os}$ group.¹⁹

In this chapter the synthesis of the previously unknown green isomer of $\text{Os}_3(\mu\text{-H})_2(\text{CO})_9(\text{CNBu}^t)$ is reported. The crystal structure indicates it contains an $\text{Os}(\mu\text{-H})_2\text{Os}$ linkage in which the hydrides are inequivalent. The mobility of the carbonyl and the hydride ligands in this cluster and in the two red isomers have also been studied.

4.2 Experimental section

Unless otherwise stated, manipulations of starting materials and products were carried out under a nitrogen atmosphere with the use of standard Schlenk techniques. Hexane was refluxed over potassium, distilled, and stored under nitrogen before use. Dichloromethane was treated similarly except that P_2O_5 was used as the drying agent. The preparations of $\text{HOs}_3(\mu\text{-H})(\text{CO})_{10}(\text{CNBu}^t)$ (2) and the red isomers of $\text{Os}_3(\mu\text{-H})_2(\text{CO})_9(\text{CNBu}^t)$ (1ra, 1rb) have been described.^{22,84} The ^{13}C O-enriched compounds were obtained from ^{13}C O-enriched $\text{Os}_3(\text{CO})_{12}$ (estimated 35-40% ^{13}C). This in turn was prepared by heating $\text{Os}_3(\text{CO})_{12}$ in toluene at 125 °C under about 1.5 atm of ^{13}C O (99% ^{13}C) for 3 days.

Infrared spectra were recorded on a Perkin-Elmer 983 spectrometer; the internal calibration of the instrument was periodically checked against the known absorption frequencies of gaseous CO. The electron-impact (70 eV) mass spectrum was obtained on a Hewlett-Packard 5985 GC-MS system; the pattern of the envelope of peaks of the parent ion matched that simulated by computer. The microanalysis was performed by M.K. Yang of the Microanalytical Laboratory of Simon Fraser University.

NMR spectra were recorded on a Bruker WM400 or a Bruker SY-100 spectrometer; ^{13}C NMR spectra were obtained on samples that had been ^{13}CO enriched. The NMR line-shape simulations were carried out with a computer program (EXCHANGE) written by Professor R.E.D. McClung of the University of Alberta, or the program DNMR3 of Kleier and Binch.¹⁰⁰ The uncertainty of the rate constants was taken to be $\pm 10\%$ of the best fit. The fit was generally better than this. The thermocouple of the temperature controller had been calibrated and shown to be accurate to ± 2 °C.

Preparation of the Green Isomer of $\text{Os}_3(\mu\text{-H})_2(\text{CO})_9(\text{CNBu}^t)$ (1g)

A small amount of $\text{HOs}_3(\mu\text{-H})(\text{CO})_{10}(\text{CNBu}^t)$ (about 5 mg) in hexane (approximately 5 mL) was refluxed rapidly in air with rapid stirring until the colour changed from yellow to green. Refluxing the solution under a nitrogen flow gave the same result. (Further heating of the solution caused

the colour to change from green to red due to the formation of the known red isomers of 1).⁸⁴ The green solution was transferred to a Schlenk tube and stored at 0 °C. The procedure was repeated several times. The green solutions were combined and the solvent removed on the vacuum line. The residue was shaken with small portions of hexane until the green component of the residue was extracted. Some yellow powder remained undissolved which was identified as unreacted starting material. The green solution was filtered through Celite and stored at -15 °C. This yielded a mixture of green and yellow crystals which were identified as the desired product and the starting material, respectively. The two types of crystals were separated by redissolving the mixture in hexane in which the green isomer dissolved rapidly whereas the starting material was almost insoluble. Storing the green solution at -15 °C afforded crystals of the pure green isomer of $\text{Os}_3(\mu\text{-H})_2(\text{CO})_9(\text{CNBu}^t)$. The preparation gave a yield of approximately 80% based on the amount of $\text{HOs}_3(\mu\text{-H})(\text{CO})_{10}(\text{CNBu}^t)$ consumed. The purification process was also attempted by chromatography on Florisil with hexane as the eluent. Although the separation was successful, the yield was much lower.

Spectroscopic and analytical data for the green isomer of $\text{Os}_3(\mu\text{-H})_2(\text{CO})_9(\text{CNBu}^t)$, 1g: IR (hexane) (Fig. 4.1) $\nu(\text{CN})$ 2177.5 (br, m), $\nu(\text{CO})$ 2084.5 (m), 2060.5 (s), 2033.5 (vs),

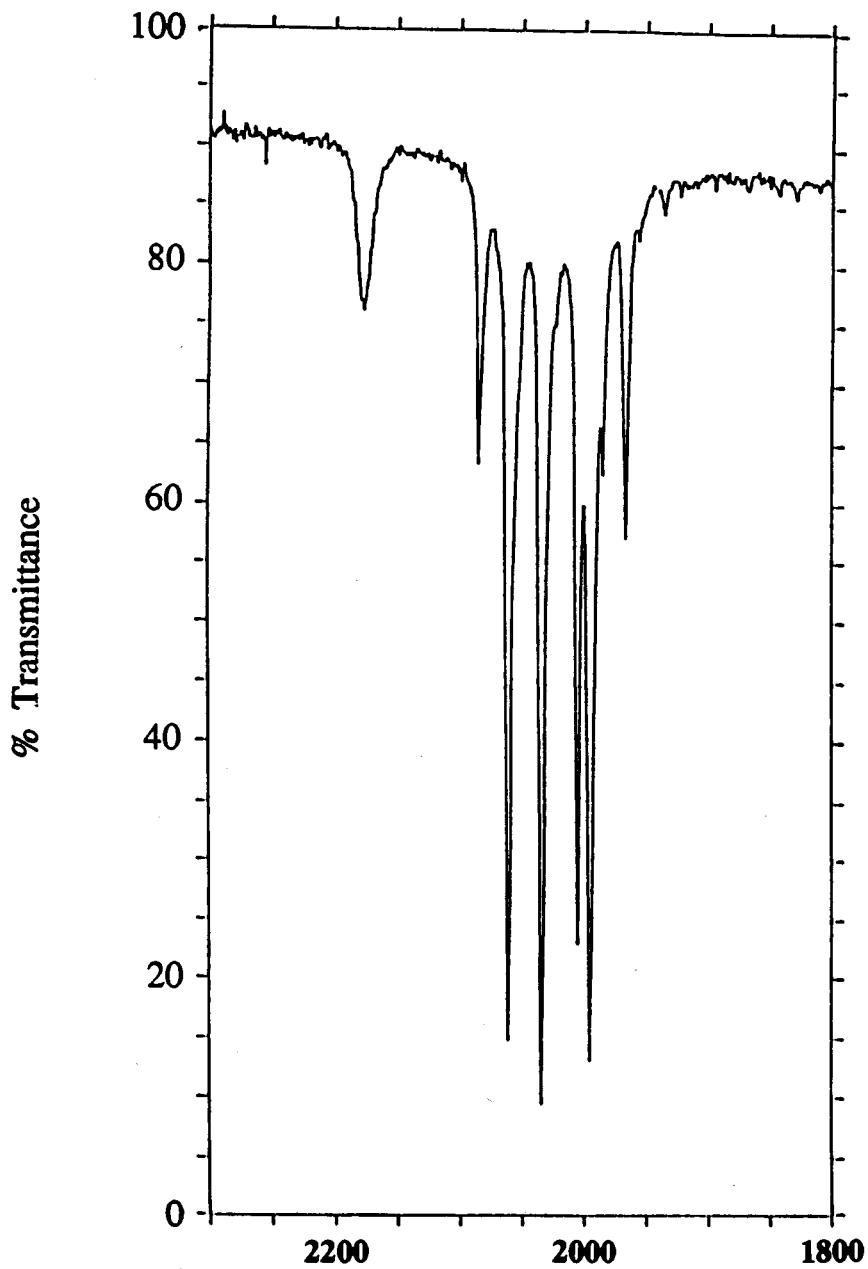


Fig. 4.1 Infrared spectrum of **1g** in hexane (terminal CO region).

2004.0 (s), 1994.5 (s), 1984.5 (m), 1965.5 (m), 1935.0 (vw) cm^{-1} ; ^1H NMR (toluene- d_8 , ambient temperature) δ 0.73, -10.94 (d, $J_{\text{H-H}} = 1.1$ Hz, $J_{\text{Os-H}} = 47.2$ Hz), -11.36 (d, $J_{\text{H-H}} = 1.1$ Hz, $J_{\text{Os-H}} = 47.2$ Hz); ^{13}C (hydrogen coupled) NMR ($\text{CH}_2\text{Cl}_2/\text{CD}_2\text{Cl}_2$, 4/1, -30 °C, CO region) δ 187.3 (2C), 185.3 (1C), 181.9 (2C), 178.0 (2C, d, $J_{\text{C-H}} = 11.6$ Hz), 177.4 (2C, d, $J_{\text{C-H}} = 11.7$ Hz); m.p. 107 - 108 °C; MS (EI) m/z 909 (M^+); Anal. Calcd for $\text{C}_{14}\text{H}_{11}\text{NO}_9\text{Os}_3$: C, 18.52; H, 1.22; N, 1.54. Found: C, 18.72; H, 1.27; N, 1.33.

4.3 Results and Discussion

Rapid heating and stirring of a hexane solution of $\text{HOs}_3(\mu\text{-H})(\text{CO})_{10}(\text{CNBu}^t)$ (**2**) to reflux in air, or under a static or flowing N_2 atmosphere in an open vessel caused the colour of the solution to change from yellow to green. The solution was outgassed by the reflux process and the rapid stirring. The green solution was identified as due to a previously unknown product of the decarbonylation of **2**. Further heating of the solution caused it to turn from green to red. The red colour was attributed to the known decarbonylation products (**1ra**, **1rb**) of **2**.⁸⁴ When **1g** or **1r** was stirred in hexane under 1 atm of carbon monoxide at room temperature, it was quantitatively reverted to **2** within 30 minutes. (It was not established whether the conversion of **1r** to **2** proceeded via **1g**.) The relationship between **2** and

the isomers of **1** is shown in Fig. 4.2. When a hexane solution of **2** was heated under vacuum at 70 °C, as reported in literature,⁸⁴ **1g** was also formed initially as evidenced by the colour change, but before a significant amount formed it isomerized to **1r**.

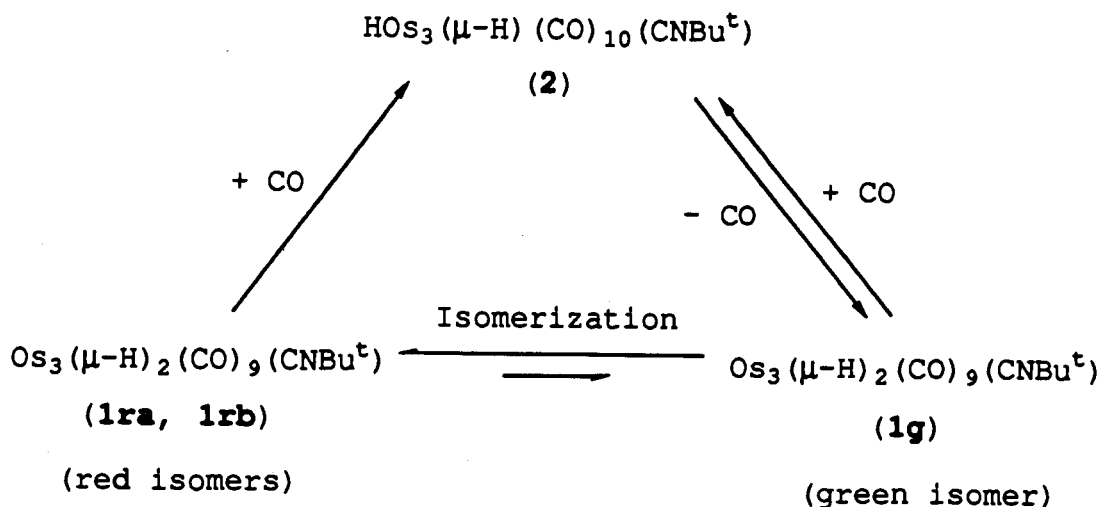


Fig. 4.2 Interconversion of **2** and the isomers of $\text{Os}_3(\mu\text{-H})_2(\text{CO})_9(\text{CNBu}^t)$.

The ^1H NMR spectrum of **1g** in toluene- d_8 at room temperature exhibited a resonance at δ 0.73 due to the hydrogen atoms of the tert-butyl group, and two resonances in the hydride region at δ -10.94 and -11.36. Both hydride signals showed a small H-H coupling of 1.1 Hz. The -5 to -15 ppm region is usually associated with resonances due to terminal hydrides of saturated triosmium clusters, with the

resonances for bridging hydrides usually in the -15 to -23 ppm region.⁸ However, in unsaturated clusters, signals due to bridging hydrides are known to appear in the terminal hydride region.⁸

The hydride resonances of **1g** also exhibited satellites attributed to coupling to ¹⁸⁷Os ($J_{\text{Os-H}} = 47.2 \text{ Hz}$).¹⁰¹ Osmium-187 has a nuclear spin of $\frac{1}{2}$ and a natural abundance of 1.6%. It has been observed that the $J_{\text{Os-H}}$ coupling constant of hydrides in $\text{Os}(\mu\text{-H})_2\text{Os}$ units is greater than about 40 Hz, while for hydrides in $\text{Os}(\mu\text{-H})\text{Os}$ units $J_{\text{Os-H}}$ is usually less than 40 Hz.¹⁹ An average Os-H coupling of about 45 Hz has been observed in $\text{Os}_3(\mu\text{-H})_2(\text{CO})_9(\text{PR}_3)$ ($\text{PR}_3 = \text{PMe}_3, \text{PPh}_3, \text{P}(\text{OMe})_3$) clusters,^a whereas in $\text{Os}_3(\mu\text{-H})_3(\text{CO})_9(\text{SiPh}_3)$, Os-H couplings of 44.1 and 44.9 Hz were found for the $\text{Os}(\mu\text{-H})_2\text{Os}$ grouping.¹⁹ This suggests that the two hydride ligands in **1g** are arranged in a dibridging $\text{Os}(\mu\text{-H})_2\text{Os}$ arrangement. Further support for this arrangement was provided by the NOE study and the HYDEX calculation as discussed in Chapter 1, and the X-ray crystal structure of **1g** described below.

a. The Os-H couplings in these clusters were measured by the author in an unrelated study.

Structure of 1g

The X-ray crystal structure of 1g is shown in Fig. 4.3. Selected bond lengths and bond angles are reported in Table 4.1(a) and 4.1(b), respectively. As is normally the case, the hydride ligands were not located in the crystal structure determination. However, the structure revealed two Os-Os bonds of 2.812(1) Å and one shorter Os-Os bond of 2.680(1) Å. The shorter Os-Os vector is characteristic of an $\text{Os}(\mu\text{-H})_2\text{Os}$ unit. For example, in $\text{Os}_3(\mu\text{-H})_2(\text{CO})_{10}$ and 1rb, similar Os-Os bond vectors of 2.683(1) Å⁴⁰ and 2.690(1) Å²², respectively, were found for the $\text{Os}(\mu\text{-H})_2\text{Os}$ linkage. The diffraction study of $\text{Os}_3(\mu\text{-H})_2(\text{CO})_{10}$ included a neutron diffraction determination in which the hydride ligands were directly located.⁴⁰ The bond lengths of the two longer Os-Os vectors in 1g are slightly shorter than that normally found in saturated triosmium clusters. For example, the average Os-Os bond length in $\text{Os}_3(\text{CO})_{12}$ is 2.877 Å.⁹ A shortening of the unbridged Os-Os bonds was also found in similar unsaturated clusters such as 1rb²² and $\text{Os}_3(\mu\text{-H})_2(\text{CO})_9(\text{L})$ (L = CO,⁴⁰ PPh_3 ¹⁰²).

The CNBu^t ligand is located in an axial position on the osmium centre which is not associated with the $\text{Os}(\mu\text{-H})_2\text{Os}$ grouping. For this reason the hydride ligands are inequivalent and two resonances are observed in the hydride region of the ¹H NMR spectrum of 1g (an equatorial

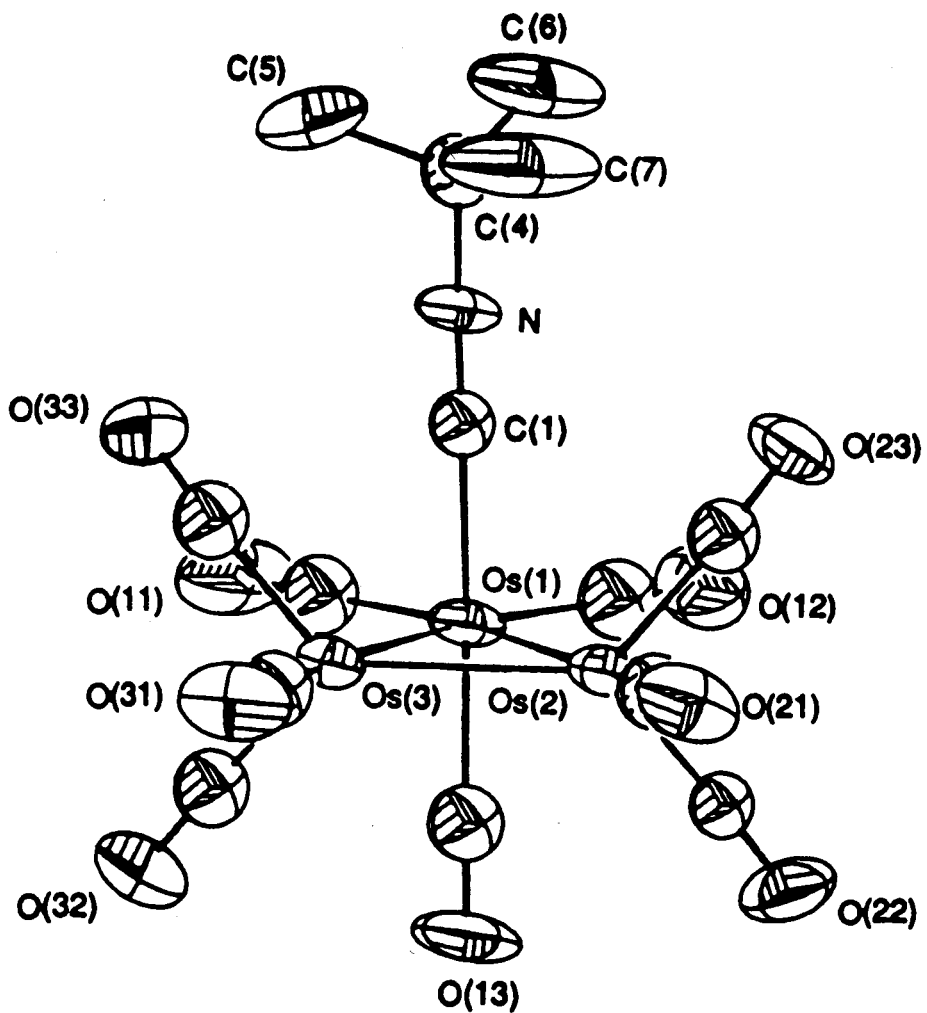


Fig. 4.3 Molecular structure of 1g.

Table 4.1(a) Selected Molecular Dimensions for 1g

Bond Lengths (Å)

Os(1)-Os(2)	2.812 (1)	C(1)-N	1.16 (2)
Os(1)-Os(3)	2.812 (1)	C(11)-O(11)	1.16 (2)
Os(2)-Os(3)	2.680 (1)	C(12)-O(12)	1.11 (2)
Os(1)-C(1)	2.00 (2)	C(13)-O(13)	1.12 (2)
Os(1)-C(11)	1.88 (2)	C(21)-O(21)	1.17 (2)
Os(1)-C(12)	1.93 (2)	C(22)-O(22)	1.13 (2)
Os(1)-C(13)	1.96 (2)	C(23)-O(23)	1.16 (2)
Os(2)-C(21)	1.90 (2)	C(31)-O(31)	1.16 (2)
Os(2)-C(22)	1.90 (2)	C(32)-O(32)	1.16 (2)
Os(2)-C(23)	1.87 (2)	C(33)-O(33)	1.14 (2)
Os(3)-C(31)	1.86 (2)	N-C(4)	1.44 (2)
Os(3)-C(32)	1.87 (2)	C(4)-C(5)	1.53 (3)
Os(3)-C(33)	1.90 (2)	C(4)-C(6)	1.53 (3)
		C(4)-C(7)	1.47 (3)

Table 4.1(b) Selected Molecular Dimensions for 1g

Bond Angles (deg)					
Os(1)-Os(2)-Os(3)	61.53	(3)	N-C(1)-Os(1)	179	(2)
Os(2)-Os(3)-Os(1)	61.55	(3)	O(11)-C(11)-Os(1)	177	(2)
Os(3)-Os(1)-Os(2)	56.91	(2)	O(12)-C(12)-Os(1)	179	(2)
C(1)-Os(1)-Os(3)	85.6	(5)	O(13)-C(13)-Os(1)	179	(2)
C(1)-Os(1)-C(11)	89.9	(7)	O(21)-C(21)-Os(2)	179	(2)
C(1)-Os(1)-C(12)	92.6	(7)	O(22)-C(22)-Os(2)	177	(2)
C(1)-Os(1)-C(13)	170.1	(7)	O(23)-C(23)-Os(2)	176	(2)
C(11)-Os(1)-C(12)	100.2	(8)	O(31)-C(31)-Os(3)	176	(2)
C(21)-Os(2)-C(22)	95.2	(8)	O(32)-C(32)-Os(3)	178	(2)
C(21)-Os(2)-C(23)	101.2	(8)	O(33)-C(33)-Os(3)	177	(2)
C(22)-Os(2)-C(23)	88.9	(7)	C(5)-C(4)-N	108	(2)
C(23)-Os(2)-Os(3)	129.0	(5)	C(6)-C(4)-N	106	(2)
C(31)-Os(3)-C(32)	95.1	(8)	C(7)-C(4)-N	111	(2)
C(31)-Os(3)-C(33)	99.4	(8)	C(1)-N-C(4)	174	(2)
C(32)-Os(3)-C(33)	88.5	(8)	C(5)-C(4)-C(6)	108	(2)
C(33)-Os(3)-Os(2)	130.2	(6)	C(5)-C(4)-C(7)	111	(2)
			C(6)-C(4)-C(7)	113	(2)

CNBut group would result in two equivalent hydrides).

The CNBut group is considered a better σ -donor but poorer π -acceptor ligand than a carbonyl.¹⁰³ It is usually found to occupy an axial site in osmium clusters and is therefore trans to a carbonyl ligand.⁷⁴ It is believed that this reduces the competition between the carbonyl ligands for the π -electron density on the Os atom. This has been discussed in Chapter 3. The CNBut group is also a sterically undemanding ligand that can occupy an axial position without causing serious steric interactions with the other axial carbonyl ligands on that side of the Os₃ plane.^{22,57,74} On the other hand, and as mentioned in Chapter 2, bulkier ligands such as phosphines are invariably found in equatorial sites in trinuclear clusters.^{24,46,104-106}

The Os-C bond to the CNBut ligand is slightly longer than that to the axial carbonyl (2.00(2) vs. 1.96(2) Å). Although the difference is barely significant it is consistent with the Os-CO having more double bond character (i.e., the CO ligand is a better π -acceptor than the CNBut ligand).

Formation of 1g from 2

When a dichloromethane solution of 1g was stirred at room temperature, 1g slowly isomerized to the red isomers of 1 over 4 days to give an equilibrium mixture of the three

isomers of 1. The approximate ratio of **1g**:**1ra**:**1rb** in the equilibrium mixture was about 1:5:1 as determined by the integration of the appropriate peaks in the ^1H NMR spectrum of the mixture. This indicates that the green isomer is the kinetic product of the decarbonylation of 2. The proposed reaction pathway of **1g** and **1r** from 2 is shown in Fig. 4.4.

It is not obvious how **1g** is initially formed from 2. It is suggested that an intermediate (**2c**) may be involved in the formation of **1g** as shown in Fig. 4.4. (Another form of **2c** is also possible that has the terminal hydride located on the same side of the Os_3 plane as the CNBu^t group.) It is known that in square planar platinum (II) chemistry a hydride ligand has a large trans effect.¹⁰⁷ A large trans effect of the H ligand in **2c** would facilitate the labilization of a CO group of the $\text{Os}(\text{CO})_4$ unit which, followed by migration of the terminal hydride to the resulting $\text{Os}(\text{CO})_3$ unit, would give the green isomer (as shown in Fig. 4.4).

The ^1H NMR spectrum of 2 at -70°C showed three weak signals at δ 1.67, -8.57 and -19.46 which were not reported in the original literature.²² These signals are consistent with the presence of another isomer of 2 such as **2c**. The isomer **2c** may be formed by the migration of the bridging hydride in **2a** or **2b** to the corresponding edge in **2c**. This process is known to have a low energy barrier in other hydrido-osmium clusters.^{5,108}

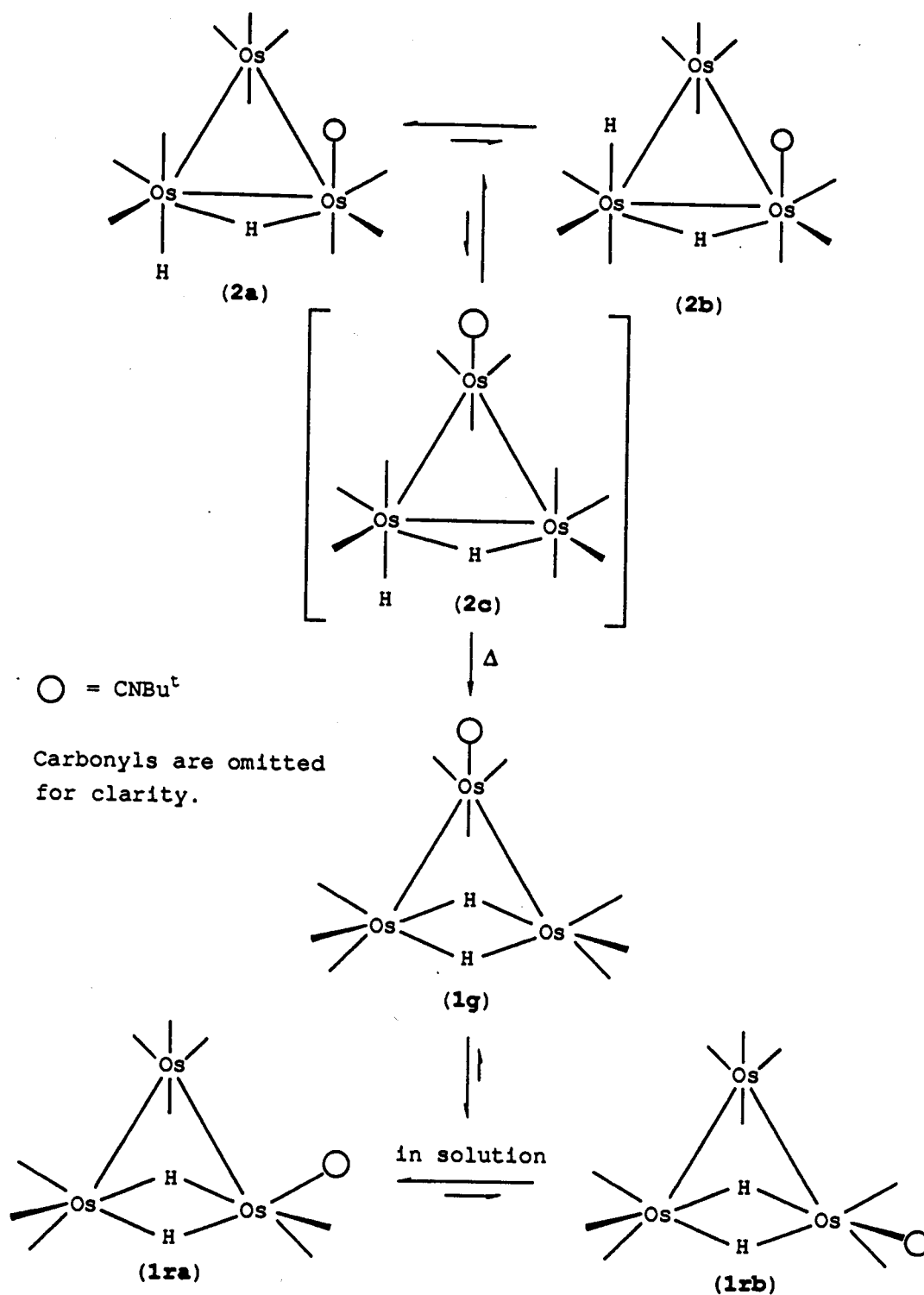


Fig. 4.4 Formation of 1g and 1r from 2.

In $\text{Os}_3(\mu\text{-H})_2(\text{CO})_{10}$, the bonding in the $\text{Os}(\mu\text{-H})_2\text{Os}$ linkage has been described as a four-centre four-electron bond.^{40,109} The small H-H couplings observed in **1g**, and **1ra**, probably indicate that there is little mixing of the molecular orbitals of the two $\text{Os}(\mu\text{-H})\text{Os}$ units in the $\text{Os}(\mu\text{-H})_2\text{Os}$ groupings in these molecules. In $\text{Os}_3(\mu\text{-H})_3(\text{CO})_9(\text{SiPh}_3)$, no coupling was observed between the hydrides of the $\text{Os}(\mu\text{-H})_2\text{Os}$ unit where it was suggested that there is no mixing of the three-centre, two-electron $\text{Os}(\mu\text{-H})\text{Os}$ molecular orbitals in the $\text{Os}(\mu\text{-H})_2\text{Os}$ grouping of this cluster.¹⁹ In the clusters $\text{Os}_3(\mu\text{-H})_2(\text{CO})_9(\text{PR}_3)$ ($\text{PR}_3 = \text{PMe}_3, \text{P(OMe)}_3$), similar small couplings (of 1.1 Hz) were also observed in the minor isomer in which the hydrides are inequivalent (see Table 4.2).

The coupling between the hydrides may, however, depend on the dihedral angle¹¹⁰ (i.e., the angle between the two $\text{Os}(\mu\text{-H})\text{Os}$ planes). The positions of the bridging hydrides of **1g** were calculated with the HYDEX program from which the dihedral angle between the two $\text{Os}(\mu\text{-H})\text{Os}$ planes was determined to be about 155° . This is consistent with the observed dihedral angle of 153° between the $\text{Os}(\mu\text{-H})\text{Os}$ planes in $\text{Os}_3(\mu\text{-H})_2(\text{CO})_{10}$. The corresponding dihedral angle in several other clusters with similar hydride arrangements have been calculated and are shown in Table 4.2. In **1ra**, where the dihedral angle is substantially smaller, only 138° , but a 1.1 Hz coupling between the hydrides was also

observed (see below). A similar angle was calculated for the $\text{Os}_3(\mu\text{-H})_2(\text{CO})_9(\text{PR}_3)$ clusters and these also exhibit small H-H coupling constants. However, in the case of $\text{Os}_3(\mu\text{-H})_3(\text{CO})_9(\text{SiPh}_3)$, where the calculated angle is 160° , no coupling was observed.¹⁹ This suggests that the dihedral angle in the $\text{Os}(\mu\text{-H})\text{Os}$ linkages does not contribute significantly to the spin-spin coupling between the hydrides.

Table 4.2 The observed H-H coupling constants and the dihedral angles in some selected unsaturated hydrido-osmium clusters. The dihedral angles are calculated from the positions of hydrides estimated from the HYDEX program and the X-ray data from the corresponding references.

	$J_{\text{H-H}}$	Dihedral angle, θ
$\text{Os}_3(\mu\text{-H})_2(\text{CO})_{10}$	equiv. hydrides	$153^\circ 40'$
1g	1.1 Hz	155°
1rb	1.1 Hz	$138^\circ 22'$
$\text{Os}_3(\mu\text{-H})_3(\text{CO})_9(\text{SiPh}_3)$	not observed	$160^\circ 19'$
$\text{Os}_3(\mu\text{-H})_2(\text{CO})_9(\text{PPh}_3)$	equiv. hydrides	$138^\circ 98'$
$\text{Os}_3(\mu\text{-H})_2(\text{CO})_9(\text{PMe}_3)$	1.1 Hz	(est. 138°) ⁹⁸
$\text{Os}_3(\mu\text{-H})_2(\text{CO})_9[\text{P}(\text{OMe})_3]$	1.1 Hz	(est. 138°) ⁹⁸

Isomerization of 1g to 1r

The mechanism of the isomerization from 1g to 1r is not clear. No intermediate species in the isomerization was detected by ^1H NMR spectroscopy. A carbonyl dissociation mechanism can, however, be excluded. This mechanism would

involve the dissociation of a carbonyl from the $\text{Os}(\text{CO})_3(\text{CNBu}^t)$ group of **1g** followed by migration of this carbonyl to the $\text{Os}(\mu\text{-H})_2\text{Os}$ linkage and the migration of the hydrides to the corresponding edge in **1r**. It is known that the carbonylation of **1g** and **1r** to **2** is fast compared to the equilibration of the isomers of **1**. Therefore, if CO dissociation occurred, **2** would be expected to be formed in the process. The ^1H NMR spectrum of the equilibrium mixture indicated that the isomerization of **1g** to **1r** is quantitative and **2** was not observed. A plausible mechanism for the isomerization would involve an intermediate with a bridging CO and CNBu^t ligand along an Os-Os edge not bridged by the hydride ligands. This is shown in Fig. 4.5. It is known that CNBu^t can act as a bridging ligand.^{103,111}

Nonrigidity of 1g

The $^{13}\text{C}\{^1\text{H}\}$ NMR spectrum of **1g** at -42°C (Fig. 4.6) exhibits five resonances at δ 187.3 (2C), 185.3 (1C), 181.9 (2C), 178.0 (2C), 177.4 (2C). The assignments shown on the spectrum follow the labelling scheme in Fig. 4.7. The proton coupled spectrum at the same temperature showed that the two high field signals at δ 178.0 and 177.4 are coupled to the hydrides with $J_{\text{C-H}} = 11.6$ and 11.7 Hz, respectively; the signal at δ 181.9 was slightly broadened compared to the other signals. The two resonances that exhibit hydrogen coupling can immediately be assigned to the

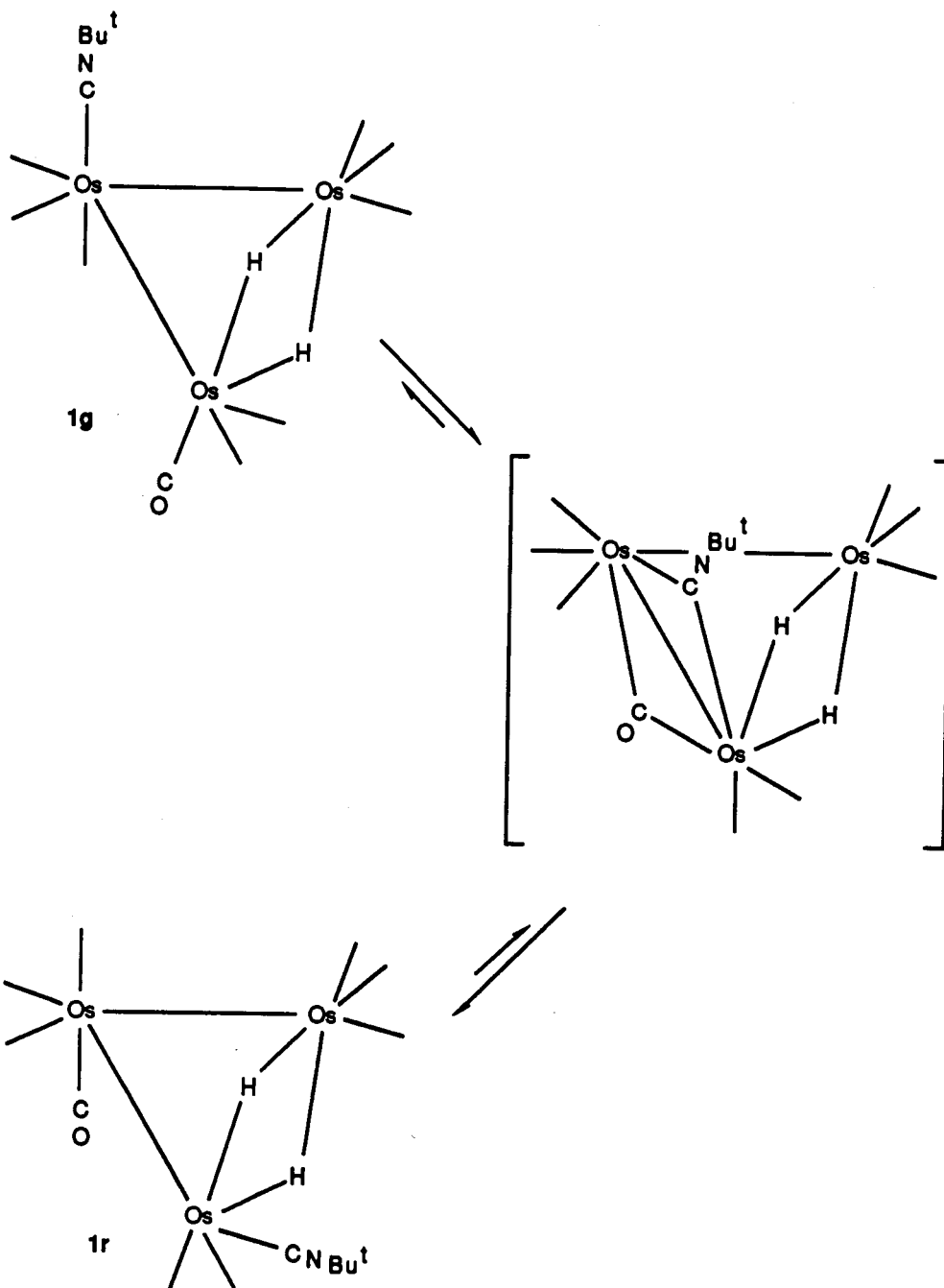


Fig. 4.5 Proposed pathway for the isomerization of 1.

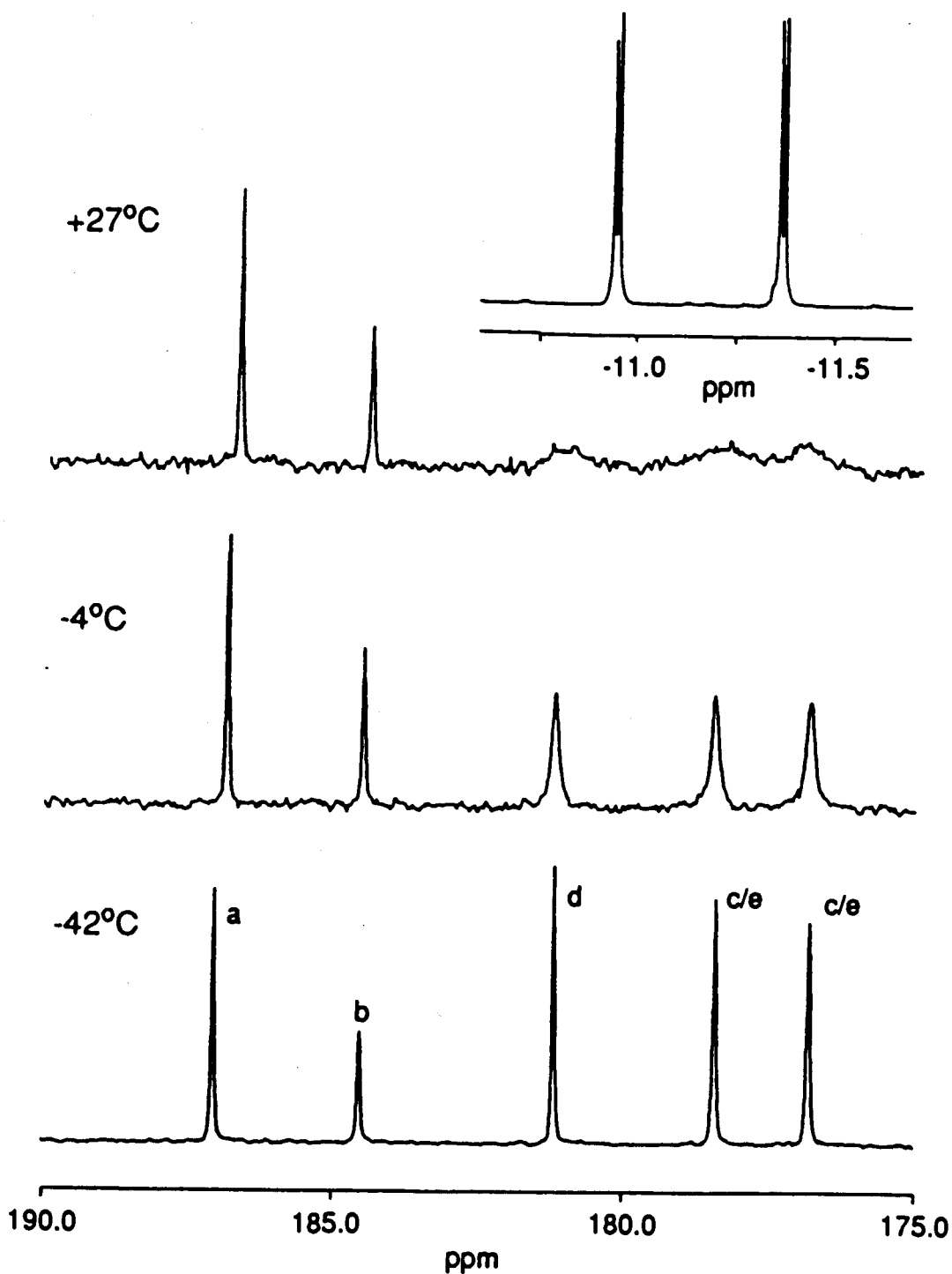
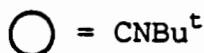
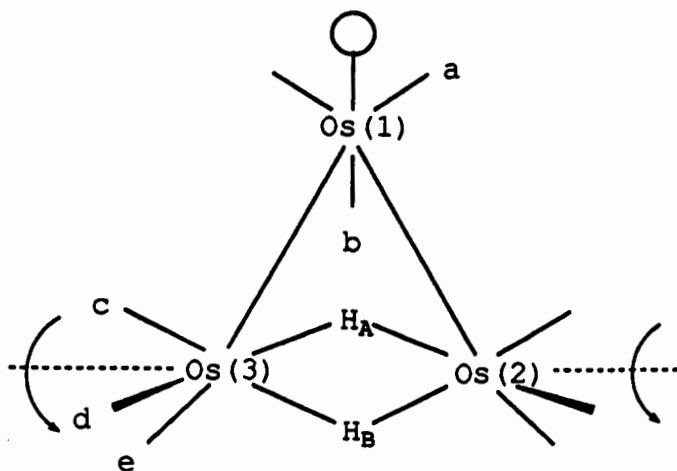


Fig. 4.6 Variable temperature 100.6 MHz ^{13}C NMR spectra of **1g** in $\text{CH}_2\text{Cl}_2/\text{CD}_2\text{Cl}_2$. Inset: 100-MHz ^1H NMR spectrum of **1g** in toluene-d_8 at 22°C .

carbonyls c and e of the $\text{Os}(\text{CO})_3$ units since they are trans to the two bridging hydrides. A similar coupling of 10.7 Hz was observed in $\text{Os}_3(\mu\text{-H})_2(\text{CO})_{10}$ for the analogous linkage.⁷⁴

These two doublets cannot be assigned more definitely from the coupled ^{13}C NMR spectrum. From the T_1 measurements of the hydrides of 1g reported in Chapter 1, the hydride that gives the ^1H NMR resonance at δ -11.36 exhibits a T_1 value of 0.31 s, slightly shorter than that which gives a resonance at δ -10.94 where the T_1 is 0.33 s. The resonance that exhibits a shorter T_1 is therefore tentatively assigned to the hydride H_A since, because of its close proximity to the CNBu^t group, it should relax through dipolar interaction more efficiently than H_B . If the ^1H resonance at δ -11.36 (i.e., H_A) is selectively decoupled, the doublet due to carbonyls e should collapse to a singlet since these carbonyls are trans to H_A (Fig. 4.7). When this was carried out, it was found that the ^{13}C resonance at δ 177.4 collapsed to a singlet. This resonance is, therefore, assigned to the carbonyls e, and that at δ 178.0 to carbonyls c.

This assignment of the ^{13}C resonances is consistent with that predicted if the magnetic anisotropy of the $\text{C}\equiv\text{N}$ group is considered. It is well-known that $\text{C}\equiv\text{N}$ bonds possess a large magnetic anisotropy.¹¹² Nuclei alongside this bond are deshielded. Due to the closer proximity of the $\text{C}\equiv\text{N}$ bond to the carbonyls c than to carbonyls e,



Carbonyls are omitted for clarity.

Fig. 4.7 Proposed mechanism of CO exchange in **1g**.

carbonyls **c** should be deshielded, and the resonance due to these carbonyls should be at a lower field to that due to carbonyls **e**.

The assignment of the other ¹³C NMR resonances in **1g** and many of those in **1ra** and **1rb** are also consistent with this view. This argument, however, cannot be applied to the assignment of the hydride resonances since the resonance attributed to H_A is assigned as upfield to that due to H_B. Since the amount of deshielding is angle and distance dependent, the sign of the shielding effect of a C≡N bond is not possible to predict. It is noted that C=O bonds also possess a large magnetic anisotropy and may offset that due to the C≡N linkage.

The slightly broadened ^{13}C resonance in the ^1H -coupled ^{13}C NMR spectrum of **1g** at δ 181.9 is assigned to the two equatorial carbonyls d. The broadness of the signal is attributed to unresolved couplings to the two bridging hydrides that are cis to these carbonyls. A coupling of 0.8 Hz was observed for the cis ^{13}C - ^1H coupling in a highly ^{13}CO enriched sample of $\text{Os}_3(\mu\text{-H})_2(\text{CO})_{10}$.⁷⁹ The assignment is consistent with the mode of collapse of the signals at higher temperatures which is discussed below. The two signals at lowest field can then be unambiguously assigned to the carbonyls of the $\text{Os}(\text{CO})_3(\text{CNBu}^t)$ group by intensity considerations. The signal at δ 185.3 of intensity one is attributed to the axial carbonyl b which is trans to the CNBu^t group. The resonance at δ 187.3 of intensity two is therefore assigned to the two equatorial carbonyls a. It has been observed in saturated triosmium clusters that resonances of axial carbonyls usually occur at a lower field than those due to equatorial carbonyls of the same group.^{78,79} The anomaly observed in this case can probably be attributed to the magnetic anisotropy of the $\text{C}\equiv\text{N}$ bond that deshields the equatorial carbonyls more than the axial carbonyls.

Variable temperature ^{13}C NMR spectra of **1g** are shown in Fig. 4.6. On warming the sample from -42°C to $+27^\circ\text{C}$, the three signals at high field collapse almost to the base line. This is rationalized in terms of a three-fold

rotation of the $\text{Os}(\text{CO})_3$ units about the $\text{Os}(2)\text{-Os}(3)$ vector as shown in Fig. 4.7. During the rotation, the two bridging hydrides which lie on either side of the rotation axis at the $\text{Os}(2)$ and $\text{Os}(3)$ centres might be expected to rotate simultaneously. However, at room temperature the two hydride signals in the ^1H NMR spectrum of **1g** were still sharp, and the small H-H couplings remained well resolved (inset in Fig. 4.6). This indicates that the hydride ligands are rigid on the NMR time scale. Indeed, this small coupling remains observable even at 70°C at which temperature isomerization of **1g** to **1r** occurs. This is consistent with the reported study of the deuterium kinetic isotope effect on the carbonyl exchange in $\text{Os}_3(\mu\text{-D})_2(\text{CO})_{10}$ from which it was concluded that the hydrides are rigid during the carbonyl exchange process.⁹⁹ (The carbonyl exchange in $\text{Os}_3(\mu\text{-H})_2(\text{CO})_{10}$ is believed to be similar to that in **1g**.)⁹⁹

Simulation of the ^{13}C NMR spectrum of **1g** at $8 \pm 2^\circ\text{C}$ (Fig. 4.8) gave a rate constant of $40 \pm 4 \text{ s}^{-1}$ which corresponds to a ΔG^\ddagger value of $14.4 \pm 0.2 \text{ kcal mol}^{-1}$. The activation energy of the CO exchange process observed in $\text{Os}_3(\mu\text{-H})_2(\text{CO})_{10}$ was calculated from the data reported by Hawkes et al.¹¹³ to be about $17.5 \text{ kcal mol}^{-1}$. The lower barrier in **1g** can be attributed to electronic rather than steric factors. The exact nature of the electronic factors is, however, uncertain.

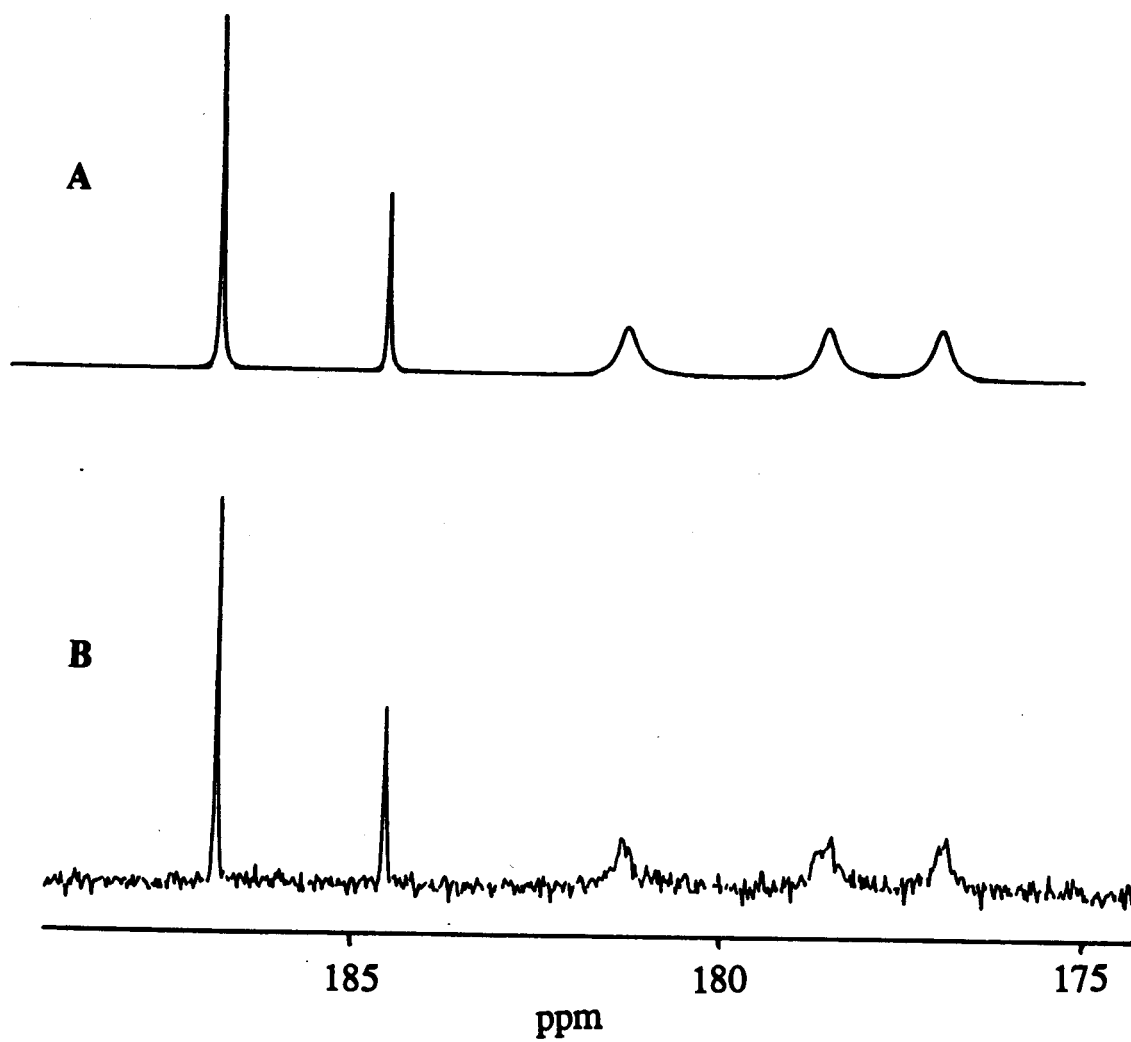


Fig. 4.8 Calculated (A) and observed (B) ^{13}C NMR spectra of **1g** at 8 °C.

The carbonyl signals due to the $\text{Os}(\text{CO})_3(\text{CNBu}^t)$ group remain sharp at room temperature and, indeed, up to 102 °C where isomerization becomes rapid (see below). This indicates that below 102 °C the carbonyls of this group do not exchange with those of the $\text{Os}(\text{CO})_3$ units.

Nonrigidity of 1r

The thermodynamic product, 1r, from the decarbonylation of 2 consists of two isomers, 1ra and 1rb, in solution (the two isomers are shown in Fig. 4.11). In the solid state 1r exists as isomer b as determined by X-ray crystallography.²² The molecular structure of 1rb revealed a triangular osmium framework with the CNBu^t group located in an equatorial position on an osmium atom of the $\text{Os}(\mu\text{-H})_2\text{Os}$ linkage (Fig. 4.9). The other isomer, 1ra, which is the major isomer in solution, has not been structurally characterized. The proposed structure of 1ra has the CNBu^t group in a pseudo-axial position of the same osmium atom in 1rb.²² The ^{13}C NMR spectrum of 1ra is in agreement with this configuration.

Both isomers of 1r are rigid at room temperature as indicated by ^{13}C NMR spectroscopy. The proton decoupled ^{13}C NMR spectrum of 1ra (^{13}CO enriched) exhibits nine resonances of relative intensity one in the terminal carbonyl region at δ 185.8, 185.1, 184.0, 183.3, 178.3, 177.1, 176.4, 176.1 and 175.0. The assignments of the ^{13}C NMR resonances are shown

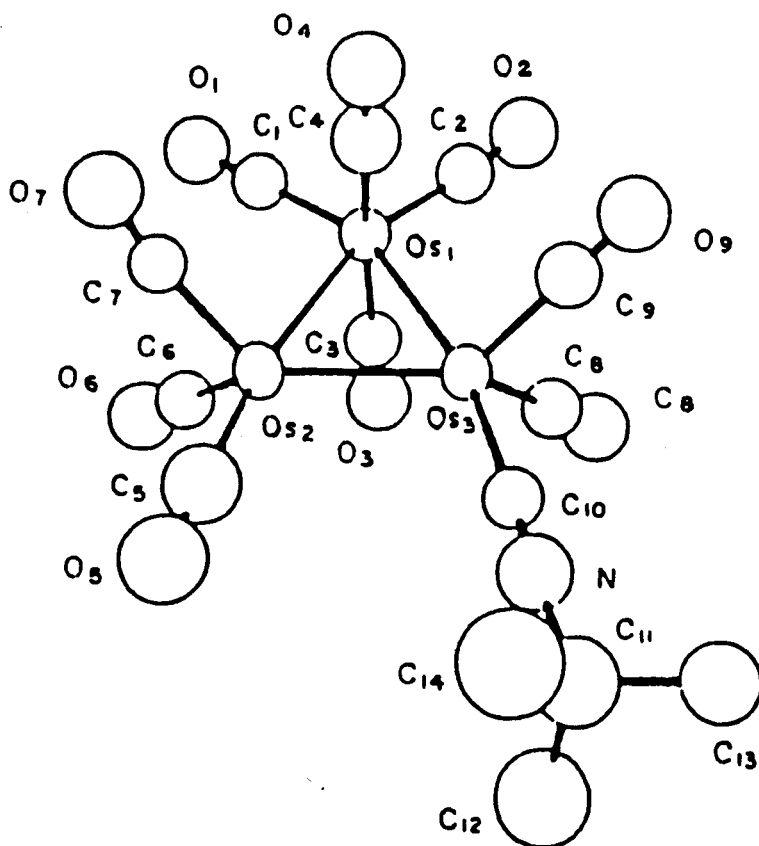


Fig. 4.9 Molecular structure of the red isomer of $\text{Os}_3(\mu\text{-H})_2(\text{CO})_9(\text{CNBut})$, 1rb.22

in Fig. 4.10 which follows the labelling scheme in Fig. 4.11. The four resonances to the low field of 180 ppm are assigned to the carbonyls of the $\text{Os}(\text{CO})_4$ group. It has been observed that signals due to carbonyls in a trans OC-Os-CO arrangement in ^{13}C -enriched carbonyl clusters exhibit ^{13}C - ^{13}C coupling.^{76,77} The resonances at δ 185.8 ($J_{\text{C-C}} = 34.7$ Hz) and 184.0 ($J_{\text{C-C}} = 34.9$ Hz) are, therefore, readily assigned to the axial carbonyls a and b, respectively. The resonance to lowest field is assigned to carbonyl a since it is closer to the CNBu^t ligand and is expected to experience the greatest deshielding effect of this ligand, as discussed above. The resonances at δ 185.1 and 183.3 are assigned to the equatorial carbonyls c and d, respectively, for the same reason. The integration of the signals and the satellite peaks indicates that the carbonyls are about 36% ^{13}C enriched.

The five resonances at the high field of 180 ppm are assigned to the carbonyls of the $(\text{OC})_3\text{Os}(\mu\text{-H})_2\text{Os}(\text{CO})_2(\text{CNBu}^t)$ grouping. In the ^1H -coupled ^{13}C NMR spectrum, the three resonances at δ 177.1 ($J_{\text{C-H}} = 12.0$ Hz), 176.4 ($J_{\text{C-H}} = 13.2$ Hz) and 176.1 ($J_{\text{C-H}} = 13.3$ Hz) exhibit ^{13}C - ^1H coupling. When the ^1H resonance of 1ra at δ -12.72 was selectively decoupled, only the signal at δ 176.4 collapsed to a singlet. Since only one carbonyl is trans to the hydride H_B , i.e. carbonyl g, this result indicates that the ^1H resonance at δ -12.72 is due to the hydride H_B and the

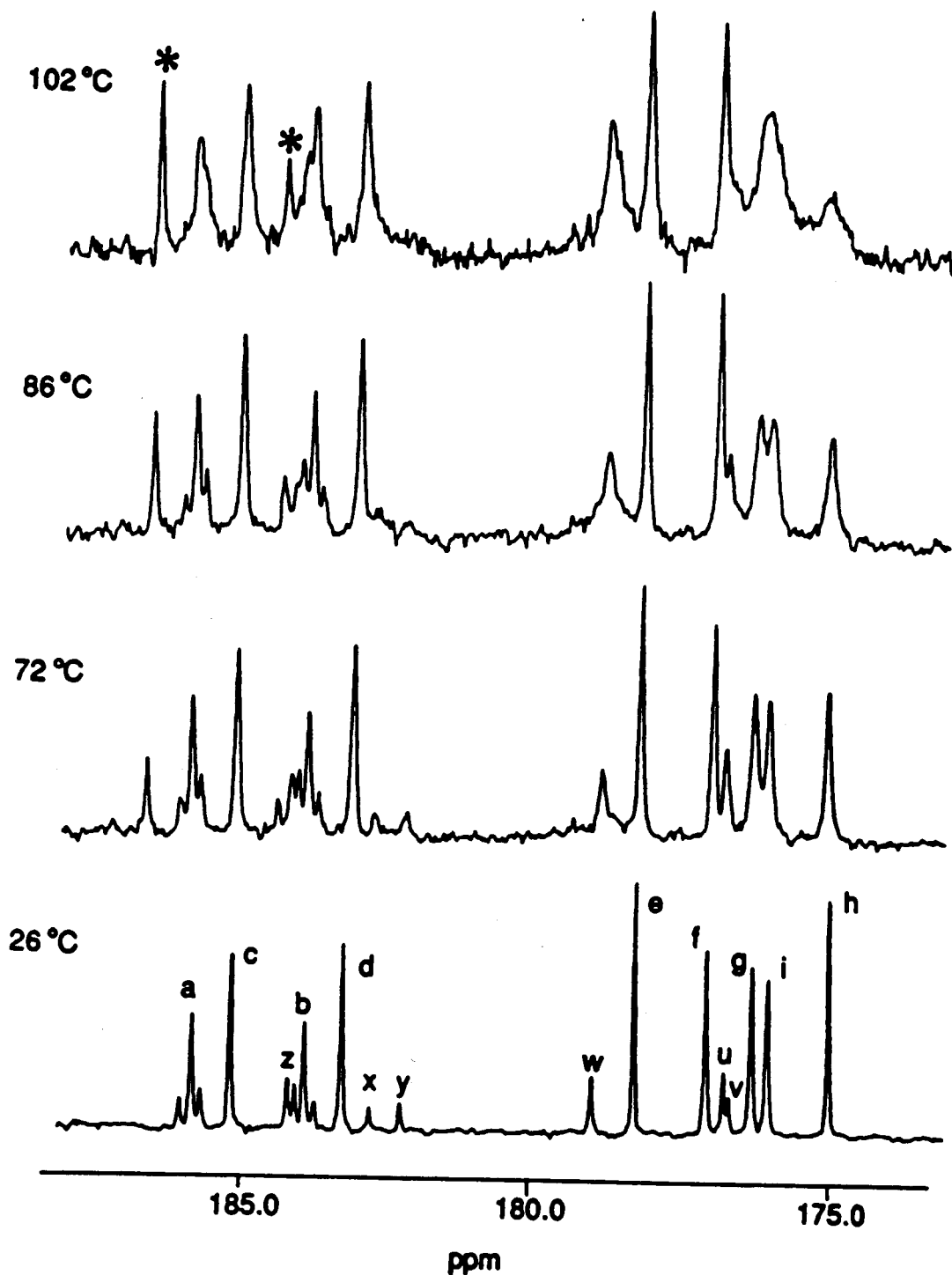


Fig. 4.10 Variable temperature ^{13}C NMR spectra of **1r** in toluene/toluene- d_8 . (The signals marked with an asterisk are due to $1g$, see text.)

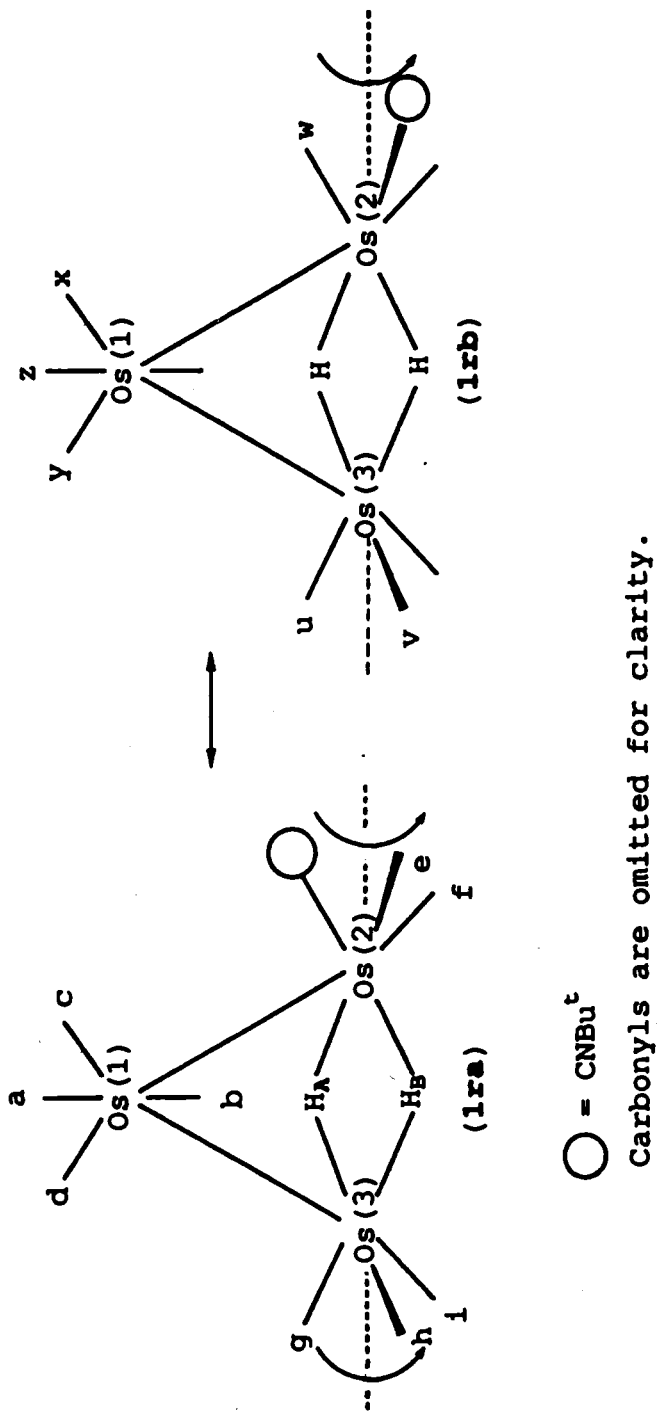


Fig. 4.11 Illustration of the three-fold rotations about the Os(2)-Os(3) axis (dotted line). The rotation at Os(2) interconverts the isomers **1ra** and **1rb**.

collapsed $^{13}\text{C}=\text{O}$ signal is due to the carbonyl g. The ^{13}C resonances at δ 177.1 and 176.1 are therefore assigned to the carbonyls f and i, respectively, based on the mode of collapse of the signals as discussed below. Likewise, the resonances at δ 178.3 and 175.0 are assigned to the carbonyls e and h, respectively.

The ^{13}C NMR spectrum of the minor isomer 1rb exhibits six resonances at δ 184.1 (2C), 182.8 (1C), 182.3 (1C), 179.0 (2C), 176.9 (2C) and 176.7 (1C). The resonances to high field of 180 ppm are assigned to the carbonyls of the $\text{Os}(\mu\text{-H})_2\text{Os}$ grouping by analogy to those of 1ra (and 1g). The resonances at δ 179.0 and 176.9 exhibit C-H couplings of 10.2 and 12.7 Hz respectively in the ^1H -coupled ^{13}C spectrum and are therefore assigned to the carbonyls w and u. (Since the hydrides in 1rb are equivalent, selective proton decoupling in this case will not yield any additional information.) The resonance at δ 176.7 of intensity one may, therefore, be assigned to the carbonyl v on the basis of its intensity. Since the chemical environment of the carbonyls u and v are similar, the chemical shifts are expected to be similar. On this basis, the resonance at δ 176.9 is tentatively assigned to the carbonyls u, and that at δ 179.0 to carbonyls w. This is also consistent with the view that, since carbonyls w are close to CNBu^t , they are deshielded by the magnetic anisotropy of CNBu^t , as mentioned above. The three resonances at low field of 180 ppm are

assigned to the carbonyls of the $\text{Os}(\text{CO})_4$ group. From intensity considerations, the resonance at δ 184.1 is assigned to the axial carbonyls z. The carbonyls x and y are assigned to the resonances at δ 182.8 and 182.3. However, a more definitive assignment of the equatorial carbonyls cannot be made at this point.

It is noted that the ^{13}C NMR resonances of the axial carbonyls of the $\text{Os}(\text{CO})_4$ group of **1ra** and **1rb** occur at a lower field than those due to the equatorial carbonyls of the same group.^{79,112} The ^{13}C NMR spectrum of $\text{Os}_3(\mu\text{-H})_2(\text{CO})_{10}$ exhibits two resonances at δ 181.8 and 182.7 due to the carbonyls of the $\text{Os}(\text{CO})_4$ unit. The assignment of these signals had been under debate for some time.¹¹³ Based on the assignment of the ^{13}C NMR resonances of **1r** the low field signal at δ 182.7 in the spectrum of $\text{Os}_3(\mu\text{-H})_2(\text{CO})_{10}$ should be assigned to the axial and that at δ 181.8 to the equatorial carbonyls. Koridze and co-workers agree with this assignment. Their assignment was based on ^{187}Os - ^{13}C O couplings measured in triosmium clusters.¹¹⁴

On warming the sample of **1r** to 72 °C, the three high field signals of **1ra** broadened while the other signals remained reasonably sharp. This is consistent with a three-fold rotation of the $\text{Os}(\text{CO})_3$ group about the $\text{Os}(2)$ - $\text{Os}(3)$ axis in **1ra** as shown in Fig. 4.11. A line shape analysis of the spectrum at 86 ± 2 °C (Fig. 4.12) gave a rate constant of $12 \pm 2 \text{ s}^{-1}$ which corresponds to a ΔG^\ddagger value of

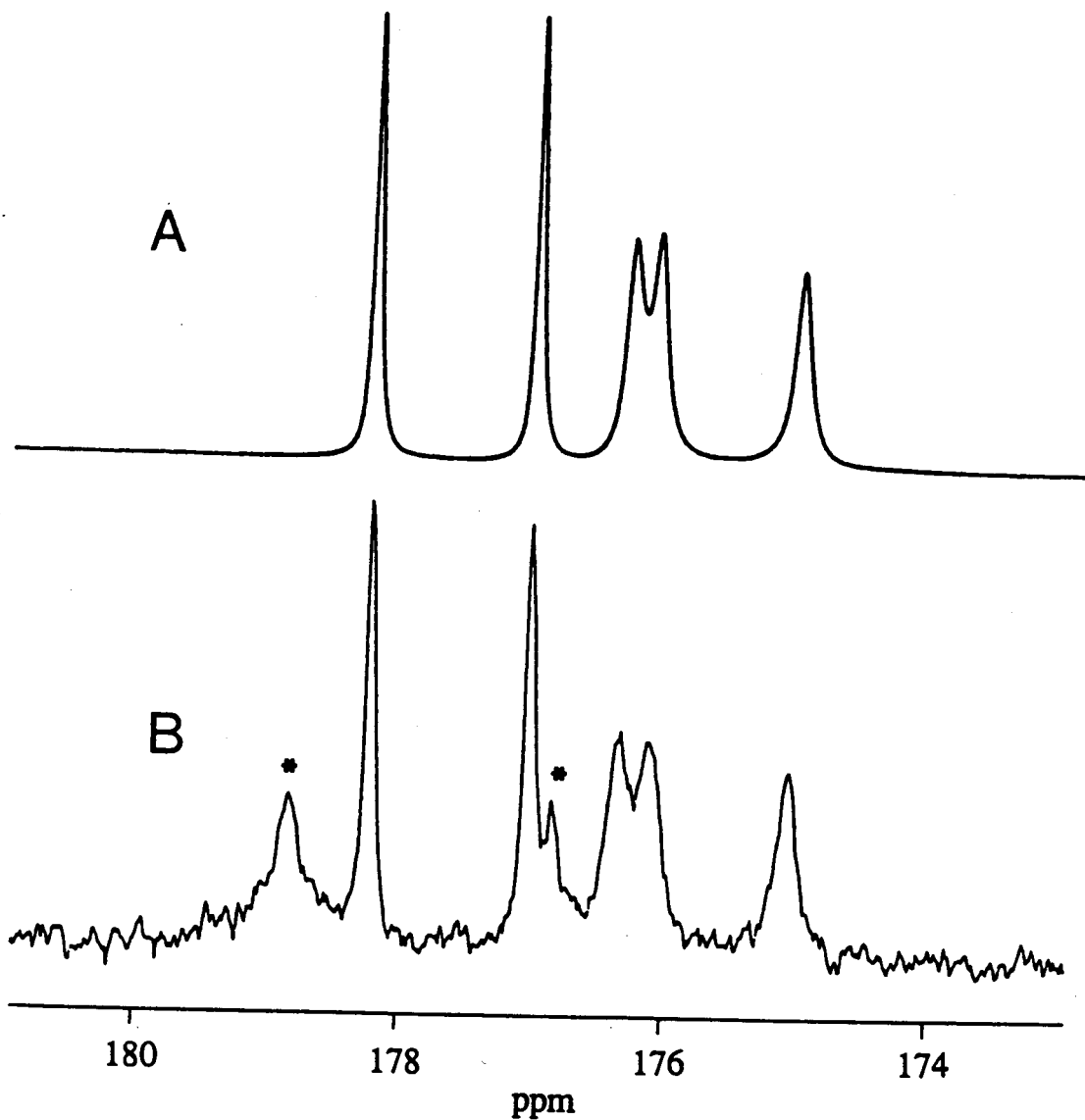


Fig. 4.12 Calculated (A) and observed (B) ^{13}C NMR spectra of **1ra** at 86 °C. (Only the part of the spectrum at high field of 180 ppm is shown; the signals marked by an asterisk are due to **1rb**.)

$19.4 \pm 0.2 \text{ kcal mol}^{-1}$. The CO exchange process of **1ra** therefore has a higher energy barrier than that observed in both $\text{Os}_3(\mu\text{-H})_2(\text{CO})_{10}$ and in **1g**. At this temperature, slow isomerization of **1r** to **1g** takes place as evidenced by the appearance of the carbonyl resonances due to the $\text{Os}(\text{CO})_3(\text{CNBu}^t)$ group of **1g** (marked by asterisks in Fig. 4.10). The resonances due to the carbonyls u and v of **1rb** coalesce at this temperature. This could be due to either rotation of the $\text{Os}(\text{CO})_3$ group as in **1ra**, or a variation of chemical shift of the two signals with temperature that renders the signals accidentally degenerate at 72°C . However, the spectrum at 86°C showed that the coalesced signal was also decreasing in intensity consistent with rotation of the $\text{Os}(\text{CO})_3$ group in **1rb**.

At 102°C , the resonances due to the carbonyls e and f started to broaden. There was also a general broadening of all signals from **1ra** and **1rb** (the two high-field signals due to **1g** remained sharp). This is attributed to the three-fold rotation at the $\text{Os}(\text{CO})_2(\text{CNBu}^t)$ unit along the Os(2)-Os(3) axis. This process will bring the CNBu^t group from a pseudo-axial position to the equatorial site and therefore interconverts **1ra** and **1rb** as shown in Fig. 4.11. When this takes place the appropriate carbonyls of **1ra** and **1rb** will equilibrate and all signals due to these isomers will broaden. As noted above, the two resonances due to the carbonyls of the $\text{Os}(\text{CO})_3(\text{CNBu}^t)$ group of **1g** remain sharp,

suggesting that these carbonyls do not exchange even at 102 °C.

The activation energy barrier to the rotation at the $\text{Os}(\text{CO})_2(\text{CNBu}^t)$ group of **1r** was also studied by ^1H NMR spectroscopy at 400 MHz. The ^1H NMR spectrum of **1r** in toluene- d_8 exhibits two resonances at δ 1.42 and 1.52 in the ratio of approximately 10:3. They are assigned to the tert-butyl groups of **1ra** and **1rb**, respectively. On warming the sample to 83 °C, the two signals coalesced which, as before, is consistent with the interconversion of the two red isomers of **1**. Simulation of the ^1H NMR spectrum at 83 ± 2 °C (Fig. 4.13) gave a rate constant of $4.4 \pm 0.4 \text{ s}^{-1}$ which corresponds to a ΔG^\ddagger value of $19.9 \pm 0.2 \text{ kcal mol}^{-1}$. The hydride signals of **1ra** and **1rb** were also broadened at this temperature. Surprisingly, the hydride ligands remain rigid on the NMR time scale up to the point of isomerization. Indeed, the hydrides may remain rigid during the isomerization process from **1g** to **1r**, but there is no simple way to confirm this.

Conclusion

The rigidity of the hydrides of the $\text{Os}(\mu\text{-H})_2\text{Os}$ group in $\text{Os}_3(\mu\text{-H})_2(\text{CO})_{10}$, **1g** and **1r** is in contrast to those in $\text{Os}(\mu\text{-H})\text{Os}$ groups in osmium clusters where the hydride is usually nonrigid.^{5,108} It was also observed that in $\text{Os}_3(\mu\text{-H})_3(\text{CO})_9(\text{SiPh}_3)$, the hydrides of the $\text{Os}(\mu\text{-H})_2\text{Os}$ unit

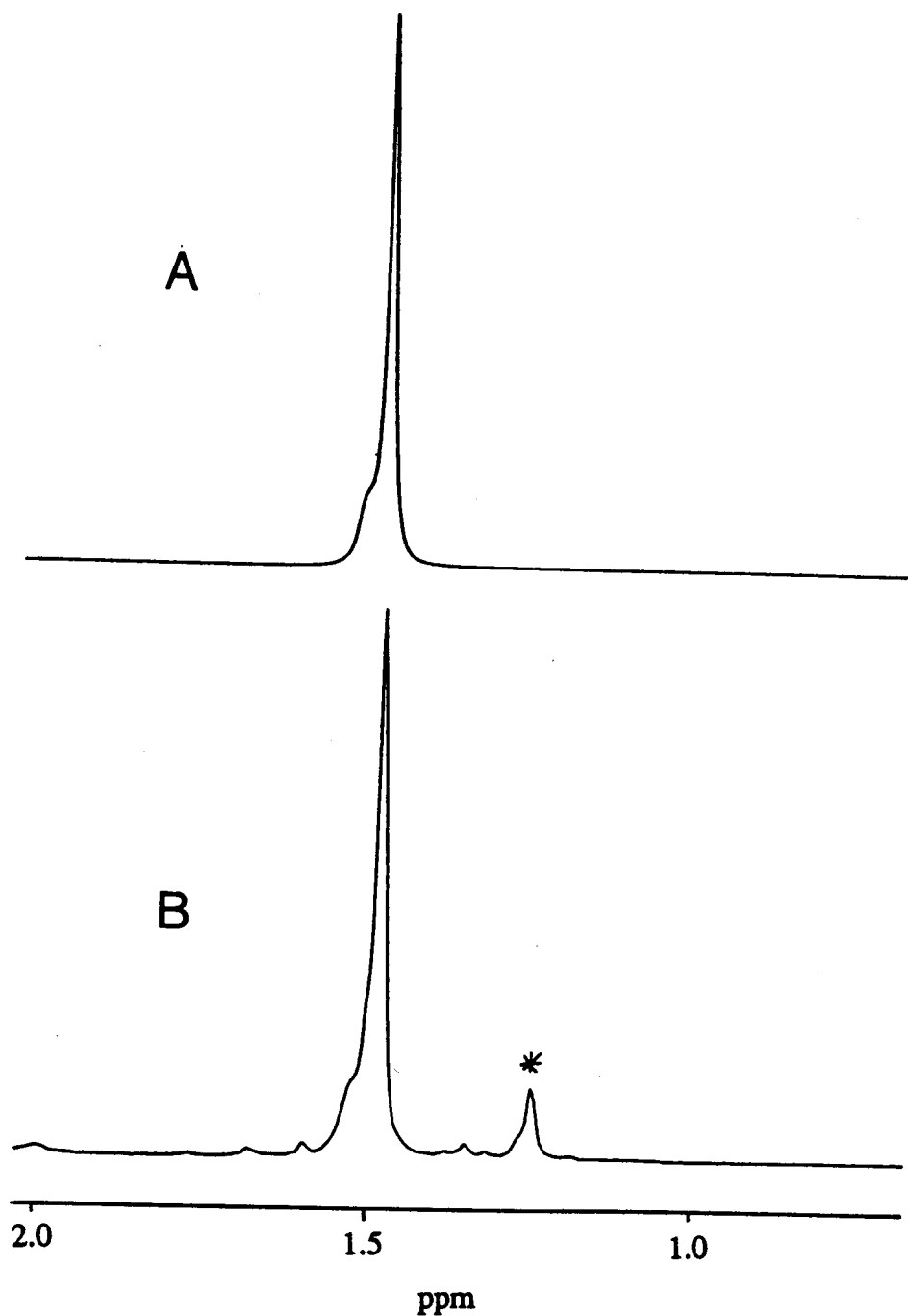


Fig. 4.13 Calculated (A) and observed (B) ^1H NMR spectra of 1r at 83 °C. (The signal marked by an asterisk is due to 1g.)

slowly exchange with that of the $\text{Os}(\mu\text{-H})\text{Os}$ group at 75 °C.¹⁹ The nonrigidity of the carbonyls in **1g** and **1r** is also in contrast with that observed in the clusters $\text{Os}_3(\mu\text{-X})(\mu\text{-H})(\text{CO})_{10}$ ($\text{X} = \text{SEt}, \text{SPh}, \text{Cl}, \text{Br}, \text{I}, \text{CO}_2\text{Me}, \text{CO}_2\text{CF}_3$) where the carbonyls of the $\text{Os}(\text{CO})_4$ group exchange rather than those in the $\text{Os}(\text{CO})_3$ unit.¹¹⁵ Also, in $[\text{Re}_3(\mu\text{-H})_4(\text{CO})_{10}]^-$, the hydrides in both the $\text{Re}(\mu\text{-H})\text{Re}$ and $\text{Re}(\mu\text{-H})_2\text{Re}$ units do not exchange nor do the carbonyls of the $\text{Re}(\text{CO})_3$ and $\text{Re}(\text{CO})_4$ groups.¹¹⁶ Similar clusters, therefore, do not necessarily have similar exchange processes. It is still not clear why apparently similar processes in metal clusters often have very different activation barriers.

Appendix I

Notation:

$f_1(2)$ = nuclear Overhauser enhancement at spin 1 when spin 2 is saturated.

R_1 = total direct relaxation rate of spin 1

$$= \sum_n \rho_{1n} + \rho_1^*$$

(n = spins that have relaxation interaction with spin 1 in the molecule.)

ρ_1^* = direct relaxation of spin 1 due to the relaxation mechanisms other than dipole-dipole relaxation.

ρ_{1n} = direct dipole-dipole relaxation between spins 1 and n (only intramolecular dipolar interaction is considered because of dilute sample).

W_{1I}, W_{1S} = transition probability for relaxation of spins I and S, respectively, by single-quantum process.

W_0 = zero-quantum process corresponding to a mutual spin-flip (no net relaxation).

W_2 = double-quantum process corresponding to a simultaneous relaxation of both spins.

τ_c = correlation time of the molecule.

For a system with two spin-1/2 nuclei, spins I and S, where the spins are not J-coupled, the energy level diagram (Solomon's diagram) is shown in Fig. A.1.

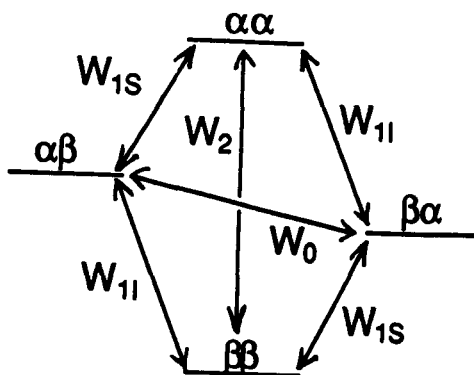


Fig. A.1 The Solomon's diagram for a 2-spin spin-1/2 system.

After spin S is saturated, the spin system will return to their equilibrium states, i.e., the equilibrium states according to the Boltzmann's distribution, mainly through spin-lattice relaxation. Other relaxation pathways will not be dealt with in this thesis because they are not important to the NOE.

Relaxation through W_1 's requires magnetic field fluctuations at a frequency of the order to the Larmor precession frequency, ω_0 , i.e., about 10^8 Hz (for a 100 MHz NMR spectrometer); while W_2 requires field fluctuations around $2\omega_0$. Because the necessary field fluctuations are produced by proton tumbling at a rate $1/\tau_c$, W_1 and W_2 are

most efficient when $\omega_0^2 \tau_c^2 \approx 1$. Fig. A.2 shows the relation of the spectral density, $J(\omega)$, or the intensity of appropriate field fluctuations, and the Larmor frequency with respect to τ_c . It can be seen that maximum $J(\omega)$ is achieved when $\omega_0^2 \tau_c^2 \approx 1$, and, hence, the relaxation is maximum. This is also illustrated in Fig. A.3. Moreover, for a correlation time of, e.g., 10^{-9} s, the relaxation rate (R_1) is higher at lower field strength (at 100 MHz) than that at a higher field strength (at 400 MHz). Better NOE is, therefore, obtained with a lower field spectrometer.

The relaxation through W_0 requires fields of low frequency and, therefore, it is most efficient when the molecular tumbling is slow, e.g., for large molecules, or for molecules in viscous solution. The NOE is useful only when $W_2 \gg W_0$. The expressions for W_0 , W_1 and W_2 are as follows:⁶

$$W_0 = \frac{1}{20} (2\pi D)^2 J(\omega_x - \omega_A)$$

$$W_1 = \frac{3}{40} (2\pi D)^2 J(\omega_A)$$

$$W_2 = \frac{3}{10} (2\pi D)^2 J(\omega_x + \omega_A)$$

where D is the dipolar interaction constant, $J(\omega)$'s is the spectral density function. It is noted that, in extreme narrowing condition (i.e., when the spectral density terms

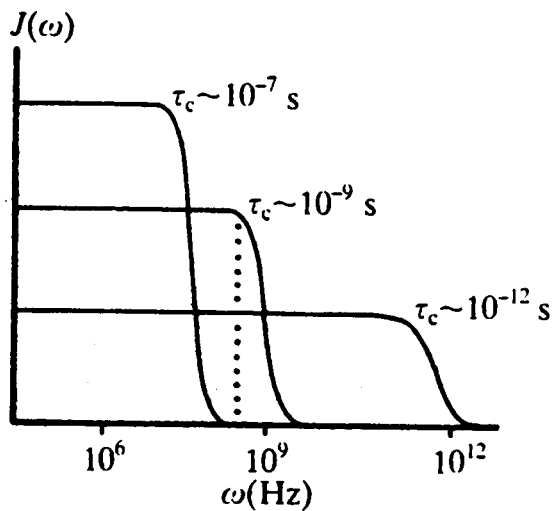


Fig. A.2 Plot of spectral density, $J(\omega)$ and the frequency, at different correlation times.

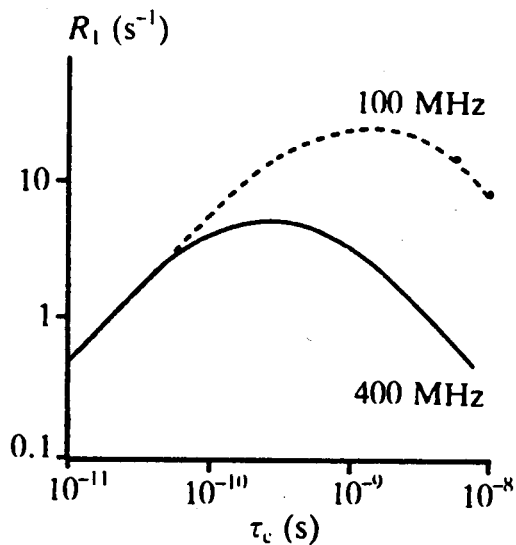


Fig. A.3 Diagram shows the relation of τ_c and the relaxation rate (R_1) at 100 and 400 MHz.

are equal), $W_0 : W_1 : W_2 = 1/6 : 1/4 : 1$, i.e., relaxation is mainly through W_2 .

The spin-lattice relaxation time, T_1 , is related to the mean-square average of the local magnetic field, H_L , by:

$$\frac{1}{T_1} = \frac{2}{3} \gamma^2 \langle H_L \rangle^2 \tau_c / (1 + \omega_0^2 \tau_c^2)$$

All nuclear interactions which contribute to H_L can cause relaxation.

In terms of the transition probabilities, W 's, T_1 can be expressed as follows:

$$\frac{1}{T_1} = W_0 + 2W_1 + W_2$$

With the substitution of the expressions of W 's, and the assumption for extreme narrowing condition, i.e., $\omega_0^2 \tau_c^2 \ll 1$,

$$\frac{1}{T_1} = \frac{3}{2} \frac{\gamma^4 \hbar^2 \tau_c}{r^6}$$

..... Eqn. A.1

Nuclear Overhauser enhancement (NOE) is the change of the absorption intensity of a nuclear spin (spin 1), when the NMR resonance of a different spin (spin 2), is saturated. If I_0 is the equilibrium intensity of the NMR resonance of spin 1, the NOE at spin 1 can be expressed by:

$$f_1(2) = \frac{\langle I_z \rangle - I_0}{I_0}$$

where $\langle I_z \rangle$ is the average value of the nuclear spin operator. When a steady state condition for spin 1 is reached, i.e., $d\langle I_z \rangle/dt = 0$, the expression of NOE, after several steps of substitutions,^a can be written in a more general form:

$$f_1(2) = \frac{\gamma_2 \rho_{12}}{2 \gamma_1 R_1} - \sum_n \frac{\gamma_n \rho_{1n} f_n(2)}{2 \gamma_1 R_1} \quad \dots\dots\dots \text{Eqn A.2}$$

where n is the spins other than spins 1 and 2; and for intramolecular dipole-dipole relaxation,

$$\rho_{12} = \frac{\gamma_1^2 \gamma_2^2 \hbar^2}{r_{12}^6} \tau_c(12)$$

where the distance information from NOE experiments is obtained.

a. The derivation of Eqn. A.2 can be found in most NMR books. The details will not be discussed here.

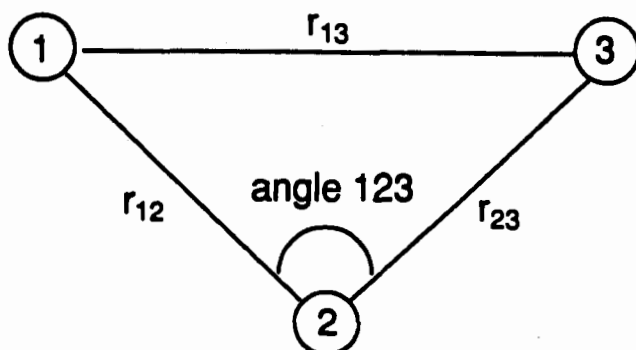
For 2-spin systems, Eqn. A.2 can be written as:

$$f_1(2) = \frac{\gamma_2}{\gamma_1} \frac{\rho_{12}}{2R_1}$$

$$= \frac{\rho_{12}}{2R_1} \text{ (for homonuclear spins 1 and 2)}$$

Therefore, if the total dipolar relaxation of spin 1 (R_1) is large, and the relaxation is not mainly through the saturated spin, the observed NOE will be small.

For 3-spin homonuclear systems (spins 1, 2, and 3) arranged as shown:



Eqn. A.2 can be written as:

$$f_1(2) = \frac{\rho_{12}}{2R_1} - \frac{\rho_{13}}{2R_1} f_3(2)$$

..... Eqn. A.3

In the case where the distance between spin 1 and spin 3, i.e., r_{13} , is relatively long compared to those of r_{12} and r_{23} , i.e., when angle 123 is large, $\rho_{13} \ll \rho_{23}$ because

$\rho \propto 1/r^6$. To a good approximation, ρ_{13} can be neglected. $f_1(2)$ and $f_3(2)$, i.e., when the central spin is saturated, can then be treated as 2-spin systems. This approximation is, however, no longer valid when the angle 123 is small. In this case, r_{13} and, therefore, ρ_{13} is not negligible.

When one of the end spins, e.g., spin 1, is saturated, $f_2(1)$ and $f_3(1)$ must be treated as 3-spin systems. This is because the direct dipole-dipole relaxation between spins 2 and 3, ρ_{23} , is not negligible in (similar for $f_3(1)$):

$$f_2(1) = \frac{\rho_{21}}{2R_2} - \frac{\rho_{23}}{2R_2} f_3(1)$$

NOE is therefore angle dependent. In fact, curves can be drawn with Eqn. A.3 when r_{13} is varied, i.e., the angle 123 is varied. This is shown in Fig. 1.22 in the thesis. It can be seen that at some angles and internuclear distances, zero or even negative enhancements may result. The negative enhancement can almost instantly provide a rough idea on the relative positions, or the arrangement, of the three spins under consideration.

For a special case in 3-spin systems where two of the spins are equivalent, i.e., a AX_2 system, the NOE is calculated as follows:

- (a) For the enhancement of spin a when both of spin x are saturated, $f_a(x)$ is obtained from Eqn. A.2:

$$f_a(x) = \frac{2 \rho_{ax}}{2 R_a}$$

Since spin a relaxes through dipole-dipole interaction with two spin x's,

$$R_a = 2 \rho_{ax} + \rho_a^*$$

$$f_a(x) = \frac{\rho_{ax}}{2 \rho_{ax} + \rho_a^*}$$

(b) For $f_x(a)$, one of the spin x's must be considered as a third spin in the system, e.g., spin d, Eqn. A.3 can be written as:

$$f_a(x) = \frac{\rho_{ax}}{2R_x} - \frac{\rho_{xd}}{2R_x} f_d(a)$$

where

$$R_x = \rho_{ax} + \rho_{xd} + \rho_x^*$$

$$\rho_{xd} = \frac{\gamma_x^2 \gamma_d^2 h^2}{r_{xd}^2} \tau_c(xd)$$

It is noted that if ρ^* is assumed negligible in the calculation of NOE, the calculated values of NOE are larger than expected.

It is normally easier to obtain an integral of 1% enhancement than that of 0.1%. Fig. A.4 shows a simulated

NOE difference spectrum on a one-proton multiplet and a three-proton singlet of the same line width. In this case, however, it is easier to "see" and measure a 0.1% enhancement at the singlet (3H) than a 1% enhancement at the multiplet (1H).²⁷ Hence, it is not correct to think that the easiest NOE to measure is the largest NOE, e.g., enhancements to methyl groups may be small but they are also easy to measure. By the analogy, in $\text{HOS}_3(\mu\text{-H})(\text{CO})_{10}(\text{L})$ clusters, the multiplet of the bridging hydride (coupled to the terminal hydride and the phosphorus atom) was saturated and enhancement was measured at the signal of the terminal hydride which is a doublet.

When the correlation time of a molecule is long, e.g., at low temperature where the solvent is viscous, the relaxation rate (R_1) will decrease, as seen from Fig. A.3. The decrease of relaxation rate will result in a smaller NOE.

For the systems where more than three spins are present, calculation of NOE with the use of Eqn. A.2 will be more complicated. Assumptions can sometimes be made to simplify the calculation. For example, the spins that are reasonably far away from both the saturated spin and the observed spin can be omitted. In the case where phenyl rings are present, and the phenyl-hydrogens are close to the observed spin, in order to simplify the calculation the interactions of the phenyl-hydrogens and the observed spin

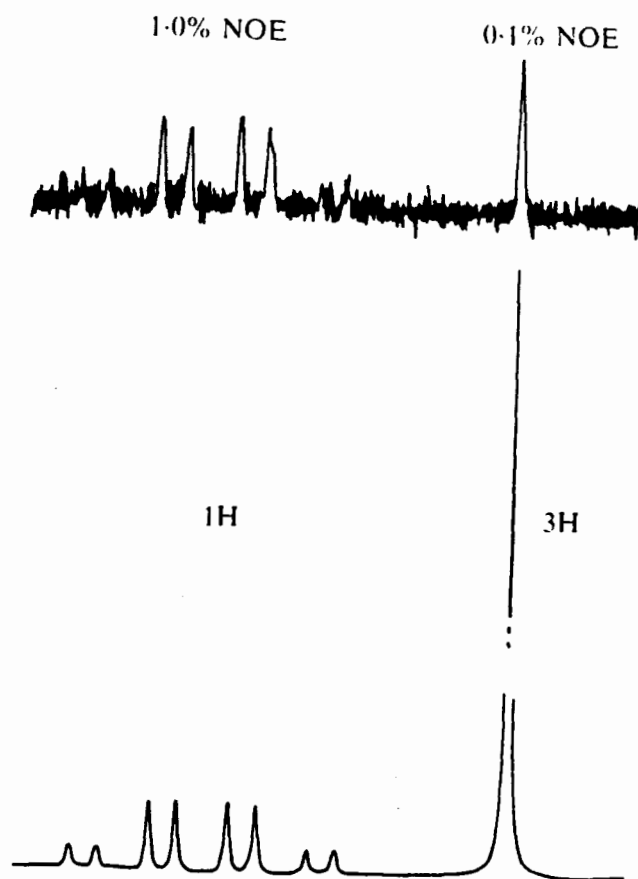


Fig. A.4 Simulated NOE's for a one-proton multiplet and a three-proton singlet.

are omitted (as reported in the thesis). Because of the rotation of the phenyl rings, the distance of the hydride and the phenyl hydrogens is non-static. The direct dipole-dipole interaction is, therefore, weak. The calculated NOE will be larger than the observed although the assumption will help simplify the calculation.

References

1. Mann, B.E. In Comprehensive Organometallic Chemistry; Wilkinson, G., Stone, F.G.A., Abel, E.W., Eds.; Pergamon: New York, 1982; Vol. 3, p 89.
2. Band, E.; Muetterties, E.L. Chem. Rev. 1978, 78, 639.
3. Geoffroy, G.L. Acc. Chem. Res. 1980, 13, 469.
4. Johnson, B.F.G.; Benfield, R.E. In Transition Metal Clusters; Johnson, B.F.G., Eds.; Wiley: Chichester, England, 1980; p 471.
5. Deeming, A.J. Adv. Organomet. Chem. 1986, 26, 1.
6. Orpen, A.G. J. Chem. Soc. Dalton Trans. 1980, 2509.
7. Bell, R.A.; Saunders, J.K. Can. J. Chem. 1970, 48, 1114.
8. Humphries, A.P.; Kaesz, H.D. Prog. Inorg. Chem. 1979, 25, 145.
9. Churchill, M.R.; DeBoer, B.G. Inorg. Chem. 1977, 16, 878.
10. Churchill, M.R.; DeBoer, B.G. Inorg. Chem. 1977, 16, 1141.
11. Churchill, M.R.; DeBoer, B.G.; Rotella, F.J. Inorg. Chem. 1976, 15, 1843.
12. Derome, A.E.; Modern NMR Techniques for Chemistry Research (Vol 6); Pergamon: U.K., p 113.
13. Noggle, J.H.; Schirmer, R.E. The Nuclear Overhauser Effect; Academic Press: New York, 1971.
14. Neuhaus, D.; Williamson, M.P. The Nuclear Overhauser Effect in Structural and Conformational Analysis; VCH: New York, 1989.
15. Harris, R.K.; Nuclear Magnetic Resonance Spectroscopy; Longman: England, 1986.
16. Brevard, C.; Granger, P.; Handbook of High Resolution Multinuclear NMR; Wiley: New York, 1981.
17. Sanders, J.K.M.; Hunter, B.K. Modern NMR Spectroscopy; Oxford: New York, 1989, p 32.

18. Knox, S.A.R.; Woepke, J.W.; Andrews, M.A.; Kaesz, H.D. J. Am. Chem. Soc. 1975, 97, 3942.
19. Willis, A.C.; Einstein, F.W.B.; Ramadam, R.M.; Pomeroy, R.K. Organometallics 1983, 2, 935.
20. Ma, A.K.; Einstein, F.W.B.; Johnston, V.J.; Pomeroy, R.K. Organometallics 1990, 9, 45.
21. Churchill, M.R.; Li, Y.-J. J. Organomet. Chem. 1985, 294, 367.
22. Adams, R.D.; Golembeski, N.M. Inorg. Chem. 1978, 18, 1909.
23. Shapley, J.R.; Keister, J.B.; Churchill, M.R.; DeBoer, B.G. J. Am. Chem. Soc. 1975, 97, 4145.
24. Churchill, M.R.; DeBoer, B.G. Inorg. Chem. 1977, 16, 2397.
25. Farrugia, L.J.; Green, M.; Hankey, D.R.; Murray, M.; Opren, A.G.; Stone, F.G.A. J. Chem. Soc., Dalton Trans. 1975, 177.
26. Wang, W.; Batchelor, R.J.; Davis, H.B.; Einstein, F.W.B.; Pomeroy, R.K. Organometallics, in press.
27. Keister, J.B.; Shapley, J.R. Inorg. Chem. 1982, 21, 3304.
28. Martin, L.R.; Einstein, F.W.B.; Pomeroy, R.K. Inorg. Chem. 1988, 27, 2986.
29. Johnson, B.F.G.; Lewis, J.; Raithby, P.R.; Azman, S.N.; Syed-Mustaffa, B.; Taylor, M.J.; Whitmire, K.H.; Clegg, W. J. Chem. Soc. Dalton Trans. 1984, 2112.
30. Einstein, F.W.B.; Pomeroy, R.K.; Willis, A.C. J. Organomet. Chem. 1986, 311, 257.
31. Ramadam, R.M.; Pomeroy, R.K. Unpublished results.
32. Ma, A.K.; Pomeroy, R.K. Unpublished results.
33. Lu, C.-Y.; Einstein, F.W.B.; Johnston, V.J.; Pomeroy, R.K. Inorg. Chem. 1989, 28, 4212.
34. Teller, R.G.; Bau, R. Struct. Bonding 1981, 44, 1.
35. Johnson, B.F.G.; Lewis, J.; Raithby, P.R.; Wong, K. J. Chem. Soc. Dalton Trans. 1980, 1248.

36. Johnston, V.J.; Einstein, F.W.B.; Pomeroy, R.K. J. Am. Chem. Soc. 1987, 109, 7220.
37. Martin, L.R.; Einstein, F.W.B.; Pomeroy, R.K. Organometallics 1988, 7, 294.
38. (a) Crabtree, R.H.; Segmuller, B.E.; Uriarte, R.J. Inorg. Chem. 1985, 24, 1949. (b) Crabtree, R.H.; Lavin, M.; Bonneviot, L. J. Am. Chem. Soc. 1986, 108, 4032.
39. Aime, S.; Botta, M.; Gobetto, R.; Osella, D. Inorg. Chem. 1987, 26, 2551.
40. Broach, R.W.; Williams, J.M. Inorg. Chem. 1979, 18, 314.
41. Riddick, J.A.; Bunger, W.B.; Sakano, T.K. Techniques of Chemistry (Vol. II): Organic Solvents, 4th ed.; Wiley: New York, 1986, p 30-36.
42. Van Buuren, G.N.; Willis, A.C.; Einstein, F.W.B.; Peterson, L.K.; Pomeroy, R.K.; Sutton, D. Inorg. Chem. 1981, 20, 4361.
43. Willis, A.C.; Van Buuren, G.N.; Pomeroy, R.K.; Einstein, F.W.B. Inorg. Chem. 1983, 22, 1162.
44. Cotton, F.G.A.; Hunter, D.L. Inorg. Chem. Acta 1974, 11, 111.
45. Aime, S.; Gambino, O.; Milone, L.; Sappa, E.; Rosenberg, E. Inorg. Chim. Acta 1975, 15, 53.
46. Johnson, B.F.G.; Lewis, J.; Reichert, B.E.; Schorpp, K.T. J. Chem. Soc., Dalton Trans. 1976, 1403.
47. Alex, R.F.; Pomeroy, R.K. Organometallics 1987, 6, 2437.
48. Tolman, C.A. Chem. Rev. 1977, 77, 313.
49. Bodner, G.M.; May, M.P.; McKinney, L.E. Inorg. Chem. 1980, 19, 1951.
50. Johnson, B.F.G.; Lewis, J.; Kilty, P.A. J. Chem. Soc. A 1968, 2859.
51. Sandström, J. Dynamic NMR Spectroscopy; Academic Press: New York, 1982; p 93.
52. Johnson, B.F.G.; Lewis, J.; Pippard, D.A. J. Chem. Soc., Dalton Trans. 1981, 407.

53. Benfield, R.E.; Johnson, B.F.G.; Raithby, P.R.; Sheldrick, G.M. Acta Crystallogr., Sect. B: Struct. Crystallogr. Cryst. Chem. 1978, B34, 666.
54. Bruce, M.I.; Matisons, J.G.; Skelton, B.W.; White, A.H. J. Chem. Soc., Dalton Trans. 1983, 2375.
55. For example: (a) Dahm, D.J.; Jacobson, R.A. J. Chem. Soc. 1968, 90, 5106. (b) Vönaläinen, T.; Pakkanen, T. Organomet. Chem. 1984, 266, 269.
56. Dawson, P.A.; Johnson, B.F.G.; Lewis, J.; Puga, J.; Raithby, P.R.; Rosales, M.J. J. Chem. Soc., Dalton Trans. 1982, 233.
57. Bruce, M.I.; Matisons, J.G.; Wallis, R.C.; Patrick, J.M.; Skelton, B.W.; White, A.H. J. Chem. Soc., Dalton Trans. 1983, 2365.
58. Bruce, M.I.; Matisons, J.G.; Patrick, J.M.; White, A.H.; Willis, A.C. J. Chem. Soc., Dalton Trans. 1985, 1223.
59. Albano, V.; Bellon, P.C.; Scatturin, V. J. Chem. Soc. Chem. Commun. 1967, 730.
60. Churchill, M.R.; Hollander, F.J.; Hutchinson, J.P. Inorg. Chem. 1977, 16, 2655.
61. Churchill, M.R.; Hutchinson, J.P. Inorg. Chem. 1978, 17, 3528.
62. Foster, A.; Johnson, B.F.G.; Lewis, J.; Matheson, T.W.; Robinson, B.H.; Jackson, W.G. J. Chem. Soc. Chem. Commun. 1974, 1042.
63. For example: (a) Bodner, G.M. Inorg. Chem. 1975, 14, 2694. (b) Bodner, G.M. Inorg. Chem. 1974, 13, 2563.
64. Braterman, P.S.; Milne, D.W.; Randall, W.; Rosenberg, E. J. Chem. Soc., Dalton Trans. 1973, 1027.
65. Cobblestick, R.E.; Einstein, F.W.B.; Pomeroy, R.K.; Spetch, E.R. J. Organomet. Chem. 1980, 195, 77.
66. (a) Mente, D.C.; Mills, J.L.; Mitchell, R.E. Inorg. Chem. 1975, 14, 123. (b) Mente, D.C.; Mills, J.L. Inorg. Chem. 1975, 14, 1862.
67. Martin, L.R.; Einstein, F.W.B.; Pomeroy, R.K. Inorg. Chem. 1985, 24, 2777.
68. Debies, T.P.; Rabalais, J.W. Inorg. Chem. 1974, 13, 308.

69. Johnston, V.J. Ph. D. Thesis, 1989, Simon Fraser University.
70. Johnston, V.J.; Einstein, F.W.B.; Ma, A.K.; Pomeroy, R.K. Organometallics 1990, 9, 52.
71. Einstein, F.W.B.; Johnston, V.J.; Pomeroy, R.K. Organometallics 1990, 9, 2754.
72. Benfield, R.E.; Johnson, B.F.G.; Lewis, J.; Raithby, P.R.; Zuccaro, C.; Hemick, K. International Union of Crystallography 1979, 2210.
73. (a) Cotton, F.A.; Wilkinson, G. Advanced Inorganic Chemistry, 5th ed.; Wiley: New York, 1988; p 62.
(b) Greenwood, N.N.; Earnshaw, A. Chemistry of the Elements; Pergamon: New York, 1984; p 349.
74. Mays, M.J.; Gavens, P.D. J. Chem. Soc. Dalton Trans. 1980, 911.
75. Ma, A.K.; Einstein, F.W.B.; Johnston, V.J.; Pomeroy, R.K. Organometallics 1990, 9, 45.
76. Tachikawa, M.; Richter, S.I.; Shapley, J.R. J. Organomet. Chem. 1977, 128, C9.
77. Aime, S.; Osella, D. J. Chem. Soc. Chem. Commun. 1981, 300.
78. Mann, B.E.; Taylor, B.F. ^{13}C NMR Data for Organometallic Compounds; Academic: New York, 1981; p 176.
79. Aime, S.; Osella, D.; Milone, L.; Rosenberg, E. J. Organomet. Chem. 1981, 213, 207.
80. (a) Einstein, F.W.B.; Pomeroy, R.K.; Rushman, P.; Willis, A.C. J. Chem. Soc. Chem. Commun. 1983, 854. (b) Fleming, M.M.; Pomeroy, R.K.; Rushman, P. J. Organomet. Chem. 1984, 274, C33.
81. Shipley, J.A.; Batchelor, R.J.; Einstein, F.W.B.; Pomeroy, R.K. Organometallics 1991, 10, 3620.
82. Alex, R.F.; Pomeroy, R.K. J. Organomet. Chem. 1985, 284, 379.
83. Gavens, P.D.; Mays, M.J. J. Organomet. Chem. 1978, 162, 389.
84. Adams, R.D.; Golembeski, N.M. J. Am. Chem. Soc. 1979, 101, 2579.

85. Johnston, V.J.; Einstein, F.W.B.; Pomeroy, R.K. J. Am. Chem. Soc. 1987, 109, 8111.
86. Allmenningen, A.; Bastiansen, O.; Skancke, P.N. Acta Chem Scand. 1961, 15, 711.
87. Bruce, M.I.; Liddel, M.J.; Hughes, C.A.; Skelton, B.W.; White, A.H. J. Organomet. Chem. 1988, 347, 157.
88. Nixon, J.F. Adv. Inorg. Radiochem. 1985, 29, 41.
89. Eady, C.R.; Johnson, B.F.G.; Lewis, J.; Reichert, B.E.; Sheldrick, G.M. J. Chem. Soc. Chem. Commun. 1976, 271.
90. Farrar, D.H.; Johnson, B.F.G.; Lewis, J.; Raithby, P.R.; Rosales, M.J. J. Chem. Soc. Dalton Trans. 1982, 2051.
91. Mason, R.; Thomas, K.M.; Mingos, D.M.P. J. Am. Chem. Soc. 1973, 95, 3802.
92. Eady, C.R.; Johnson, B.F.G.; Lewis, J.; Mason, R.; Hitchcock, P.B.; Thomas, K.M. J. Chem. Soc. Chem. Commun. 1977, 385.
93. Eady, C.R.; Johnson, B.F.G.; Lewis, J. J. Chem. Soc. Dalton Trans. 1975, 2606.
94. Pomeroy, R.K. J. Organomet. Chem. 1990, 383, 387.
95. Morrison, R.T.; Boyd, R.N. Organic Chemistry, 3rd ed.; Prentice-Hall: New Delhi, 1975; p 423.
96. Davis, H.B.; Einstein, F.W.B.; Glavina, P.G.; Jones, T.; Pomeroy, R.K.; Rushman, P. Organometallics 1989, 8, 1030.
97. Shapley, J.R.; Keister, J.B.; Churchill, M.R.; DeBoer, B.G. J. Am. Chem. Soc. 1975, 97, 4145.
98. Deeming, A.J.; Hasso, S. J. Organomet. Chem. 1976, 114, 313.
99. Rosenberg, E.; Anslyn, E.V.; Barner-Thorsen, C.; Aime, S.; Osella, D.; Gobetto, R.; Milone, L. Organometallics 1984, 3, 1790.
100. Kleier, D.A.; Binsch, G. QCPE 1970, 11, 165.
101. Constable, E.C.; Johnson, B.F.G.; Lewis, J.; Pain, G.N.; Taylor, M.J. J. Chem. Soc. Chem. Commun. 1982, 754.

102. Benfield, R.E.; Johnson, B.F.G.; Lewis, J.; Raithby, P.R.; Zuccaro, C.; Henrick, K. Acta Crystallogr., Sect. B: Struct. Crystallogr. Cryst. Chem. 1981, B35, 2210.
103. (a) Treichel, P.M. Adv. Organomet. Chem. 1973, 11, 21.
 (b) Yamamoto, Y. Coord. Chem. Rev. 1980, 32, 193.
 (c) Harvey, P.D.; Butler, I.S.; Harris, G.W.; Coville, N.J. Inorg. Chem. 1986, 25, 3608.
104. Dahm, D.J.; Jacobson, R.A. J. Am. Chem. Soc. 1968, 90, 5106.
105. Benfield, R.E.; Johnson, B.F.G.; Raithby, P.R.; Sheldrick, G.M. Acta Crystallogr., Sect. B: Struct. Crystallogr. Cryst. Chem. 1978, B34, 666.
106. Alex, R.F.; Einstein, F.W.B.; Jones, R.H.; Pomeroy, R.K. Inorg. Chem. 1978, 26, 3175.
107. Cotton, F.A.; Wilkinson, G. Advanced Inorganic Chemistry, 5th ed.; Wiley: New York, 1988; p 1299.
108. Some examples: (a) Ewing, P.; Farrugia, L.J.; Rycroft, D.S. Organometallics 1988, 7, 859. (b) Kneuper, H.-J.; Shapley, J.R. Organometallics 1987, 6, 2455.
 (c) VanderVelde, D.G.; Holmgren, J.S.; Shapley, J.R. Inorg. Chem. 1987, 26, 3077. (d) Aime, S.; Bertocello, R.; Buseti, V.; Gobetto, R.; Granozzi, G.; Osella, D. Inorg. Chem. 1986, 25, 4004. (e) Hsu, L.-Y.; Hsu, W.-L.; Jan, D.-Y.; Shore, S. G. Organometallics 1986, 5, 1041.
109. Sherwood, D.E.; Hall, M.B. Inorg. Chem. 1982, 21, 3458.
110. Karplus, M. J. Chem. Phys. 1959, 30, 11.
111. For example: (a) Bassett, J.-M.; Barker, G.K.; Green, M.; Howard, J.A.K.; Stone, F.G.A.; Wolsey, W.C. J. Chem. Soc. Dalton Trans. 1981, 219. (b) Howell, J.A.S.; Rowan, A.J. J. Chem. Soc. Dalton Trans. 1980, 503. (c) Ennis, M.; Kumar, R.; Manning, A.R.; Howell, J.A.S.; Mathur, P.; Rowan, A.J. J. Chem. Soc. Dalton Trans. 1981, 1251.
112. Günther, H. NMR Spectroscopy; Wiley: New York, 1980; p 73.
113. (a) Hawkes, G.E.; Randall, E.W.; Aime, S.; Osella, D.; Elliot, J.E. J. Chem. Soc. Dalton Trans. 1984, 279.
 (b) Hawkes, G.E.; Lian, L.Y.; Randall, E.W.; Sales, K.D.; Aime, S. Ibid 1985, 225.
114. Koridze, A. Dokl. Akad. Nauk. SSSR, 1989.

115. Bryan, E.G.; Forster, A.; Johnson, B.F.G.; Lewis, J.; Matheson, T.W. J. Chem. Soc. Dalton Trans. 1978, 196.
116. Beringhelli, T.; Ciani, G.; D'Alphonso, G.; Molinavi, H.; Sironi, A. Inorg. Chem. 1985, 24, 2666.